12TH INTERNATIONAL AMR PATHOLOGY SLIDE SEMINAR SYMPOSIUM IN ANATOMIC PATHOLOGY

Case – 1

Gynecologic and breast pathology

Contributed by: Ira Bleiweiss

Clinical History

A 68-year-old presented with a non-palpable, spiculated left breast mass found on screening mammography. Her prior imaging was unavailable, as she had recently moved from Ghana. Ultrasound revealed an irregular solid mass measuring 1.4x1.7 x 1.4 cm. Ultrasound-guided core biopsy was performed and was diagnosed at a commercial lab as a "well differentiated invasive papillary carcinoma, grade I" with receptors (ER/PR/Her2neu) all negative. A second opinion at an outside hospital was similar, and both the pathologist and the medical oncologist showed great surprise that such a low-grade lesion was triple negative. It was therefore decided to proceed to surgery and repeat the markers on the surgical specimen rather than treat with neoadjuvant chemotherapy as was originally contemplated.

Pathological Findings

The excision again revealed a irregular 2.1cm papillary lesion which was clearly invasive and contained tall columnar cells with nearly identical nuclei. Immunohistochemical stains revealed complete loss of calponin and p63 staining confirming the invasive nature of the tumor, and once again the tumor proved to be triple negative for estrogen receptor (ER), progesterone receptor (PR), and Her2neu. However, this time the pathologist recognized the unusual histology of the tumor, namely being made-up of tall columnar cells with reversed nuclear polarity (nuclei at the apical rather than basal poles of the cells), so-called breast carcinoma resembling tall cell variant of papillary thyroid carcinoma, more recently renamed papillary breast carcinoma with reverse polarity. Both sets of slides were sent to me for a confirmatory second opinion. The submitted slides are from the surgical excision specimen. Margins of the specimen were negative for tumor, as were three sentinel lymph nodes; and the patient has no evidence of disease approximately three years after her surgery.

Diagnosis

Invasive mammary tall cell breast carcinoma with reversed polarity

Comments

Tall cell carcinoma with reversed polarity (TCCRP), first reported by Eusebi et al in 2003, is a rare variant of breast carcinoma with distinct morphologic, immunohistochemical, and molecular findings. The entity was initially described as a breast tumor resembling the tall cell variant of papillary thyroid carcinoma based on its distinctive morphologic features.

This lesion is usually encountered in post-menopausal women in their 6th to 7th decades. Histologically, TCCRP is characterized by papillary, solid, or follicular architecture, lined by columnar epithelial cells displaying reverse polarity with abundant cytoplasm and apically located nuclei. The nuclear characteristics are reminiscent of papillary thyroid carcinomas, including optical clearing,

grooves, and occasional nuclear inclusions. The nuclear features are generally low grade with no few if any mitoses, and low Ki-67 proliferation rates, and minimal if any necrosis. Lymphatic and perineural invasion are typically not seen. The tumors are characteristically negative for ER, PR, and Her2 (so-called triple negative), positive for both low- and high-molecular-weight keratins, variably positive for breast markers (GCDFP-15, Mammoglobin, and Gata-3), and negative for thyroid markers (TTF-1 and thyroglobulin). While metastasis from a thyroid carcinoma should be a consideration, the immunohistochemical stains as well as the irregular, spiculated nature (as opposed to round, well-circumscribed metastases) confirm that the lesion is a breast primary, even in the absence of an intraductal component. In more recent molecular studies TCCRP has been associated with *IDH2* p.Arg172 hotspot mutations and *PIK3CA* missense mutations.

Various terms have been used to describe the lesion, including invasive solid papillary breast carcinomas resembling the tall cell variant of papillary thyroid neoplasms and solid papillary carcinoma with reverse polarity, however in 2019, the World Health Organization (WHO) classified the tumor in the "rare and salivary gland tumors" group and named tall cell carcinoma with reversed polarity (TCCRP). TCCRP generally shows an indolent clinical course with most patients being disease free during the follow up period and has been categorized as a breast carcinoma with low malignant potential with to date only 80 cases reported in the literature. Rare reports of local reoccurrence, nodal involvement and bone metastasis have, however, been described and are generally associated with larger tumors. Conservative surgical intervention is first line treatment for these lesions, but the utility of chemotherapy and/or radiation is currently controversial. The variable terminology, overlapping features with other papillary carcinomas of the breast, and lack of consensus concerning the clinical course complicate the diagnosis and management of these lesions.

Perhaps of greatest importance is the recognition of this entity's paradoxical triple negative staining pattern, more typical of poorly differentiated invasive breast carcinomas. This is a major hint to the diagnosis, and, as demonstrated in this case, a key to avoiding inappropriate neoadjuvant chemotherapy.

References

1. Eusebi V, Damiani S, Ellis IO, et al. breast tumor resembling the tall cell variant of papillary thyroid carcinoma: report of 5 cases. Am J Surg Pathol 23:1114-1118, 2003.
2. Cameselle-Teijeiro J, Abdulkader I, Barreiro-Morandeira F, et al. Breast tumor resembling the tall cell variant of papillary thyroid carcinoma: a case report. Int J Surg Pathol 14:79-84,2006.
3. Tosri AL, Ragazzi M, Asioli S, et al. Breast tumor resembling the tall cell variant of papillary thyroid carcinoma: report of 4 cases with evidence of malignant potential. Int J Surg Pathol 15:14-19,2007.
4. Chang SY, Fleiszer DM, Mesurolle B, et al. Breast tumor resembling the tall cell variant of papillary thyroid carcinoma. Breast J 15:531-535,2009.
5. Foschini M, Asioli S, Foreid S, et al. Solid papillary breast carcinomas resembling the tall cell variant of papillary thyroid neoplasms: a unique invasive tumor with indolent behavior. Am J Surg Pathol 41;887-895,2017.
6. Alsadoun N, MacGrogan G, Truntzer C, et al. Solid papillary carcinoma with reverse polarity of the breast harbors specific morphologic, immunohistochemical and molecular profile in comparison with other benign or malignant papillary lesions of the breast: a comparative study of 9 additional cases. Mod Pathol 31:1367-1380,2018.
7. Tumours Editorial Board of the WHO Classification. Classification of Breast Tumours, 5th edition. Lyon: IARC Press, 2019.

8. Fresia P, da Silva EM, Frosina D, et al. Immunohistochemical analysis of IDH2 R172 hotspot mutations in breast papillary neoplasms: applications in the diagnosis of tall cell carcinoma with reverse polarity. Mod Pathol 33:1056–1064,2020.
9. Trihia HJ, Lampropoulos P, Karelis L, et al. Tall cell carcinoma with reversed polarity: A case report of a very rare breast tumor entity and mini-review. Breast J 27:369-376,2019.
10. Schnitt SJ, Fend F, and Decker T. Breast carcinomas of low malignant potential. Virchows Archs 480:50-19,2022.

12TH INTERNATIONAL AMR PATHOLOGY SLIDE SEMINAR SYMPOSIUM IN ANATOMIC PATHOLOGY

Case – 2

Gynecologic and breast pathology

Contributed by: Ira Bleiweiss

Clinical History and Microscopic Findings

A 70 year old female former nurse presented with recurrent right axillary adenopathy. Approximately fifteen years previously (in 2008) she noted swelling in her left axilla. Excision at the time revealed 2 lymph nodes with metastatic carcinoma with extranodal extension. It was positive for estrogen receptor (ER), progesterone receptor (PR), and Her2neu (3+). After imaging detected a spiculated lesion in her left breast, a lumpectomy and axillary dissection was performed in early 2009, revealing invasive poorly differentiated duct carcinoma (1.5 cm) with lymphatic invasion. Metastatic carcinoma was present in an additional three out of twenty (3/20) left axillary lymph nodes. She received chemotherapy (Adriamycin/Cytoxan x4, taxol/Herceptin x12) followed by weekly Herceptin, a course of radiation to the left breast and axilla, and finally aromatase inhibitor (arimidex) for 3 years.

In 2018 (approximately 9 years after radiation treatment, she presented with an area of bruising along the medial aspect of her left breast. She was told that it might represent delayed healing from radiation; however, it enlarged, and a red raised area developed after a few months. After a skin biopsy revealed high grade angiosarcoma, a mastectomy was performed, revealing a 5.0 cm partially necrotic mass of high grade epithelioid and spindle cell angiosarcoma in the skin and focally involving the underlying breast tissue. Because of lingering neuropathy from her prior chemotherapy, she declined systemic treatment with paclitaxel.

Two years later (in 2020) she developed contralateral (right sided) pain, swelling, and axillary adenopathy, excision of which revealed metastatic angiosarcoma enlarging and replacing one out of three lymph nodes with extranodal involvement. Immunohistochemical stains showed that the tumor cells were positive for CD31, ERG, and C-myc. She again declined chemotherapy.

Two years later (in 2022) she again developed a right sided axillary mass which proved to be recurrent metastatic high grade epithelioid angiosarcoma in four out of six (4/6) lymph nodes and in surrounding adipose tissue. The slides are from this limited axillary dissection. Unfortunately, two months later she was incidentally found to have a 3.0cm, node negative pancreatic ductal adenocarcinoma for which a Whipple procedure was performed. She refused additional therapy and is NED at this writing, about 4 months after surgery.

Diagnosis

Radiation-related high grade epithelioid angiosarcoma of breast skin, recurrently metastatic to contralateral axillary lymph nodes-

Comments

Angiosarcoma of the breast is a rare entity, often histologically deceptively bland in appearance looking relative to its behavior, probably first described by Stewart and Treves in 1948 as “lymphangiosarcoma” in women with post mastectomy lymphedema. Lymphedema-associated

angiosarcoma is now rare because of currently more conservative surgical treatment of both the breast (lumpectomy) and axilla, particularly as sentinel lymph node excision has become standard, and complete axillary dissection has become rare. Whole breast irradiation is a frequent adjuvant treatment after most (but not all) lumpectomies performed for many invasive carcinomas and many intraductal carcinomas, often including radiation to the axilla in patients with smaller amounts of lymph node metastasis. In addition, chest wall/axillary radiation following mastectomy is often recommended in patients with certain pathologic indicators such as greater than 4 positive axillary lymph nodes, extensive lymphatic invasion in the breast, larger (generally >5cm) invasive tumors, carcinoma invading the deep margin (usually skeletal muscle), and/or skin invasion/ulceration by the tumor.

Despite the fact that radiation therapy in breast cancer treatment has become so commonplace, the absolute risk of developing angiosarcoma in a post-irradiated breast has remained low (well below 1 percent). On the other hand, angiosarcoma comprises a high percentage of radiation-induced sarcomas. While the latency period for such cases is shorter (average 10-11 years, ranging from 6 months to 44 years), survival is generally poor. There is no proven benefit to adjuvant chemotherapy or radiation therapy (which has in cases been attempted, oddly enough). The majority of radiation-induced angiosarcomas arise in the skin presenting as reddish areas usually with raised reddish nodules. Microscopically they are usually high grade and often so epithelioid as to be difficult to differentiate from recurrent invasive breast carcinoma. The key in such lesions is to look at the periphery of the lesion, away from the cellular epithelioid elements, where one will encounter the more typical interanastomosing blood vessels lined by plump atypical endothelial cells which then merge with spindle cells and epithelioid cells. Immunohistochemical stains are quite helpful in this differential, as the tumor cells will be positive for vascular markers, such as CD31, CD34, and/or factor VIII-related antigen; however, the vast majority of radiation-induced angiosarcomas of breast are positive for c-myc protein, so much so as to be practically pathognomonic of the entity.

Atypical vascular lesions of the skin appear to be precursors to full-fledged tumor as they may precede or coincide with adjacent sarcoma, but current studies show MYC gene amplification in radiation-induced angiosarcomas but not in the atypical vascular lesions or non-radiation related sarcomas. Although the literature describes atypical vascular lesions as non-obligate precursors of angiosarcoma, in my experience, the majority of patients with such lesions do develop angiosarcoma, despite their excision.

References

1. Yap J, Chuba PJ, Thomas R, et al. Sarcoma as a second malignancy after treatment for breast cancer. Int J Radiation Oncology Biol Phys 52:1231-1237,2002.
2. Brenn T and Fletcher CDM. Radiation-associated cutaneous atypical vascular lesions and angiosarcoma. Clinicopathologic analysis of 42 cases. Am J Surg Pathol 29:983-996,2005.
3. Manner J, Radlwimmer B, Hohenberger P, et al. MYC high level gene amplification is a distinctive feature of angiosarcomas after irradiation or chronic lymphedema. Am J Pathol 176:34-39,2010.
4. Guo T, Zhang L, Chang N, Singer S, Maki RG, Antonescu CA. Consistent MYC and FLT4 gene amplification in radiation-induced angiosarcoma but not in other radiation-associated atypical vascular lesions. Genes Chromosomes Cancer 50:25-33,2011.
5. Fernandez AP, Sun Y, Tubbs RR, et al. FISH for MYC amplification and anti-MYC immunohistochemistry: useful diagnostic tools in the assessment of secondary angiosarcoma and atypical vascular proliferations. J Cutan Pathol 39:234-242,2012.

6. Ginter PS, Mosquera JM, McDonald TY, et al. Diagnostic utility of MYC amplification and anti-MYC immunohistochemistry in atypical vascular lesions, primary or radiation-induced mammary angiosarcomas, and primary angiosarcomas of other sites. Hum Pathol 45:709-716,2014.

12TH INTERNATIONAL AMR PATHOLOGY SLIDE SEMINAR SYMPOSIUM IN ANATOMIC PATHOLOGY

Case – 3

Gynecologic and breast pathology

Contributed by: Maria Pia Foschini

Clinical History

A 61-year-old woman presented with a 2 cm nodule located in the UOQ of the right breast. A core needle biopsy was performed resulting in a B3 lesion. At the multidisciplinary meeting a decision to remove the nodule was taken. After surgical removal of the lesions, the patient was follow-up with mammography every year. Seven years after surgery, microcalcifications appeared on the UOQ of the right breast, in strict connection with the surgical scar. After the diagnosis of high grade duct in situ carcinoma (DCIS), performed on vacuum assisted biopsy, surgical resection with clear margins was performed; the sentinel node biopsy was negative. The surgical resection evidenced invasive carcinoma, no special type (NST), grade 2, associated with high grade DCIS and lobular in situ carcinoma (LCIS). The patient, followed up with annual mammography, is presently alive with no evidence of disease.

Microscopic Findings

The nodule had well defined, pushing margins, focally permeative.

The nodule was composed of a proliferation of small glands, surrounded by two types of cells. The outer layer was composed of clear cells, while the inner layer was composed of eosinophilic cells. A thick basal membrane surrounded each gland (fig. 1). Focal the tumour showed polypoid intraductal growth. Mitotic figures were quite rare. No necrosis was seen. On immunohistochemistry the clear cells were positive for the myoepithelial markers, as smooth muscle actin, calponin and p63. The inner, eosinophilic cells were positive for low molecular weight cytokeratins. Oestrogen (ER), Progesterone (PR) receptors and HER2 were negative; proliferative index, evaluated by Ki67 was lower than 5% of the neoplastic cells.

The breast parenchyma surrounding the nodule showed multiple foci of lobular in situ carcinoma, classical type.

The present case was diagnosed as adenomyoepithelioma (AME), without features of malignancy.

The area with microcalcifications, detected 7 years after surgery, on histology was composed of ductal in situ carcinoma of high nuclear grade, solid with comedo-type necrosis. It did not show any immunohistochemical evidence of myoepithelial cell differentiation. On surgical resection, a 0.5 cm. area of invasive carcinoma, no special type was additionally seen in association with DCIS. Both DCIS and invasive carcinoma were devoid of any myoepithelial cell differentiation (calponin, smooth muscle actin and CK14 negative); in addition, they were ER/PR positive, HER2 negative (fig. 2). The remaining breast parenchyma showed multiple foci of LCIS classical type.

Diagnosis

Adenomyoepithelioma (AME), without features of malignancy, followed by high grade in situ duct carcinoma associated with invasive carcinoma NST.

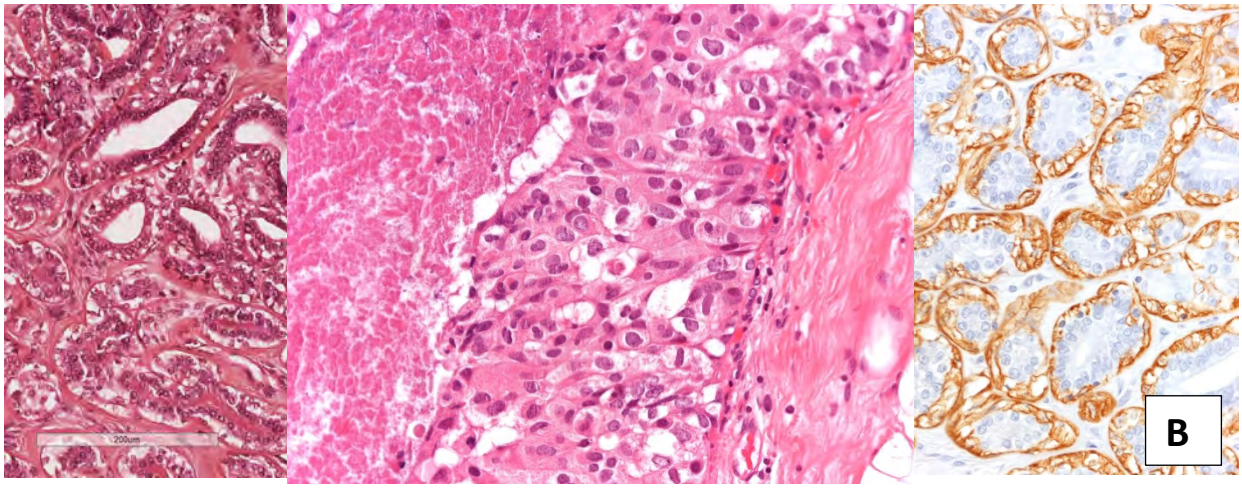

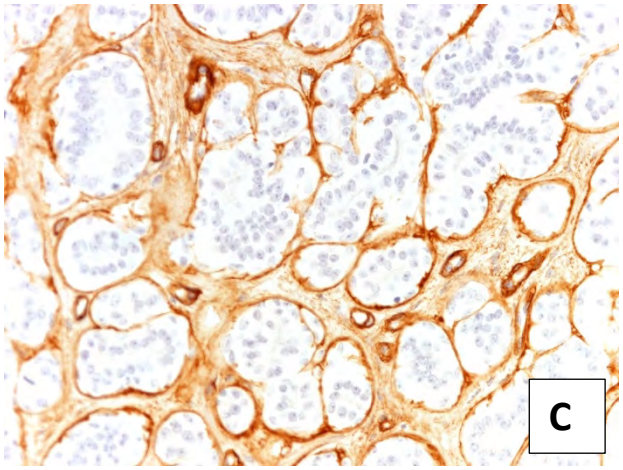

Fig. 1: A) on H&E the tumour showed a biphasic component, with epithelial and myoepithelial cells; B) Smooth muscle actin is strongly positive in the myoepithelial cells; C) Collagen IV evidences the basal membrane.

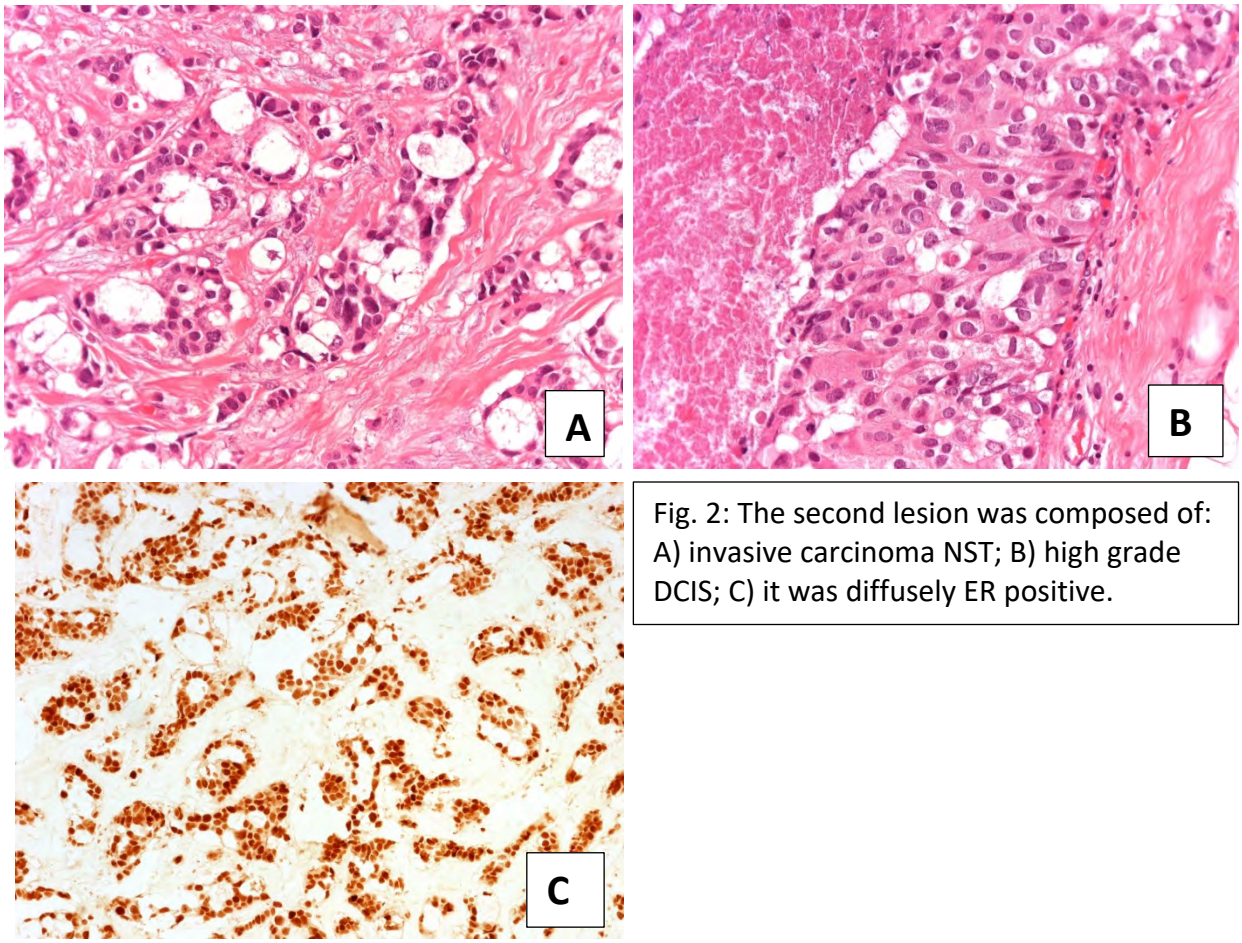

Fig. 2: The second lesion was composed of: A) invasive carcinoma NST; B) high grade DCIS; C) it was diffusely ER positive.

Comments

According to the WHO blue book classification, 5th edition, AME is defined as "a biphasic neoplasm (usually benign) characterized by small epithelium-lined spaces with inner luminal ductal cells and a proliferation of variably enlarged and clearly noticeable abluminal myoepithelial cells. Malignant transformation may occur from either the luminal or myoepithelial component." (1). The present case, on its initial presentation, completely fulfilled all those criteria.

AME can present a great variety of morphological features (2,3,4), sometimes difficult to classify, but suggesting a propensity to malignant transformation (5).

In AME malignant transformation can involve both (epithelial and myoepithelial) components. Features of malignancy involving the myoepithelial components are known since the first AME studies (6,7) while the spectrum of malignant transformation of the epithelial component has been matter of debate only recently (3,4).

DCIS can arise in AME (3,4), being characterized by atypical epithelial cells surrounded by the prominent myoepithelial component typical of AME.

On the contrary, the present case of AME, at initial presentation did not show any feature of malignancy. It showed a tubular architecture, that should be differentiated from microglandular adenosis and from other being microglandular proliferations (8).

In present case, DCIS and invasive carcinoma, epithelial type, arose in the breast tissue surrounding the surgical scar. The relation between the AME and the subsequent pure epithelial carcinoma is difficult to assess. Cases of AME showing DCIS in the tissue adjacent have been described

(9), but at the moment it is not clear if the epithelial malignancy can have a clonal relation with the AME or it is a second, unrelated tumour.

References

1. WHO Classification of Tumours Editorial Board. Breast tumours [Internet]. Lyon (France): International Agency for Research on Cancer; 2019. (WHO classification of tumours series, 5th ed.; vol. 2). Available from: https://tumourclassification.iarc.who.int/chapters/32.
2. Cima L, Kaya H, Marchiò C, Nishimura R, Wen HY, Fabbri VP, Foschini MP. Triple-negative breast carcinomas of low malignant potential: review on diagnostic criteria and differential diagnoses. Virchows Arch. 2022 Jan;480(1):109-126. doi: 10.1007/s00428-021-03174-7. Epub 2021 Aug 30. PMID: 34458945; PMCID: PMC8983547.
3. Rakha E, Tan PH, Ellis I, Quinn C. Adenomyoepithelioma of the breast: a proposal for classification. Histopathology. 2021 Oct;79(4):465-479. doi: 10.1111/his.14380. Epub 2021 Jun 13. PMID: 33829532.
4. Foschini MP, Nishimura R, Fabbri VP, Varga Z, Kaya H, Cserni G. Breast lesions with myoepithelial phenotype. Histopathology. 2023 Jan;82(1):53-69. doi: 10.1111/his.14826. PMID: 36482278.
5. Hayes MM. Adenomyoepithelioma of the breast: a review stressing its propensity for malignant transformation. J Clin Pathol. 2011 Jun;64(6):477-84. doi: 10.1136/jcp.2010.087718. Epub 2011 Feb 9. PMID: 21307156.
6. Eusebi V, Casadei GP, Bussolati G, Azzopardi JG. Adenomyoepithelioma of the breast with a distinctive type of apocrine adenosis. Histopathology. 1987 Mar;11(3):305-15. doi: 10.1111/j.1365-2559.1987.tb02635.x. PMID: 2828217.
7. Kiaer H, Nielsen B, Paulsen S, Sørensen IM, Dyreborg U, Blichert-Toft M. Adenomyoepithelial adenosis and low-grade malignant adenomyoepithelioma of the breast. Virchows Arch A Pathol Anat Histopathol. 1984;405(1):55-67. doi: 10.1007/BF00694925. PMID: 6438900.
8. Foschini MP, Eusebi V. Microglandular adenosis of the breast: a deceptive and still mysterious benign lesion. Hum Pathol. 2018 Dec;82:1-9. doi: 10.1016/j.humpath.2018.06.025. Epub 2018 Jun 24. PMID: 29949742.
9. Kamei M, Daa T, Miyawaki M, Suehiro S, Sugio K. Adenomyoepithelioma of the breast coexisting with ductal carcinoma in situ: a case report and review of the literature. Surg Case Rep. 2015 Sep 11;1:81. doi: 10.1186/s40792-015-0083-8. PMID: 26380805; PMCID: PMC4567590.

12TH INTERNATIONAL AMR PATHOLOGY SLIDE SEMINAR SYMPOSIUM IN ANATOMIC PATHOLOGY

Case – 4

Gynecologic and breast pathology

Contributed by: Masaharu Fukunaga

Clinical History

A 54-year-old, G1P1, female was admitted with a six-month history of abnormal uterine bleeding. She had no history of malignancy. Image analyses indicated an endometrial tumor in the fundus. Cervical and endometrial cytology showed “adenocarcinoma”(high grade serous or endometrioid carcinoma, grade 3, suggested）Endometrioid biopsy indicated a high grade endometrial carcinoma. A total abdominal hysterectomy, bilateral salpingo-oophorectomy and pelvic lymph nodes dissection was scheduled but declined by the patient and her family. She has not visited our hospital again so far.

Microscopic Findings

Microscopically, two components were identified. The first was endometrioid carcinoma, grade 2. characterized by glandular, papillary, and cribriform proliferations of cuboidal cells with round or oval nuclei with small nucleoli and moderate amount of cytoplasm. The second was predominant and composed of a poorly differentiated carcinoma. It showed solid sheet or trabecular arrangements without any obvious glandular differentiation. The tumor cells had enlarged round nuclei, prominent nucleoli and multivacuolated clear or eosinophilic cytoplasm. The interphase between the two components was abrupt. There was a prominent lymphoplasmacytic infiltration in the stroma.

Immunohistochemical findings: The endometrioid carcinoma, grade 2, component was positive for AE1/AE3, EMA, ER, PgR, PAX8, E cadherin, p16 (focally), p53 (wild type), and negative for vimentin, synaptophysin and chromogranin. The poorly differentiated carcinoma was positive for AE1/AE3, EMA, PAX8, E cadherin, p16 (focally), p53 (wild type) and negative for vimentin, ER, PgR and negative for vimentin, synaptophysin, chromogranin A. p40, CK5/6 and NapsinA.

Diagnosis

Endometrioid carcinoma, grade 3.

Comments

Differential diagnoses include serous carcinoma and neuroendocrine carcinoma and dedifferentiated carcinoma/undifferentiated carcinoma (1-4). Serous carcinoma is characterized by a papillary, slit - like glandular arrangements or solid proliferation and high grade cytological features, and aberrant p53 immunohistochemical expression. Neuroendocrine carcinoma is positive for neuroendocrine markers such as synaptophysin and chromogranin A. Dedifferentiated carcinoma is composed of an undifferentiated carcinoma and a differentiated component (typically of FIGO grade 1 or grade 2 endometrioid carcinoma). It shows a solid proliferation composed of small to intermediate sized cells arranged in sheet without any obvious glandular differentiation. It often

shows dyscohesive or rhabdoid features. It lacks expression of PAX8, ER, and ER but up to 20% of tumor cells may show focal staining with these markers. E cadherin labeling is absent or minimal. Distinguishing between grade 3 endometrioid carcinoma and dedifferentiated carcinoma/dedifferentiated carcinoma is of clinical importance. The later is more aggressive than the former. Dedifferentiated carcinoma/dedifferentiated carcinoma is highly aggressive, with recurrence or death from disease occurring in 55-95% of cases and required extended surgery (2, 4, 5). The presence of an undifferentiated carcinoma component, regardless of the percentage, can portend worse prognosis.

References

1. Tafel LJ, et al. Endometrial and ovarian carcinomas with undifferentiated components: clinically aggressive and frequently underrecognized neoplasms. Mod Pathol 2010, 23:781-9
2. Silva EG, et al. Association of low grade endometrioid carcinoma of the uterus and ovary with undifferentiated carcinoma: a new type of dedifferentiated carcinoma? Int J Gynecol Pathol 2006, 25:248-58.
3. Murali R. High grade endometrial carcinomas: morphologic and immunohistochemical features, diagnostic challenges and recommendations. In J Gynecol Pathol 2019, 38:40-63
4. Hoang.LN. Immunophenotypic features of dedifferentiated endometrial carcinoma: insights from BRG1/INI1-deificent tumors. Histopathol 2016, 69:560-9.
5. Coatham, M, et al. Concurrent ARIDIA and ARID18 inactivation in endometrial and ovarian dedifferentiated carcinomas Mod Pathol 2016, 29:1586-93.

12TH INTERNATIONAL AMR PATHOLOGY SLIDE SEMINAR SYMPOSIUM IN ANATOMIC PATHOLOGY

Case – 5

Gynecologic and breast pathology

Contributed by: Ricardo Lastra

Clinical History

A 48-year-old woman with 4 cm mass in the upper pole of the left kidney, 11 cm left adnexal simple cyst, and a 2.3 cm solid mass in the right ovary. The patient underwent partial nephrectomy for clinical-radiologic concern for clear cell renal cell carcinoma, and right salpingo-oophorectomy for the solid right ovarian mass. Frozen section evaluation of the right ovarian mass was diagnosed as metastatic renal cell carcinoma.

Pathological Findings

Gross findings: Gross evaluation of the right ovary demonstrated a 6 cm intact ovary with a smooth external surface. Cut sections revealed a vaguely circumscribed, yellow nodule measuring 1.2 cm, predominantly involving the ovarian hilum.

Microscopic examination: Section of the right ovarian lesion demonstrated a papillary and tubulocystic proliferation with slender and delicate fibrovascular cores, lined by cytologically bland cells with cuboidal nuclei with uniform chromatin, inconspicuous nucleoli, and no appreciable mitotic activity. Nuclear polarization to either the apical or basal portion of the cells was present, with areas of cytoplasmic clearing, focally imparting a secretory endometrium-like appearance.

Differential Diagnosis:

- Metastatic clear cell renal cell carcinoma
- Endometrioid carcinoma with secretory change
- Ovarian sex-cord stromal proliferation
- Clear cell papillary cystadenoma

Immunohistochemistry: The lesional cells were positive for a number of epithelial markers (including MOC-31 and BerEp4), as well as multiple mesothelial markers (including CK5/6, WT-1, calretinin, and D2-40). In addition, the cells were positive for CK7, PAX-8, EMA, and CA-IX, and were negative for CD10, RCC, AMACR, inhibin, Napsin-A, TTF-1, Melan-A, HMB45, ER, and PR. BAP-1 expression was retained.

Molecular findings: Next-generation sequencing revealed a pathogenic point mutation in the VHL gene (VHL c.343C>T, p.H115Y) with low allele frequency, suggesting a somatic rather than germline mutation.

Diagnosis

Clear cell papillary cystadenoma of the broad ligament/ovarian hilum.

Comments

Papillary cystadenoma of the epididymis and broad ligament is an uncommon benign neoplasm which may morphologically resemble metastatic clear cell renal cell carcinoma. Bilateral disease has been associated with germline mutations in the VHL gene, indicative of Von Hippel-Lindau disease, but unilateral lesions in non-syndromic patients have also been shown to harbor somatic alterations in VHL. Non-syndromic cases have been described in patients ranging in age from 20 to 65 years. Histologically, the lesions are composed of cystic, glandular, and papillary structures lined cuboidal to columnar nuclei with cytoplasmic clearing, minimal cytologic atypia, and absent (or rare) mitotic figures. Often, the neoplastic nuclei are located towards the apical portion of the cells, imparting a secretory endometrium-like appearance. Immunohistochemically, the tumors demonstrate positivity for high molecular weight cytokeratins, EMA, and CK7, and absence of RCC expression (which may be useful to distinguish these from metastatic clear cell renal cell carcinoma). In addition, they demonstrate an unusual and overlapping pattern of epithelial and mesothelial marker expression, with positivity of BerEp4 and MOC-31 in a significant number of cases, as well as expression of WT-1, calretinin, and HBME-1. CA-IX is often positive with a peculiar "cup-like" staining pattern, with membranous expression limited to the basolateral portion of the cells, without staining in the apical portion. Lastly, the tumor cells are often positive for PAX-8, and generally negative for AMACR (although cases with focal/weak expression have been reported).

Given the morphologic feature of cytoplasmic clearing, together with the expression of CK7, PAX-8, and CA-IX, metastatic clear cell renal cell carcinoma is a significant diagnostic pitfall. In general, however, the morphology of clear cell papillary cystadenoma is not entirely reminiscent of clear cell renal cell carcinoma, and the absence of expression of RCC and AMACR in these tumors is useful in aiding in this differential. A more difficult differential includes clear cell papillary renal cell carcinoma, which has a similar staining pattern as clear cell papillary cystadenoma, with positivity for PAX-8, but negative staining for both RCC and AMACR. Clinical and radiologic correlation are crucial in dealing with this differential.

Other potential differential diagnoses include endometrioid carcinoma with secretory change, although the absence of ER and PR expression, together with the presence of mesothelial marker expression would be highly unusual for endometrioid carcinomas. Lastly, mesothelial proliferations may fall into the differential given the diffuse expression of all mesothelial markers. However, the extent of positivity for epithelial markers seen in clear cell papillary cystadenoma would be unusual for a mesothelial proliferation, as would be the diffuse expression of PAX-8 (although it is now well known that a subset of both benign and malignant mesothelial proliferations can demonstrate variable degree of PAX-8 expression).

In conclusion, clear cell papillary cystadenoma is an uncommon benign neoplasm most often found in the epididymis, but also occasionally encountered in the broad ligament and ovarian hilum. While it is usually associated to von Hippel-Lindau disease, sporadic cases with somatic mutations in the VHL gene have also been described. The unusual staining pattern, which includes overlapping expression of both epithelial and mesothelial markers, can cause confusion if this entity is not considered in the histological differential diagnosis. Distinction of this lesion from variants of renal cell carcinoma and mesothelial lesions is important for patient management, and for potential referral to genetic counseling.

References

1. Sharma AE, Hamedani FS, Barroeta JE, *et al.* Clear cell papillary cystadenoma of the ovary masquerading as metastatic clear cell renal cell carcinoma: A case report and review of literature. *Int J Gynecol Pathol.* 2021 May 1;40(3):290-295.

2. Seok JY, Kang M, An J, *et al.* Papillary cystadenoma of the fallopian tube not associated with von Hippel-Lindau disease: a case report. *Korean J Pathol.* 2014 Oct;48(5):382-6.
3. Gilcrease MZ, Schmidt L, Zbar B, *et al.* Somatic von Hippel-Lindau mutation in clear cell papillary cystadenoma of the epididymis. *Hum Pathol.* 1995 Dec;26(12):1341-6.
4. Cox R, Vang R, Epstein JI. Papillary cystadenoma of the epididymis and broad ligament: morphologic and immunohistochemical overlap with clear cell papillary renal cell carcinoma. *Am J Surg Pathol.* 2014 May;38(5):713-8.

Case – 6

Gynecologic and breast pathology

Contributed by: Maria Pia Foschini

Clinical History

A 54-year-old woman presented a 2 cm. nodule located in the IUQ of the right breast, classified on ultrasound as U3. After a core needle biopsy diagnosed as B3, the nodule was removed. After the diagnosis of benign lesion, the patient did not receive any further therapy. Four years later she presented a second nodule located in the UOQ of the right breast, that was histologically diagnosed as fibroadenoma.

The present, presently followed-up in the local breast screening program, does not present any further breast lesion.

Microscopic Findings

On histology the nodule had well defined, pushing margins and was composed of a proliferation of spindle cells in a fibro-myxoid stroma. The cells had bland, elongated nuclei and eosinophilic cytoplasm.

No atypical mitotic figures or necrosis were seen. Some mammary ducts were present within the lesion, reminiscent of fibroadenoma. The neoplastic cells seemed in close contact with the myoepithelial cells surrounding these ducts.

On immunohistochemistry the neoplastic cells were strongly positive for markers of myoepithelial cell differentiation, as smooth muscle actin, calponin, p63, CK14. In addition, low molecular weight CK (CAM 5.2) was also positive. CD34 was negative. (Fig. 1).

Diagnosis

Benign myoepithelioma with fibroadenoma-like features / fibroadenoma with diffuse myoepithelial cell differentiation.

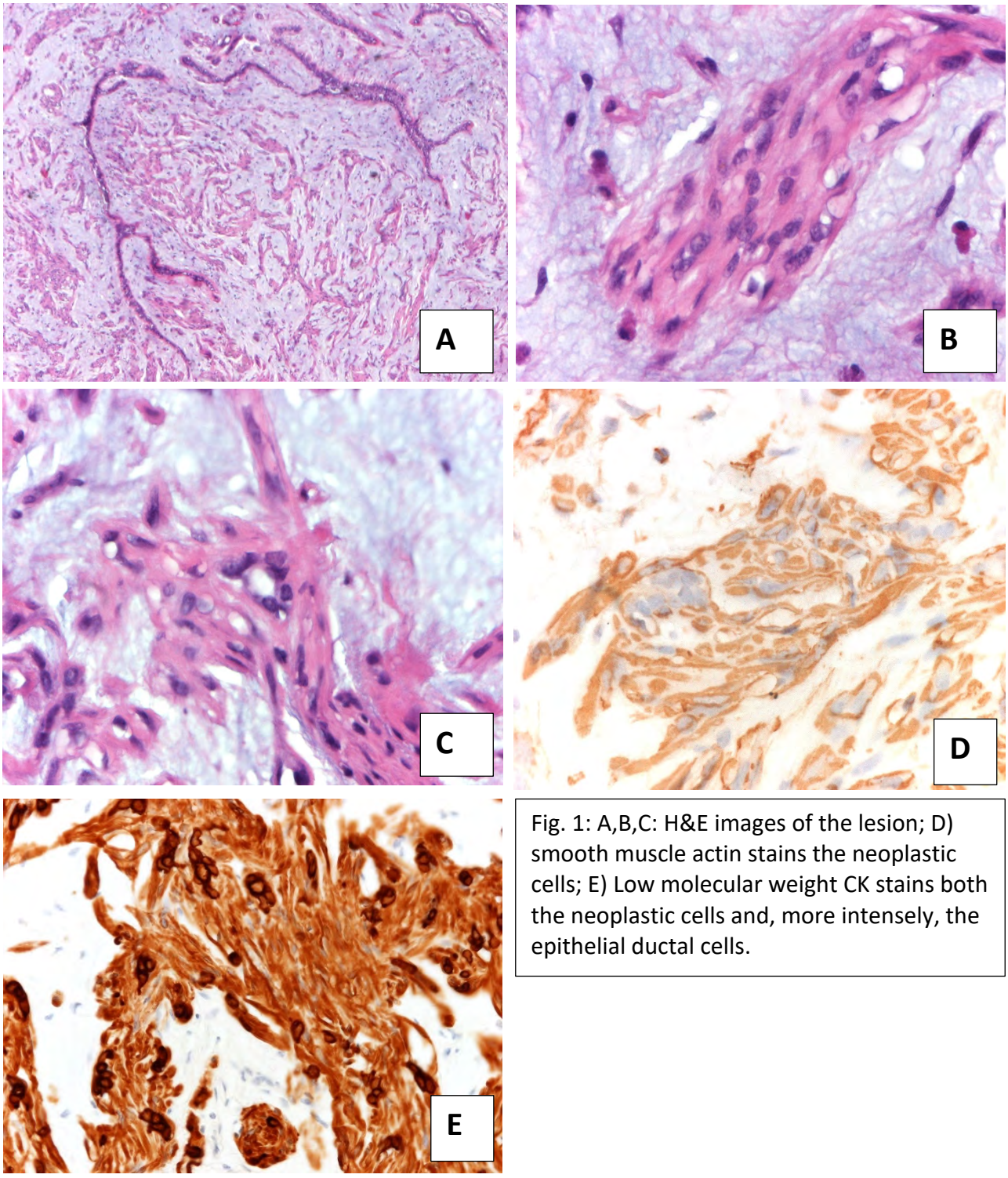

Fig. 1: A,B,C: H&E images of the lesion; D) smooth muscle actin stains the neoplastic cells; E) Low molecular weight CK stains both the neoplastic cells and, more intensely, the epithelial ductal cells.

Comments

Benign myoepithelioma (BM) is an exceedingly rare tumour, entirely composed of myoepithelial cells (review in references 1 and 2). BM is usually composed of cells with eosinophilic or clear cytoplasm showing, on immunohistochemistry or on ultrastructure, myoepithelial cell differentiation (1,2, 3). BM affect adult/elderly patients, presenting as breast nodule, more rarely as a cystic lesion. Prognosis is usually good, at least according to the rare papers reporting follow-up information. Nevertheless, in spite of apparently benign looking neoplastic cells, one case showed infiltrative pattern (4) and one case gave rise to metastasis (5). Differential diagnosis should be carried out with fibroadenoma with myoid stroma.

Bittesini et al. (6) described a fibroepithelial tumour, with myoid stromal cells containing actin rich intracytoplasmic globules. This diagnosis was excluded as the present case lacked the intracytoplasmic globules. Furthermore, rare cases of breast hamartoma with myoid features are on record (7,8).

In the present case, the positivity for high and low molecular weight cytokeratins, in addition to the positivity for smooth muscle actin and calponin, supports more myoepithelial rather than myoid differentiation. The presence of ducts within the lesion, can be interpreted as entrapped or part of the tumour.

The close continuity between the neoplastic cells and the myoepithelial cells surrounding the ducts indicate that the ducts are part of the tumour. Both morphological features and the 4-years long follow-up confirm that the lesion is benign.

References

1. Foschini MP, Nishimura R, Fabbri VP, Varga Z, Kaya H, Cserni G. Breast lesions with myoepithelial phenotype. Histopathology. 2023 Jan;82(1):53-69. doi: 10.1111/his.14826. PMID: 36482278.
2. Foschini MP, Morandi L, Asioli S, Giove G, Corradini AG, Eusebi V. The morphological spectrum of salivary gland type tumours of the breast. Pathology. 2017 Feb;49(2):215-227. doi: 10.1016/j.pathol.2016.10.011. Epub 2016 Dec 30. PMID: 28043647.
3. Enghardt MH, Hale JH. An epithelial and spindle cell breast tumour of myoepithelial origin. An immunohistochemical and ultrastructural study. Virchows Arch. A Pathol. Anat. Histopathol. 1989; 416; 177–184. 40.
4. Erlandson RA, Rosen PP. Infiltrating myoepithelioma of the breast. Am. J. Surg. Pathol. 1982; 6; 785–793. 39.
5. Jennens RR, Rosenthal MA, Gonzales M. Metastatic myoepithelioma of the breast. ANZ J. Surg. 2004; 74(12); 1135– 1137. 41.
6. Bittesini L, Dei Tos AP, Doglioni C, Della Libera D, Laurino L, Fletcher CD. Fibroepithelial tumor of the breast with digital fibroma-like inclusions in the stromal component. Case report with immunocytochemical and ultrastructural analysis. Am J Surg Pathol. 1994 Mar;18(3):296-301. doi: 10.1097/00000478-199403000-00010. PMID: 8116798.
7. Khoo JJ, Alwi RI, Abd-Rahman I. Myoid hamartoma of breast with chondroid metaplasia: a case report. Malays J Pathol. 2009 Jun;31(1):77-80. PMID: 19694319.
8. Aminpour N, Sogunro O, Towfighi P, Park BU, Boisvert M. Clinical management of myoid hamartomas of the breast: A case report and literature review. Heliyon. 2022 Nov 17;8(11):e11723. doi: 10.1016/j.heliyon.2022.e11723. PMID: 36439748; PMCID: PMC9691934.

12TH INTERNATIONAL AMR PATHOLOGY SLIDE SEMINAR SYMPOSIUM IN ANATOMIC PATHOLOGY

Case – 7

Gynecologic and breast pathology

Contributed by: Masaharu Fukunaga

Clinical History

A 25-year-old, G0P0, female was admitted because of abnormal uterine bleeding. A diagnosis of endometrial curettage in other hospital was carcinosarcoma and a total hysterectomy and chemotherapy were considered. The patient visited our hospital for asking a second opinion and a conservative treatment. On the review of the slide, a diagnosis of corded and hyalinized endometrioid carcinoma was rendered and hormonal (medroxyprogesterone acetate, MPA) therapy has been performed. She is well without recurrent four years after the therapy.

Microscopic Findings

Microscopically, the tumor was composed of two components. One was a conventional endometrioid carcinoma showing glandular and cribriform proliferation of cuboidal cells with round nuclei and moderate amount of cytoplasm with focal squamous differentiation. The other was a sex-cord-like component with hyalinization showing round, ovary or spindle cell proliferations in cord-like, small nest, trabecular, and fascicular arrangements and focal osteoid-like changes. These cells showed mild to moderate atypia and the mitotic activity was 1/10HPF. No necrosis was noted.

By immunohistochemistry, the sex cord-like component was positive for vimentin and p53 (wild type) and negative for AE1/AE3, ER, PgR, inhibin, calretinin, D2-40. CD10.

Diagnosis

Corded and hyalinized endometrioid carcinoma (CHEC) of the endometrium.

Comments

CHECs are usually low grade, low stage, and present at a young age and exhibit squamous differentiation at an increased frequency compared to typical endometrioid carcinoma (1-4).

Differential diagnoses include carcinosarcoma and uterine tumor resembling ovarian sex cord tumor (UTROSCT). Carcinosarcomas are characterized by a high-grade adenocarcinoma component and apparent sarcoma component. Heterologous elements in endometrioid carcinomas are histologically benign, whereas heterologous elements in carcinosarcomas are charlatanically highly malignant, and most often represented by rhabdomyosarcoma. UTROST is characterized by round or spindle cell proliferation in sex cord pattern without component of endometrial stroma nor endometrial epithelial tumor. It has a polyphenotypic immunohistochemical profile.

Unlike carcinosarcomas, which frequently harbor 53 mutations, CHECs usually exhibit wild-type p53 and nuclear beta-catenin expression, indicative of underlying CTNNB1 mutations. According to the TCGA (The Cancer Genome Atlas) subgroups of endometrial carcinoma, the majority of CHECs appear to fall into the copy number low (no specific molecular profile) subgroup (2). Molecularly,

sequence analysis showed mutations in the exon 3 of beta-catenin gene in the areas of sex cord-like formations (3)

Follow up research revealed that the prognosis of this variant was similar to the conventional endometrioid carcinoma.

References

1. Murray S et al. Endometrioid carcinomas of the uterine corpus with sex cord-like formation, hyalinization and other unusual morphologic features: a report of 31cases of a neoplasm that may be confused with carcinosarcoma and other uterine neoplasms. Am J Surg, 2005, 29:157-66
2. Safdar NS et al. Corded and hyalinized and spindle endometrioid endometrial carcinoma: a clinicopathologic and molecular analysis of 9 tumors based on the TCGA Classifier. Am J Surg Pathol. 2021, 45:1038-46
3. Wani Y, et al. Aberrant nuclear beta-catenin expression in the spindle or corded cells in so-called corded and hyalinized endometrioid carcinoma. Another critical role of the unique morphological features. Histol Histopathol.2009. 24:149-55.
4. Jia M. et al. Uterine lesions with sex cord-like architectures: a systematic review. Diagn Pathol 2019 PMID 31739799.

12TH INTERNATIONAL AMR PATHOLOGY SLIDE SEMINAR SYMPOSIUM IN ANATOMIC PATHOLOGY

Case – 8

Gynecologic and breast pathology

Contributed by: Anais Malpica

Clinical History

A 36-year-old female with a history of advanced stage ovarian tumor, status-post bilateral salpingo-oophorectomy, omentectomy and tumor debulking, adjuvant chemotherapy (4 cycles of BEP), and on maintenance treatment with Arimidex, was found to have progression of her residual abdomino-pelvic disease on a follow-up visit. At this time, she also reported abdominal pain and nausea. Of note, the initial diagnosis had been rendered 7 years earlier and although the patient had had some residual disease, this had remained stable and she was asymptomatic. Her last imaging studies showed nodules of variable size, the largest measuring several cm and located in the left upper quadrant. The patient underwent partial tumor debulking and resection of the transverse colon. Currently, she is on a temozolomide trial.

Pathological Findings

Gross Features

The largest mass was 8 cm in greatest dimension, white, firm and located in the adipose tissue adjacent to the distal transverse colon. The smallest nodule was 0.6 cm and located in the small bowel mesentery.

Microscopic Features

The tumor shows a large area with a proliferation of mostly polygonal cells and focally spindle cells with atypia arranged in sheets, nests, and trabeculae. The mitotic index is 41 mitoses/10 HPFs. Towards the periphery, there are perivascular pseudorosettes and ependymal rosettes with bland looking cells and rare mitotic figures. Necrosis and hemorrhage are seen.

Immunohistochemical Features

The tumor cells are positive for GFAP, S-100, WT-1, ER, and PR. They are also focally positive for CD99 and PAX-8 while negative for keratin, neurofilament, and SALL4.

MDACC MAPP (Mutation Analysis Precision Panel) Results

Different somatic mutations were detected in the recurrent and initial tumors as seen in the panels in page 2.

SNVs/Indels	CNVs	Fusions	TMB	MSI
NF2	*None*	*None*	1 mut/Mb	Stable (MSS)

Somatic Mutations (SNVs/Indels)

Gene	DNA	Protein	Location	VAF	Type
NF2	c.496_513del	p.E166_K171del	Exon 5	61%	Deletion - Deletion

SNVs/Indels	CNVs	Fusions	TMB	MSI
CTNNB1	*None*	*None*	1 mut/Mb	Stable (MSS)

*Somatic Mutations (SNVs/Indels)****

Gene	DNA	Protein	Location	VAF	Type
CTNNB1	c.133T>C	p.S45P	Exon 3	13%	SNV - Missense

Diagnosis

Recurrent anaplastic ependymoma, extra-axial type, of ovarian origin.

Comments

Extra-axial ependymoma is a rare tumor that can occur in different anatomical sites. The latter can be grouped as follows: pelvic (ovary, paraovarian tissue, broad ligament, uterosacral ligament, endometrium, fallopian tube, pelvis and peritoneum), extrapelvic (omentum, peritoneum, small bowel, liver, lung, posterior mediastinum, and cervical paraspinal region), and presacral region (presacral soft tissue or subcutaneous tissue of the sacrococcygeal region). Tumors occurring in pelvic and extrapelvic sites are seen only in women while tumors in the presacral region are more common in women than in men. Patients range in age from 13 years to 76 years (mean, 38 years). Tumors are usually unilateral, cystic/solid or solid, and range in size from 1 cm to 20 cm. Ovarian ependymomas can be associated with mature or immature teratomas.

Microscopically, extra-axial ependymomas are characterized by histological heterogeneity including solid, macrocystic, microcystic, papillary, cribriform, and trabecular patterns. Vascular pseudorosettes and ependymal rosettes are typical seen. Tumors can be low grade or anaplastic. Psammoma bodies can be seen and the presence of cartilage is uncommon. The degree of mitotic activity is variable. The differential diagnosis is wide and includes: serous tumors, including borderline tumors and low and high grade serous carcinomas, endometrioid tumors, including borderline tumors and carcinomas, FATWO, PNET, MMMT, struma ovarii, granulosa cell tumor and Sertoli-Leydig cell tumor.

Immunohistochemically, extra-axial ependymoma is positive for keratin AE1/AE3, CK7, CK18, keratin 34βE12, Cam 5.2, EMA, GFAP, ER, PR, WT-1, and PAX8. The expression of CD99 is less prevalent than in axial ependymomas. Tumors arising in the context of a teratoma may have an immunophenotype similar to axial ependymomas.

This tumor can present as disseminated disease or have recurrences/metastases to the peritoneum, regional or distant lymph nodes, lung and pleura. The clinical course is indolent or slow growing in most cases, even for anaplastic tumors. Recurrences may occur decades after the initial diagnosis and rare patients have died of disease.

The cornerstone of treatment is surgery. Adjuvant chemotherapy has been used and more recently endocrine therapy (Tamoxifen, Letrozole, GnRH analogue, and aromatase inhibitors) has been successfully used to control tumor growth.

Recently, a case with *CHEK2p.H371Y* germline mutation has been described. This finding could indicate a potential role for targeted therapy (poly ADP-ribose polymerase-1 inhibitors) to treat this disease.

References

1. Vazzano JL, Swanson BJ, Wakely PE. Primary Peritoneal Ependymoma: A case report and literature review. AJSP: Reviews & Reports (26) 6;311-314, 2021.
2. Stolnicu S, Furtado A, Sanches A, et al.. Ovarian ependymomas of extra-axial type or central immunophenotypes. Hum Pathol. 2011 Mar;42(3):403-8.
3. Idowu MO, Rosenblum MK, Wei XJ, et al. Ependymomas of the central nervous system and adult extra-axial ependymomas are morphologically and immunohistochemically distinct--a comparative study with assessment of ovarian carcinomas for expression of glial fibrillary acidic protein. Am J Surg Pathol. 2008 May;32(5):710-8.
4. Liang L, Olar A, Niu N, Jiang Y, Cheng W, Bian XW, Yang W, Zhang J, Yemelyanova A, Malpica A, Zhang Z, Fuller GN, Liu J. Primary Glial and Neuronal Tumors of the Ovary or Peritoneum: A Clinicopathologic Study of 11 Cases. Am J Surg Pathol. 2016 Jun;40(6):847-56.
5. Yin J, Yao M, Lu H, et al. Primary uterine broad ligament ependymoma with CHEK2 p.H371Y germline mutation: A CARE-compliant case report uterine broad ligament ependymoma. J Obstet Gynaecol Res. 2022 Jan;48(1):266-270.
6. Inukai R, Kawai T, Nishikawa R, et al. Ependymoma of the broad ligament mimicking an ovarian surface epithelial tumor. Radiol Case Rep. 2020 Nov 20;16(1):210-214.
7. Deval B, Rousset P, Bigenwald C, et al. Treatment of ovarian anaplastic ependymoma by an aromatase inhibitor. Obstet Gynecol. 2014 Feb;123(2 Pt 2 Suppl 2):488-491.
8. Zhou F, Song J, Mikolaenko I, et al. Pelvic Ependymoma With Clinical Response to GnRH Analog Therapy: A Case Report With an Overview of Primary Extraneural Ependymomas. Int J Gynecol Pathol. 2015 Sep;34(5):450-8.
9. Murdock T, Orr B, Allen S, et al. Central Nervous System-type Neuroepithelial Tumors and Tumor-like Proliferations Developing in the Gynecologic Tract and Pelvis: Clinicopathologic Analysis of 23 Cases. Am J Surg Pathol. 2018 Nov;42(11):1429-1444.
10. Gorski JW, Taylor JS, Zhang J, et al. Hormonal based treatment of ovarian anaplastic ependymoma with anastrozole. Gynecol Oncol Rep. 2017 Mar 14;20:93-96.

12TH INTERNATIONAL AMR PATHOLOGY SLIDE SEMINAR SYMPOSIUM IN ANATOMIC PATHOLOGY

Case – 9

Gynecologic and breast pathology

Contributed by: Ricardo Lastra

Clinical History

A 22-year-old woman with two prior pregnancies (one resulting in a first trimester abortion, and the second resulting in intrauterine fetal demise at 26 weeks gestation), presenting at 34 weeks 6 days gestation by ultrasound with decreased to absent fetal movements for the prior 8 hours. Ultrasound performed in the emergency department was consistent with intrauterine fetal demise. The pregnancy had been complicated by abnormal placental ultrasound findings, most notably an area concerning for a large chorangioma, and severe fetal growth restriction. Additional differential diagnosis from a radiologic perspective included a twin gestation with a partial hydatidiform mole component. The patient underwent induction of labor and vaginal delivery. Fetal autopsy was significant for a slightly small fetus for gestational age, without other overt gross or microscopic abnormalities.

Microscopic Findings

Gross findings: Gross evaluation of the received placental tissue demonstrated a 14.5 x 13.0 x 3.8 cm discoid placenta weighing 298 grams. The umbilical cord and fetal membranes were grossly unremarkable. Sectioning through the placental disc revealed multiple pale areas with erythematous center, measuring up to 1.9 cm in greatest dimension, and encompassing approximately 25% of the overall placental volume. Additionally, a 7.3 cm firm area with white discoloration and punctate vasculature was also identified.

Microscopic examination: Sections of the three-vessel umbilical cord and fetal membranes were unremarkable, demonstrating no significant inflammation. Section of the placenta disc demonstrated areas of relatively normal villous development, architecture, and overall morphology for this gestational age. However, other areas correlating with the grossly identified pale to white/firm areas demonstrated a distinctly different villous morphology, characterized by large villi with stromal hydropic change, increased stromal cellularity, focal stromal myxoid change, and prominent thick-walled stromal vessels. Mild peripheral scalloping was identified, but significant peripheral trophoblastic proliferation or trophoblastic pseudoinclusions were not present. Increased perivillous fibrin deposition was identified in the areas of abnormal villous morphology.

Differential Diagnoses:

- Twin pregnancy with complete hydatidiform mole component
- Twin pregnancy with partial hydatidiform mole component
- Non-molar chromosomal abnormality
- Placental mesenchymal dysplasia

Immunohistochemistry: p57 immunohistochemical stain demonstrated retained expression in the cytotrophoblast, with loss of expression in the villous stromal cells.

Diagnosis

Placental mesenchymal dysplasia.

Comments

Placental mesenchymal dysplasia is a rare placental disorder first described in 1991 by Moscoso *et al.* as a "placental vascular anomaly with diffuse mesenchymal stem villous hyperplasia". It is characterized by stem villous enlargement, cystic dilatation, and vesicle formation, often associated to placentomegaly and abnormal vascular structures (most commonly large thick-walled stem villous vessels). Since the abnormal chorionic villi are often admixed with more normal appearing villi, they are often misdiagnosed as twin pregnancies with a molar component coexisting with a normal fetus. However, other features classically associated to molar pregnancies, including peripheral trophoblastic hyperplasia and trophoblastic pseudoinclusions are generally absent.

The developing fetus is disproportionally female (82% in one study), and is at increased risk for Beckwith-Wiedemann syndrome and other genetic abnormalities. Additionally, they often demonstrate intrauterine growth restriction (33-50%) and are at increased risk for intrauterine fetal demise (13-43%) and preterm labor (33%). However, unlike molar pregnancies, a significant number of cases of placental mesenchymal dysplasia will feature a normal fetus without significant alterations, with a pregnancy extending into the third trimester.

From a genetic perspective, most cases of placental mesenchymal dysplasia demonstrate a normal female karyotype (46, XX). However, short tandem repeat analysis has shown a significant number of these to be either androgenetic/biparental mosaicism or androgenetic/biparental chimerism, with the presence of androgenetic cells resulting in abnormal imprinting. Beckwith-Wiedemann syndrome, an imprinting disorder with complex and diverse phenotypes (most commonly exomphalos, macroglossia, and gigantism) and an increased risk for the development of embryonal tumors, often also demonstrates androgenetic/biparental mosaicism (amongst other causative genetic alternations), and approximately 20% of cases of placental mesenchymal dysplasia will occur in the setting of Beckwith-Wiedemann syndrome.

In contrast to complete hydatidiform moles, which demonstrate loss of expression of p57 in both the cytotrophoblast and villous stromal cells (in the majority of the cases, not including mosaic CHM), placental mesenchymal dysplasia demonstrates loss of expression of p57 in the villous stromal cells (which contain the androgenetic genome) with retained expression in the cytotrophoblast (which contain the biparental genome). A subset of placental mesenchymal dysplasia cases, however, are composed entirely of biparental cells; in these cases, the abnormalities are thought to result from aberrant hypomethylation of various placenta-specific differentially methylated regions.

From a morphologic perspective, placental mesenchymal dysplasia can also be confused with partial hydatidiform moles (either as a single conception or as part of a twin conception). However, the characteristic peripheral scalloping, focal trophoblastic hyperplasia, and trophoblastic pseudoinclusions seen in partial hydatidiform moles are generally not seen in placental mesenchymal dysplasia, and partial hydatidiform moles demonstrate retained expression of p57 in both the cytotrophoblast and villous stromal cells. From a genetic perspective, partial hydatidiform moles are characterized by diandric triploidy, which is not seen in cases of placental mesenchymal dysplasia.

In conclusion, placental mesenchymal dysplasia is an uncommon placental disorder often demonstrating androgenetic/biparental mosaicism/chimerism, associated in a significant number of

cases to Beckwith-Wiedemann syndrome. While often confused with either partial or complete hydatidiform moles (generally as twin gestations with a concurrent “normal” gestation), placental mesenchymal dysplasia lacks some of the characteristic histologic features of molar villi, including trophoblastic proliferation and trophoblastic pseudoinclusions; the distinction form molar pregnancies is important for patient management and follow-up.

References

1. Moscoso G, Jauniaux E, Hustin J. Placental vascular anomaly with diffuse mesenchymal stem villous hyperplasia. A new clinico-pathological entity? *Pathol Res Pract*. Mar 1991;187(2-3):324-8.
2. Soejima H, Hara S, Ohba T, Higashimoto K. Placental Mesenchymal Dysplasia and Beckwith-Wiedemann Syndrome. *Cancers (Basel)*. Nov 12 2022;14(22).
3. Pawoo N, Heller DS. Placental mesenchymal dysplasia. *Arch Pathol Lab Med*. Sep 2014;138(9):1247-9.
4. Pham T, Steele J, Stayboldt C, Chan L, Benirschke K. Placental mesenchymal dysplasia is associated with high rates of intrauterine growth restriction and fetal demise: A report of 11 new cases and a review of the literature. *Am J Clin Pathol*. Jul 2006;126(1):67-78. yftp
5. Nayeri UA, West AB, Grossetta Nardini HK, Copel JA, Sfakianaki AK. Systematic review of sonographic findings of placental mesenchymal dysplasia and subsequent pregnancy outcome. *Ultrasound Obstet Gynecol*. Apr 2013;41(4):366-74.
6. Parveen Z, Tongson-Ignacio JE, Fraser CR, Killeen JL, Thompson KS. Placental mesenchymal dysplasia. *Arch Pathol Lab Med*. Jan 2007;131(1):131-7.

12TH INTERNATIONAL AMR PATHOLOGY SLIDE SEMINAR SYMPOSIUM IN ANATOMIC PATHOLOGY

Case – 8

Gynecologic and breast pathology

Contributed by: Anais Malpica

Clinical History

A 32-year-old female presented to the emergency room with acute abdomen. Imaging studies showed a showed a 15.0 cm right ovarian mass. Her serum CA125 was 500 U/mL. She underwent a TAHBSO and staging.

Pathological Findings

Gross Findings

The ovarian tumor was solid and cystic, tan/yellow with areas of hemorrhage and measured 15.5 cm. There were tumors in multiple specimens from the pelvis and omentum.

Microscopic Findings

The tumor shows a combination of architectural patterns: nested, trabecular and follicular. Most of the neoplastic cells show scanty cytoplasm. In areas, large cells with abundant eosinophilic cytoplasm are noted. Mitotic figures are numerous. The stroma is fibrous.

Immunohistochemical Findings

The tumor cells are positive for keratin 18 (patchy), keratin cocktail (patchy), MOC31 (patchy), EMA (patchy), WT-1 (strong), SALL4 (patchy), glypican 3 (patchy), synaptophysin (patchy), inhibin (focal), p16 (diffuse) while negative for keratin 7, panMel, chromogranin and SOX-10; p53 expression is wild type. The tumor cells show no expression of SMARCA4 (BRG1).

Diagnosis

Ovary, Small Cell Carcinoma, Hypercalcemic Type

Comments

Origin

Small cell carcinoma, hypercalcemic type, was initially mentioned by Dr. Robert Scully in a 1979 AFIP fascicle where he indicated that this tumor had an unknown origin. The first article on this neoplasm was published in 1982, and it showed that patients affected by this disease were young, with an average age of 22 years, usually with hypercalcemia and a poor outcome. At that time, it was felt that the tumor could represent either a poorly differentiated granulosa cell tumor or a primitive germ cell tumor. In 1987, Dr. Thomas Ulbright and his group reported a small series of 6 cases, were similar findings regarding age, hypercalcemia and poor outcome were noted. In addition, some similarities with yolk sac tumor were observed in the immunohistochemical and electron microscopic studies (ie, laminin and α-1 antitrypsine expression in 3 cases and the presence of intercellular basement membrane-like substance by EM). A comparison with a testicular tumor associated with

seminoma and teratoma was also made and it was suggested that this tumor had a germ cell origin. In 2013, Dr. Jolanta Kupryjanczyk, who was intrigued by the presence of glandular elements lined by mucinous epithelium in some examples of small cell carcinoma, hypercalcemic type, decided to examine exhaustively two tumors of this type. After obtaining multiple sections, she found an association with immature teratoma in both cases, one case also had a yolk sac tumor component. This prompted a comparison with other tumors and she found a similarity with atypical teratoid/rhabdoid tumor of the central nervous system and malignant rhabdoid tumor. Then, she stained the cases with SMARC4 IHC which showed the loss of this marker and that triggered PCR studies that showed a SMARCA4 mutation.

Confounding Clinical Features

This tumor affects mostly young women, however, it can be seen in infants and postmenopausal patients. Hypercalcemia is common, but 40% of the patients have normal calcium values. A rare case of dual *BRCA2* and *SMARCA4* mutations has been described as well as a patient with *Tp53* germline mutation. Some cases can present with manifestations secondary to disseminated disease (ie, a neck mass).

Confounding Histological Features

In up to 40% of the cases, there is a component of large cells, when they predominate it can be difficult to recognize this neoplasm, especially if there is a predominant myxoid background. The presence of the latter also can difficult the recognition of tumors composed of small cells exclusively. Numerous glandular elements lined by mucinous epithelium, spindle cells or the presence of another tumor also represent confounding factors.

Confounding Immunohistochemical Features

SMARCA4 (BRG1) is lost in >95% of the cases, but not in all cases. Occasionally, there is loss of SMARCB1 (INI-1), SMARCA2 (BRM), or dual loss of SMARCA4 and SMARCA2. This tumor is variably positive for keratin, MOC-31, claudin, EMA, calretinin, CD10, SALL4, CD56, synaptophysin, chromogranin, and inhibin (focally); p53 expression is wild type.

Genetic Considerations

Genetic testing for germline *SMARCA4* pathogenic mutations is recommended for all patients with the diagnosis of small cell carcinoma, hypercalcemic type, as up to 43% of tested patients were found to have a germline mutation for this gene. However, the penetrance of this mutation remains unclear.

References

1. Dickersin GR, Kline IW, Scully RE. Small cell carcinoma of the ovary with hypercalcemia: a report of eleven cases. Cancer. 1982 Jan 1;49(1):188-97.
2. Young RH, Oliva E, Scully RE. Small cell carcinoma of the ovary, hypercalcemic type. A clinicopathological analysis of 150 cases. Am J Surg Pathol. 1994 Nov;18(11):1102-16.
3. Kupryjańczyk J, Dansonka-Mieszkowska A, Moes-Sosnowska J, et al.. Ovarian small cell carcinoma of hypercalcemic type - evidence of germline origin and SMARCA4 gene inactivation. a pilot study. Pol J Pathol. 2013 Dec;64(4):238-46.
4. Ulbright TM, Roth LM, Stehman FB, et al. Poorly differentiated (small cell) carcinoma of the ovary in young women: evidence supporting a germ cell origin. Hum Pathol. 1987 Feb;18(2):175-84.
5. Atwi D, Quinton MR, Kiser RM, et al. Small Cell Carcinoma of the Ovary, Hypercalcemic Type, in a 12-Month-Old Girl. Pediatr Dev Pathol. 2021 Sep-Oct;24(5):493-497.
6. Simões MFE, da Costa AABA, Silva TN, et al. Case Report of Small Cell Carcinoma of the Ovary, Hypercalcemic Type (Ovarian Rhabdoid Tumor) with *SMARCB1* Mutation: A Literature Review of a Rare and Aggressive Condition. Curr Oncol. 2022 Jan 18;29(2):411-422.

7. Sanders BE, Wolsky R, Doughty ES, et al. Small cell carcinoma of the ovary hypercalcemic type (SCCOHT): A review and novel case with dual germline SMARCA4 and BRCA2 mutations. Gynecol Oncol Rep. 2022 Oct 6;44:101077.
8. Tischkowitz M, Huang S, Banerjee S, et al. Small-Cell Carcinoma of the Ovary, Hypercalcemic Type-Genetics, New Treatment Targets, and Current Management Guidelines. Clin Cancer Res. 2020 Aug 1;26(15):3908-3917.
9. Auguste A, Blanc-Durand F, Deloger M, et al. Small Cell Carcinoma of the Ovary, Hypercalcemic Type (SCCOHT) beyond *SMARCA4* Mutations: A Comprehensive Genomic Analysis. Cells. 2020 Jun 19;9(6):1496.
10. Kommoss FKF, Schmidt D, Kommoss F, et al. . Small-cell carcinoma of the ovary hypercalcaemic type shows a wild-type immunohistochemical staining pattern of p53. Histopathology. 2023 Apr 17. doi: 10.1111/his.14926. Epub ahead of print. PMID: 37067676.
11. Jelinic P, Schlappe BA, Conlon N, et al. Concomitant loss of SMARCA2 and SMARCA4 expression in small cell carcinoma of the ovary, hypercalcemic type. Mod Pathol. 2016 Jan;29(1):60-6
12. Karnezis AN, Wang Y, Ramos P, et al. Dual loss of the SWI/SNF complex ATPases SMARCA4/BRG1 and SMARCA2/BRM is highly sensitive and specific for small cell carcinoma of the ovary, hypercalcaemic type. J Pathol. 2016 Feb;238(3):389-400.
13. Witkowski L, Goudie C, Foulkes WD, et al. Small-Cell Carcinoma of the Ovary of Hypercalcemic Type (Malignant Rhabdoid Tumor of the Ovary): A Review with Recent Developments on Pathogenesis. Surg Pathol Clin. 2016 Jun;9(2):215-26.
14. Callegaro-Filho D, Gershenson DM, Nick AM, et al. Small cell carcinoma of the ovary-hypercalcemic type (SCCOHT): A review of 47 cases. Gynecol Oncol. 2016 Jan;140(1):53-7.
15. Agaimy A, Thiel F, Hartmann A, Fukunaga M. SMARCA4-deficient undifferentiated carcinoma of the ovary (small cell carcinoma, hypercalcemic type): clinicopathologic and immunohistochemical study of 3 cases. Ann Diagn Pathol. 2015 Oct;19(5):283-7.
16. Conlon N, Silva A, Guerra E, Jelinic P, et al. Loss of SMARCA4 Expression Is Both Sensitive and Specific for the Diagnosis of Small Cell Carcinoma of Ovary, Hypercalcemic Type. Am J Surg Pathol. 2016 Mar;40(3):395-403.
17. Tandon B, Hagemann IS, Maluf HM, et al. Association of Li-Fraumeni Syndrome With Small Cell Carcinoma of the Ovary, Hypercalcemic Type and Concurrent Pleomorphic Liposarcoma of the Cervix. Int J Gynecol Pathol. 2017 Nov;36(6):593-599.

12TH INTERNATIONAL AMR PATHOLOGY SLIDE SEMINAR SYMPOSIUM IN ANATOMIC PATHOLOGY

Case – 11

Gastrointestinal and Liver Pathology

Contributed by: Volkan Adsay

Clinical History

This 47-year-old man presented with epigastric pain and underwent abdominal ultrasound that disclosed a 6 cm mass in the liver, along with multiple smaller liver lesions. A needle core biopsy of the liver mass was performed (the scanned slide of this biopsy is available online), which was diagnosed as hepatocellular carcinoma in the outside institution. The patient was referred to our hospital to be evaluated for a liver transplantation. We re-reviewed the outside biopsy and came to different interpretation which led to more detailed analysis including MR and DOTA-PET scans which disclosed also a portal vein thrombosis and a pancreatic lesion. Based on the revised diagnosis, the patient underwent lutetium therapy followed by the post-neoadjuvant resection of the main liver mass, along with resection/ablation of smaller liver tumors, resection of portal vein thrombus and distal pancreatectomy (represented in the resection slides that were submitted for your review).

Pathological Findings

In the biopsy (available online), microscopically, this tumor shows a distinctly hepatoid morphology such that it was classified as hepatocellular carcinoma (HCC) in the biopsy in the outside institution. It has trabecules/nests seprated by sinusoidal-like vasculature. The cells have abundant amphophilic cytoplasm, round monotonous nuclei and single prominent nucleoli are often visible in close inspection. However, at the same time they have features that do not exactly fit to hepatocellular carcinomas. For example, a hepatocellular carcinoma of this pattern would be expected to have more small-cell change and/or more atypia. Also, while the nucleoli are visible, they are not exactly of the type that is seen in HCCs. The cytoplasmic granularity is also peculiar. In reviewing this biopsy, we thought the overall pattern was more in keeping with the oncocytic/hepatoid pancreatic neuroendocrine tumors (PanNET) that we have seen and thus performed immunohistochemistry for chromogranin and synaptophysin both of which showed diffuse strong positivity, while arginase, HepPar-1 and glypican-3 were negative. Trypsin was also negative. Based on this revised diagnosis, abdominal MR and PET-scans were performed and disclosed the portal vessel involvement and a mass in the pancreas head and patient underwent lutetium treatment. The pancreatic tumor has more infiltrative borders than ordinary PanNETs. There is portal vessel involvement. Both tumors show prominent hyalinization which is at least partly secondary to the lutetium treatment.

Diagnosis

- **(Pancreas /Portal): Well differentiated pancreatic neuroendocrine tumor (PanNET), grade 3 of 3 (Ki67, 25%), oncocytic type, highly-infiltrative, with post-therapy hyalinization; LN met: 2/23.**
- **(Liver): Metastatic PanNET, grade 3 of 3 (Ki67, 32%), oncocytic type.**

Comments

Oncocytic/ hepatoid ("metabolic cell type" PanNETs)

Oncocytic / hepatoid variants are increasingly being recognized as clinically significant subsets of PanNETs which are highly prone to be misdiagnosed. In fact, we have now seen several cases other than the one represented here which had been originally mis-interpreted as HCC or other cancers. Although not observed in this particular case hepatocellular differentiation in PanNETs often extends to the immunohistochemical level with arginase and HepPar positivity and even steatohepatitic changes. So far, such examples (with full-blown hepatocellular differentiation) that we have seen were the primary tumors in the pancreas and not in metastasis; but they are bound to happen also in the metastatic examples but we have just not seen (yet, or perhaps missed). Oncocytic PanNETs without overt hepatoid differentiation (by IHC or steatohepatitic changes) are a lot more common. Because the oncocytic and hepatoid cells also have close resemblance to other metabolically active cells such as luteal, adrenocortical, steroid-cell we collectively refer to these as "metabolic" cell type, for the lack of a better term. Rhabdoid examples as well as those that resemble solid-pseudopapillary neoplasms also appear to belong to this category. All of these also tend to form more broad bands and sheets than the typical nested/trabecular/festoon patterns of conventional PanNETs. It is becoming clear that this group, especially oncocytic, is more aggressive than the ordinary PanNETs, with higher proliferative rate, larger tumor, more infiltrative, more advanced and more prone to metastasis and aggressive behavior. This becomes more striking when they are compared to the variants that form the less aggressive group (i.e, mature/organoid/degenerative group including the symplastic/pleomorphic, paraganglioid and ductulo-insular PanNETs). Therefore, recognition of these variants like oncocytic and hepatoid may be important not only for accurate diagnosis but also for their potential for more aggressive behavior.

Grading of PanNETs (importance of giving the exact percentage of Ki67)

PanNETs are graded based on mitotic activity rate and Ki67 labeling index (G1: < 3%; G2: 3-20; and G3 > 20), whichever is higher. In our experience, in PanNETs, Ki67 count, if done correctly, always trumps the mitotic count and that is why it is the more important determinant. Counting with AI is very promising, and we are testing that in our research extensively, however, until the programs are perfected, we continue to use the manual count of printed captured image of the hot spot. It is becoming appreciated that it is important to provide the exact figure because current grading cut-offs appear to be too wide and perhaps imperfect in reflecting the biology of the tumor. In fact, for this reason, we are proposing to sub-grade grade 2 cases as 2a (3-10%) and 2b (10-20%) because G2 cases Ki67 > 10% are beginning to be managed differently in the oncology literature and we have also observed this group that we call 2b to have much higher metastatic rates than lesser grade lesions (7x more metastasis rate than G1). In other words, not surprisingly, a G2 that is 4 % is different than a G2 that is 18%, and G3 that is 21 % is different than a G3 that is 48%. That is why it is important to provide the nominal figure of Ki67 in the reports. In this case, the Ki index was 25 % in the primary but 32% in the metastasis.

NET-G3 vs PDNEC

Neuroendocrine neoplasms in GI and PB tracts are currently regarded in two very distinct categories based primarily (in fact, solely) on their morphology: 1) NE tumors (those that look like carcinoids, or islet cell tumors/carcinomas) versus 2) NE carcinomas which are fundamentally the counterpart of small cell or large cell neuroendocrine carcinomas of the lung. These 2 groups are highly

distinct in their behavior as well as molecular genetic background and clinicopathologic associations. NECs, which we report as “poorly diff NE carcinoma” in daily practice, are highly aggressive malignancies with median survival of about a year. Their Ki67 is typically far higher than 50%. They are often negative with DOTA PET but light up with FDG-PET. They require platinum-based therapy. They show molecular-genetic profile that establishes that they can be viewed as stem-cell/neuroendocrine version of adenocarcinomas: For example, they have SMAD4 and Rb loss, and p53 overexpression, which if present, supports the diagnosis. In contrast, NETs, which we diagnose as “well-differentiated neuroendocrine tumor”, have a much more protracted clinical course (5-yr, 70%, estimated 10-yr 40%), and in fact, curable when they are small and low grade. The NE neoplasms that arise from familial/genetic syndromes such as von Hippel-Lindau, MEN, Mahvash and tuberosclerosis are almost always WDNETs, not PDNECs.

In other words, there is a dichotomous classification of NENs (as WDNETs vs PDNECs) which is very valid and important. However, increasingly we are encountering unclassifiable/transitional cases. These are rare and seem to come in 2 flavors:

1) “Ambigious” group in which the morphology may be difficult to tell as WDNET or PDNEC, especially of large cell type, especially in small biopsies. The immunostains and molecular alterations of the respective entities may help determine which category this gray zone tumor belongs. Such “ambigious” cases also usually have Ki67 30-50%; if it is higher than 50-60%, it is probably a PDNEC.

2) Transformation cases, i.e., cases that clearly start life as a WDNET but in time start to look and act like a PDNEC, both by rapid growth/dissemination but also acquisition of molecular/genetic as well as PET characteristics (transforming from DOTA to FDG).

Oncocytic neuroendocrine neoplasms illustrated in this case are by definition WDNETs, however, they need to be distinguished from large cell PDNECs which can also show fair amount of cytoplasm. These oncocytic PanNETs often display aggressive features such as larger size, more infiltrative patterns, metastatic behavior as well as high Ki67, typically at least G2. We have seen several examples of this entity that transformed from G2 to G3 over the follow up period.

Infiltration pattern of PanNETs

In endocrine tumors such as thyroid, the degree of invasiveness in the advancing edge is one of the most important prognosticators to an extent that it by itself changes the diagnosis from adenoma to carcinoma to high grade carcinoma. Until recently, this parameter was not at all considered in prognostic evaluation of PanNETs. We have recently proposed a grading system for invasiveness, and found that highly infiltrative PanNETs are much more aggressive. Confirmatory studies are being published, consolidating the value of interpreting this parameter.

In the case illustrated here, the tumor was highly infiltrative both by gross examination as well as microscopic. In our experience, a oncocytic PanNETs are often highly infiltrative as in this example.

Therapy in PanNETs

The treatment of primary PanNETs is resection. In fact, even if there is limited number of metastasis, resection and ablation are attempted because these can achieve long term survival. As they are relatively slow growing tumors, PanNETs usually do not respond well to cytotoxic therapy, they typically remain stable but do not show significant shrinkage. In contrast, PDNECs are sensitive to platinum treatment and often show remarkable shrinkage but also rapid regrowth and dissemination shortly after. Whereas, PanNETs grow slowly with or without treatment. However,

those with more proliferative activity such as the oncocytic variants may benefit from the therapies and show remarkable shrinkage. Lutetium is one of the more specific and effective medications used for PanNETs. Therapy often leads to marked hyalinization as seen in this case.

References

1. Xue Y, Reid MD, Pehlivanoglu B, Obeng RC, Jiang H, Memis B, Lui SK, Sarmiento J, Kooby D, Maithel SK, El-Rayes B, Basturk O, Adsay V. Morphologic Variants of Pancreatic Neuroendocrine Tumors: Clinicopathologic Analysis and Prognostic Stratification. *Endocrine Pathology*. 31(3):239-253. 2020 Jun
2. Basturk O, Yang Z, Tang LH, Hruban RH, Adsay V, McCall CM, Krasinskas AM, Jang KT, Frankel WL, Balci S, Sigel C, Klimstra DS. The High- grade (WHO G3) Pancreatic Neuroendocrine Tumor Category Is Morphologically and Biologically Heterogenous and Includes Both Well Differentiated and Poorly Differentiated Neoplasms. *American Journal of Surgical Pathology*. 39(5):683-90, 2015.
3. Adsay NV, Klimstra DS, Klöppel G, Öberg K, Papotti M, Rindi G, Scarpa A; Neoplasms of the Neuroendocrine Pancreas. Pancreatic Neuroendocrine Carcinoma (Poorly Differentiated Neuroendocrine Neoplasm). In: WHO Classification of Tumours of Endocrine Organs, IARC, 4 th Edition; 2017.
4. Adsay NV, Perren A, Singhi AD. Tumours of the Pancreas. Pancreatic Neuroendocrine Carcinoma. Edited by International Agency for Research in Cancer and the WHO Classification of Tumours Editorial Board. In: WHO Classification of Tumours of the Digestive System, IARC, 5th Edition, 2019.
5. Basturk O, Tang L, Hruban RH, Adsay V, Yang Z, Krasinskas AM, Vakiani E, La Rosa S, Jang KT, Frankel WL, Liu X, Zhang L, Giordano TJ, Bellizzi AM, Chen JH, Shi C, Allen P, Reidy DL, Wolfgang CL, Saka B, Rezaee N, Deshpande V, Klimstra DS. Poorly differentiated neuroendocrine carcinomas of the pancreas: a clinicopathologic analysis of 44 cases. *American Journal of Surgical Pathology*. 38(4):437-47, 2014.
6. Basturk O, Tang L, Hruban RH, Adsay V, Yang Z, Krasinskas AM, Vakiani E, La Rosa S, Jang KT, Frankel WL, Liu X, Zhang L, Giordano TJ, Bellizzi AM, Chen JH, Shi C, Allen P, Reidy DL, Wolfgang CL, Saka B, Rezaee N, Deshpande V, Klimstra DS. Poorly differentiated neuroendocrine carcinomas of the pancreas: a clinicopathologic analysis of 44 cases. *American Journal of Surgical Pathology*. 38(4):437-47, 2014.
7. Taskin OC, Reid MD, Bagci P, Balci S, Armutlu A, Demirtas D, Pehlivanoglu B, Saka B, Memis B, Bozkurtlar E, Leblebici CB, Birceanu A, Xue Y, Erkan M, Kapran Y, Baygul A, Sokmensuer C, Scarpa A, Luchini C, Basturk O, Adsay V. Infiltration pattern predicts metastasis and progression better than the T-stage and grade in pancreatic neuroendocrine tumors: a proposal for a novel infiltration-based morphologic grading. *Mod Pathol. 2022 Jun;35(6):777-785*.
8. Reid MD, Bagci P, Ohike N, Saka B, Erbarut Seven I, Dursun N, Balci S, Gucer H, Jang KT, Tajiri T, Basturk O, Kong SY, Goodman M, Akkas G, Adsay V. Calculation of the Ki67 index in pancreatic neuroendocrine tumors: a comparative analysis of four counting methodologies. *Modern Pathology*. 28(5):686-94, 2015.
9. Asa SL, La Rosa S, Basturk O, Adsay V, Minnetti M, Grossman AB. Molecular Pathology of Well-Differentiated Gastro-entero-pancreatic Neuroendocrine Tumors. *Endocr Pathol*. 32(1):169-191. 2021 Jan 18.

12TH INTERNATIONAL AMR PATHOLOGY SLIDE SEMINAR SYMPOSIUM IN ANATOMIC PATHOLOGY

Case – 12

Gastrointestinal and Liver Pathology

Contributed by: Luca Di Tommaso

Clinical History

A 30-year-old woman with history of oral contraceptive performed US during a check-up for renal colic. US revealed two lesions in the liver, the major > 5 cm. Imaging (PET; CT; MNR) suggestive for hepatocellular adenoma. CEA, Ca19.9, NSE: negative. Pre-operative diagnosis: hepatocellular adenoma.

Pathological Findings

Liver resection 11x6x4 (IV and V segments); 5 cm, whitish lesion with pushing margins (see gross image). The lesion was constituted by epithelioid cells containing clear vacuoles embedded in a rich vascular network. Neoplastic cells showed the following immunoprofile: Hepar1+, LFABP-, vimentin-, HMB45-, MelanA-.

Diagnosis

Hepatocellular adenoma (HCA), with inactivation of Hepatocyte Nuclear Factor 1a (HNF1-α) or "steatotic" HCA.

Comments

Steatotic HCA represent about a third of HCAs and are characterized by biallelic inactivation (90% of the times somatic alterations) of the HNF1-α gene. They tend to occur in young women with a history of OC use, as well as MODY3 (Maturity onset diabetes of the young, type 3). In the clinical setting, the detection of liver adenomatosis (> 10 HCA in the liver) should prompt to start family screen for the HNF-1A germline mutation and MODY3 diabetes. HNF1-α regulates FABP1 gene which encodes for liver fatty acid binding protein (LFABP) which is therefore absent in H-HCA. Hepatocellular carcinoma has been reported to arise in the settings of sporadic HCAs as well in patients with MODY3, especially in female patients with multiple lesions without significant steatosis and presence of myxoid change, peliosis and sinusoidal dilatation.

References

1. Nault JC, et al. Nat Rev Gastroenterol Hepatol. 2022; 19:703-716
2. Bioulac-Sage P, et al. Histopathology. 2022; 80:878-897.

12TH INTERNATIONAL AMR PATHOLOGY SLIDE SEMINAR SYMPOSIUM IN ANATOMIC PATHOLOGY

Case – 13

Gastrointestinal and Liver Pathology

Contributed by: Volkan Adsay

Clinical History

This 70-year-old man with hypertension and diabetes presented with progressively increasing malaise in the last six months. Serologic tests were unremarkable other than increased C-reactive protein. When his symptoms and signs did not subside, he eventually underwent more detailed analysis involving abdominal MRI disclosing a complex cystic lesion with a differential diagnosis of "cystadenocarcinoma" or a hydatid cyst. The patient underwent left hepatectomy that revealed a 12x9x6 cm relatively demarcated partially cystic and partially solid mass. The tumor also displayed intraductal growth.

Pathological Findings

This tumor is characterized by a multilocular cystic lesion with many of the loculi filled with beige tan material (please see the two gross photos). In careful gross inspection, the intraductal nature of the cysts can be appreciated. The tan nodules filling the cysts correspond to florid papillary proliferation. Architecturally, the papillae are highly complex, arborizing. They are lined by pseudostratified epithelium of 1-5 cell layers. Intraepithelial lumina formation is prominent. These are microcystic spaces of 1-3 cell size, punctuating the epithelium without obvious polarization of cells around them. This creates cribriform appearance. Some contain mucin. Cytologically, the cells are cuboidal, and have round nuclei with prominent, eccentric nucleoli. The cytoplasm is abundant, acidophilic and finely granular. Despite the monotony of the cells and their low nucleocytoplasmic ratio (due to the abundance of cytoplasm), architectural complexity and cytologic features are quite atypical. The cysts are lined by the same type of epithelium.

Diagnosis

- **Intraductal oncocytic papillary neoplasm of the bile ducts with extensive high-grade dysplasia/CIS, indefinite for invasion.**
- **Not: Lesion submitted entirely but no definitive invasion is identified.**

Comments

Intraductal oncocytic papillary neoplasm (IOPN) is an entity that we had described originally in the pancreas in 1996. Later on, it also began to be appreciated in the biliary tract and the liver. However, most of the data on these tumors is based on their more common pancreatic counterpart. In 2000's IOPN was regarded as the oncocytic "variant" of IPNBs (intraductal papillary neoplasms of the bile ducts), or in the pancreas, of intraductal papillary mucinous neoplasms). However, as more experience accumulated, its distinctive characteristics began to be appreciated, and in WHO 2019 it was recognized as a separate entity with a CPT code of 8455/2.

Overall, as a member of the generic “intraductal neoplasia” category of the pancreatobiliary tract, IOPNs share several characteristics with the other tumors in the group (namely, pancreatic intraductal papillary mucinous neoplasms, biliary intraductal papillary neoplasms, pancreatic/biliary intraductal tubulopapillary neoplasms, intra-ampullary papillary tubular neoplasms, and intracholecystic neoplasms). In essence these are all “adenoma-carcinoma sequence” entities, aka tumoral intraepithelial neoplasms. However, IOPNs have some distinctive features among this group. First, although they are designated “intraductal” they typically present as complex multilocular cystic neoplasms that are deceptively aggressive- and infiltrative-appearing, and they radiologically get diagnosed as “cystadencarcinoma”. Their intraductal nature is often not clearly evident. More importantly, despite being highly complex and aggressive-appearing, they in fact seldom have conventional invasive carcinoma. And perhaps most important is the fact that even when they are invasive they have a very protracted clinical course, with most cases cured with complete resection. This is in stark contradiction with other complex intraductal neoplasia which exhibit invasive carcinoma in more than 2/3 of the cases, and more than 30-60 % of the patients die at 5 years. Whereas, a majority of IOPNs live for even 10 years. In addition to all these distinctive clinicopathologic characteristics, IOPNs were also found to have a fairly specific molecular alteration, namely DNAJB1-PRKACA fusion, which is an unusual alteration seen in fibrolamellar HCCs but not in other intraductal or biliary neoplasia of any kind. This finding consolidated IOPNs nature as a distinct tumor category.

For the diagnosis of biliary/hepatic IOPN, the recognition of its morphologic repertoire is the key.

As mentioned previously, grossly they form multilocular cystic-solid masses and their intraductal nature may not be readily evident. The most characteristic feature of IOPNs, even beyond the oncocytic nature of the cells is its distinctive arborizing papillary architecture in which the papillae are very exuberant and highly complex and delicately branching. The distribution of cells lining the papilla is also highly distinctive. The cells are round and fairly-uniform, which is striking considering the complexity of the lesion and the overall atypical appearance. They form 1-5 cells without a specific layering. The epithelium is often punctuated by multicell size vacuoles, some of which may contain mucin. The cells have abundant granular cytoplasm which is more commonly acidophilic and granular creating a very oncocytic appearance; however, it can be paler and mucin-like in some cases like this particular example. Invariably, the nuclei are round and exhibit single prominent and eccentrically located nucleoli. The lining of the cysts is also similar in nature, although some ducts with secondary dilatation may have more gastric like or endocervical-like epithelium. Granular debris can be seen in the cyst contents. Immunohistochemically, they are keratin positive, often express MUC6, and typically lack CDX2 and MUC2. Heppar1 (hepatocellular marker) can show some positivity, and some cases pick up acinar markers. IHC is generally not needed for the diagnosis.

In small biopsies, due to the cellularity, complexity and cytology, biliary IOPNs are typically misdiagnosed as “ordinary cholangiocarcinoma”. Careful attention to the monotonous cytology (round nuclei with single prominent nucleoli; acidophilic nature of the cytoplasm) and the formation of papillary units should help recognize and distinguish them from cholangiocarcinomas. This distinction is of utmost significance because IOPNs are curable by complete resection while cholangiocarcinomas are aggressive and typically rapidly mortal. Additionally, IOPNs may not require chemotherapy unless overtly invasive, and in fact, being slow-growing tumors they may not benefit from chemotherapy.

The same cytologic features are also helpful in distinguishing IOPNs from other intraductal neoplasia. The main intraductal neoplasm of the bile ducts, IPNBs, are essentially biliary counterparts of IPMNs. A significant proportion of IPNBs look like colonic villous or tubulovillous adenomas with intestinal cytology, showing pseudostratified columnar cells with cigar shaped nuclei. They show

expression of intestinal markers CDX2/MUC2. Thus, both morphologically and immunophenotypically these intestinal IPNBs are clearly distinct from IOPNs. Some IPNBs have more gastric type mucin, and may resemble pyloric gland adenomas. More papillary examples of gastric-type IPNBs have columnar cells with abundant intracytoplasmic pale mucin of the type seen in gastric mucosa. In the less complex areas these may overlap with IOPNs but the overall tumor with the complex papillary configuration is not a feature of gastric IPNBs. The variant of IPNB that IOPNs overlap the most with are the pancreatobiliary type because the nuclei are round and nucleoli are prominent. However, instead of the arborizing and delicate papillary configuration and monotonous (neat and clean) appearance of IOPNs, these PB IPNBs show marked atypia, pleomorphism and disorganization. Being mucin-poor and with round nuclei, ITPNs (intraductal tubulo-papillary neoplasms) may resemble IOPNs in cytologic preparations; they are also both MUC6 positive; however, the architectural features of these two entities differ greatly, with ITPNs showing a distinct tubular architecture, while the delicate arborizing papillae of IOPN are probably its most pathognomonic feature.

By default, due to the complexity of the papillae as well as their cytologic atypia, all IOPNs, by convention, qualify as HGD/CIS (high grade dysplasia / carcinoma in-situ). Most IOPNs look alike in terms of their complexity and as to what constitutes HGD/CIS.

IOPNs grow extensively into the feeding branch ducts, and this retrograde pagetoid spread, combined with the background atrophy (that often accompany the tumor) lead to multifocal foci of pseudo-invasion. With the exuberant complexity of these lesions and the difficulty in distinguishing pseudo-invasion from a true invasion, pathologists often diagnose these tumors as “micro-invasive”. The reported rate of invasion may in fact be lower in reality if only the cases with overt invasion are considered. This may be one of the reasons why even cases reported as “invasive” are often cured with complete resection

Overall, clinical behavior of IOPNs is very good, and in fact, almost-excellent, with 10 year survival percentage in the 90’s.

References

1. Adsay NV, Adair CF, Heffess CS, et al.: Intraductal oncocytic papillary neoplasms of the pancreas. *Am J Surg Pathol* 1996, 20:980-94.
2. Rouzbahman M, Serra S, Adsay NV, Bejarano PA, Nakanuma Y, Chetty R. Oncocytic papillary neoplasms of the biliary tract: a clinicopathological, mucin core and Wnt pathway protein analysis of four cases. *Pathology*. 2007 Aug;39(4):413-8.
3. Basturk O, Tan M, Bhanot U, Allen P, Adsay V, Scott SN, Shah R, Berger MF, Askan G, Dikoglu E, Jobanputra V, Wrzeszczynski KO, Sigel C, Iacobuzio-Donahue C, Klimstra DS. The oncocytic subtype is genetically distinct from other pancreatic intraductal papillary mucinous neoplasm subtypes. Mod Pathol. 2016 Sep;29(9):1058-69. doi: 10.1038/modpathol.2016.98. Epub 2016 Jun 10. PMID: 27282351
4. Wang T, Askan G, Adsay V, Allen P, Jarnagin WR, Memis B, Sigel C, Seven IE, Klimstra DS, Basturk O. Intraductal Oncocytic Papillary Neoplasms: Clinical-Pathologic Characterization of 24 Cases, With An Emphasis on Associated Invasive Carcinomas. Am J Surg Pathol. 2019 May;43(5):656-661.
5. Wang T, Askan G, Ozcan K, Rana S, Zehir A, Bhanot UK, Yantiss RK, Rao DS, Wahl SJ, Bagci P, Balci S, Balachandran V, Jarnagin WR, Adsay NV, Klimstra DS, Basturk O. Tumoral Intraductal Neoplasms of the Bile Ducts Comprise Morphologically and Genetically Distinct Entities. Arch Pathol Lab Med. 2023 Feb 23
6. Pea A, Paolino G, Martelli F, Bariani E, Piccoli P, Sereni E, Salvia R, Lawlor RT, Cheng L, Chang D, Scarpa A, Luchini C. Characterization and digital spatial deconvolution of the immune microenvironment of intraductal oncocytic papillary neoplasms (IOPN) of the pancreas. Virchows Arch. 2023 Apr 22.

7. Reid MD, Stallworth CR, Lewis MM, Akkas G, Memis B, Basturk O, Adsay V. Cytopathologic diagnosis of oncocytic type intraductal papillary mucinous neoplasm: Criteria and clinical implications of accurate diagnosis. Cancer Cytopathol. 2016 Feb;124(2):122-34.
8. Armutlu A, Quigley B, Choi H, Basturk O, Akkas G, Pehlivanoglu B, Memis B, Jang KT, Erkan M, Erkan B, Balci S, Saka B, Bagci P, Farris AB, Kooby DA, Martin D, Kalb B, Maithel SK, Sarmiento J, Reid MD, Adsay NV. Hepatic Cysts: Reappraisal of the Classification, Terminology, Differential Diagnosis, and Clinicopathologic Characteristics in 258 Cases. *Am J Surg Pathol*. 2022 Sep 1;46(9):1219-1233.
9. Wang T, Askan G, Ozcan K, Rana S, Zehir A, Bhanot UK, Yantiss RK, Rao DS, Wahl SJ, Bagci P, Balci S, Balachandran V, Jarnagin WR, Adsay NV, Klimstra DS, Basturk O. Tumoral Intraductal Neoplasms of the Bile Ducts Comprise Morphologically and Genetically Distinct Entities. Arch Pathol Lab Med. 2023 Feb 23.
10. Pehlivanoglu B, Adsay V. Intraductal tubulopapillary neoplasms of the bile ducts: identity, clinicopathologic characteristics, and differential diagnosis of a distinct entity among intraductal tumors. Hum Pathol. 2023 Feb

12TH INTERNATIONAL AMR PATHOLOGY SLIDE SEMINAR SYMPOSIUM IN ANATOMIC PATHOLOGY

Case – 14

Gastrointestinal and Liver Pathology

Contributed by: Abbas Agaimy

Clinical History

A 53-year-old man without other relevant previous clinical history presented with new-onset symptoms and clinical signs of Cushing disease. Biochemical investigations revealed highly elevated serum cortisol and ACTH, but CRH was very low. With a suspicion of probable ACTH-producing pituitary adenoma, imaging studies were performed but failed to show any abnormalities in the Sella turcica or the surrounding organs, so that genuine or ectopic pituitary adenoma could be ruled out. An abdominal and thorax CT was performed which revealed no intrathoracic lesions. The adrenal glands appeared diffusely enlarged without focal mass-forming lesions. However, the pancreas showed a large contrast-enhancing mass occupying most of the head and body, measuring 8 cm in maximum diameter. Coe needle biopsies revealed differentiated neuroendocrine neoplasm with Ki67 index >20%. Immunohistochemistry confirmed expression of ACTH in the neoplastic cells as the origin of the ACTH. Total pancreatectomy was performed followed by transient normalization of his Cushing, but liver metastases appeared soon with re-elevated ACTH levels. Bilateral adrenalectomy was performed as a palliative measure to alleviate his severe uncontrollable Cushing symptoms. The patient was then put on palliative systemic chemotherapy.

Pathological and Molecular Findings

Macroscopic features

The pancreatectomy specimen showed a large multinodular tan-yellow soft mass involving most of the pancreatic head and body and extending into the peripancreatic tissue with multiple involved peripancreatic lymph nodes.

Histological and immunohistochemical findings

Histological examination showed a cellular neoplasm composed of uniform neuroendocrine-type cells with moderate rim of eosinophilic cytoplasm and fine granular pepper-salt chromatin pattern disposed into organoid nests and larger confluent aggregates with multiple foci of comedo-type necrosis. Mitotic activity was brisk (>10 inn 10 hpf). Immunohistochemistry (IHC) revealed consistent expression of pankeratin, synaptophysin, chromogranin A, and SSTR2A (3+), but not ISL1, TTF1, CDX2 or CK20. TP53 and Rb1 showed wildtype expression pattern. Strong cytoplasmic expression of ACTH was seen in most of the tumor cells. Ki67 labeled variably <20% - 55% of the neoplastic cells. BCOR IHC showed weak nuclear staining.

Molecular findings

Targeted RNA sequencing (TruSight Panel, Illumina) revealed an *EWSR1::BEND2* fusion. The t(X;22)(p22;q12) fusion breakpoints mapped to exon 10; 3'-end of *EWSR1* (chr22:29688158) fused to exon 2; 5'-end of *BEND2* (chrX:18234853). The *EWSR1* rearrangement was confirmed using a *EWSR1*

split apart FISH probe. No pathogenic mutations in *DAXX, ATRX, MEN1, TSC1/2 or BCOR* were detected using the TSO500 DNA Panel.

Diagnosis

ACTH-producing pancreatic neuroendocrine neoplasm (NET, grade 3) associated with ectopic Cushing with a novel *EWSR1::BEND2* gene fusion.

Comments

Ectopic Cushing syndrome is a diagnostically and therapeutically challenging rare clinical disorder resulting from excessive adrenocorticotrophic hormone (ACTH) secreted by neoplasms of non-pituitary origin. These ACTH-producing tumors are generally divided into two main categories: highly aggressive poorly differentiated carcinomas (mostly small cell lung cancer), and well differentiated neuroendocrine tumors (NET) of diverse organs. Among the latter, bronchopulmonary carcinoids, gastroenteropancreatic NETs, pheochromocytoma/ paraganglioma, and much less frequently, thymic NET, medullary thyroid carcinoma, NET of unknown origin, and rare anecdotal sites have been reported. Rarely, non-neuroendocrine neoplasms may be associated with ectopic Cushing syndrome that resolves after tumor resection.

Pancreatic ACTH-producing neuroendocrine neoplasms (NENs) are rare with <150 cases reported to date, mostly as single case reports or rare case series. They are generally more aggressive with an overall 5-year-survival of 35%, compared to 72% - 97% for most other hormone-secreting NETs. Their histology is not significantly different from their conventional counterparts, but they tend to display more eosinophilic cytoplasm, aggressive histological features (higher mitotic activity, necrosis, lymphovascular invasion and locally invasive growth). They occur predominantly I females (2/3) of cases) at a mean age of 42 years (compared to a mean age of 59 years for pancreatic NETs in general).

The pathogenetic mechanisms underlying the ectopic ACTH production by certain NENs and their genotypes remained obscure. Several theories have been postulated to explain the ectopic hormone production, but none could be proven. Based on the fusion findings in this index case presented herein, we recently have examined 21 ACTH-producing NENs from pancreatic, pulmonary, thymic and renal origins to test the hypothesis that the *EWSR1::BEND2* or other alternate gene fusions might be enriched among these rare tumors. All four successfully tested pancreatic tumors revealed a gene fusion (2 had a *EWSR1::BEND2* fusion and 1 case each had a *KMT2A::BCOR* and a *TFG::ADGRG7* fusion), while none of the non-pancreatic cases did.

The frequency of the EWSR1::BEND2 fusion among unselected pancreatic NENs is <2% (Scarpa et al). In retrospect, one of the two tumors with this fusion that were included in the Scarpa et al study turned out to be associated with ectopic Cushing (personal communication with Dr. Scarpa), so that overall, 3 of the 4 pancreatic tumors with this fusion were ACTH-producing (75%). This is in sharp contract with the very low overall prevalence of the fusion in pancreatic NETs (<2%), suggesting close association between the fusion and the ectopic ACTH secretion. The observation that, these fusions are likely driver events in these tumors as they proved to be mutually exclusive with *ATRX, DAXX* and *MEN1* mutations (as the most frequently mutated genes in NETs) in all four fusion-positive cases, suggest the ACTH-producing NENs are distinct subset of pancreatic NETs and does not represent a mere coincidence of ACTH production.

The association between gene fusions and paraneoplastic phenomena has been well documented in mesenchymal neoplasms: *STAT6:NAB2* (hypoglycemia in 5% of solitary fibrous tumors), *ETV6::NTRK3* (neonatal hypercalcemia in infantile fibrosarcoma/ congenital mesoblastic nephroma), and *EWSR1::CREB1* (hyper-Interleukin-6 in angiomatoid fibrous histiocytoma). In

angiomatoid fibrous histiocytoma, the presence of a CREB-binding site in the IL-6 promotor region has been proposed to explain the fusion-induced IL-6 overexpression observed in this rare tumor type.

We postulate that, molecular/ structural homology between parts of the *EWSR1::BEND2* fusion transcript and the promoter of POMC or other pre-ACTH precursors might be responsible for the overexpression of the ACTH precursors in these rare pancreatic tumors, but this remains currently speculative and merits functional verification in future studies.

Figure 1

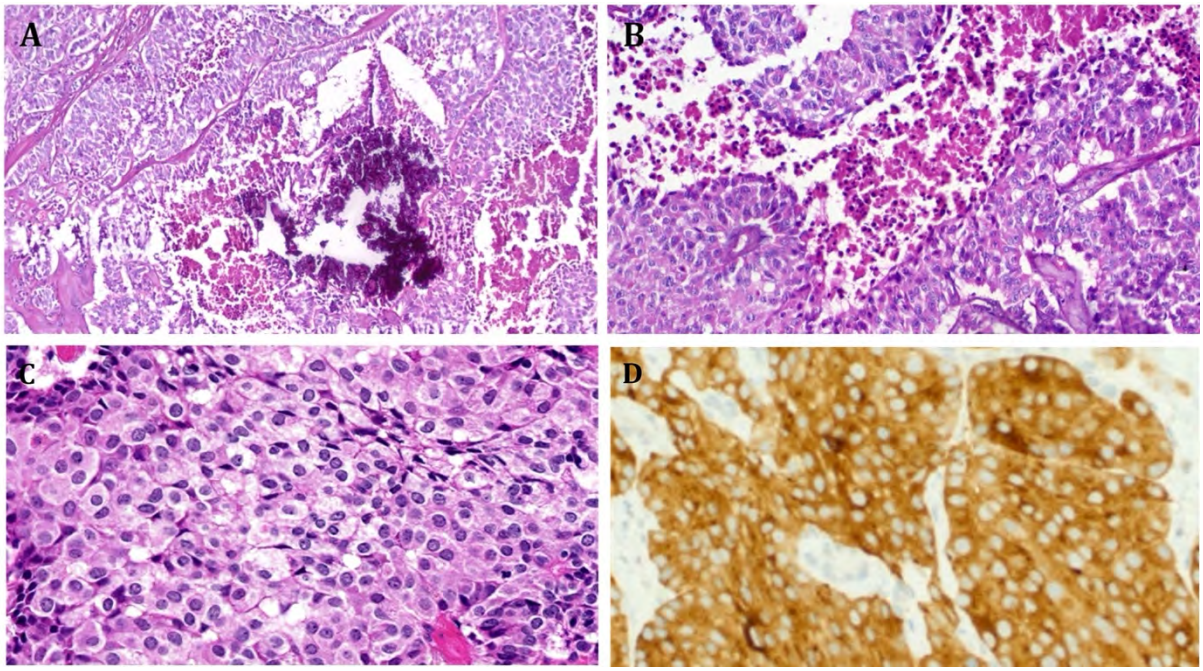

A, B, C: pancreatic ACTH-secreting neuroendocrine neoplasm shows features of NETG3 with extensive foci of necrosis and organoid arrangement of cells and moderate cytoplasmic eosinophilia. **D**: Almost all the tumor cells expressed cytoplasmic ACTH.

References

1. Agaimy A. Paraneoplastic disorders associated with miscellaneous neoplasms with focus on selected soft tissue and Undifferentiated/ rhabdoid malignancies. Semin Diagn Pathol 2019;36: 269-278.
2. Agaimy A, Kasajima A, Stoehr R, Haller F, Schubart C, Pfarr N, von Werder A, Pavel ME, Sessa F, Uccella S, La Rosa S, Klöppel G. Gene Fusions Are Frequent in ACTH-secreting Neuroendocrine Neoplasms of The Pancreas, But Not in Their Non-pancreatic Counterparts. Virchows Arch 2023;482: 507-516.
3. Akiyama M, Yamaoka M, Mikami-Terao Y, Yokoi K, Inoue T, Hiramatsu T, Ashizuka S, Yoshizawa J, Katagi H, Ikegami M, Ida H, Nakazawa A, Okita H, Matsumoto K. Paraneoplastic Syndrome of Angiomatoid Fibrous Histiocytoma May Be Caused by EWSR1-CREB1 Fusion-induced Excessive Interleukin-6 Production. J Pediatr Hematol Oncol 2015;37:554-9.
4. Coates PJ, Doniach I, Howlett TA, Rees LH, Besser GM. Immunocytochemical study of 18 tumours causing ectopic Cushing's syndrome. J Clin Pathol 1986;39: 955-60.
5. Guilmette JM, Nosé V. Neoplasms of the Neuroendocrine Pancreas: An Update in the Classification, Definition, and Molecular Genetic Advances. Adv Anat Pathol 2019;26:13-30.

6. Isidori AM, Kaltsas GA, Pozza C, Frajese V, Newell-Price J, Reznek RH, Jenkins PJ, Monson JP, Grossman AB, Besser GM. The ectopic adrenocorticotropin syndrome: clinical features, diagnosis, management, and long-term follow-up. J Clin Endocrinol Metab 2006;91: 371-7.
7. Lucas CG, Gupta R, Wu J, Shah K, Ravindranathan A, Barreto J, Gener M, Ginn KF, Prall OWJ, Xu H, Kee D, Ko HS, Yaqoob N, Zia N, Florez A, Cha S, Perry A, Clarke JL, Chang SM, Berger MS, Solomon DA. EWSR1-BEND2 fusion defines an epigenetically distinct subtype of astroblastoma. Acta Neuropathol 2022;143: 109-113.
8. Mao W, Xu J, Lu H, Wang Y, Zhang L, Chen M. A rare case report of renal Ewing sarcoma/primitive neuroectodermal tumor with ACTH production. BMC Urol. 2022;22:103.
9. Maragliano R, Vanoli A, Albarello L, Milione M, Basturk O, Klimstra DS, Wachtel A, Uccella S, Vicari E, Milesi M, Davì MV, Scarpa A, Sessa F, Capella C, La Rosa S. ACTH-secreting pancreatic neoplasms associated with Cushing syndrome: clinicopathologic study of 11 cases and review of the literature. Am J Surg Pathol 2015;39: 374-82.
10. Scarpa A, Chang DK, Nones K, et al. Whole-genome landscape of pancreatic neuroendocrine tumours. Nature 2017;543: 65-71.
11. Shimizu N, Hasumi M, Hamano T, Iijima M, Yoshioka T, Yamazaki Y, Sasano H. Renal primitive neuroectodermal tumor with elevated plasma adrenocorticotropic hormone levels: A case report. IJU Case Rep. 2019;2:128-131.
12. Volante M, Mete O, Pelosi G, Roden AC, Speel EJM, Uccella S. Molecular Pathology of Well-Differentiated Pulmonary and Thymic Neuroendocrine Tumors: What Do Pathologists Need to Know? Endocr Pathol 2021;32: 154-168.
13. White A, Clark AJ, Stewart MF. The synthesis of ACTH and related peptides by tumours. Baillieres Clin Endocrinol Metab 1990;4: 1-27.
14. Wu Y, Yue L, Li J, Yuan M, Chai Y. Cushing's syndrome secondary to typical pulmonary carcinoid with mutation in BCOR gene: A case report. Medicine (Baltimore) 2017;96:e7870.

12TH INTERNATIONAL AMR PATHOLOGY SLIDE SEMINAR SYMPOSIUM IN ANATOMIC PATHOLOGY

Case – 15

Gastrointestinal and Liver Pathology

Contributed by: Abbas Agaimy

Clinical History

A 46-year-old man underwent heart transplantation for dilatative cardiomyopathy 6 years ago. He has been under regular monitoring without signs of transplant rejection. Currently, he presented with abdominal pain and fatigue. Hemoccult test was positive. Upper GI endoscopy was unremarkable, but colonoscopy revealed multiple polypoid lesions in the left colon measuring up to 8 mm in size with variable superficial ulcerations. Abdominal CT showed in addition multiple liver nodules measuring up to 3.5 cm. Core needle biopsies was obtained from a liver lesion, followed then by left hemicolectomy and partial hepatectomy. No additional findings in other organs were seen on further imaging.

Pathological Findings

Macroscopic features

The colectomy specimen revealed multiple polypoid and intramural nodules measuring up to 2.5 cm in size with brownish to tan-yellow cut surface and focal mucosal ulceration. The liver specimen contained multiple grey-whitish nodule with soft consistency measuring up to 3.5 cm in diameter.

Histological and immunohistochemical findings

Histological examination of the colon sections showed an admixture of well differentiated paucicellular mature looking smooth muscle nodules with variably increased cellularity and abrupt foci of small primitive looking atypical areas lacking smooth muscle features. The mitotic activity was highly variable 8absent in the well differentiated areas and brisk in the cellular atypical smooth muscle looking or primitive looking foci). The liver nodules showed a highly cellular neoplasm composed of small hyperchromatic primitive looking ovoid cells diffusely set into sparse fibrous stroma with variable scattered small mature lymphocytes in the background and at the interphase to the normal liver tissue. The mitotic activity was brisk with >50 mitoses in 10 HPFs. Foci of necrosis were seen only in the liver nodules.

The immunohistochemistry showed diffuse expression of SMA and variable expression of h-caldesmon. Desmin was focally positive but varied from one nodule to another. The EBER was positive in both the liver and the colonic nodules. The TP53 showed aberrant pattern in the liver nodules but was of wildtype reactivity in the colon tumors. The Rb1 showed retained nuclear reactivity in both manifestations.

Diagnosis

Multifocal EBV-associated post-transplant smooth muscle neoplasms of the GI tract (colon) and the liver occurring 6 years after heart transplantation.

Comments

EBV-associated smooth muscle neoplasms (EBV-SMNs) are rare. They may occur at any body site, also in anatomic sites usually not involved by sporadic smooth muscle neoplasms. The have been reported in association with immunodeficiency in the context of primary immunodeficiency, HIV infection and in iatrogenic immunosuppression in solid organ transplant recipients. Certain site distributions have been linked to the underlying immune defect with HIV/AIDS-related cases showing predilection for the central nervous system (axial or extra-axial in up to 40% of cases), while iatrogenic immunodeficiency-associated tumors are more frequently encountered in the liver (56%), the lungs (31%) and the gastrointestinal tract (15%). Up to 29 – 71% of cases are multifocal with the frequency of multifocality again being associated with the underlying immune defect.

The clinical symptoms of EBV-SMNs are essentially nonspecific and are defined by the site and extent of involvement. The age at presentation varies greatly (1 – 66 y), with the majority of primary immune defect associated cases presenting in children. Post-transplant tumors on the other hand are mostly diseases of adults and they occur more frequently in kidney transplant patients followed by heart, liver, and hematopoietic stem cells transplantation. Cases occurring under immunosuppressive therapy for autoimmune diseases have been rarely reported. The latency between the immunodeficiency and the tumor presentation ranges from months to years. Lack of any apparent cause of immunodeficiency at time of presentation should warrant careful clinical and immunological workup of the patient to verify the possibility of undiagnosed occult immune defects in any case of EBV-SMNs.

The exact pattern of EBV latency is controversial. Positivity for EBV-encoded small RNA (EBER), EBNA2, and LMP1 have been described, but varied with the type of immune defect with inconsistent EBNA2 expression and absent LMP1 in the majority of posttransplant and a subset of HIV-associated EBV-SMNs. From a molecular pathogenetic perspective, overexpression of MYC and activation of the AKT/mTOR signaling pathway have been implicated in the pathogenesis of EBV-SMNs. Notably, multiple EBV infection events have been found responsible for the multifocality of neoplasms, indicating involvement of independent viral clones and not tumor dissemination or metastasis from a single primary neoplasm.

Grossly, EBV-associated SMNs range in size from microscopic to > 20 cm. Their borders may be well demarcated or infiltrative. Histologically, they display features of smooth muscle cells, in addition a to a second cell population displaying small primitive looking round to oval cells. A hemangiopericytoma-like pattern is noted in a subset of cases. Cytological atypia varies from mild to moderate and is rarely marked and mitotic activity is variable as well. Intratumoral T-cell infiltrates are observed frequently but are usually limited. Immunohistochemistry shows consistent expression of SMA and h-caldesmon, but desmin is frequently only focal or negative. EBER is diagnostic.

The prognosis varies with the underlying disease and immune status. Most tumors do not metastasize. Posttransplant cases may respond to reduction of the immunosuppression.

There is still no established grading scheme for these rare neoplasms. Histologically, they vary from well differentiated benign- looking (leiomyoma-like) to atypical SMNs of unknown malignant potential to frankly malignant high-grade sarcomas. Those high-grade looking tumors frequently show no clear-cut smooth muscle features, so diagnosis requires a high suspicion index. The presence of scattered or aggregated lymphocytes in the background and hemangiopericytoma-like vessels in many cases combined with incomplete smooth muscle immunophenotype should alert to this possibility and warrant EBV testing. Retained Rb1 expression and/ or TP53 wildtype pattern in any presumable high-grade leiomyosarcoma is also a potential hint to an EBV-SMN. In the current case, it is formally impossible to rule out that the liver nodules are metastases from the poorly differentiated components of the colonic tumors as the liver nodules were all high-grade and lacked any differentiated component in contrast to the colonic lesions.

Figure 1

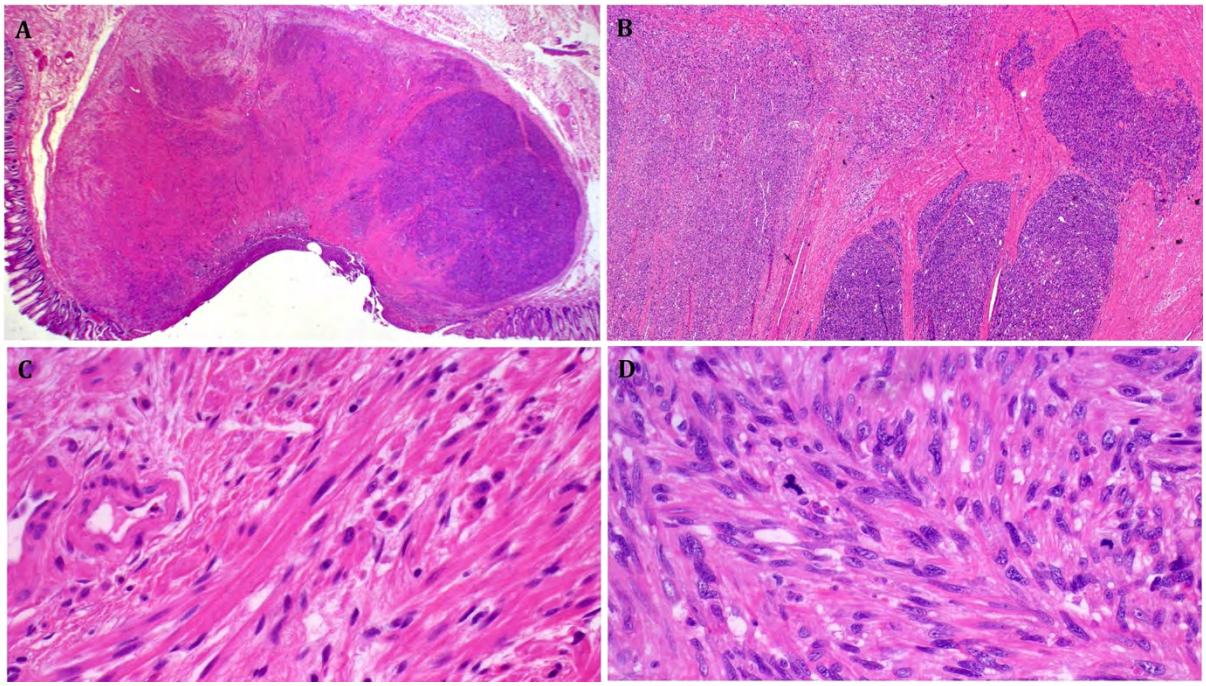

A: overview of an ulcerated submucosal colonic EBV-SMN showing non-invasive borders with transition from eosinophilic well differentiated to a dark-stained primitive looking component. **B**: Another intramural colonic lesion showing invasive borders within the M. propria and biphasic morphology. **C**: higher magnification of a colonic lesion shows leiomyoma-like mature smooth muscle morphology. **D**: another colonic lesion with conventional leiomyosarcoma-like morphology, note atypical mitotic activity.

Figure 2

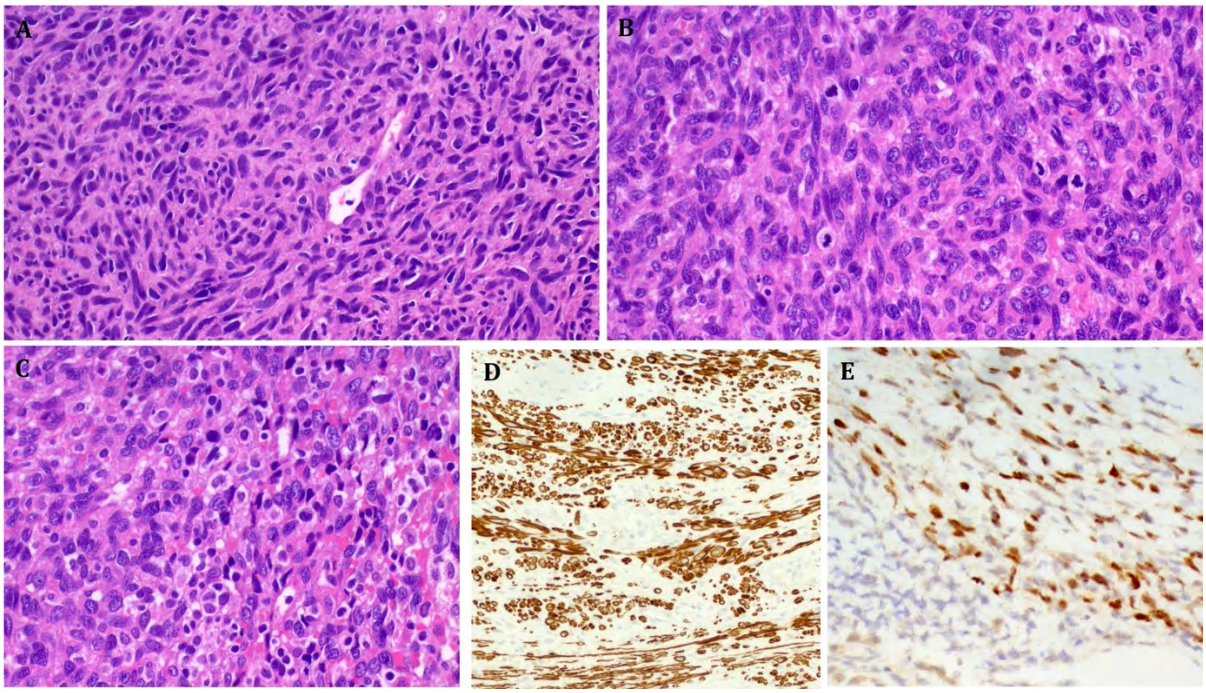

A, B: the liver lesions showed frankly malignant neoplasms with a predominance of primitive dark-stained ovoid to plump spindle cells with brisk mitotic activity. **C**: a few mature lymphocytes were seen

within the stroma and at the border to the liver. **D**: strong expression of h-caldesmon. E: EBER shows strong nuclear reactivity in the neoplastic cells but not in the inflammatory cells at left lower field.

References

1. Cohen JI, Dropulic L, Hsu AP, et al. Association of GATA2 Deficiency With Severe Primary Epstein-Barr Virus (EBV) Infection and EBV-associated Cancers. Clin Infect Dis. 2016;63:41-7.
2. Deyrup AT, Lee VK, Hill CE, et al. Epstein-Barr virus-associated smooth muscle tumors are distinctive mesenchymal tumors reflecting multiple infection events: a clinicopathologic and molecular analysis of 29 tumors from 19 patients. Am J Surg Pathol 2006;30:75-82.
3. Hussein K, Rath B, Ludewig B, et al. Clinico-pathological characteristics of different types of immunodeficiency-associated smooth muscle tumours. Eur J Cancer. 2014;50:2417-24.
4. Jonigk D, Laenger F, Maegel L, et al. Molecular and clinicopathological analysis of Epstein-Barr virus-associated posttransplant smooth muscle tumors. Am J Transplant. 2012;12:1908-17.
5. Magg T, Schober T, Walz C, et al. Epstein-Barr Virus^{+} Smooth Muscle Tumors as Manifestation of Primary Immunodeficiency Disorders. Front Immunol. 20189:368.
6. Moore Dalal K, Antonescu CR, Dematteo RP, et al. EBV-Associated Smooth Muscle Neoplasms: Solid Tumors Arising in the Presence of Immunosuppression and Autoimmune Diseases. Sarcoma. 20082008:859407.
7. Ong KW, Teo M, Lee V, et al. Expression of EBV latent antigens, mammalian target of rapamycin, and tumor suppression genes in EBV-positive smooth muscle tumors: clinical and therapeutic implications. Clin Cancer Res. 2009;15:5350-8.
8. Parta M, Cuellar-Rodriguez J, Freeman AF, et al. Resolution of Multifocal Epstein-Barr Virus-Related Smooth Muscle Tumor in a Patient with GATA2 Deficiency Following Hematopoietic Stem Cell Transplantation. J Clin Immunol. 2017;37:61-66.
9. Tan CS, Loh HL, Foo MW, et al. Epstein-Barr virus-associated smooth muscle tumors after kidney transplantation: treatment and outcomes in a single center. Clin Transplant. 201327:E462-8.

12TH INTERNATIONAL AMR PATHOLOGY SLIDE SEMINAR SYMPOSIUM IN ANATOMIC PATHOLOGY

Case – 16

Gastrointestinal and Liver Pathology

Contributed by: Luca Di Tommaso

Clinical History

A 55-year-old woman with history of lipoma of the breast performed US during a check-up for abdominal pain. US revealed a 5 cm lesion in the liver. Imaging (PET; CT; MNR) negative for other lesions. CEA and alfa-fetoprotein: negative; Ca19.9: 69 U/ml. Pre-operative diagnosis: hepatocellular carcinoma.

Pathological Findings

Liver resection 10x9x4 (VIII segment); 4.7 cm, whitish lesion with pushing margins (see gross image). The lesion was constituted by clear, epithelioid and eosinophilic, spindle cells, embedded in a rich vascular network. Neoplastic cells showed the following immunoprofile: Hepar1-, vimentin+, HMB45+, MelanA+.

Diagnosis

Angiomyolipoma of the liver.

Comments

Primary hepatic angiomyolipoma (PHA) are rare tumors (1). As compared to the most common renal cases, hepatic lesions are rarely associated with tuberous sclerosis and characterized by LOH involving TSC2 (chromosome 16p13), rather than mutation on TSC1 or TSC2 reported in renal angiomyolipoma. PHA are highly variable at histological level, with mixture of epithelioid and spindle cells, blood vessel and fat; in addition PHA show a disarrangement of the reticulin framework. In some cases, the pure morphological features can be misleading, especially on tiny biopsy. Indeed cases showing a trabecular pattern of growth and clear, epithelioid cells can be interpreted as hepatocellular adenoma or even carcinoma.

References

1. Goodman Z and Ishak K. Am J Surg Pathol 1984; 8: 745-50
2. Tsui et al. Am J Surg Pathol 1999; 66: 695-705
3. Klompenhouwer et al. Liver Int. 2017; 37: 1272-1280.

Case – 17

Gastrointestinal and Liver Pathology

Contributed by: Irene Gullo & Fátima Carneiro

Clinical History

A 70-year-old male with previous history of oral squamous cell carcinoma was submitted to upper endoscopy. A 3cm elevated and sessile lesion (IIa+Is by Paris classification) was found in the subcardic region (**Figure 1**). The endoscopic biopsy showed (low-grade) dysplasia of gastric phenotype. The lesion was removed by endoscopic submucosal dissection (ESD).

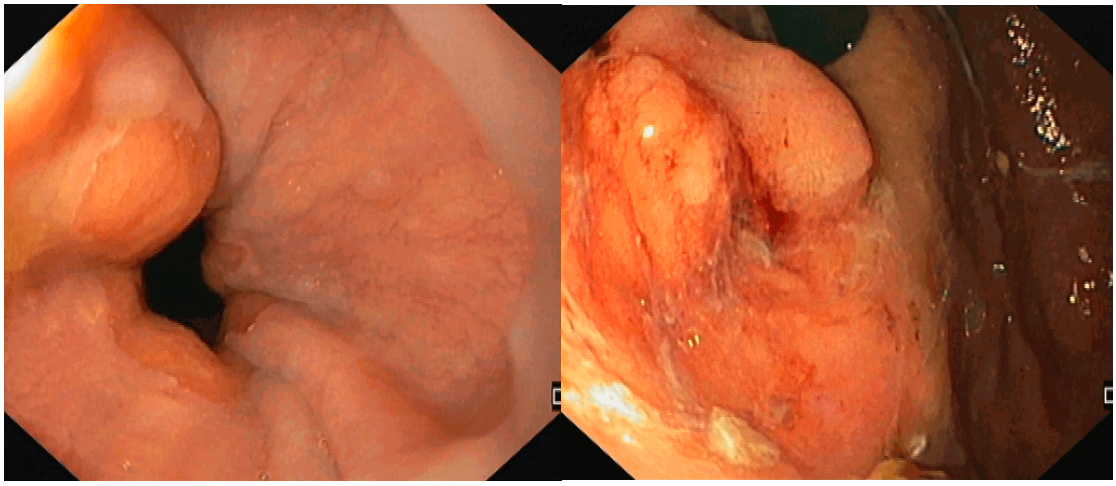

Figure 1

Pathological and Molecular Findings

Histopathological analysis showed GC with two juxtaposed components: GC with lymphoid stroma (GCLS) and tubulo-papillary (TP) adenocarcinoma (low-grade) (**Figure 2**).

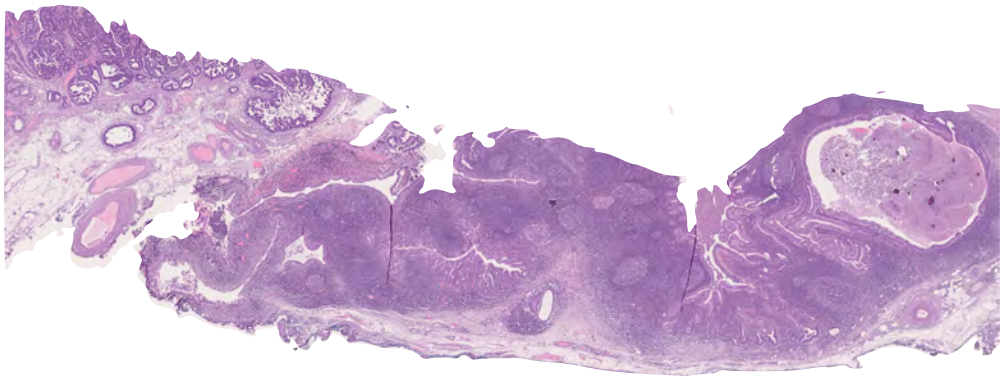

Figure 2

EBV-encoded small RNAs (EBER) *in situ* hybridization revealed positivity in the GCLS component, while TP component was negative (**Figure 3**). By immunohistochemistry, both components were mismatch-repair proteins (MMR) proficient.

Figure 3

To investigate if the tumour was clonal (despite the two components) or, otherwise, a collision tumour, shallow Whole Genome Sequencing (sWGS) of both components was performed. The molecular analysis showed similar amplification/deletion profile, pointing to a clonal origin of the two components. By contrast, EBV read counts were positive in the GCLS component (n=73) but totally negative in TP component.

Since TP GC showed lymphatic invasion and the endoscopic resection was incomplete (vertical margin), total gastrectomy was performed. No residual tumour or lymph node metastases (0/50) were observed.

Diagnosis

Bi-phenotypic gastric carcinoma with GCLS (EBV+) and TP (EBV-) components.

Comments

Gastric carcinoma (GC) is highly heterogeneous both from morphologic and molecular standpoints [1]. The morphological features of GC with lymphoid stroma have been associated with Epstein-Barr virus (EBV) infection [2]. We aim to report a case of GC showing remarkable morphomolecular heterogeneity. The coexistence of EBV+ and EBV- components in GC has been reported only in few cases in which distinct tumour clonality (*i.e.*collision tumour) was observed, rather than a single tumour with distinct phenotypes [3,4]. In our case, GCLS and TP components were considered clonal by shallow WGS, despite showing different EBV status. To our knowledge, this is the first case report of a “bi-phenotypic” GC showing a morphological switch from GCLS to TP adenocarcinoma on the basis of EBV status.

References

1. Cancer Genome Atlas Research Network. Comprehensive molecular characterization of gastric adenocarcinoma. Nature. 2014;11;513(7517):202-9. doi: 10.1038/nature13480.
2. Gullo I, Carvalho J, Martins D, Lemos D, Monteiro AR, Ferreira M, Das K, Tan P, Oliveira C, Carneiro F, Oliveira P. The Transcriptomic Landscape of Gastric Cancer: Insights into Epstein-Barr Virus Infected and Microsatellite Unstable Tumors. Int J Mol Sci. 2018;17;19(7):2079. doi: 10.3390/ijms19072079.
3. Shinozaki-Ushiku A, Kunita A, Fukayama M. Update on Epstein-Barr virus and gastric cancer (review). Int J Oncol. 2015;46(4):1421-34. doi: 10.3892/ijo.2015.2856.
4. Miyabe K, Saito M, Koyama K, Umakoshi M, Ito Y, Yoshida M, Kudo-Asabe Y, Saito K, Nanjo H, Maeda D, Matsusaka K, Goto A, Kono K. Collision of Epstein-Barr virus-positive and -negative gastric cancer, diagnosed by molecular analysis: a case report. BMC Gastroenterol. 2021;2;21(1):97. doi: 10.1186/s12876-021-01683-y.

12TH INTERNATIONAL AMR PATHOLOGY SLIDE SEMINAR SYMPOSIUM IN ANATOMIC PATHOLOGY

Case – 18

Gastrointestinal and Liver Pathology

Contributed by: Christopher Hartley

Clinical History

A 62-year-old man with a history of non-alcoholic steatohepatitis-associated cirrhosis was found to have two enlarging LI-RADs 5 lesions in the liver on routine screening for hepatocellular carcinoma. A biopsy of one of the masses was performed, and following the diagnosis, liver transplantation was performed within 2 weeks.

Pathological Findings

Macroscopic Features: The explanted liver showed five tumor nodules grossly, ranging from 1.2 cm to 5.3 cm in greatest dimension with extensive necrosis.

Histological and Immunohistochemical Findings: Sections of the core biopsy show two distinct lower power morphologies present in separate cores, as well as in a single fragmented core (Figure 1). Higher power view of each histology reveals separate hepatoid and sarcomatoid proliferations (Figure 2).

Figure 1:

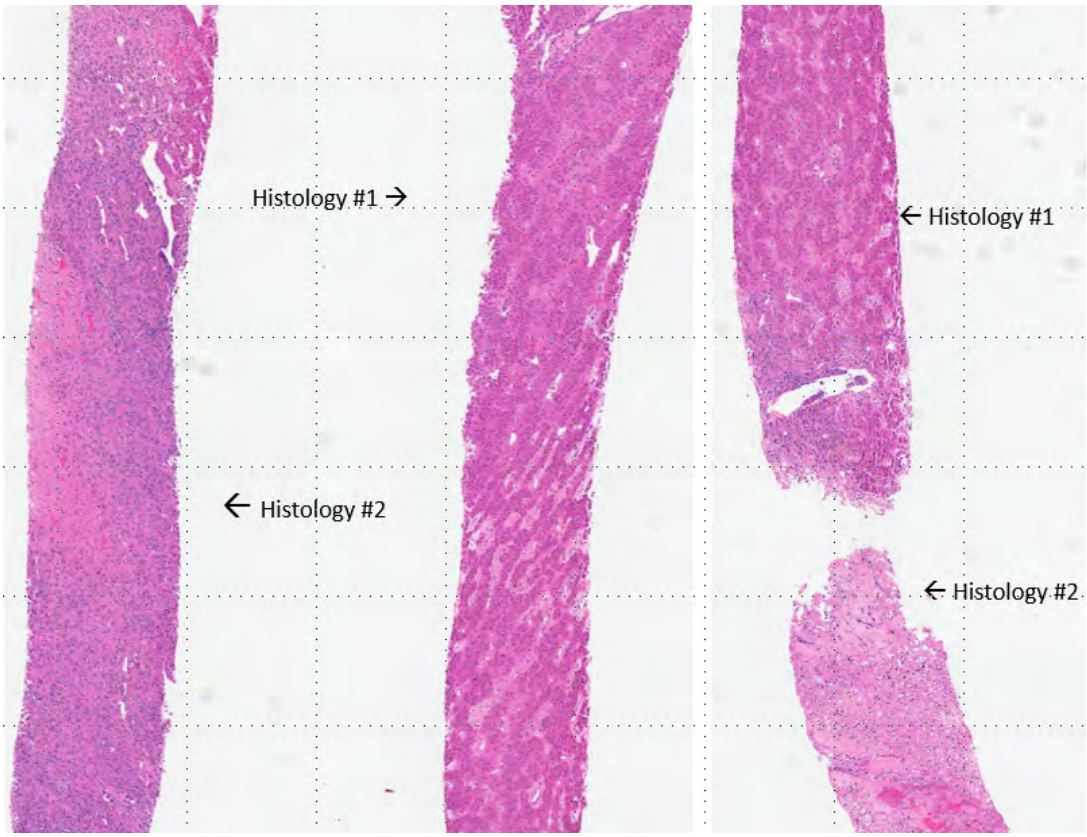

Immunostains on the core biopsy show that the sarcomatoid areas are positive for CK7 and Desmin, while the hepatoid areas are positive for Arginase (Figure 3). The hepatoid areas were also positive for HepPar1 and Albumin in-situ hybridization (not shown). Calponin was also focally positive in the sarcomatoid area, while reticulin showed loss of fibers in the hepatoid component (Figure 4).

Figure 2:

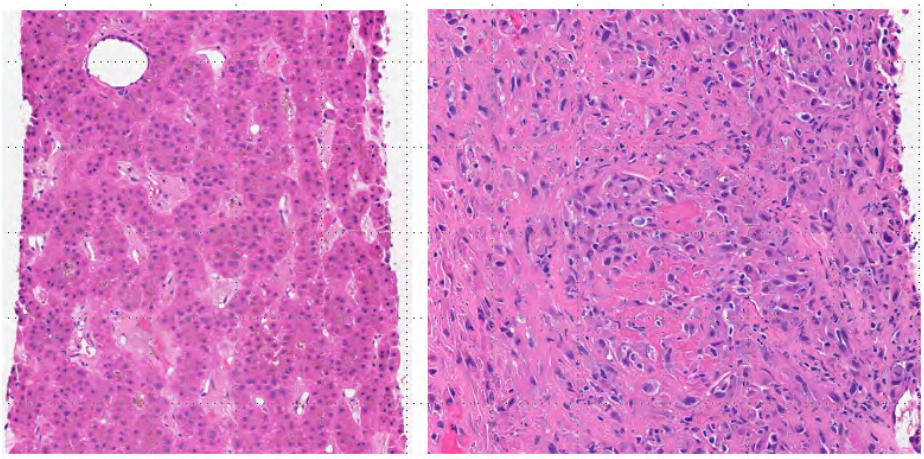

Figure 3:

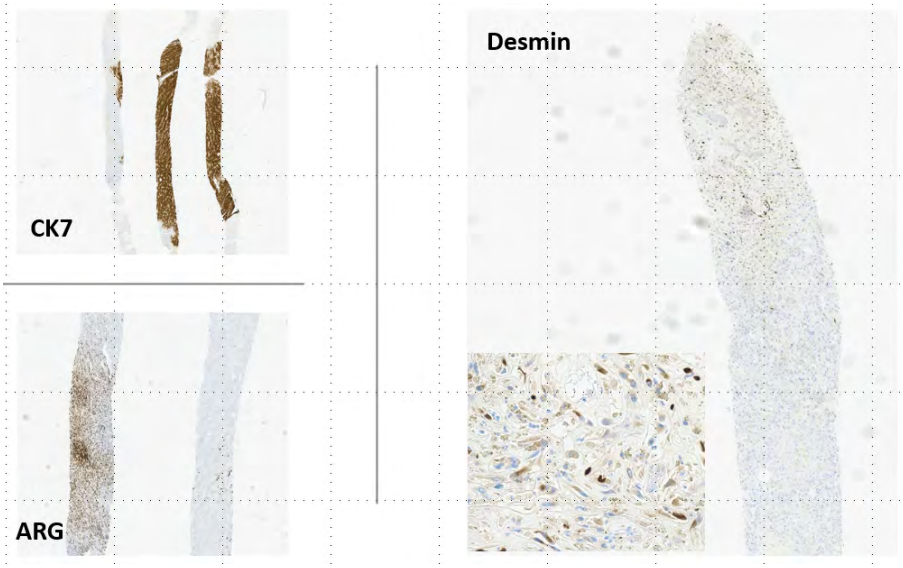

Figure 4:

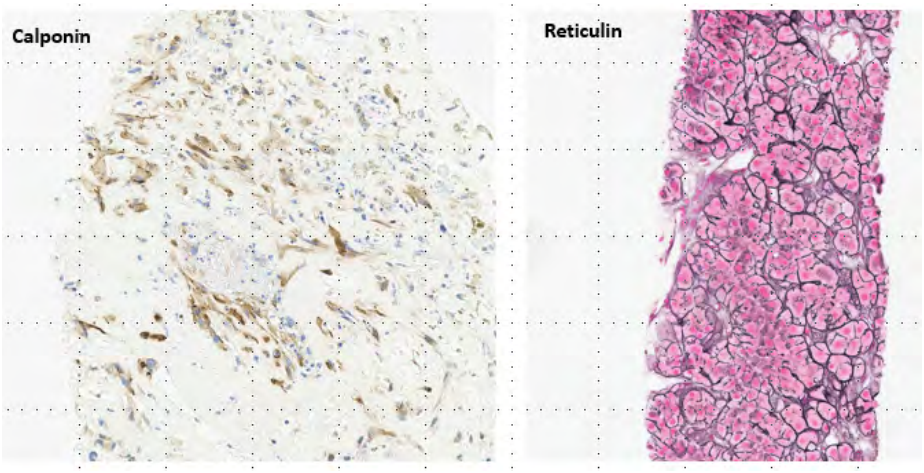

Additional immunostains showed that the sarcomatoid area was negative for MyoD1, Myogenin, SOX10, and CD31.

Sections of the nodules in the explanted liver showed extensive necrosis, but also more viable sarcomatoid areas with better-preserved histology (Figure 5). No hepatocellular component was appreciated in sampling of any of the 5 nodules, despite generous sampling.

Figure 5:

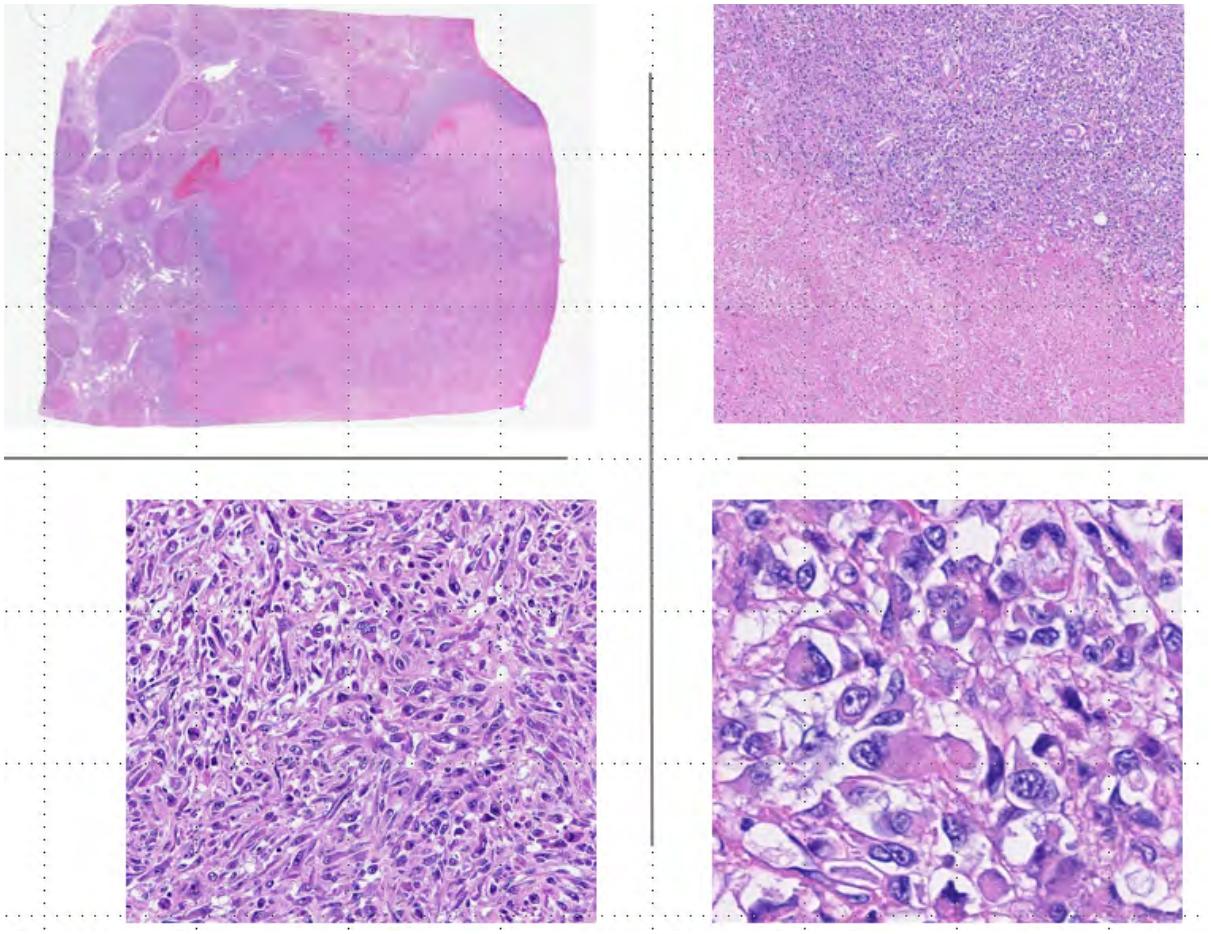

Diagnosis

Hepatocellular carcinoma with sarcomatoid myogenic differentiation (also sometimes referred to as rhabdoid heterologous differentiation).

Comments

I found this case particularly interesting due to prominence and much-better preserved well to moderately differentiated hepatocellular component, compared to the more subtle, less-preserved sarcomatoid morphology on the core biopsy, whose malignant cells could be overlooked as either degenerating/necrotic hepatocellular carcinoma, or perhaps a reactive myofibroblastic proliferation. Also, within a single partially fragmented core, there is an abrupt transition from hepatocellular carcinoma to sarcomatoid carcinoma, without intervening poorly differentiated hepatocellular carcinoma, mimicking a “collision tumor.”

Immunostains confirmed the hepatocellular differentiation of the well to moderately differentiated component, and lack thereof in the sarcomatoid component. The presence of the hepatocellular component was critical to avoid a diagnosis of leiomyosarcoma. Strong CK7 with patchy Desmin and Calponin confirm rhabdoid/myogenic sarcomatoid differentiation. Previously, sarcomatoid hepatocellular carcinoma was thought to be associated with embolization/prior treatment, but sarcomatoid HCC as been increasingly reported in cases without a history or prior treatment, such as this case [1]. Sarcomatoid HCC can show rhabdoid, osteoid, or chondroid heterologous differentiation.

References

1. Wang JP, Yao ZG, Sun YW, Liu XH, Sun FK, Lin CH, Ren FX, Lv BB, Zhang SJ, Wang Y, Meng FY, Zheng SZ, Gong W, Liu J. Clinicopathological characteristics and surgical outcomes of sarcomatoid hepatocellular carcinoma. World J Gastroenterol. 2020 Aug 7;26(29):4327-4342. doi: 10.3748/wjg.v26.i29.4327. PMID: 32848337; PMCID: PMC7422543.

Case – 19

Gastrointestinal and Liver Pathology

Contributed by: Fátima Carneiro

Clinical History

Male, 38-year-old, with multiple polyps, submitted to total gastrectomy. Numerous small polyps were observed in the body and fundus (**Figure 1A**), sparing the antrum (**Figure 1B**). Polyps were not identified in the duodenum and colon.The patient was not taking PPIs (proton pump inhibitors). The family history was irrelevant. The patient was lost for follow-up.

Figure 1A

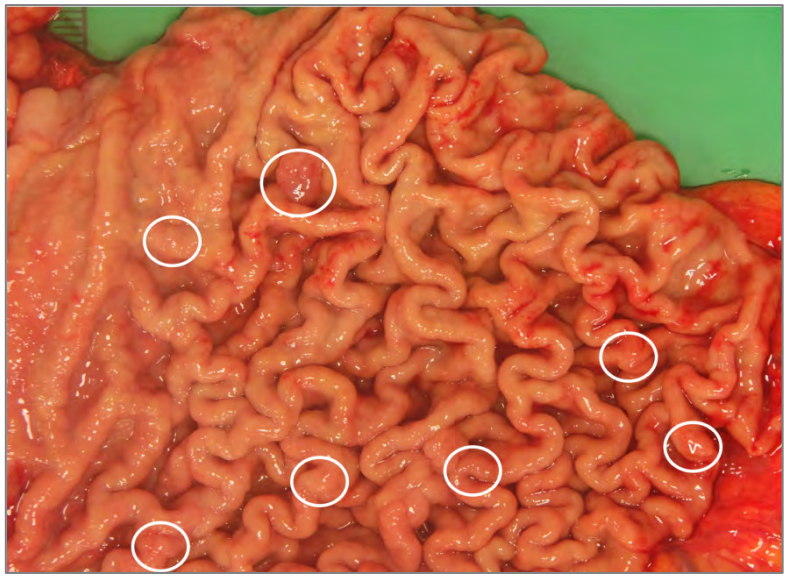

Figure 1B

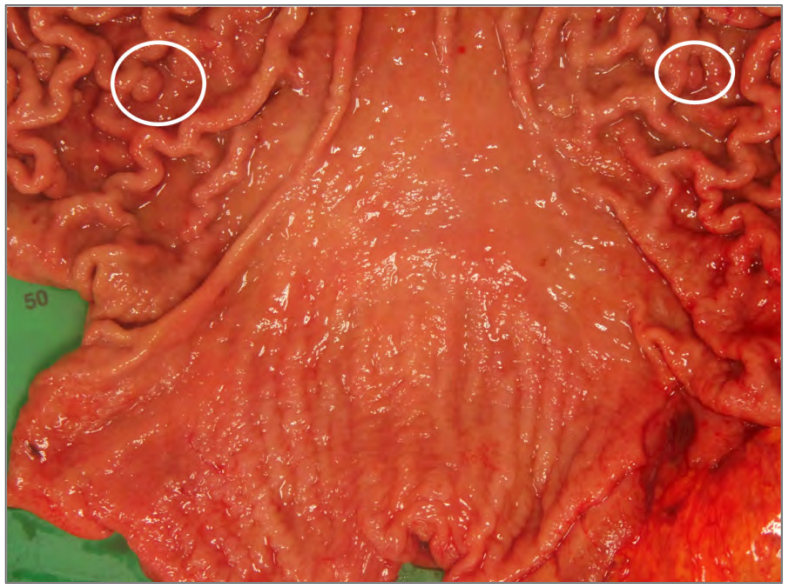

Histological features

The gastric polyps displayed the features of fundic gland polyps and fundic gland–like polyps, with cystic glands (**Figure 2A**) lined by mucin secreting epithelium. At the periphery, proliferated glands were observed, focally with the features the so called "hyperproliferative aberrant pits" (**Figure 2B**). Dysplasia was focally observed (**Figure 2C**). In one of the polyps, a focus of intramucosal adenocarcinoma was identified (not shown).

Figure 2A

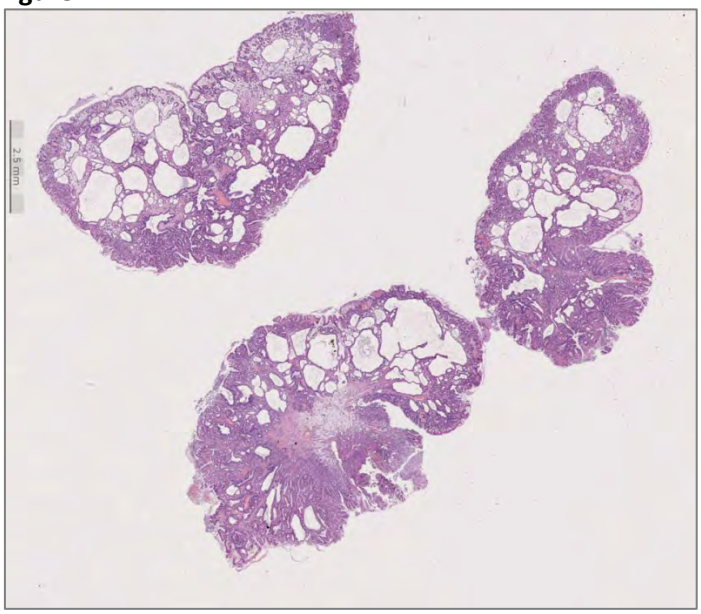

Figure 2B

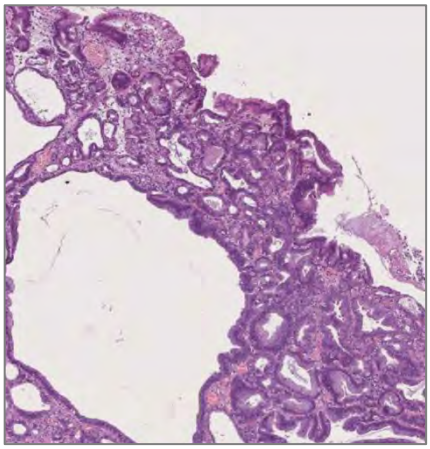

Figure 2C

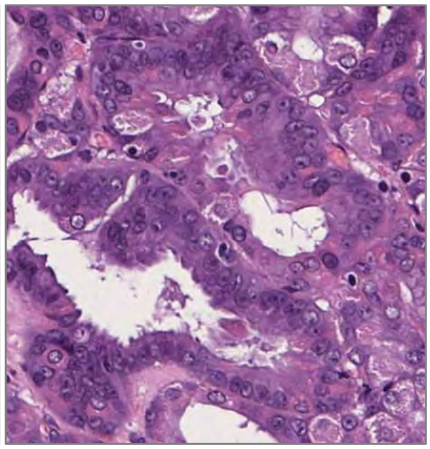

Genetic study

The genetic study was directed to APC gene, namely the region of the promoter 1B. Mutations within the Ying Yang 1(YY1) binding motif of the *APC* gene (c.-191T>C, c.-192A>G and c.-195A>C) were not identified. The genetic study was repeated, giving the same results. No other mutations were found in the *APC* gene.

Diagnosis

GAPPS-like fundic gland proximal polyposis of the stomach

Comments

GAPPS (Gastric Adenocarcinoma and Proximal Polyposis of the Stomach) is an autosomal dominant gastric polyposis syndrome, first described in 2012 (1,2). After the identification of GAPPS, several families have been described in the literature (3-7). A range of microscopic features can be observed in GAPPS, including fundic gland polyps (FGPs), dysplastic FGPs, fundic gland–like polyps, hyperproliferative aberrant pits (HPAPs), hyperplastic polyps, gastric-type adenomas, and adenocarcinomas (tubular/intestinal and mixed with a poorly cohesive component) (8). HPAP appear to be unique lesions that have not been described in any other setting of gastric pathology (8). The criteria for the diagnosis of GAPPS are summarized in **Table 1**, encompassing essential and supportive criteria (9).

Table 1

Essential criteria (1 and 2)	Supportive criteria (any)
1.Phenotypic features • Proximal (body and fundus) gastric polyposis with antral sparing; no evidence of colorectal or duodenal polyposis[a]. No evidence of colorectal or duodenal polyposis; • > 100 polyps carpeting the proximal stomach in the index patient or > 30 polyps in a first-degree relative of another patient; • Predominantly fundic gland polyps and/or fundic gland–like polyps;	**1.**Spectrum of other histological lesions: • Hyperproliferative aberrant pits • Hyperplastic polyps • Gastric-type adenomas
2. Proband or family member with either dysplastic fundic gland polyps or gastric adenocarcinoma. **3.** Mutation in the chr5: 112,043,220–12,043,224 region of promoter 1B of APC[b]	2.Family history (autosomal dominant pattern of inheritance)

[a]Exclusions include other heritable gastric polyposis syndromes and use of PPIs. In patients on PPIs it is recommended to repeat the endoscopy off therapy.

[b]The point mutations that segregate with GAPPS (c.-191T>C, c.-192A>G and c.-195A>C) are all positioned within the Ying Yang 1(YY1) binding motif of the APC gene.

In the case herein presented, most essential clinical criteria for the diagnosis of GAPPS were present, namely extensive involvement of the fundus and body of the stomach with fundic gland polyps and fundic gland–like polyps, sparing the antrum and lesser curvature; presence of hyperproliferative aberrant pits (HPAPs), dysplastic fundic gland polyps and gastric adenocarcinoma; absence of involvement of the duodenum or large bowel (excluding the diagnosis of FAP and attenuated FAP).

However, none of the "GAPPS mutations" described in 2016 (10) was identified, precluding the diagnosis of GAPPS. In face of these findings, two options may be considered for this GAPPS-like gastric polyposis: either there is a (germline) new mutation not identified in the genetic test; otherwise, it may represent the sporadic counterpart of GAPPS syndrome.

References

1. Worthley DL, Phillips KD, Wayte N, et al. Gastric adenocarcinoma and proximal polyposis of the stomach (GAPPS): a new autosomal dominant syndrome. Gut. 2012; 61(5):774-779.
2. Yanaru-Fujisawa R, Nakamura S, Moriyama T, et al. Familial fundic gland polyposis with gastric cancer. Gut. 2012; 61(7):1103-1104.

3. Mitsui Y, Yokoyama R, Fujimoto S, Kagemoto K, Kitamura S, Okamoto K, et al. First report of an Asian family with gastric adenocarcinoma and proximal polyposis of the stomach (GAPPS) revealed with the germline mutation of the APC exon 1B promoter region. Gastric Cancer. 2018;21:1058-1063.
4. Repak R, Kohoutova D, Podhola M, Rejchrt S, Minarik M, Benesova L, et al. The first European family with gastric adenocarcinoma and proximal polyposis of the stomach: case report and review of the literature. Gastrointest Endosc. 2016;84:718-725.
5. Rudloff U. Gastric adenocarcinoma and proximal polyposis of the stomach: diagnosis and clinical perspectives. Clinical and experimental gastroenterology. 2018;11:447-459.
6. Foretova L, Navratilova M, Svoboda M, Grell P, Nemec L, Sirotek L, et al. GAPPS – Gastric Adenocarcinoma and Proximal Polyposis of the Stomach Syndrome in 8 Families Tested at Masaryk Memorial Cancer Institute - Prevention and Prophylactic Gastrectomies. Klin Onkol. 2019; 32:109-117.
7. Grossman A, Colavito J, Levine J, Thomas KM, Greifer M. Filling in the "GAPPS": an unusual presentation of a child with gastric adenocarcinoma and proximal polyposis of the stomach Gastric Cancer. 2022 Mar; 25(2):468-472.
8. de Boer WB, Ee H, Kumarasinghe MP. Neoplastic Lesions of Gastric Adenocarcinoma and Proximal Polyposis Syndrome (GAPPS) are Gastric Phenotype. Am J Surg Pathol. 2018; 42:1-8.
9. Carneiro F, Chenevix-Trench G, de Boer WB, Kumarasinghe MP, Worthley DL. GAPPS and other fundic gland polyposes. In: Board WCoTE, ed. WHO Classification of Tumours. Digestive System Tumours. Fifth Edition. 5th edition ed. Lyon (France): International Agency for Research on Cancer; 2019:526-528.
10. Li J, Woods SL, Healey S, Beesley J, Chen X, Lee JS, et al. Point Mutations in Exon 1B of APC Reveal Gastric Adenocarcinoma and Proximal Polyposis of the Stomach as a Familial Adenomatous Polyposis Variant. Am J Hum Genet. 2016; 98: 830-842.

12TH INTERNATIONAL AMR PATHOLOGY SLIDE SEMINAR SYMPOSIUM IN ANATOMIC PATHOLOGY

Case – 20

Gastrointestinal and Liver Pathology

Contributed by: Katherine Hagen

Clinical History

A 59-year-old man with recent COVID-19 infection presented with gastrointestinal symptoms including diarrhea, anorexia, nausea, and weight loss (approximately 90 lbs.). He also noted hyperpigmentation on his hands.

Pathological Findings

Macroscopic Features: On endoscopy, diffuse edema, erythema, and friability was noted in the stomach, duodenum, terminal ileum, and colon. The entire colon was affected without skip lesions Inflammatory type polyps were noted in the stomach and colon.

Histological and Immunohistochemical Findings: Biopsies throughout the gastrointestinal tract showed variable inflammation, edema, and architectural distortion. Biopsies obtained from both the background colonic mucosa and polypoid colonic mucosa appeared morphologically similar. CMV immunostain, GMS, and AFB stains were negative for organisms. SARS-CoV2 ddPCR performed on the colon biopsy was negative.

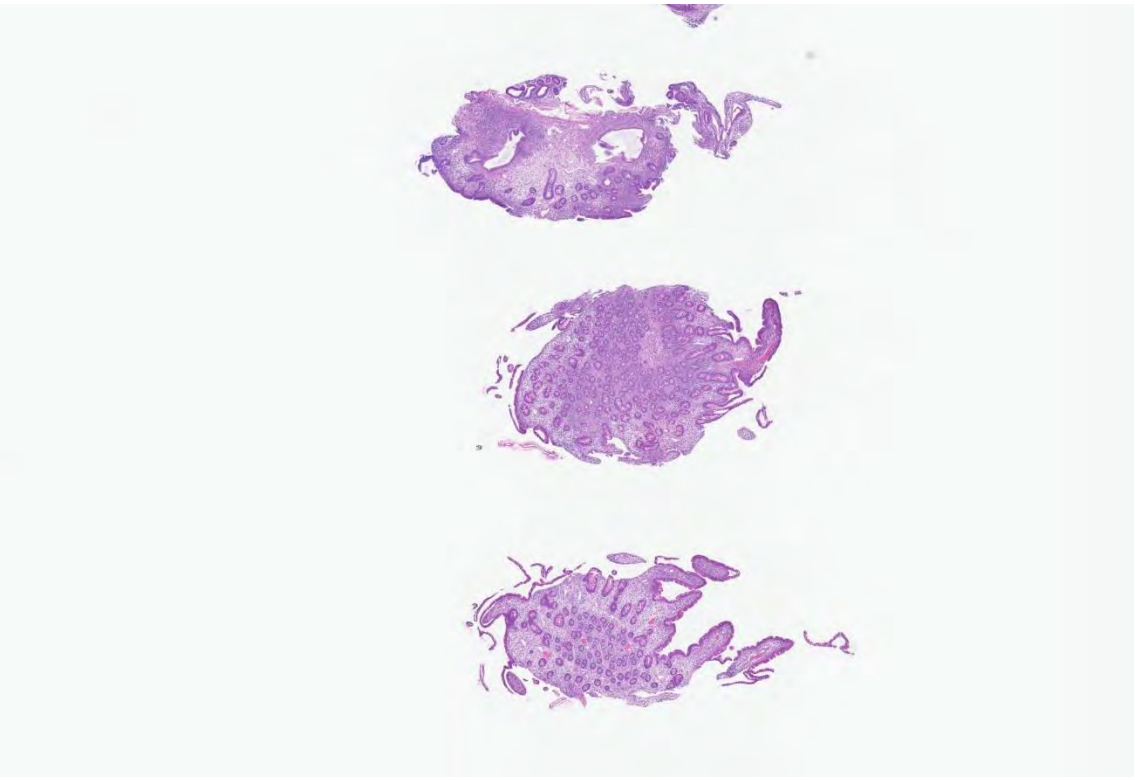

Figure 1: Duodenal biopsy shows variable villous blunting and lamina propria edema at low power

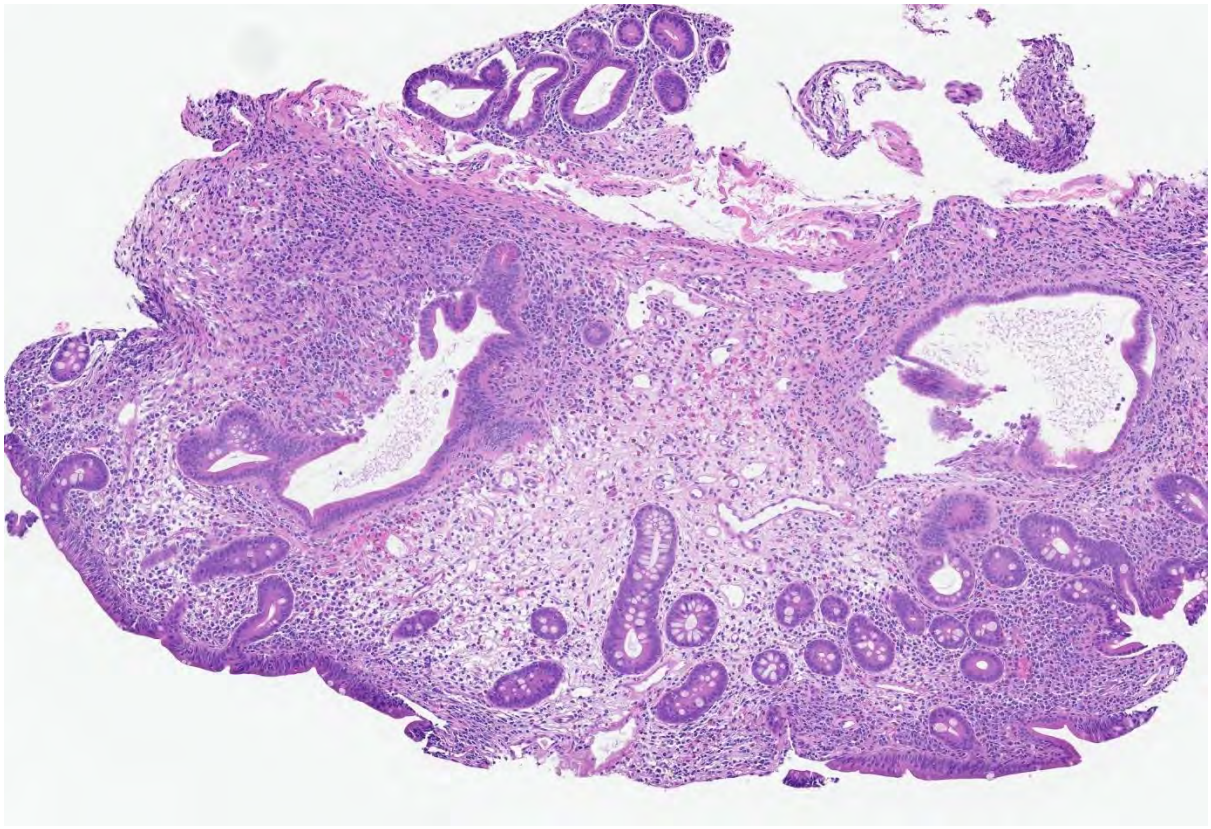

Figure 2: At higher power, the duodenum shows areas of villous blunting, intraepithelial lymphocytosis, lamina propria edema, and cystic dilation of glands

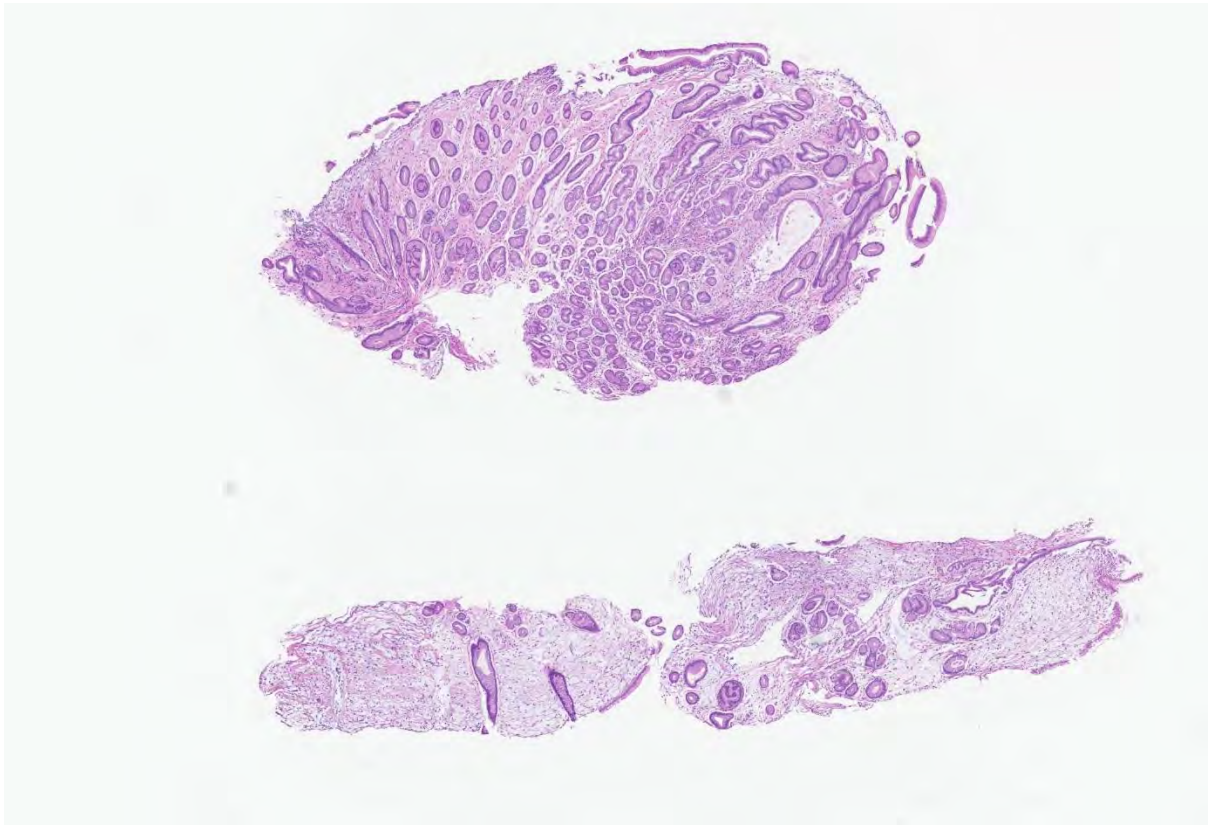

Figure 3: Gastric biopsies show prominent lamina propria edema and focal dilation of gastric pits

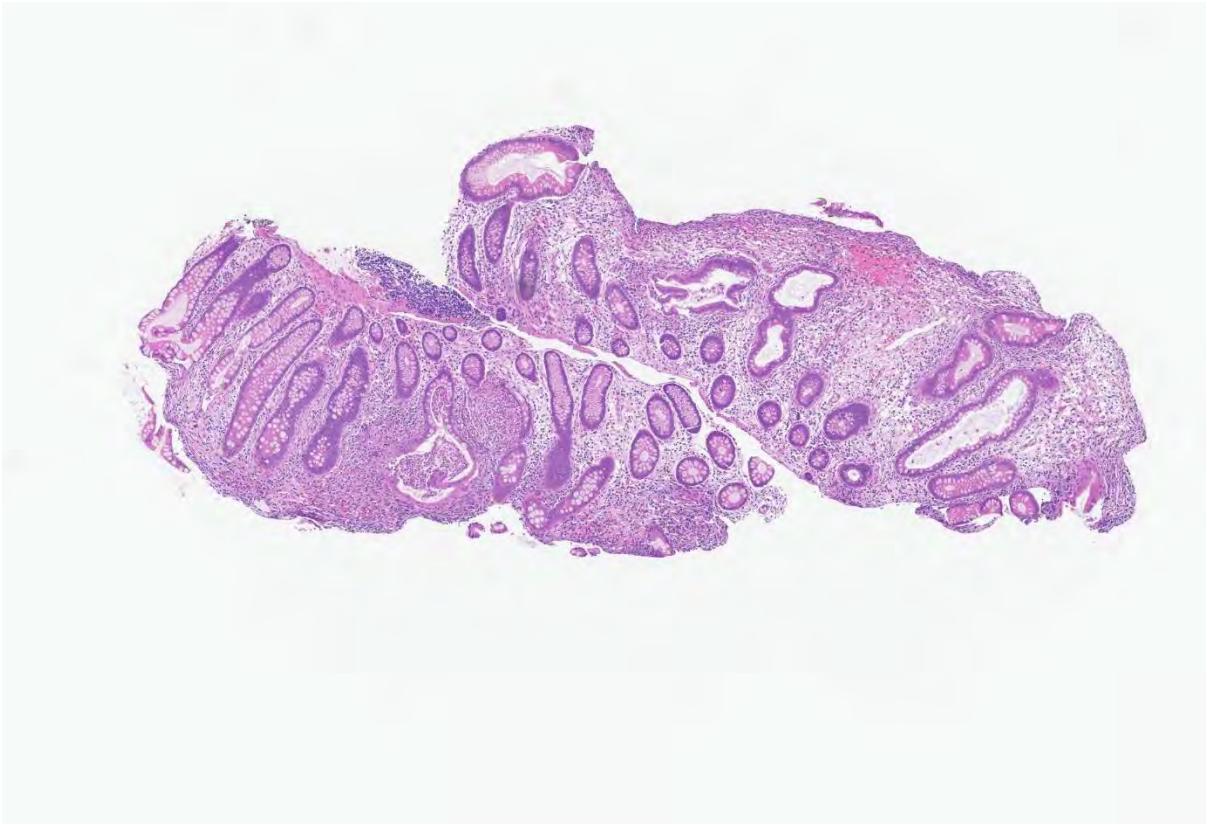

Figure 4: Biopsies of the background colonic mucosa show focal acute inflammation, lamina propria edema, and cystic dilation of crypts

Figure 5: Biopsies from colonic polyps appear morphologically similar to the background colonic mucosa with evidence of acute inflammation, lamina propria edema and cystic dilation of crypts reminiscent of a juvenile-type inflammatory polyp.

Diagnosis

Cronkhite-Canada Syndrome.

Comments

Cronkhite-Canada syndrome is a rare polyposis syndrome of unknown etiology. Patients typically present in middle adulthood with variable symptoms including diarrhea, nausea, vomiting, anorexia, and weight loss. Polyps can be seen anywhere throughout the gastrointestinal tract other than the esophagus. Biopsies from the polyps show cystically dilated glands associated with an edematous inflammatory stroma, appearing morphologically similar to juvenile type inflammatory polyps. Biopsies of the intervening background mucosa appears morphologically similar to the polypoid mucosa (in juvenile polyposis syndrome the intervening mucosa is morphologically normal) [1]. Characteristic extraintestinal manifestations include alopecia, nail atrophy, and skin hyperpigmentation. Patients typically have a poor prognosis due to nutritional complications as a result of malabsorption. Treatment typically consists of immunosuppression and nutritional supplementation.

Some limited data suggests that Cronkhite-Canada syndrome may be an autoimmune disorder, although the etiology remains largely unknown [2]. COVID-19 has been associated with autoimmune sequalae in some patients [3]. Whether the recent COVID-19 infection in this patient was unrelated or somehow triggered an immune response in this patient is uncertain, but certainly an interesting association to ponder.

References

1. Burke AP, Sobin LH. The pathology of Cronkhite-Canada polyps. A comparison to juvenile polyposis. Am J Surg Pathol. 1989;13(11):940-946.
2. Riegert-Johnson DL et al. Cronkhite-Canada syndrome hamartomatous polyps are infiltrated with IgG4 plasma cells. Digestion. 2007;75(2-3):96-97.
3. Ehrenfeld, M et al. Covid-19 and autoimmunity. Autoimmune Rev. 2020;19(8):102597.s

12TH INTERNATIONAL AMR PATHOLOGY SLIDE SEMINAR SYMPOSIUM IN ANATOMIC PATHOLOGY

Case – 21

Head and Neck Pathology

Contributed by: ***Alena Skálová***

Clinical History

A 66-year-old man presented with a tumor of the nasal cavity, that was originally diagnosed as high grade squamous cell carcinoma. The new excision was performed at another hospital with diagnosis of acinic carcinoma with high-grade transformation. Due to an uncertain diagnosis, the tumor was sent to us for second opinion.

Six months after primary excision, the patient presented with huge recurrent tumor in the nasal cavity, with a cervical lymph node metastasis. The patient died 10 months after primary surgery having been treated by chemotherapy.

Pathological Findings

Microscopically, the tumor was uniformly high-grade, exhibiting solid alveolar growth pattern, mild nuclear pleomorphism and elevated mitotic rate. The neoplastic cells displayed slightly irregular oval nuclei with one small distinct nucleolus. The cytoplasm was mostly pale, in places also empty looking, finely granular or plasmacytoid and eosinophilic with resemblance to high grade myoepithelial carcinoma. The tumor cells were arranged in small nests and trabeculae separated by thin fibrous septa, with rare glandular formation.

By immunohistochemistry, the tumor cells were entirely SMARCB1-deficient, with positive internal control in lymphocytes. The SMARCA4 marker showed intact expression in tumors cells. The tumor cells were positive for cytokeratins AE1/3, CK7, CK18, and EMA while entirely negative for CK20, CDX2, STAB2, DOG1, SOX10, melan A, S-100 protein and GATA3. The proliferative activity was high with MIB1 index about 60%.

Molecular findings: using TruSight Oncology 500 (Illumina), we detected a clinically significant mutation of the *ARID1B* gene c.1469G>A p.(Trp490Ter) AF: 6%; *SMARCB1* c.157C>T p.(Arg53Ter) AF: 20%; and *MGA* c.3724C>T p.(Arg1242Ter) AF: 8% in the examined sample. Low mutation load (TMB: Low; 6.4 mut/Mb) and low microsatellite instability (MSI-L; 2% loci) were demonstrated. No clinically significant numerical changes in the examined genes were detected.

Diagnosis

SMARCB1-deficient sinonasal adenocarcinoma.

Comments

The classification of poorly differentiated sinonasal carcinomas has experienced tremendous developments during the last two decades. Among these new achievements, recognition of carcinoma subtypes driven by defects in the Switch/Sucrose nonfermentable (SWI/SNF) chromatin remodeling complex represents a major discovery **(1-3).** There are four sinonasal entities driven solely or

predominantly by SWI/SNF complex deficiency: 1) SMARCB1(INI1)-deficient sinonasal carcinoma (lacking gland formation and frequently displaying a basaloid, and less frequently eosinophilic/oncocytoid morphology, 2) SMARCB1-deficient sinonasal adenocarcinoma (with unequivocal glandular differentiation or yolk sac-like growth pattern), 3) SMARCA4-deficient undifferentiated (SNUC-like) carcinoma (lacking glandular or squamous immunophenotypes), and 4) SMARCA4-deficient subset of sinonasal teratocarcinosarcoma **(4)**.

SMARCB1-deficient sinonasal adenocarcinoma is a rare variant of SMARCB1-deficient sinonasal carcinoma defined by presence of unequivocal glandular differentiation or by presence of features characteristic of adenocarcinoma **(5).** Less than 20 cases have been described to date but this tumor type might be under-reported or included in the spectrum of nonspecified SMARCB1-deficient sinonasal carcinoma **(6).** SMARCB1-deficient sinonasal adenocarcinomas display a higher predilection for males (5:1) compared to undifferentiated non-glandular SMARCB1-deficient sinonasal carcinoma. Most tumors originate in the nasal cavity while some involve multiple sinonasal sites. Less often, the ethmoid or the maxillary sinuses may be involved selectively.

Most SWI/SNF-deficient malignancies pursue a highly aggressive clinical course resulting in wide-spread disease dissemination either at or soon after diagnosis, ultimately causing patients´ death soon after diagnosis, despite apparently curative treatment intention. To date, no satisfactorily effective systemic chemotherapy has been established for treating these patients.

References

1. Agaimy A, Koch M, Lell M, Semrau S, Dudek W, Wachter DL, Knöll A, Iro H, Haller F, Hartmann A. SMARCB1(INI1)-deficient sinonasal basaloid carcinoma: a novel member of the expanding family of SMARCB1-deficient neoplasms. *Am J Surg Pathol.* 2014;38:1274- 81.
2. Bishop JA, Antonescu CR, Westra WH. SMARCB1 (INI-1)-deficient carcinomas of the sinonasal tract. *Am J Surg Pathol.* 2014;38:1282-9.
3. Agaimy A, Hartmann A, Antonescu CR, Chiosea SI, El-Mofty SK, Geddert H, Iro H, Lewis JS Jr, Märkl B, Mills SE, Riener MO, Robertson T, Sandison A, Semrau S, Simpson RH, Stelow E, Westra WH, Bishop JA. SMARCB1 (INI-1)-deficient Sinonasal Carcinoma: A Series of 39 Cases Expanding the Morphologic and Clinicopathologic Spectrum of a Recently Described Entity. *Am J Surg Pathol.* 2017;41:458-471.
4. Rooper LM, Agaimy A, Gagan J, Simpson RHW, Thompson LDR, Trzcinska AM, Ud Din N, Bishop JA. Comprehensive Molecular Profiling of Sinonasal Teratocarcinosarcoma Highlights Recurrent SMARCA4 Inactivation and CTNNB1 Mutations. *Am J Surg Pathol*. 2023 Feb 1;47(2):224-233
5. Shah AA, Jain D, Ababneh E, Agaimy A, Hoschar AP, Griffith CC, Magliocca KR, Wenig BM, Rooper LM, Bishop JA. SMARCB1 (INI-1)-Deficient Adenocarcinoma of the Sinonasal Tract: A Potentially Under-Recognized form of Sinonasal Adenocarcinoma with Occasional Yolk Sac Tumor-Like Features. *Head Neck Pathol*. 2020;14:465-472.
6. Agaimy A. SWI/SNF-deficient Sinonasal Carcinomas. *Adv Anat Pathol.* 2023 Mar 1;30(2):95-103.s

12TH INTERNATIONAL AMR PATHOLOGY SLIDE SEMINAR SYMPOSIUM IN ANATOMIC PATHOLOGY

Case – 22

Head and Neck Pathology

Contributed by: ***Fredrik Petersson***

Clinical History

A 51 y/o Chinese male, ex-smoker with G6PD, presented with a painless base of tongue tongue lesion which had bled for 2 days. On clinical examination, a tumor was seen located to BOT/lateral pharyngeal wall. An MRI-study was performed and showed a 5 cm tumor in the left lateral oro-pharyngeal wall, centred in the parapharyngeal space. A PET-CT was negative for distant spread. An incision biopsy was done. The tumor was resected at another hospital, where also a repeat biopsy was performed (showing the same features as in the first biopsy specimen). The resected specimen contained a 5.2 cm tumor which displayed the same histological features as in the biopsies. No necrosis, HGT or PNI was seen, but focal LVI was present. All margins were negative (7-18 mm). Bilateral modified neck dissections revealed no LN metastasis.

Pathological Findings

The tumor was comprised of variably sized nests (focally separated by thin fibrovascular septae) as well as sheets of neoplastic cells. The (epithelioid to spindly) neoplastic cells demonstrated ample eosinophilic to clear cytoplasm, and ovoid to spindle-shaped nuclei. There was low-grade nuclear atypia and visible nucleoli. PAS/DPAS stains demonstrated intra-cytoplasmic glycogen. DPAS- and Mucicarmine-stains were negative for mucin. IHC: Neoplastic cells express cytokeratins (AE1/3) and CK7. There was no expression of CK20, CK5/6, NUT1, S100-protein, HMB45, Melan A, GFAP, desmin, SMA, synaptophysin, PAX8, TTF1 and TFE3. TLE1 showed weak patchy nuclear expression and only rare single cell displayed some immuno-positivity for p63. There was retained nuclear expression of SMARCB1/INI1. The Ki67 proliferation index was variable (10-20% in hot spots). The case was signed out as: “Carcinoma with unusual features, most likely salivary gland-type.” Slides were sent to A.Agaimy (Erlangen):

“Most likely a monomorphic clear cell variant of a salivary-analogue carcinoma (the differential includes in particular monomorphic variant of muco-epidermoid carcinoma in addition to other unusual entities)”. TruSight-RNA-fusion-panel-testing (Illumina panel) showed presence of the classical CRTC1:MAML2 fusion (for MEC).

Diagnosis

Monomorphic (clear cell and focally spindle cell) variant of mucoepidermoid carcinoma.

Comments

MEC was first described by Stewart et al in 1945 and is a malignant epithelial neoplasm that classically comprises mucous, intermediate, and epidermoid cells in variable combinations, and in both cystic and solid/nested formations [1]. Adding to the histopathological complexity of MEC is the fact that these tumors may exhibit a wide range of nuclear atypia (minimal to pronounced), mitotic

activity, proportions of solid to cystic architecture, and infiltrative patterns. In addition, MECs may display extensive clear-cell and oncocytic change [2]. Other less-common variants include sclerosing MEC with/without eosinophilia, unicystic-, sebaceous-, psammomatous-, and Warthin-like MEC. a goblet cell-rich aggressive variant [3,4]. MEC with a focal spindle cell component is not uncommonly encountered, but MEC with a predominance of spindle cells is rare and has only been documented in a few previous studies [5-9]. In most of these cases (spindle cell MEC), there has been a component of either goblet cells/mucocytes and/or glandular differentiation observed. Both these histomorphological features were conspicuously absent in the case presented here (hence the designation “monomorphic”).

Demonstration of the classical CRTC1:MAML2 fusion (NGS) provides very strong support of the diagnosis. The t(11:19)(q21-23;p13) translocation (fusing the CRTC1- MAML2-genes) can be found in up to 80% of MECs of the salivary glands as well as of other organs, including lung, thyroid, cervix, and lacrimal gland. This translocation is seen in both conventional as well as unusual types of MECs, including clear cell predominant, oncocytic, and Warthin-like variants. A subset of salivary gland MECs has also been shown to harbor t(11;15) CRTC3-MAML2 fusion. However, it is important to be aware of that the spectrum of neoplasms associated with this gene fusion has been expanded to include tumors such as metaplastic variants of Warthin tumor, clear cell hidradenoma and hidradenocarcinoma of the skin, and mammary hidradenoma. In addition, a subset of goblet cell-rich odontogenic cysts (not meeting the traditional diagnostic criteria for MEC), also have shown MAML2-rearrangement on FISH [10].

From a differential diagnostic point of view, it is important to be familiar with the much wider histomorphologic spectrum of MEC, than what is currently described in many textbooks. In fact, extension of this phenomenon (e.g. that more uncommon histo-/cytopathological patterns/appearances in classically defined entities), is a most likely outlook in tomorrow’s world of surgical pathology, where based on increasingly available molecular genetic data, much of the taxonomic landscape of neoplastic oncology, is being if not re-written, at least is getting a serious overhaul whereby new tumor entities arise, old categories are being diversified and/or split and where new patterns of commonalities between seemingly diverse tumors are being explored and discovered. The truth of the matter is that none of the definitions, descriptions, and illustrations of MEC hitherto offered in standard text books are applicable to the “monomorphic” variant/pattern of MEC. Based on the nested growth pattern separated by thin blood vasculature, variable cytoplasmic clearing and a mixture of plump spindle-type and epithelioid cells, it is very fair to consider either a myoepithelial neoplasm, a paraganglioma, clear cell sarcoma or a perivascular epithelioid cell tumor (PECOMA) in this case.

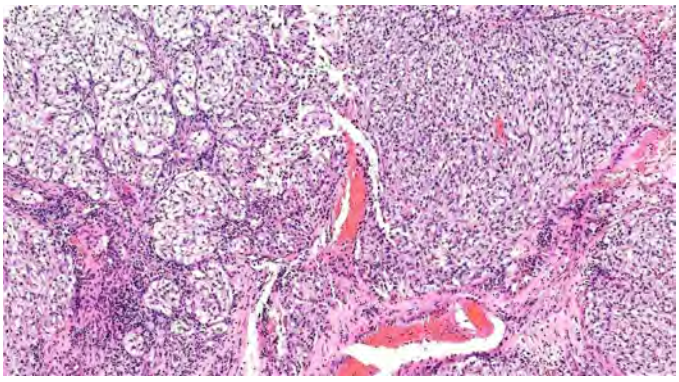

Nested and confluent architectural patterns

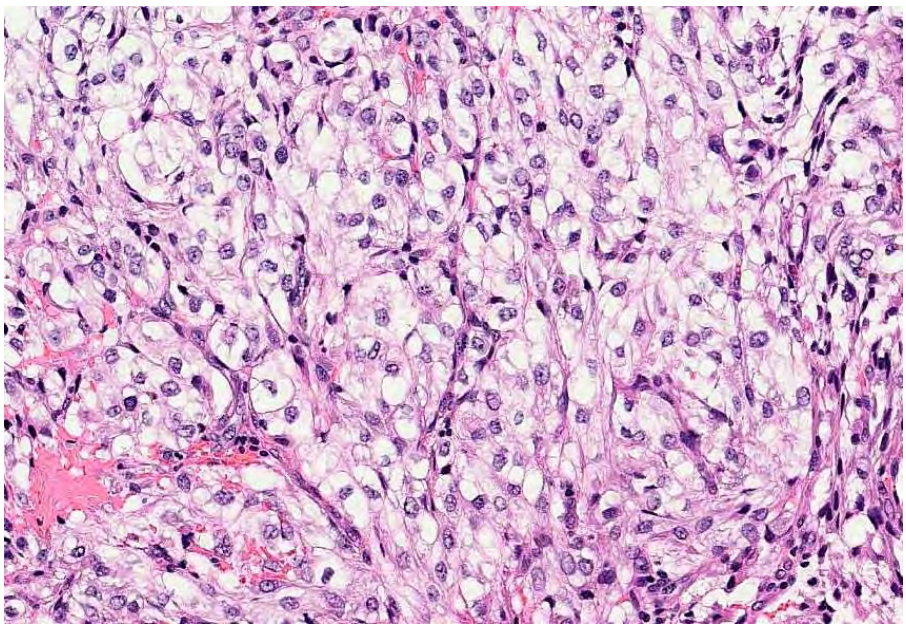

Monomorphic cells with low-grade nuclear features and clear cytoplasm

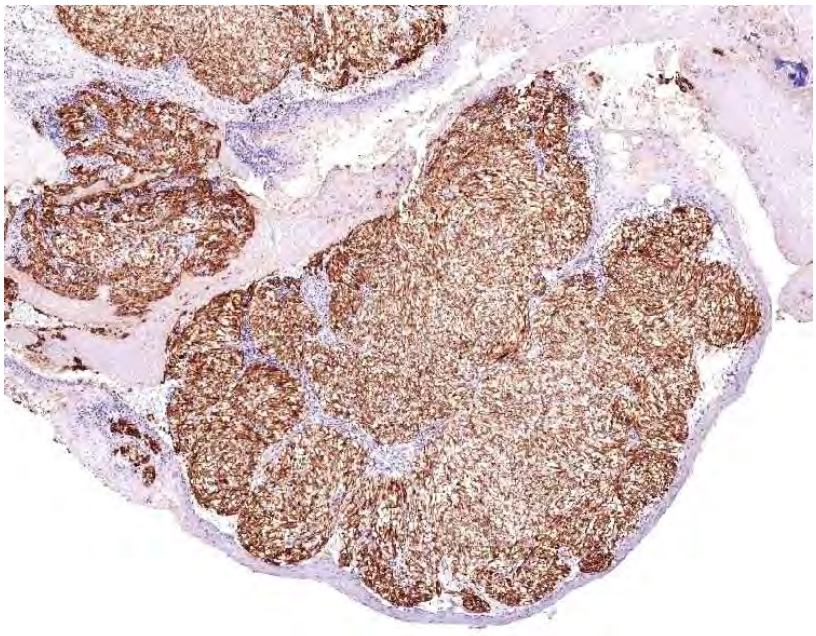

Strong expression of CK7.

References

1. Stewart FW, Foote FW, Becker WF. Muco-epidermoid tumors of salivary glands. Ann Surg. 1945;122:820-844.

2. Weinreb I, Seethala RR, Perez-Ordoñez B, Chetty R, Hoschar AP, Hunt JL. Oncocytic mucoepidermoid carcinoma: clinicopathologic description in a series of 12 cases. Am J Surg Pathol. 2009;33:409-416.
3. Brandwein MS, Ivanov K, Wallace DI, et al. Mucoepidermoid carcinoma: a clinicopathologic study of 80 patients with special reference to histological grading. Am J Surg Pathol. 2001;25:835-845.
4. Luna MA. Salivary mucoepidermoid carcinoma: revisited. Adv Anat Pathol. 2006;13:293-307.
5. Ide F, Mishima K, Saito I. Mucoepidermoid carcinoma with spindle cell change: a low grade lesion potentially mistaken for sarcomatoid dedifferentiation. Head Neck Pathol. 2008;2:227-230.
6. Liyanage RL, Wadusinghearachchi NS, Siriwardena BS, Jayasooriya PR, Tilakaratne WM. Pigmented mucoepidermoid carcinoma with spindle cell differentiation. Oral Surg Oral Med Oral Pathol Oral Radiol. 2014;117:e449-e451.
7. Lucas RB. Pathology of Tumours of the Oral Tissues. London, UK: Churchill; 1964:228-232.
8. Love GL, Sarma DP. Spindle cell mucoepidermoid carcinoma of submandibular gland. J Surg Oncol. 1986;31:66-68.
9. Goh GH, Lim CM, Vanacek T, Michal M, Petersson F. Spindle Cell Mucoepidermoid Carcinoma of the Palatine Tonsil With CRTC1-MAML2 Fusion Transcript: Report of a Rare Case in a 17-Year-Old Boy and a Review of the Literature. Int J Surg Pathol. 2017 Dec;25(8):705-710.
10. sArgyris PP, Wehrs RN, García JJ, Koutlas IG.Fluorescence in-situ hybridization identifies Mastermind-like 2 (MAML2) rearrangement in odontogenic cysts with mucous prosoplasia: a pilot study. Histopathology. 2015 May;66(6):791-797.

12TH INTERNATIONAL AMR PATHOLOGY SLIDE SEMINAR SYMPOSIUM IN ANATOMIC PATHOLOGY

Case – 23

Head and Neck Pathology

Contributed by: ***Alena Skálová***

Clinical History

It was a tumor of the left parotid gland of a 69-year-old man. The tumor measured 50x45 mm, it had a solid consistency and whitish color. After resection, the patient had paresis of n. facialis on the left side. The postoperative irradiation of the parotideal area and neck on the left was administered with a total dose of 60 Gy in 30 fractions. The radiotherapy was completed in Decemnber 2022 and the patient is now without any oncological treatment. On the last check from 2/2/2023 he was without evidence of disease.

Pathological Findings

The tumor demonstrated a lobulated appearance at low power. There were prominent nests, trabeculae and lobules of neoplastic cells divided by fibrous stromal septa with focal myxoid stromal change and production of abundant hyalinized basement membrane-like material in other places. The tumor cells were monotonous with minimal clear to basophilic cytoplasm, round to ovoid or vesicular nuclei, with single prominent nucleoli.

By immunohistochemistry, the tumor was strongly and diffusely positive for p40, p63, cytokeratin AE1/AE3, OSCAR, CK14, CD99 and NKX2.2, while completely negative for CK7, S100, SOX10, GFAP, NUT1, HMGA2, CK20, AR and TTF1. Proliferative activity was high with Ki-67 index 40%.

Molecular findings: FISH for both the *EWSR1* and *FLI1* gene rearrangements were positive supporting the presence of a translocation. The t(11;22) translocation with *EWSR1-FLI1* fusion transcript was detected by next generation sequencing.

Diagnosis

Adamantinoma-like Ewing sarcoma of parotid gland.

Comments

Adamantinoma-like Ewing sarcoma (ALES) is an unusual tumor that is currently classified as a variant of Ewing sarcoma (ES) with complex epithelial differentiation **(1).**

ALES demonstrates the *EWSR1::FLI1* translocation characteristic of Ewing sarcoma despite overt epithelial differentiation including diffuse expression of cytokeratins and p40/p63 **(2).** Although ALESs harbor the *EWSR1::FLI1* translocation **(1)** and corresponding immunohistochemical positivity for CD99 and NKX2.2 characteristic of ES **(3),** they also demonstrate overt evidence of squamous differentiation including cohesive growth, keratin pearl formation, peripheral nuclear palisading, and diffuse positivity for pancytokeratin and p40 **(4).** Not only does this unique morphology and immunophenotype show substantial overlap with various types of carcinoma, but a few cases that likely represent the same entity have been reported as “carcinoma with Ewing family tumor elements”

(4). However, because the *EWSR1::FLI1* translocation has traditionally been considered pathognomonic for ES, most tumors that demonstrate these features have been classified as the variant ALES **(5-7).**

ALES presents a conspicuous diagnostic challenge when it arises in the salivary glands owing to its epithelial differentiation and morphologic overlap with a wide spectrum of basaloid and myoepithelial salivary gland carcinomas **(2).** The morphologic and immunohistochemical findings make ALES susceptible to misclassification as various other salivary tumors including basal cell adenocarcinoma, adenoid cystic carcinoma, squamous cell carcinoma, NUT carcinoma, and myoepithelial carcinoma. Nevertheless, monotonous cytology, despite highly infiltrative growth, and positivity for p40 and CD99 can provide important clues for consideration of ALES, and identification of the defining *EWSR1::FLI1* translocations can confirm the diagnosis. Owing to its rarity, little information is available on the clinical course as well as the optimal treatment of ALES, although there are reports of outcomes similar to or a slightly more favorable one than Ewing sarcoma after treatment with surgery, adjuvant chemotherapy, and radiotherapy **(8).**

References

1. Rooper LM, Bishop JA, Flucke U, Weinreb I. Ewing sarcoma. In: Hellivel T, Lazar AJ, eds. eds. WHO Classification of Tumours Editorial Board. Head and neck tumours [Internet; beta version ahead of print]. Lyon, France, 2022, International Agency for Research on Cancer, (WHO classification of tumours series, 5th ed.; vol. 9). Available from: https://tumourclassification.iarc.who.int/chapters/52
2. Bishop JA, Alaggio R, Zhang L, et al. Adamantinoma-like Ewing family tumors of the head and neck: a pitfall in the differential diagnosis of basaloid and myoepithelial carcinomas. *Am J Surg Pathol.* 2015; 39(9):1267-74.
3. Shibuya R, Matsuyama A, Nakamoto M, et al. The combination of CD99 and NKX2.2, a transcriptional target of EWSR1-FLI1, is highly specific for the diagnosis of Ewing sarcoma. *Virchows Arch.* 2014;465:599–605.
4. Oliveira G, Polonia A, Cameselle-Teijeiro JM, et al. EWSR1 rearrangement is a frequent event in papillary thyroid carcinoma and in carcinoma of the thyroid with Ewing family tumor elements (CEFTE). *Virchows Arch*. 2017;470:517–525.
5. Bal M, Shah A, Rekhi B, et al. Adamantinoma-Like Ewing Sarcoma of the Head and Neck: A Case-Series of a Rare and Challenging Diagnosis. *Head Neck Pathol*. 2022;16(3):679-694.
6. Rooper LM, Jo VY, Antonescu CR, Nose V, Westra WH, Seethala RR, Bishop JA. Adamantinoma-like Ewing Sarcoma of the Salivary Glands: A Newly Recognized Mimicker of Basaloid Salivary Carcinomas. *Am J Surg Pathol.* 2019;43(2):187-194.
7. Lezcano C, Clarke MR, Zhang L, et al. Adamantinoma-like Ewing sarcoma mimicking basal cell adenocarcinoma of the parotid gland: a case report and review of the literature. *Head Neck Pathol.* 2015;9:280–285.
8. Rooper LM, Bishop JA. Soft Tissue Special Issue: Adamantinoma-Like Ewing Sarcoma of the Head and Neck: A Practical Review of a Challenging Emerging Entity. *Head Neck Pathol*. 2020;14:59–69.

12TH INTERNATIONAL AMR PATHOLOGY SLIDE SEMINAR SYMPOSIUM IN ANATOMIC PATHOLOGY

Case – 24

Head and Neck Pathology

Contributed by: ***Göran Elmberger***

Clinical History

An 81-year-old man with epistaxis since 1.5 years. Previous history of gastric DLCBCL 14 years previously. CT H&N revealed a 3x4.2x5 cm sized destructive sinonasal lesion interpreted as malignant tumor. First, a biopsy was taken and later tumor reducing curettage was performed.

Pathological Findings

Imprint cytology from biopsy showed macrophage like cells with intracytoplasmic negative staining rod like structures. Biopsy and resection showed a dense proliferation of spindle cells with somewhat epithelioid cytoplasm occasionally forming storiform patterns and a rare non-necrotizing granuloma. A sparse focal infiltrate of lymphocytes and plasma cells was noted. No necrosis. No significant cellular atypia. In more central parts of the resection specimen sclerotic areas were seen. Focally, destructive invasion of hyaline cartilage. In some areas, the tumefactive process could be seen around nerves and diffusely infiltrating soft tissues. Focally lesional cells revealed a more foamy character of the cytoplasm. Few areas of neutrophilic microabscesses detected. After initial evaluation, ancillary stains were performed to narrow down the broad differential diagnoses of sinonasal fibroinflammatory lesions considering reactive, infectious and neoplastic entities.

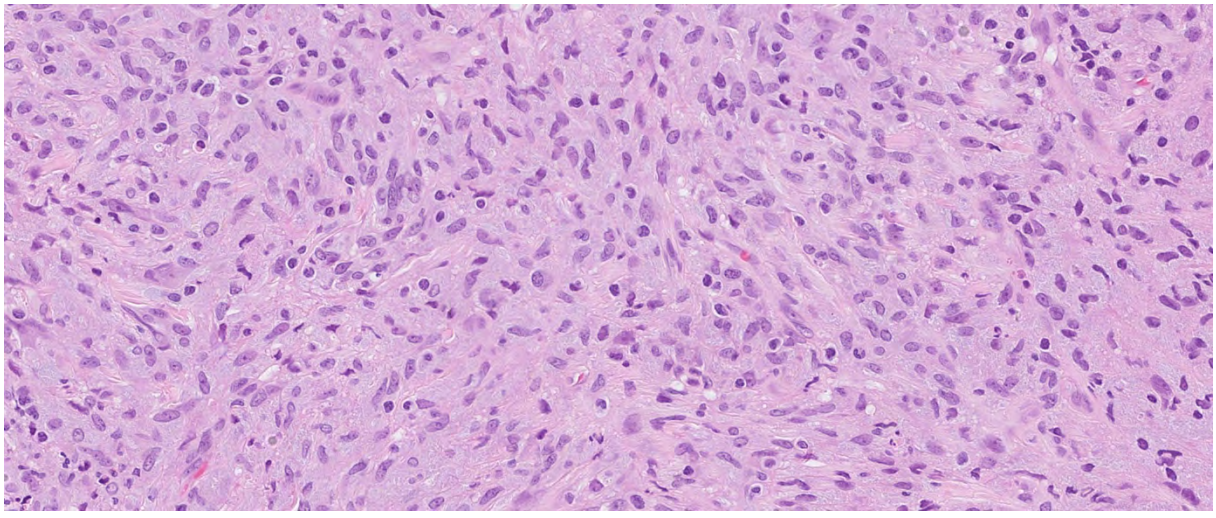

HE x 40.

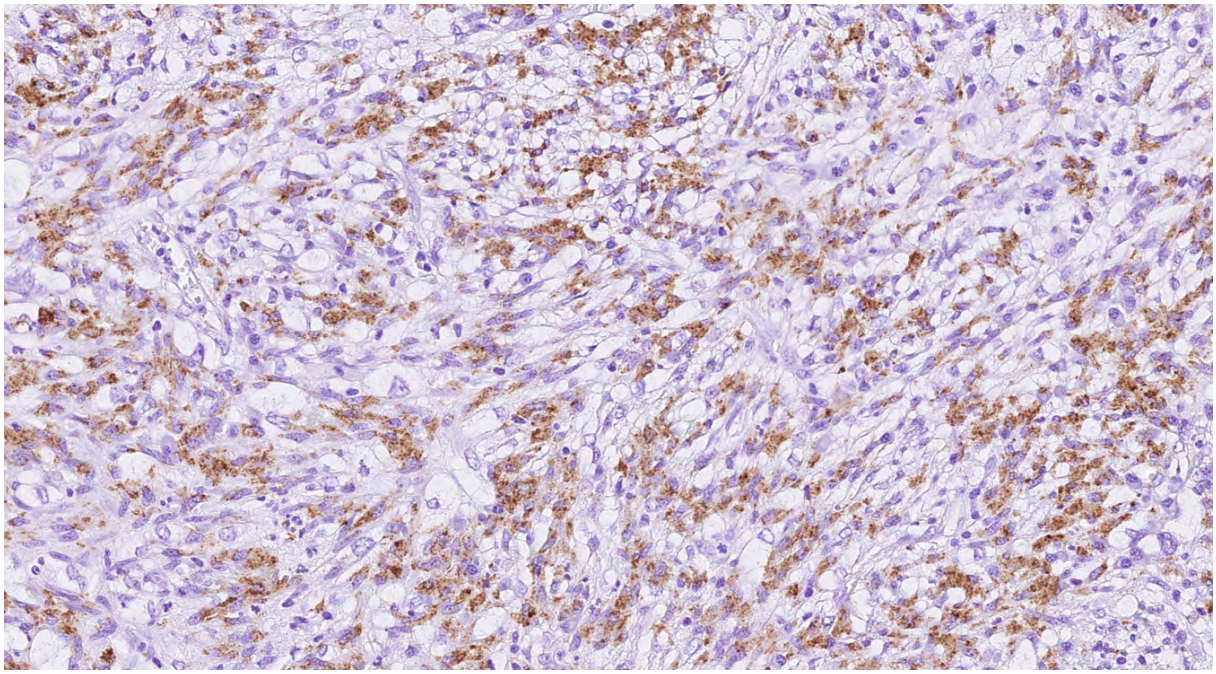

IHC TB x 40.

Antibody/Histochemical stain	Result
CKMNF116	-
SMA, Desmin	-
CD5,10,20,23,25,117,138	-
S100, SOX10	-
CD68, CD163	+
TB IHC	+
TB histochemistry ZN	+
PAS+/-D	-
Gram	-

A newly validated local confirmative molecular RT-PCR based analysis confirmed presence of non-tuberculous mycobacteria (NTM).

Diagnosis

Sinonasal Mycobacterial Spindle Cell Pseudotumor.

Comments

Follow-up

Microbiological work-up revealed Mycobacterium Avium Intracellulare (MAI) and the patient received proper medical treatment. Disease stabilized radiologically. Treatment still administered 10 months after diagnosis. Reviewing our LIS specimen history, I noted that the patient had a biopsy from a chronic ulcer at vestibulum nasi five years previously with findings of pseudoepitheliomatous squamous epithelial hyperplasia and diffuse histiocytic infiltrate in lamina propria. At that time, TB IHC was strongly positive with plentiful intracellular mycobacteria but external molecular analysis could not confirm TBC or NTM with PCR. In addition, a 16S ribosomal RNA subunit analysis could not detect any infectious bacterial, fungal or yeast infectious agents including TBC or NTM. In retrospect, this probably was a first manifestation of atypical mycobacteriosis where unfortunately molecular pathological analysis could not confirm the diagnosis. In the final report, the local pathologist still suspected infection and further microbiological work-up was recommended. Unfortunately, a clear diagnosis of atypical mycobacteriosis was not made at that time and somehow the correct diagnosis and therapy was thus delayed and allowed for this large and destructive sinonasal tumor to develop. In retrospect, one can feel that a strongly positive IHC or histochemical finding of mycobacteria should not be negated by a probably false negative molecular finding. The patient is probably immunocompromised after gastric lymphoma and aggressive chemotherapy.

Algorithmic Approach to Fibroinflammatory Sinonasal Tract Lesions

Fibroinflammatory lesions of the sinonasal tract are one of the most common head and neck lesions submitted to surgical pathology. When the fibroinflammatory pattern represents the lesion (i.e., not surface reactive ulceration), an algorithmic approach can be useful. Separated into reactive, infectious, and neoplastic, and then further divided based on common to rare, this logical progression through a series of differential considerations allows for many of these lesions to be correctly diagnosed. The reactive lesions include chronic rhinosinusitis and polyps, granulomatosis with polyangiitis, and eosinophilic angiocentric fibrosis. Infectious etiologies include acute invasive fungal rhinosinusitis, rhinoscleroma, and mycobacterial infections. The neoplastic category includes lobular capillary hemangioma, inflammatory myofibroblastic tumor, and NK/T-cell lymphoma, nasal type. Utilizing patterns of growth, dominant cell types, and additional histologic features, selected ancillary studies help to confirm the diagnosis, guiding further clinical management.

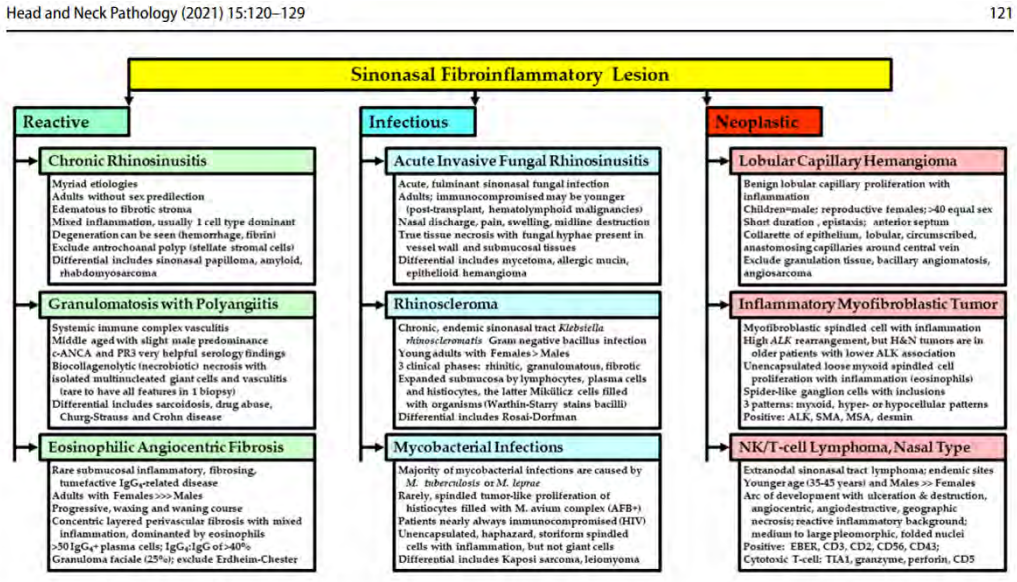

Fig. 1 A representation of several major categories to consider in the evaluation of sinonasal tract fibroinflammatory lesions

From Lester Thompson (Reference 7)

Mycobacterial spindle cell pseudotumor

Mycobacterial spindle cell pseudotumor (MSP) is a rare tumor-like lesion characterized by the proliferation of spindle cells engorged with mycobacterial microorganisms. This entity has been described by several names and histologic presentations and as mimicking neoplastic processes. Most reported cases of MSP occur in the lymph nodes, skin, spleen, and brain in patients who are immunocompromised, particularly following solid organ transplant and in those with AIDS. It can present as a single mass or multiple masses and the term "pseudotumor" has been coined because the clinical and imaging findings of the lesion mimic those of malignant tumors. Although the imaging features of MSP can be nonspecific, understanding of the pathophysiologic features and natural history is important in the preoperative differential diagnosis of soft-tissue malignant lesions and its recognition can prevent unnecessary surgical intervention. Mycobacterial spindle cell pseudotumor should be included in the differential diagnoses of a spindle cell lesion especially in immunosuppressed patients.

Clinical issues

Pseudoneoplastic spindle cell proliferation usually caused by M. Avium-Intracellulare nearly always in an immunocompromised host. Rarely occur in mucosal sites such as sinonasal tract.

Epidemiology

This is a rare lesion but incidence is increasing. Condition occurs over wide age range. Equal sex distribution.

Histological features

Cellular proliferation of bland spindle-shaped histiocytic cells in storiform to fascicular pattern. Admixed sheets of foamy histiocytes occur. Often associated lymphocytes and plasma cells. Effacement of mucosal architecture and focal necrosis may be seen. No granulomas or multinucleated histiocytic cells.

Histochemistry

Lots of AFB in Ziehl-Nielsen stain or other mycobacterial stain. Bacilli are engulfed by the spindle cells acting as macrophages.

Immunohistochemistry

Mycobacterial IHC usually strongly positive.

Genetic testing

PCR based techniques can be used to verify and subtype mycobacteria species.

Treatment

Guidelines based on species of mycobacteria and susceptibility testing of isolate. Often prolonged multi-therapy is needed to cure condition.

Differential diagnosis

- Rhinoscleroma
- Fibrohistiocytic neoplasm
- Fibrosarcoma
- Kaposi sarcoma
- Smooth muscle neoplasms
- Inflammatory myofibroblastic tumor

- Biphenotypic sinonasal sarcoma
- HD nodular sclerosis

Non-Tuberculous Mycobacteria (NTM)

Nontuberculous mycobacteria (NTM) species are mycobacterial species other than those belonging to the Mycobacterium tuberculosis complex (eg, M. tuberculosis, Mycobacterium bovis, Mycobacterium africanum, and Mycobacterium microti) and Mycobacterium leprae. NTM are generally free-living organisms that are ubiquitous in the environment. Molecular identification techniques, including whole-genome sequencing, have identified approximately 200 NTM species. Although anyone can get an NTM infection, NTM are opportunistic pathogens placing some groups at increased risk, including those with underlying lung disease or depressed immune systems. These pathogens are typically not transmitted person-to-person. NTM are environmental organisms that can be found in soil, dust, and water including natural water sources such as lakes, rivers, and streams and municipal water sources such as water that people drink or shower in. NTM can form difficult-to-eliminate biofilms, which are collections of microorganisms that stick to each other, and adhere to surfaces in moist environments, such as the insides of plumbing in buildings.

NTMs can cause infections in a wide variety of body sites, most commonly the lungs and in the following areas:

- Skin and soft tissue (typically following surgery, trauma, injection of medications or other substances)
- Device associated infections (e.g., central line associated bloodstream infection, exit site infections, pacemaker pocket site infections, etc.)
- Lymph nodes (most commonly in children)
- Blood or other usually sterile locations in the body (disseminated) (most commonly in immunocompromised patients, such as those with HIV or AIDS, but may also be due to invasive medical devices or procedures)

Symptoms can be vague and nonspecific, such as:

- Fever
- Weight loss
- Night sweats
- Decreased appetite
- Loss of energy

Other symptoms depend on the site of infection and can include cough, shortness of breath, blood in the sputum, and rashes.

Table 1-1. Atypical *Mycobacterium* Species

Slow Growing[a]	Rapid Growing
Established pathogens	**Established pathogens**
M. avium-intracellulare complex	
M. haemophilum	*M. abscessus*
M. kansasii	*M. chelonae*
M. leprae	*M. fortuitum*
M. malmoense	
M. marinum	**Newly discovered or emerging mycobacteria**
M. scrofulaceum	
M. simiae	*M. agri*
M. szulgae	*M. alvei*
M. ulcerans	*M. bonickei*
M. xenopi	*M. brumae*
	M. chitae
Newly discovered or emerging mycobacteria	*M. confluentis*
	M. fortuitum biovariant subtypes
M. bohemicum	*M. hassiacum*
M. branderi	*M. houstonense*
M. celatum	*M. immunogenum*
M. conspicuum	*M. mageritense*
M. genavense	*M. mucogenicum*
M. heckeshornense	*M. novocastrense*
M. heidelbergense	*M. porcinum*
M. interjectum	*M. senegalense*
M. intermedium	*M. septicum*
M. kubiacae	*M. smegmatis* group
M. lentiflavum	*M. goodie*
M. triplex	*M. peregrinum*
M. tusciae	*M. smegmatis (sensu stricto)*
	M. wolinskyi

[a]Other notable slow-growing mycobacteria, such as *M. gordonae* and *M. terrae*, are questionable pathogens.

Somoskovi A, Mester J, Hale YM, Parsons LM, Salfinger M. Laboratory diagnosis of nontuberculous mycobacteria. Clin Chest Med 2002;23:585–97.

Conclusions

- Even though there is wide diversity in the fibroinflammatory category of sinonasal tract lesions, a systematic approach based on general categories (reactive, infectious, neoplastic) and proceeding from the most common to the rare, will allow for appropriate diagnosis utilizing selected ancillary techniques
- While infectious pseudotumors are rarely encountered in the practice of surgical pathology, it is of importance to realize that infectious processes can closely mimic neoplastic lesions. Identification of these processes and the causative organisms is of particular significance since they can be cured by antibiotic therapy
- Mycobacterial spindle cell pseudotumors should be considered in the differential diagnosis of tumours with spindle cell proliferation
- Mycobacterial spindle cell pseudotumor is a rare condition associated primarily with immunodeficiency, especially with HIV infection
- The use of acid-fast stain is a simple and sensitive method to distinguish MSP from other rare spindle cell lesions
- TB IHC is sensitive and in our laboratory detect TBC and NTM
- Molecular diagnosis should be applied for typing and is usually a sensitive and specific ancillary technique
- Microbiological cultivation and drug sensitivity testing is golden standard but often time consuming and sometimes insensitive
- More sophisticated techniques sometimes does not work and a negative answer cannot rule out infection if IHC and or histochemical stains are positive
- In a case with typical histology and affirmative special stains a definitive diagnosis should be made even in absence of molecular and microbiological confirmation

- Different Mycobacteria have been implicated but Mycobacterium Avium complex is the most common mycobacterium in MSP
- Antimycobacterial therapy is significantly associated with successful outcome in patients with MSP and antimicrobial susceptibility testing is currently recommended by expert panels on a routine basis. Antimycobacterial treatment is continued for at least 12 months

References

1. Helliwell TR. Non-infectious inflammatory lesions of the sinonasal tract. Head Neck Pathol. 2016;10(1):32–9.
2. Sfeir MM, Schuetz A, Van Besien K, et al. Mycobacterial spindle cell pseudotumour: epidemiology and clinical outcomes. J Clin Pathol. 2018;71(7):626–30.
3. Ilyas S, Youssef D, Chaudhary H, Al-Abbadi MA. Mycobacterium-avium intracellulare associated inflammatory pseudotumor of the anterior nasal cavity. Head Neck Pathol. 2011;5(3):296–301.
4. Brandwein M, Choi HS, Strauchen J, Stoler M, Jagirdar J. Spindle cell reaction to nontuberculous mycobacteriosis in AIDS mimicking a spindle cell neoplasm. Evidence for dual histiocytic and fibroblast-like characteristics of spindle cells. Virchows Arch A. 1990;416(4):281–6.
5. Gunia S, Behrens MH, Stosiek P. Mycobacterial spindle cell pseudotumor (MSP) of the nasal septum clinically mimicking Kaposi's sarcoma: case report. Rhinology. 2005;43(1):70–1.
6. Herdman AV, Steele JC Jr. The new mycobacterial species emerging or newly distinguished pathogens. Clin Lab Med. 2004;24(3):651–90 vi.
7. Algorithmic Approach to Fibroinflammatory Sinonasal Tract Lesions. Thompson LDR. Head Neck Pathol. 2021 Mar;15(1):120-129.
8. Atypical mycobacteria: an important differential for the general physician. Rahama O, Thaker H. Clin Med (Lond). 2013 Oct;13(5):504-6.
9. Inflammatory pseudotumor: the great mimicker. Patnana M, Sevrukov AB, Elsayes KM, Viswanathan C, Lubner M, Menias CO. AJR Am J Roentgenol. 2012 Mar;198(3):W217-27.
10. The great mimicker: a rare case of head and neck inflammatory pseudotumour in the presence of human immunodeficiency virus. Ramotar H, Cheung L, Pitkin L.
11. J Laryngol Otol. 2016 Jan;130(1):107-10. Inflammatory pseudotumor of the nasal cavity. Huang WH, Dai YC. Am J Otolaryngol. 2006 Jul-Aug;27(4):275-7.
12. Nontuberculous mycobacteria-associated spindle cell pseudotumor of the nasal cavity: a case report. Ohara K, Kimura T, Sakamoto K, Okada Y. Pathol Int. 2013 May;63(5):266-71.
13. The Rise of Non-Tuberculosis Mycobacterial Lung Disease. Ratnatunga CN, Lutzky VP, Kupz A, Doolan DL, Reid DW, Field M, Bell SC, Thomson RM, Miles JJ. Front Immunol. 2020 Mar 3;11:303.

12TH INTERNATIONAL AMR PATHOLOGY SLIDE SEMINAR SYMPOSIUM IN ANATOMIC PATHOLOGY

Case – 25

Head and Neck Pathology

Contributed by: ***Paul Wakely***

Clinical History

A 75-year-old woman (history of hypothyroidism and rheumatoid arthritis) presented with a L neck mass originating from anterior inferior parotid gland that had been present for 10 years. It has increased in the last 8 months with occasional pain. Ultrasound showed a 3 cm. nodule in parotid gland with calcifications. Core needle biopsy showed fibrous tissue with aggregates of atypical glandular epithelium. She underwent L superficial parotidectomy, facial nerve preservation, and selective neck dissection. She is without evidence of disease 1 year later.

Pathological Findings

The specimen consisted of a 33.0 gram 5.2 x 4.2 x 3.8 cm. parotid gland mass with attached lymph nodes and submandibular gland. Cut sections revealed a 3.1 x 3.0 x 2.8 cm. circumscribed tan-brown mass with foci of calcifications. The mass did not involve the attached submandibular gland. Neck dissection showed no metastatic disease. Light microscopy showed a partially encapsulated multinodular tumor with scattered foci of dystrophic calcification, and coagulation necrosis. The tumor contained a monotonous proliferation of small bilayered ducts within an eosinophilic hyalinized matrix. Ducts showed a biphasic histology with an eosinophilic luminal cell layer, and an abluminal clear cell layer. Abluminal myoepithelial cells had abundant optically clear cytoplasm and discrete cell borders. In areas, larger ducts with wider luminal spaces were lined by larger cells containing single macronuclei. Immunohistochemical (IHC) staining showed positive staining of luminal cells with EMA and CAM 5.2, and staining of the clear abluminal myoepithelial cells with calponin, smooth muscle actin, p63, SOX-10, and p40.

Diagnosis

Epithelial-myoepithelial carcinoma of parotid.

Comments

Epithelial-myoepithelial carcinoma (EMC) is a low-grade salivary gland (SG) malignancy occurring in the 6th -7th decade of life accounting for only about 1% of all SG tumors. Over 50% arise within the parotid gland, about 13% in the submandibular gland, and the remaining cases in minor SG. The histologic hallmark is a solid proliferation of bilayered ducts with small lumens having eosinophilic inner luminal cells and outer abluminal myoepithelial cells. This outer layer contains conspicuous cytoplasmic clearing which in some cases is so predominant that it mimics a solid clear cell carcinoma. Papillary and cystic foci may also be seen. Oncocytic and sebaceous variants of EMC have been described. Molecularly, no specific translocation has been found in EMC although a significant number of EMCs harbor *HRAS* mutations.

Differential diagnoses includes other biphasic SG tumors including adenoid cystic CA (AdCCA), pleomorphic adenoma, basal cell adenocarcinoma, myoepithelial CA, and clear cell CA. Clinically, the most important neoplasm to separate from EMC is AdCCA. Although EMC may have a cribriform growth pattern imitating AdCCA, when present it is typically focal. IHC staining is similar in both tumors. In difficult cases, a positive *MYB* FISH test would indicate a diagnosis of AdCCA.

References

1. Skálová A et. Al. Epithelial-myoepithelial carcinoma. WHO Classification of Tumours, 5th ed. 2023.
2. Corio RL, et al. Epithelial-myoepithelial carcinoma of intercalated duct origin. A clinicopathologic and ultrastructural assessment of sixteen cases. Oral Surg Oral Med Oral Pathol. 1982;53:280-7.
3. Bishop JA et al. AFIP Atlases of Tumor Pathology. Tumors of the Salivary Glands, Fascicle 5, 5th series. 2021; 445-61.
4. Seethala R et al. Epithelial-myoepithelial carcinoma: a review of the clinicopathologic spectrum and immunophenotypic characteristics in 61 tumors of the salivary glands and upper aerodigestive tract. Am J Surg Pathol. 2007;31: 44-57.
5. Vazquez et al. Epithelial-myoepithelial carcinoma of the salivary glands: an analysis of 246 cases. Otolaryngol Head Neck Surg 2015; 153: 569-74.

12TH INTERNATIONAL AMR PATHOLOGY SLIDE SEMINAR SYMPOSIUM IN ANATOMIC PATHOLOGY

Case – 26

Head and Neck Pathology

Contributed by: ***Franco Fedeli***

Clinical History

A 41-year-old man presented with a tumor of the parotid gland.

Pathological Findings

*Macroscopic findings***:** cut surfaces of the unfixed resection specimen revealed a well circumscribed 3,5cm mass with a spongiform, granular and focally cystic cut surface.

*Histological Findings***:** microscopically, the tumor was well circumscribed, composed of cords and islands of epithelium with sebaceous differentiation, associated with lymphoid tissue including germinal centers. Cystic spaces were lined by multilayered epithelium including sebaceous and squamous cells.

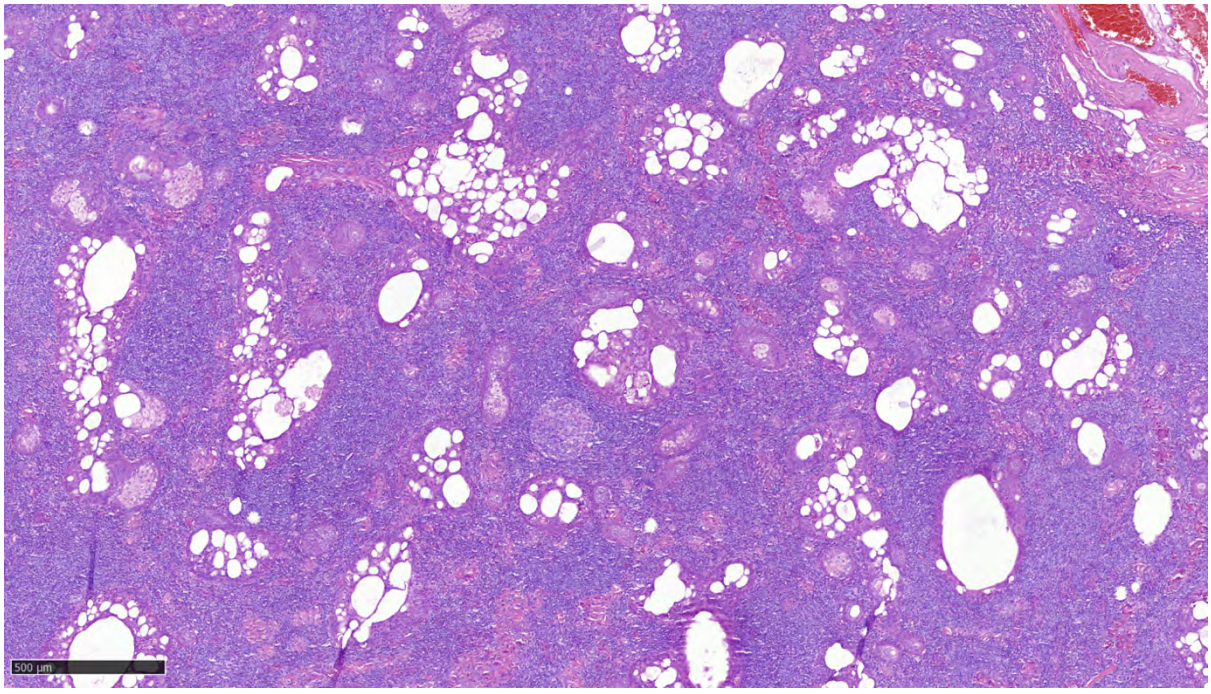

Immunohistochemical Findings: the epithelial cells expressed basal cell markers p63, 34BE12, CK5/6, and the luminal glandular cells expressed CK7. Myoepithelial cells stained with calponin were absent.

Diagnosis

Sebaceous Lymphadenoma.

Comments

Although most commonly associated with hair follicles, ectopic sebaceous glands can be identified independently. These lesions can be found mainly on the eyelids and oral mucosa. Occasionally it may arise in the major salivary glands. Benign tumors can rarely originate from these sebaceous glands, such as sebaceous adenoma, sebaceous lymphadenoma or sebaceous carcinoma. Despite the common occurrence of sebaceous differentiation in salivary glands, sebaceous lymphadenomas are very rarely encountered in major salivary gland.

Sebaceous lymphadenoma is a rare benign tumor of the parotid gland accounting for only 0.196% of all adenomas which is histologically characterized by islands of epithelium showing sebaceous differentiation distributed in hyperplastic lymphoid tissue. Rawson and Horn (1) first described this benign neoplasm in 1950 and the name "sebaceous lymphadenoma" was given by McGavran et al. in 1960 (2). The majority of these lesions occur in the parotid glands or periparotid lymph nodes. Sebaceous lymphadenoma of the parotid gland typically presents as a painless mass in patients over 50 years of age. It is known to occur equally in both sexes.

The origin of sebaceous lymphadenoma is controversial. The commonly accepted sources are branchial clefts and salivary gland inclusions in lymph nodes (3). The theory is based on the fact that ectopic salivary gland tissue in intraparotid or periparotid lymph nodes is a common findings. Published case reports of sebaceous lymphadenoma do not often give a pre-operative diagnosis. In those cases where a pre-operative diagnosis was made on clinical, radiological or cytological grounds, they are found to be varied.

Sebaceous lymphadenoma was not correctly identified by pre-operative investigations in the majority of cases. Boyle and Meschter in a single case report (4), suggested that the FNA findings in a sebaceous lymphadenoma were distinctive and accurately reflected the histological morphology, although the lesion is so rare that the diagnosis may be easily overlooked (tab1). The clinical presentation of sebaceous lymphadenoma is similar to that of pleomorphic adenoma i.e., a painless parotid swelling with no facial nerve involvement. Complete surgical excision is the modality of therapy for sebaceous lymphadenoma. Recurrence is rare following complete removal. Transformation to a sebaceous lymphadenocarcinoma has been reported but is extremely rare (5).

Table I. Examples of case reports with documented pre-operative diagnosis and final diagnosis of sebaceous lymphadenoma of parotid gland.

Pre-operative diagnosis	Age (yrs)/ Sex	Author	Pre-operative investigation	Surgery	Follow-up
Sebaceous lymphadenoma	56/F	Firat et al. (2000)	FNAC & CT scan	Superficial parotidectomy	NER at 12 months
Sebaceous lymphadenoma	75/M	Boyle & Meschter (2004)	FNAC	Excison (unspecified)	Not stated
Warthin's tumour	72/M	Case 1	FNAC	Superficial parotidectomy	NER at 16 months
Pleomorphic adenoma	57/M	Case 2	FNAC	Superficial parotidectomy	NER at 12 months
Pleomorphic adenoma	53/F	Kwon et al. (2002)	CT scan	Superficial parotidectomy	Not stated
Pleomorphic adenoma*	68/F	Shukla & Panicker (2003)	FNAC	Total conservative parotidectomy	Not stated
Acinic cell adenocarcinoma†	78/F	Mayorga et al. (1999)	FNAC	Superficial parotidectomy	NER at 13 months
Mucoepidermoid carcinoma	65/F	Assor (1970)	Needle biopsy (unspecified)	Total parotidectomy	NER at 6 months

* Final diagnosis was synchronous ipsilateral sebaceous lymphadenoma and squamous cell carcinoma
† Final diagnosis was synchronous ipsilateral sebaceous lymphadenoma and acinic cell adenocarcinoma
NER = No evidence of recurrence

References

1. Rawson AJ, Horn RC Jr. Sebaceous glands and sebaceous gland-containing tumors of the parotid salivary gland; with a considera- tion of the histogenesis of papillary cystadenoma lymphomatosum. Surgery. 1950;27(1):93–101
2. McGavran MH, Bauer WC, Ackerman LV. Sebaceous lymphadenoma of the parotid salivary gland. Cancer 1960;13:1185-7.
3. Gnepp DR, Brannon R. Sebaceous neoplasms of salivary gland origin. Report of21 cases. Cancer 1984;53:2155-70.
4. Boyle Jl, Meschter Sc. Fine needle aspiration cytology of a sebaceous lymphadenoma. Acta Cytol 2004;48:551-4.
5. Seethala RR, Thompson LDR, Gnepp DR, Barnes EL, Skalova A, Montone K, *et al*. Lymphadenoma of the salivary gland: Clinicopathological and immunohistochemical analysis of 33 tumors. Mod Pathol 2012;25:26–35.

12TH INTERNATIONAL AMR PATHOLOGY SLIDE SEMINAR SYMPOSIUM IN ANATOMIC PATHOLOGY

Case – 27

Head and Neck Pathology

Contributed by: ***Franco Fedeli***

Clinical History

A 36-year-old woman presented with a tumor of the soft palate.

Pathological Findings

Macroscopic findings: macroscopically a submucosal nodule of 2x1,5x1 cm without surface ulceration was seen. The tumor cross section manifested as an unencapsulated, multilobulated, firm, beige to tan mass with lobulated and infiltrative borders.

Histological Findings: histopathological examination revealed an unencapsulated tumor within the underlying connective tissue approximating the surface epithelium, with a varied pattern of arrangement of tumor cells that included solid nests, strands, ducts, tubular and papillary patterns and was lined by 1-2 layers of oval/cuboidal cells. Tumor cells were small and uniform, with bland, minimally hyperchromatic nuclei, inconspicuous to slightly enlarged nucleoli, and scant to moderately abundant, clear to eosinophilic cytoplasm. Mitoses were rare. Atypical mitotic figures were not found. Necrosis was not seen. Perineural growth was seen at the periphery of the lesion.

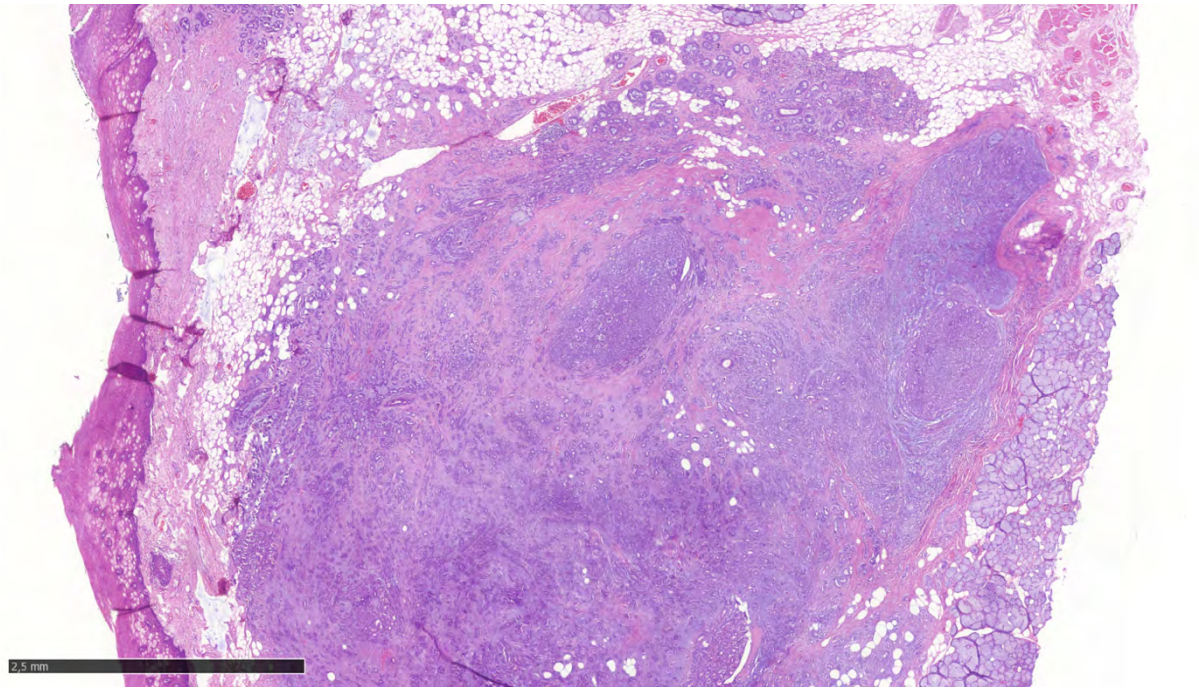

Immunohistochemical Findings: Immunohistochemically the tumor cells were positive for cytokeratin, vimentin and S-100. Molecular study was not available.

Diagnosis

Polymorphous (low-grade) adenocarcinoma.

Comments

The term polymorphous low-grade adenocarcinoma was coined by Evans and Batsakis (1) in 1984 when reporting a series of 14 cases of a salivary gland tumor with new distinctive histological features and lobular carcinoma by Freedman *et al*. (2) Currently, this neoplasm is documented and known as polymorphous adenocarcinoma (PAC) by WHO Classification of Salivary Gland Tumors (2017)

PAC is nowadays widely recognized and considered to be the most common malignant intraoral salivary tumor second to mucoepidermoid carcinoma.

Palate (49%–77.8%) is the most common site of origin of PAC, followed by buccal mucosa or upper lip (7.4%–13.4%). It may also involve the tongue, floor of the mouth, alveolar ridge, and lower lip. (3) Very rarely, it involves major salivary glands such as parotid, submandibular, and sublingual in <5% cases. Furthermore, it is also seen in other sites like breast, vagina, lung. PAC is mainly seen in adult patients from 3rd to 7th decades with a highest incidence from 5th to 6th decades of life. It occurs most commonly in females than in males. Some reports have suggested that it arises *de novo* or as neoplasms developing in a preexistent pleomorphic (carcinoma ex pleomorphic adenoma)

This tumor shows a variety of growth patterns solid, tubular, cribriform, and papillary, but consist of one basic cell type with ovoid nuclei with powdery chromatin. The tumor stroma is composed of fibrous tissue that shows varying degrees of hyalinization and myxoid change; however, the chondromyxoid matrix that typifies PA is absent.

Papillary predominant tumors and extra-palatal tumors are generally more aggressive. Immunohistochemical staining aids in the diagnosis of PAC, as tumor cells stain positive with S100, Epithelial membrane antigen (EMA), and CK7. p63 also stains positive.

Pleomorphic adenoma, monomorphic adenoma, and adenoid cystic carcinoma share the histologic characteristics as PAC, so they are considered the differential diagnosis. Lack of infiltration is seen in pleomorphic adenoma and monomorphic adenoma and pleomorphic adenoma presents with chondromyxoid matrix so they can be distinguished from PAC but they have the propensity for perineural invasion. Pleomorphic adenoma stains are positive for glial fibrillary acidic protein, but PAC is negative. PAC is often confused with adenoid cystic carcinoma because of similarities in growth pattern and neurotropism. Adenoid cystic carcinoma shows histologic patterns such as cribriform, tubular and solid, and exhibit basaloid cells with scant cytoplasm, PAC illustrates some spindling. PAC shows strong diffuse positivity S100 and EMA while adenoid cystic carcinoma stains much less diffusely.

Low-grade papillary adenocarcinoma (LGPA) is also considered a differential for PAC. However, LGPA demonstrates a more aggressive behavior, and the rate of local recurrence and regional lymph node metastasis are higher.

Polymorphous adenocarcinoma, cribriform subtype (cribriform adenocarcinoma of salivary glands; CASG) was initially reported at the base of the tongue and later in other minor salivary gland sites. CASG is characterized by a multinodular growth pattern separated by fibrous septa, relatively uniform solid, cribriform and microcystic architecture, and optically clear nuclei. Glomeruloid and papillary structures, peripheral palisading and clefting may be observed. Compared with classic PAC,

CASG is associated with a propensity to base of the tongue location and a higher risk of lymph node metastasis and may require additional treatments (e.g., neck dissection).

PAC is associated with PRKD1 mutations and adenoid cystic carcinoma shows MYB or MYBL1 gene rearrangements (4). These genetic abnormalities are pathognomonic of the tumors and can also be useful in the differential diagnosis. PAC sometimes erodes the underlying bone and may even show perivascular or perineural invasion. Metastases are very rare and even if present is mostly restricted to the regional lymph nodes.

Wide limited local excision is the choice of treatment approach. If tumor is seen at surgical margin, then postoperative radiotherapy is suggested. Adjuvant radiotherapy and radical surgical excision are recommended in cases of cervical metastases. In recurrent cases, radical surgery is done.

References

1. Batsakis JG, Pinkston GR, Luna MA, Byers RM, Sciubba JJ, Tillery GW. Adenocarcinomas of the oral cavity: A clinicopathologic study of terminal duct carcinomas. J Laryngol Otol 1983;97:825-35.
2. Freedman PD, Lumerman H. Lobular carcinoma of intraoral minor salivary gland origin. Report of twelve cases. Oral Surg Oral Med Oral Pathol 1983;56:157-66.
3. Gnepp DR, Chen JC, Warren C. Polymorphous low-grade adenocarcinoma of minor salivary gland. An immunohistochemical and clinicopathologic study. Am J Surg Pathol 1988;12:461-8.
4. Weinreb I, Zhang L, Tirunagari LM, Sung YS, Chen CL, Perez-Ordonez B, et al. Novel PRKD gene rearrangements and variant fusions in cribriform adenocarcinoma of salivary gland origin. Genes Chromosomes Cancer 2014;53:845-56.

12TH INTERNATIONAL AMR PATHOLOGY SLIDE SEMINAR SYMPOSIUM IN ANATOMIC PATHOLOGY

Case – 28

Head and Neck Pathology

Contributed by: ***Vania Nosé***

Clinical History

A 19-year-old female presented with an incidental finding of a palpable mass in the left lobe of the thyroid gland. She had no relevant past medical history. Her family history, however, included a sister with rhabdomyosarcoma at age of 19, a maternal cousin with Wilms' tumor at age 5, and a history of papillary thyroid carcinoma and breast cancer in other family members. The patient's paternal family history also included breast and pancreatic cancer. On physical examination, the patient had neck swelling with intermittent difficulty swallowing. She was referred by her clinician for ultrasonography. The ultrasound demonstrated a dominant, solid, mildly left-sided nodule with increased vascularity that nearly replaced the left thyroid lobe, and measured 4.9 x 3.3 x 5.9 cm. The mass at the base of the left thyroid lobe deviated the trachea to the right and partially narrowed it. Two weeks later, a follow-up CT of the neck with intravenous contrast showed a slight increase in size to 5.1x4.7x6.1 cm without definite evidence of extension beyond the thyroid surface or substernal extension.

Clinical Follow-Up

In follow-up, the patient received radioactive iodine therapy. Five months later, an interval imaging of the neck showed residual abnormal tissue. A PET scan then showed FDG-avid cervical lymphadenopathy bilaterally. The suspicious lymph nodes were biopsied, one on each side of the neck, and found to contain metastatic thyroblastoma. Subsequently, a bilateral neck dissection was performed.

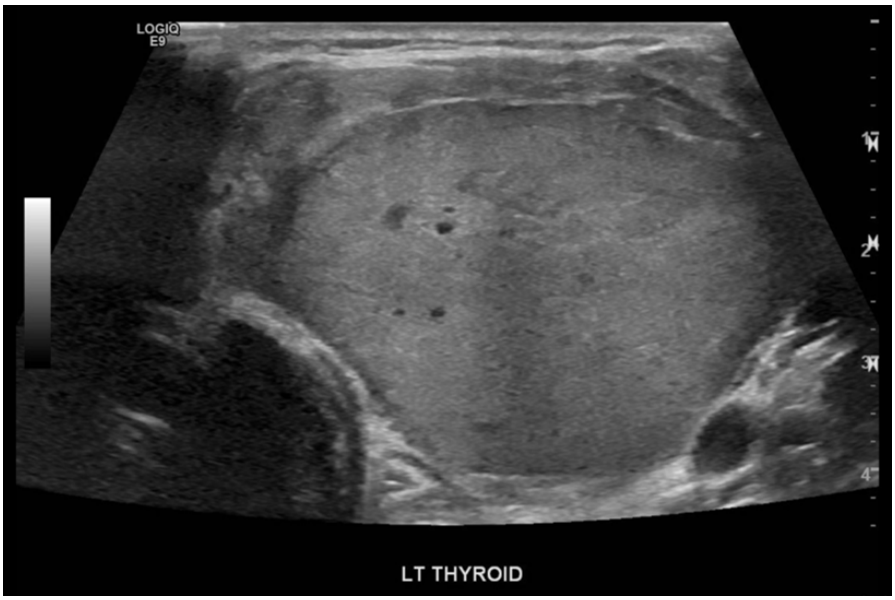

Ultrasonographic finding of the left thyroid nodule. The ultrasound demonstrated a dominant, solid, mildly hypoechoic left-sided nodule with increased vascularity that nearly replaced the left thyroid lobe

Pathological Findings

Gross Examination

Received fresh in the frozen section lab, labeled left thyroid lobe and isthmus, is a 61 g hemithyroidectomy specimen with a large, fleshy, soft, solid red-brown nodule replacing the left lobe, 5.9 cm. The lesion is likely invasive into the adjacent parenchyma. In the superior pole there are multiple white-tan firm nodules ranging in size and from 0.2 to 0.4 cm in greatest dimension. Located in the superior to mid medial pole, is a 1.3 cm lobulated and encapsulated lesion with a minimal residual parenchyma identified.

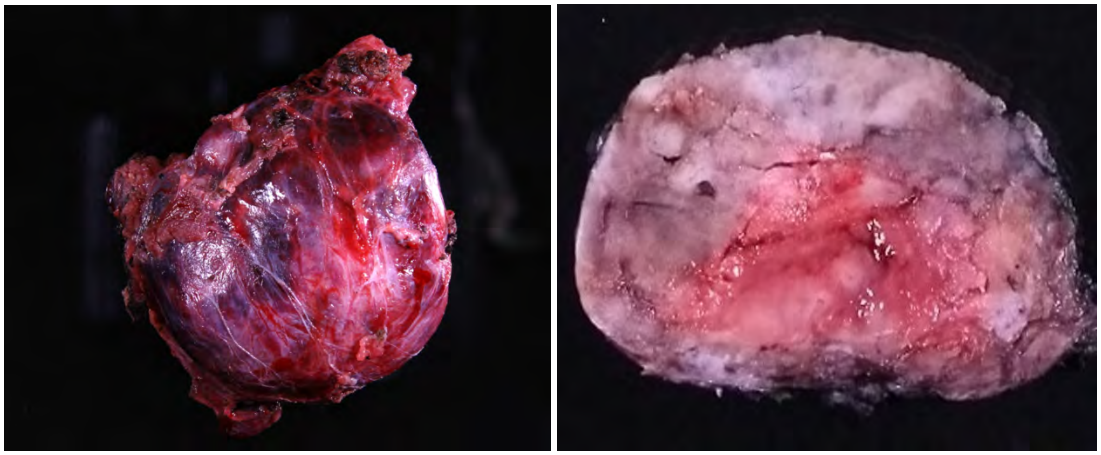

The thyroidectomy specimen contained a large, fleshy, friable, solid red-brown mass measuring 5.9 cm with nearly complete replacement of the left lobe of the thyroid and extension into adjacent parenchyma.

Frozen Section and touch prep: Microfollicular-patterned lesion

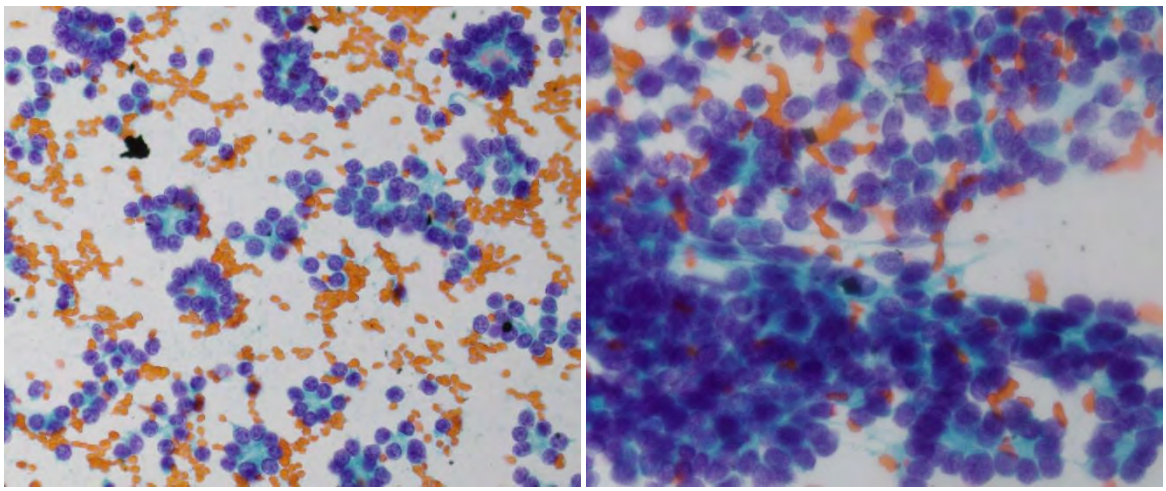

Histologic evaluation revealed a hypercellular neoplasm comprised of primitive morular groups of high N/C cells, solid arrays of follicular cells, and many small rosettes. In addition, a spindled mesenchymal component was also present. Mitoses up to 5 per 50 HPFs were observed.

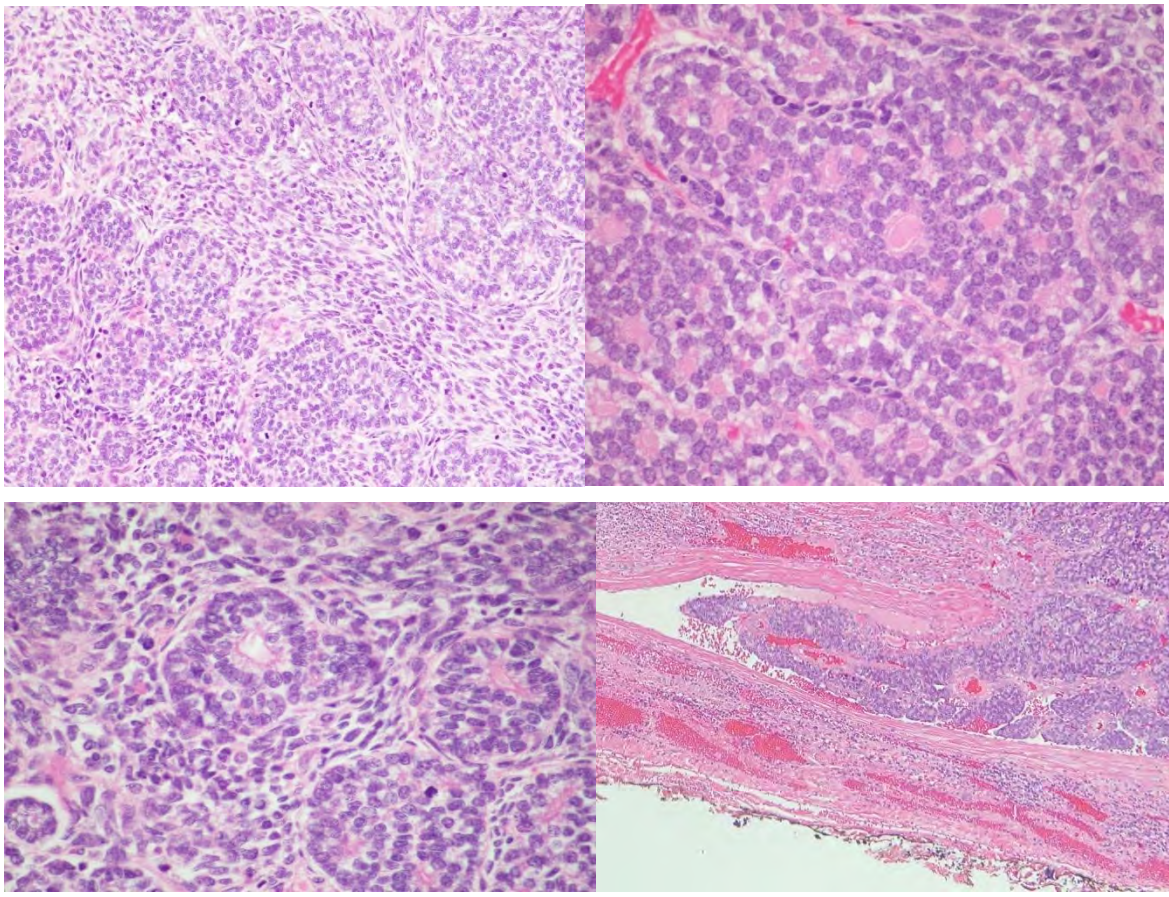

The extratumoral non-involved thyroid showed marked chronic lymphocytic thyroiditis, as well as multiple adenomatous and hyperplastic nodules.

Four lymph nodes were identified, and all were positive for metastatic tumor with extranodal extension

Immunohistochemical profile revealed the epithelial component to be diffusely positive for PAX8 and TTF1 but negative for all other markers, including thyroglobulin, CD5, p53, and neuroendocrine markers. The stromal spindle cell component showed diffuse and weak expression for TTF1, and focal expression for both p63 and p53 but were negative for PAX8, thyroglobulin, and CD5. The Ki67 proliferation index was > 60%.

Ultrastructural studies showed a glandular differentiated tumor with surface microvilli. Some lumens appeared to contain colloid, and some cells contained colloid droplets.

Molecular Studies

A somatic *DICER1* single nucleotide variant c.5437G>A (p.Glu1813Lys) was detected using a Targeted RNA next-generation sequencing (NGS) assay. This pathogenic somatic *DICER1* variant was present. The SNAPSHOT-NGS-V2 Assay also revealed single nucleotide variant of *ATM* c.3872T>G (p.Leu1291Arg).

Diagnosis

Thyroblastoma

Microfollicular neoplasm, widely invasive, involving the entire lobe, with extensive lymphovascular invasion into with intrathyroidal spread with the multiple satellite tumor nodules in the focal microscopic extrathyroidal extension. See note.

Note: This is a very unusual neoplasm which does not fit any currently described classification. The microfollicular pattern shows a more primitive type of a follicular development reminiscent of the thyroid in the first trimester of them prior changes. The tumor is predominantly formed by microfollicles with a small spindle cell stromal component. Due to the morphological features of this neoplasm in the lack of a better classification, this neoplasm is best classified as a **thyroblastoma** (signed in 2019).

Comments

Thyroblastoma is a recently recognized embryonal thyroid neoplasm with a highly aggressive biologic behavior. This primary primitive thyroid malignancy is reminiscent of early fetal embryology, and it lacks teratoid elements.

Definitions

- Thyroblastoma is an embryonal high-grade thyroid neoplasm composed of primitive thyroid-like follicular cells surrounded by a primitive small cell component and mesenchymal stroma with variable differentiation (WHO 2022)
- Thyroblastoma is an embryonal neoplasm that resemble fetal thyroid within the first trimester of embryogenesis - around 12 weeks

Synonyms

Used but not recommended:

- Malignant thyroid teratoma
- Malignant teratoid tumor
- Immature teratoma
- Carcinosarcoma
- Teratocarcinosarcoma

Etiology/Pathogenesis

***DICER1* mutations**

- Somatic mutations in the *DICER1* gene, which encodes an enzyme involved in micro RNA processing
- DICER1 mutations have been detected in all tested thyroblastoma cases
- Considered as a sporadic neoplasm, unrelated to the hereditary DICER1 syndrome due to the higher age at presentation and lack of personal or family history of DICER1 syndrome

Histologic Features

- Thyroblastoma is an embryonal neoplasm that mostly resemble fetal thyroid within the first trimester of embryogenesis
- Embryonal thyroid epithelium forming primitive follicle-like structures, or fetal-type tubules or squamous-like epithelium, primitive small cell blastemal component with variable neuroectodermal features, mesenchymal stromal with or without rhabdomyoblastic differentiation
- A conventional thyroid carcinoma component, a conventional germ cell component
- Expression of specific germ cell markers are absent

Pathologic Interpretation Pearls

- Thyroblastoma is composed of three cellular components:
- Fetal-type primitive TTF1+/PAX8+/focal thyroglobulin+ primitive-appearing thyroid follicles

- Fetal-type glands
- Primitive small round to oval cells
  - These components are surrounded by a spindle cell stroma of variable cellularity arranged into fascicles
- Positive for smooth muscle actin, desmin, and myogenin

In summary, although most thyroid carcinomas with underlying DICER1 mutations are usually indolent, thyroblastoma is an aggressive DICER1-related thyroid malignancy which is important to recognize. Due to the highly aggressive nature of thyroblastoma, the identification of specific genetic signatures for DICER1 mutation becomes critical in its diagnosis and treatment. However, due to its rarity and likely underrecognized occurrence, there are still many questions regarding the pathogenesis and tumorigenesis of thyroblastoma that remain to be answered.

References

1. Agaimy A, Nosé V, Sobrinho-Simoes M. Thyroblastoma. In: WHO Classification of Endocrine and Neuroendocrine Tumours. 5th ed. WHO Classification of Tumours Editorial Board. Lyon, France: International Agency for Research on Cancer; 2022
2. Nosé V, Gill A, Teijeiro JMC, Perren A, Erickson L. Overview of the 2022 WHO Classification of Familial Endocrine Tumor Syndromes. Endocr Pathol. 2022;33(1):197-227. doi:10.1007/s12022-022-09705-5
3. Son EJ, Nosé V. Familial follicular cell-derived thyroid carcinoma. Front Endocrinol (Lausanne). 2012;3:61. Published 2012 May 3. doi:10.3389/fendo.2012.00061
4. Nosé V. DICER1 gene alterations in thyroid diseases. Cancer Cytopathol. 2020;128(10):688-689. doi:10.1002/cncy.22327
5. Agaimy A, Witkowski L, Stoehr R, et al. Malignant teratoid tumor of the thyroid gland: an aggressive primitive multiphenotypic malignancy showing organotypical elements and frequent DICER1 alterations-is the term "thyroblastoma" more appropriate?. Virchows Arch. 2020;477(6):787-798. doi:10.1007/s00428-020-02853-1
6. Guilmette J, Dias-Santagata D, Lennerz J, et al. Primary Thyroid Neoplasm with Fetal Morphology Associated with DICER1 Mutations: Expanding the Diagnostic Profile of Thyroblastoma. Thyroid. 2022;32(11):1423-1428. doi:10.1089/thy.2022.0060
7. Rooper LM, Bynum JP, Miller KP, et al. Recurrent DICER1 Hotspot Mutations in Malignant Thyroid Gland Teratomas: Molecular Characterization and Proposal for a Separate Classification. Am J Surg Pathol. 2020;44(6):826-833. doi:10.1097/PAS.0000000000001430
8. Riedlinger WF, Lack EE, Robson CD, Rahbar R, Nosé V. Primary thyroid teratomas in children: a report of 11 cases with a proposal of criteria for their diagnosis. Am J Surg Pathol. 2005;29(5):700-706. doi:10.1097/01.pas.0000151934.18636.d5
9. Rooper LM. From Malignant Thyroid Teratoma to Thyroblastoma: Evolution of a Newly-recognized DICER1-associated Malignancy [published online ahead of print, 2022 Sep 7]. Adv Anat Pathol. 2022;10.1097/PAP.0000000000000364.
10. Nosé V, Guilmette J: Thyroblastoma. In: Diagnostic Pathology: Endocrine, 3rd Ed, Elsevier 310-315, 2023.

12TH INTERNATIONAL AMR PATHOLOGY SLIDE SEMINAR SYMPOSIUM IN ANATOMIC PATHOLOGY

Case – 29

Head and Neck Pathology

Contributed by: ***Göran Elmberger***

Clinical History

An 85-year-old man with fatigue. Previous history of idiopathic membranous glomerulonephritis 1992, prostatic adenocarcinoma Gleason 3+4=7 2003, polyarthritis 2008, and multiple skin basal cell carcinomas now presenting with a left sided neck lump in regio Ib. Radiology reveal a 36 mm sized expansile tumor in submandibular gland. FNA performed but was non-informative due to lack of diagnostic material. A core needle was later performed under clinical suspicion of malignancy but the pathological interpretation was rather inconclusive since both a reactive inflammatory condition and a biphasic salivary gland tumor of uncertain malignant potential (SUMP) could be discussed. However, overexpression of IgG4 positive plasma cells was noted in IHC. Finally, left glandula submandibularis with tumor was resected for histopathological examination.

Pathological Findings

Macroscopically a multinodular hard well-circumscribed but not encapsulated infiltrate was seen. The color was somewhat white-yellowish.

Microscopically with preservation of the salivary gland with lobular architecture and separation by thickened interlobular fibrous bands. In higher magnification, acinar atrophy was prominent. Further, storiform-type fibrosis and a dense lymphoplasmacytic infiltrate with florid follicular lymphoid hyperplasia was characteristic. Focally, well visualized in elastinvan Gieson stain, obstructive endophlebitis was seen.

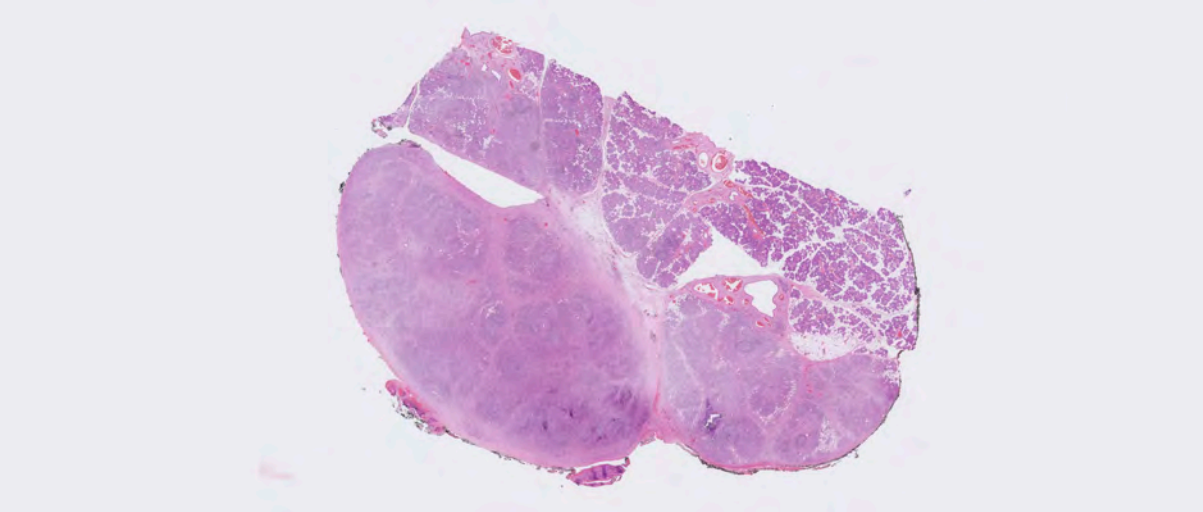

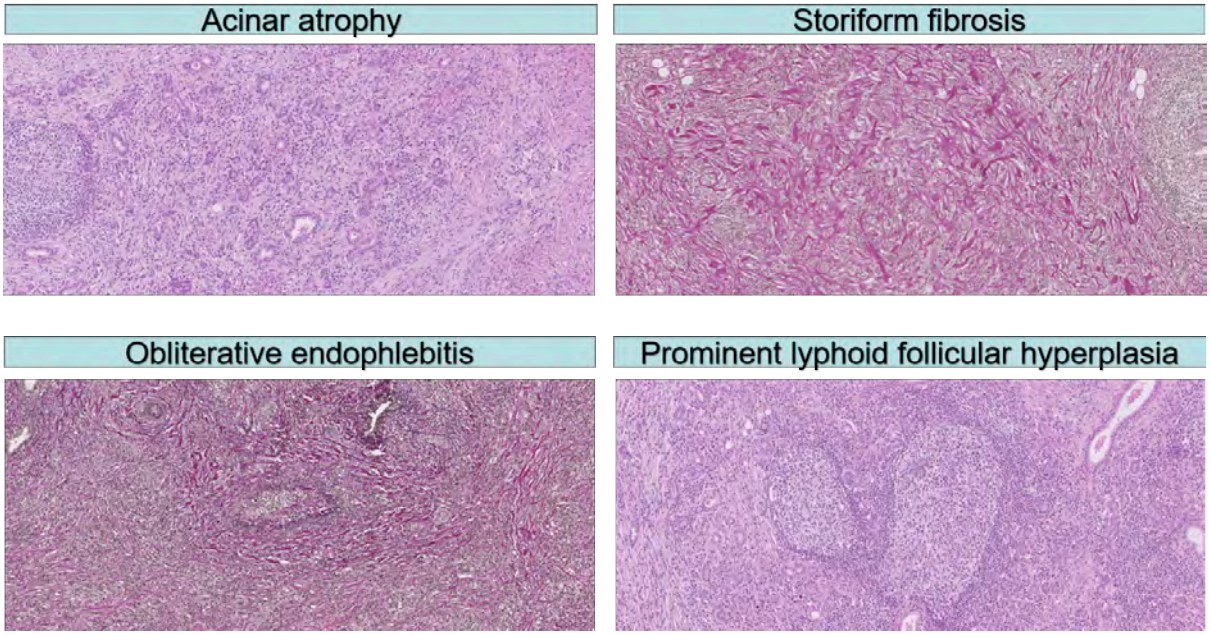

Immunohistochemistry showed 185 IgG4 positive plasma cells per HPF and the IgG4/IgG ratio of plasma cells was 90%.

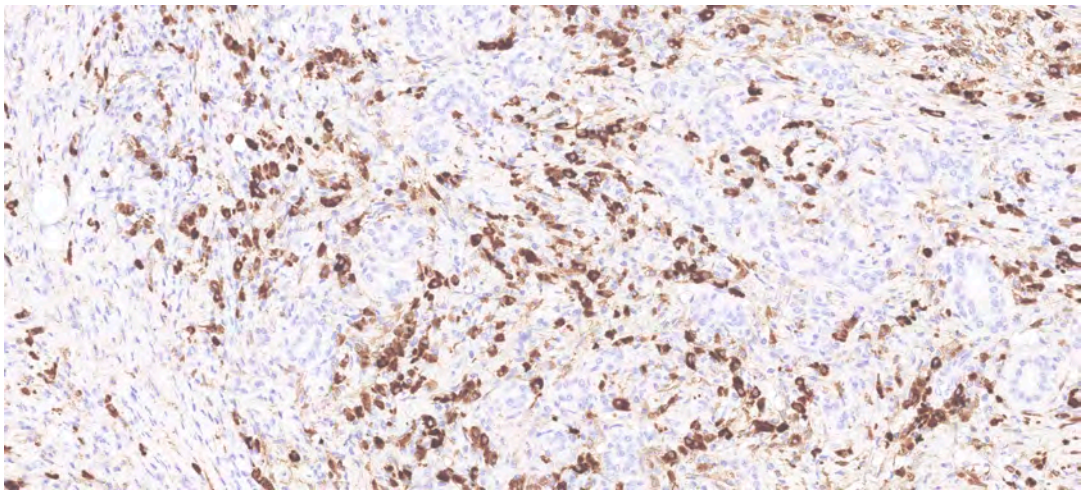

Figure. IgG4 IHC

Diagnosis

IgG4-related salivary gland disease in submandibular gland (Kùttner tumor).

Comments

Follow-up

Serological investigation showed increased s-IgG4 (200 mg/dl). As part of IgG4 RD workup CT thorax revealed bilateral pulmonary infiltrates that could be consistent with IgG4 RD in the lung. A bronchial endoscopic biopsy was performed revealing only normal probably nonrepresentative histomorphological findings. VATS biopsy recommended. Patient selfmedicated with hydrocortisone 5 mg daily due to increased musculoskeletal problems and at CT control pulmonary infiltrates were regressing. Rheumatologists considered therapy change to prednisone 40 mg daily and rituximab. CT abdomen showed slight perirenal infiltrates of post inflammatory type. Total follow-up time 8 months without evidence of further multisystem manifestations of IgG4 RD.

IgG4 related disease in general

IgG4-related disease (IgG4-RD) is a systemic autoimmune fibroinflammatory disease that produces sclerotic, tumefactive masses containing dense lymphoplasmacytic infiltrates rich in immunoglobulin IgG4 positive plasma cells. Initially characterized as a form of autoimmune pancreatitis, the distinctive histopathology of IgG4-RD has now been described in almost every organ system. However, because the clinical manifestations of IgG4-RD are diverse and nonspecific, the disease may go unsuspected until a biopsy or resection specimen is obtained to diagnose a presumed malignancy. Pathologists thus play a key role in the diagnosis of IgG4-RD, and familiarity with its histopathologic features is essential to prevent unnecessary surgery and the irreversible comorbidities resulting from delayed treatment of index manifestations and later associated manifestations of this often systemic and treatable disease. The incidence of IgG4-RD across all organ systems is difficult to determine, since the disease has only recently been described and global population-based data are lacking. Unlike most autoimmune diseases, IgG4-RD is more prevalent in middle-aged and elderly males, although the extent of this male predominance varies with the anatomic site of involvement. The most common clinical manifestation is the development of a mass lesion that produces site-specific symptoms and raises suspicion for malignancy. The effects range from simple swelling of the affected organs (salivary and lacrimal glands, lymph nodes) to obstruction (pancreaticobiliary, ureteral), organ dysfunction (pituitary insufficiency secondary to hypophysitis, kidney disease), and even frank medical emergency (aortic dissection, pachymeningitis, pancreatitis). Apart from the mass effects, a small number of patients may experience constitutional symptoms such as fever and weight loss.

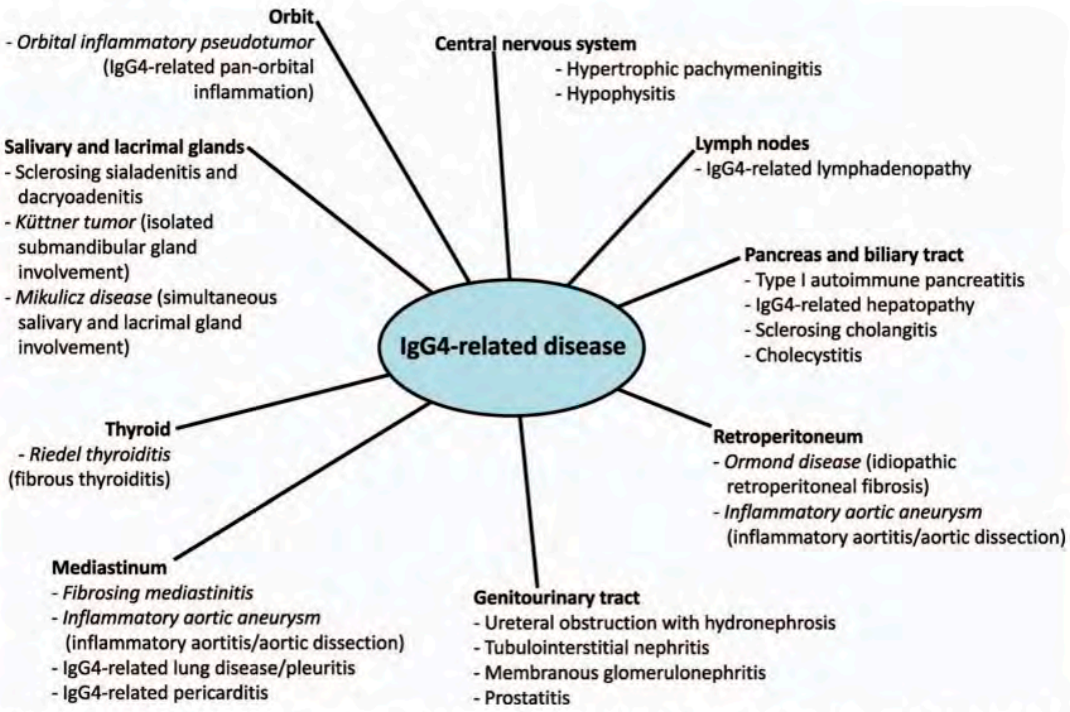

Figure 1. *Some of the many clinical manifestations of IgG4-related disease, including the names of historic fibrosing diseases (italicized) subsequently linked to the disorder. Abbreviation: IgG4, immunoglobulin G4.*

The diagnosis of IgG4 RD is often difficult and need a clinical, serological and pathological component. General and organ specific comprehensive diagnostic criteria exists. Patients with IgG4-RD frequently present with simultaneous or metachronous lesions in multiple organs. An elevated serum IgG4 (>135mg/dl) represents the only validated blood based biomarker. However, elevated serum IgG4 is detected in only half the patients with this disease. Histology continues to represent the gold standard for the diagnosis of IgG4 related disease. A definitive diagnosis of IgG4 related disease also requires the presence of elevated numbers of IgG4 positive plasma cells in tissue samples as well as an IgG4 to IgG ratio of greater than 40 %. In isolation, elevated numbers of IgG4 positive plasma cells represents a non-specific feature, detected in a variety of other inflammatory as well as neoplastic diseases. Attention to the clinical context, histological features, as well as an elevated IgG4 to IgG ratio is critical to avoiding overdiagnosis of IgG4 related disease.

Table 2. The 2020 Revised comprehensive diagnostic (RCD) criteria for IgG4-RD.

[Item 1] clinical and radiological features
One or more organs show diffuse or localized swelling or a mass or nodule characteristic of IgG4-RD. In single organ involvement, lymph node swelling is omitted.
[Item 2] serological diagnosis
Serum IgG4 levels greater than 135 mg/dl.
[Item 3] pathological diagnosis
Positivity for two of the following three criteria:
① Dense lymphocyte and plasma cell infiltration with fibrosis.
② Ratio of IgG4-positive plasma cells /IgG-positive cells greater than 40% and the number of IgG4-positive plasma cells greater than 10 per high powered field
③Typical tissue fibrosis, particularly storiform fibrosis, or obliterative phlebitis
Diagnosis:
Definite: 1) +2) +3)
Probable: 1) +3):
Possible: 1) +2)

IgG4 related disease in Head & Neck

IgG4 related disease of the head and neck region represents one of the more common manifestations of IgG4 related disease. Involvement of the submandibular and parotid glands, the orbit and thyroid represent are some of the more common sites involved by IgG4 related disease. Although major salivary glands are commonly affected by IgG4-related disease, the minor salivary glands of the oral cavity can also be involved, and a lower lip biopsy may be an auxiliary diagnostic tool. IgG4 related disease also involves the nasal sinuses, the nasal cavity, the nasopharynx, as well as the tracheobronchial tree and larynx. Eosinophilic angiocentric fibrosis, Mikulicz disease and Riedel thyroiditis are also members of the family of IgG4 related disease.

IgG4 related salivary gland disease

In IgG4-RD, the involvement of salivary glands is observed in 27% to 53% of the patients. Several organ-specific conditions, now recognized as different manifestations of IgG4-related sialoadenitis, were viewed in the past as individual disease entities. For example, Mikulitz disease, a dramatic bilateral painless swelling of parotid, lacrimal, and submandibular glands, was previously linked and not clearly distinguished from Sjögrens syndrome until 2005, because of their similar glandular histological aspects. Similarly, the Kùttner's tumor or chronic sclerosing sialoadenitis, characterized by severe swelling of the submandibular glands, was initially considered as an individual disease entity. IgG4 RD is now recognized as an autoimmune mediated disease.

Clinical issues

IgG4-RD, the swelling of lacrimal and salivary glands is mostly, but not exclusively, bilateral and persists generally for more than 3 months. Submandibular glands are more frequently affected, but parotid, sublingual, and labial salivary glands are also involved. Pain often associated with eating is common. May be a localized finding or systemic with sclerosing lesions in extra-salivary gland tissues. A diagnostic work-up including CT/PET of H&N, thorax and abdomen recommended.

History

Originally reported by Hermann Kùttner from Thùbingen Germany 1896 in "Ueber enzùndliche Tumoren der Submaxillar Speichel drùse". The concept of IgG4 RD as a new entity was reported 2003 by T Kamisawa – "A new clinicopathological entity of IgG4-related autoimmune disease".

Epidemiology

Incidence is still unknown since recently outlined entity with problems in underdiagnosis.

Histological features

Well-defined to circumscribed lesions involving variable proportion of a salivary gland. Preservation of lobular orientation of glands separated by fibrosis including thickened interlobular septa. Storiform fibrosis sometimes seen. There is a dense lymphoplasmacytic infiltrate including sheets of mature plasma cells and irregular large lymphoid follicles with germinal center formations. Acinar atrophy in later phases. Obliterative phlebitis is one hallmark lesion better seen in elastin van Gieson stain.

Immunohistochemistry or in situ hybridization

More than 100 IgG4 + plasma cells per HPF. IgG4/IgG plasma cell ratio > 40 % is a more powerful tool. ISH is a better stain especially in small biopsy specimens due to increased sensitivity and specificity. Special stains are supportive but still need to be interpreted with histopathological findings and clinical information for definitive diagnosis.

Laboratory tests

Elevated s-IgG4 levels >135 mg/dl may be seen. However, this is non-sensitive and nonspecific. Biopsy confirmed cases could have normal s-IgG4.

Treatment

Excellent response to steroids and B-cell depleting agent Rituximab. Prognosis Treated cases have excellent response but patient need lifelong surveillance to prevent organ damage in recurring local or other systemic exacerbations. Rarely extra-nodal marginal zone B-lymphoma (MALT) and salivary duct carcinoma may arise in background of CSS.

Differential diagnosis

- Neoplasm
- Chronic sialadenitis NOS
- Sjögren Syndrome
- Sialolithiasis
- Sarcoidosis

IgG4 positive plasma cells in non-specific inflammatory conditions

IgG4-positive plasma cells constitute a common component of the inflammatory infiltrates in non-specific, non-IgG4 related chronic inflammatory lesions of different localisations. Thus increased numbers of IgG4 + plasma cells and often increased s-IgG4 can be seen in other autoimmune conditions, rheumatoid arthritis, asthma, allergies, plasma cell dyscrasias, multicentric Castlemans disease and malignant epithelial tumors. The intensity of IgG4- positive plasma cells in non-specific inflammation varies greatly depending on the lesion type and site. The ubiquity and the wide range of IgG4-positive plasma cells in non-specific chronic inflammation largely limit the establishment of a universally valid threshold of IgG4- positive plasma cell count for diagnosis of IgG4 SD. The presence of a tumefactive inflammatory infiltrate with prominent accompanying sclerosis and obliterative phlebitis are of particular importance when rendering a diagnosis of IgG4 RD. The plasma cell counts should be interpreted cautiously even in the context of these typical histopathological features, thereby taking the serum IgG4 levels and other clinical findings (particularly the presence of similar manifestation in other organ systems) into consideration.

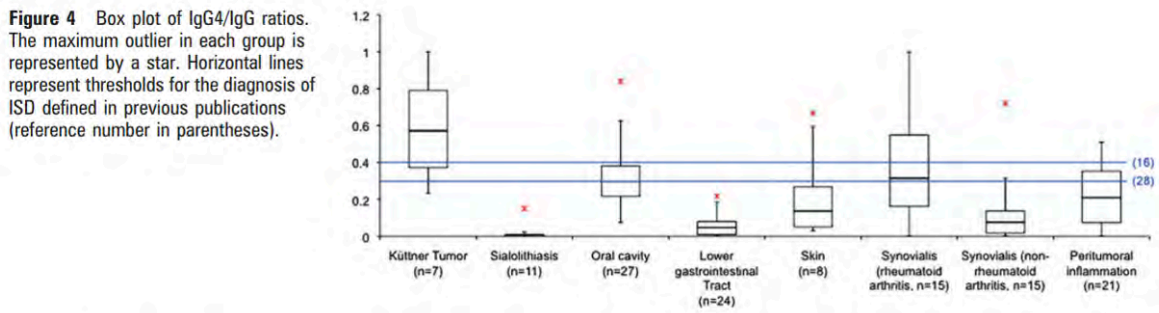

Figure 4 Box plot of IgG4/IgG ratios. The maximum outlier in each group is represented by a star. Horizontal lines represent thresholds for the diagnosis of ISD defined in previous publications (reference number in parentheses).

Cytology

The majority of IgG4 RD present as a mass forming lesion that can mimic a neoplasm, both clinically as well as on radiological examination. Cytological interpretation of these lesions can be difficult as there can be a broad range of cytological features and none is considered as diagnostic. IgG4 RD is a potential pitfall in the FNA interpretation of salivary gland lesions, especially if there is a previous history of head and neck malignancy. Low cellularity, epithelial atypia and non-representative nondescript background often cause a faulty diagnosis. However, a general awareness

of the entity, patient history, radiological features, and cytology features such as abundant plasma cells, fibroblast and epithelial atypia could raise the suspicion of this entity.

Core biopsy

In the head and neck region, CNB has been reported to have significantly higher sensitivity and specificity than fine needle aspiration. Studies that are more recent emphasize the value of CNB for diagnosis of salivary gland neoplasms. However, the accuracy of CNB in the diagnosis of IgG4-DS CNB less studied. Some report it is a potentially accurate diagnostic tool for evaluation of IgG4-RD. Others conclude that small biopsies from patients with a presumptive diagnosis of IgG4-RD often fail to meet consensus histological criteria. An elevated IgG4/total IgG ratio has been reported as the most sensitive pathological feature, and ISH provides a more robust quantification platform. It can be recommended that tumefactive lymphoplasmacytic infiltrates with increased IgG4/IgG ratio, should be evaluated for IgG4- RD regardless of histological features.

Challenge in diagnosis with small biopsy specimens

Biopsy of IgG4-RD lesions ubiquitously show lymphoplasmacytic infiltrate, but often lacking either storiform fibrosis or obliterative phlebitis. Furthermore, needle biopsy are less capable of detecting IgG4/HPF count and is inferior in diagnoing IgG4-RD, especially in salivary gland lesions.

Idiopathic membranous nephropathy and IgG4

IgG4-related disease (IgG4-RD) often affects the kidneys, and is characterized by interstitial nephritis, obstructive nephropathy, and in rare cases glomerulopathy (including membranous nephropathy). In patients with membranous nephropathy (MN) that is accompanied by multisystem damage, impaired renal function, elevated IgG4 levels, negative PLA2R, and/or renal interstitial plasma cell infiltration, the possibility of IgG4-related kidney disease (IgG4-RKD) should be carefully assessed. IgG4-related kidney disease with membranous nephropathy has been reported as initial manifestation of systemic IgG4 RD.

Conclusions

- A characteristic case of IgG4 related salivary gland disease with typical clinical, pathological and serological findings
- In retrospective this probably represent the second clinically detected manifestation of disease in this patient where the first overlooked was idiopathic membranous glomerulonephritis detected 30 years previously
- Probably the bilateral pulmonary infiltrates found at work-up could also be a manifestation of IgG 4 related disease even if bronchial biopsies were nonrepresentative
- Detected perirenal fibrosis might be a form fruste of IgG4 related retroperitoneal fibrosis
- Most probably under recognized and underreported disease entity
- IgG4 related disease is a systemic multiorgan autoimmune condition
- Preferred treatment is medical organ sparing and not surgery
- The goal is to make early diagnosis pre-op from cytology, core biopsy and clinical radiological correlation
- mRNA ISH performs better than IHC – less background
- Early diagnosis can be lifesaving in some cases
- Late stages are hallmarked by fibrosis and unlikely respond to therapy
- Diagnosis require high index of suspicion
- Diagnosis is not only tissue based but also need clinical. serological and radiological correlation
- Previous medical history need to be carefully investigated

- Radiological workup including CT and PET of the chest, abdomen and pelvis to detect possible multiorgan involvement
- Diagnosis motivates life-long surveillance for early diagnosis and organ/tissue sparing early medical treatment
- Undiagnosed prognosis is poor with progressive fibrosis
- Serious pitfall for overdiagnosis of malignancy
- Diagnosis with FNA and core biopsies challenging with many pitfalls

References

1. Kamisawa T et al: A new clinicopathological entity of IgG4-related autoimmune disease. J Gastroenterol. 38(10):982-4, 2003
2. Kamisawa T et al: IgG4-related sclerosing disease. World J Gastroenterol. 14(25):3948-55, 2008
3. IgG4-related disease. Stone JH, Zen Y, Deshpande V.N Engl J Med. 2012 Feb 9;366(6):539-51.
4. Mahajan VS et al: IgG4-related disease. Annu Rev Pathol. 9:315-47, 2014
5. IgG4-related disease: review of the histopathologic features, differential diagnosis, and therapeutic approach. Bledsoe JR, Della-Torre E, Rovati L, Deshpande V. APMIS. 2018 Jun;126(6):459-476.
6. Tsuboi H et al: Pathogenesis of IgG4-related disease. Comparison with Sjögren's syndrome. Mod Rheumatol. 1-10, 2019
7. Deshpande V: The pathology of IgG4-related disease: critical issues and challenges. Semin Diagn Pathol. 29(4):191-6, 2012
8. Deshpande V et al: Consensus statement on the pathology of IgG4-related disease. Umehara H et al: A novel clinical entity, IgG4-related disease (IgG4RD): general concept and details. Mod Rheumatol. 22(1):1-14, 2012
9. The 2019 American College of Rheumatology/European League Against Rheumatism classification criteria for IgG4-related disease. Wallace ZS, Naden RP, Chari S, Choi HK, Della-Torre E, Dicaire JF, Hart PA, Inoue D, Kawano M, Khosroshahi A, Lanzillotta M, Okazaki K, Perugino CA, Sharma A, Saeki T, Schleinitz N, Takahashi N, Umehara H, Zen Y, Stone JH; Members of the ACR/EULAR IgG4-RD Classification Criteria Working Group.Ann Rheum Dis. 2020 Jan;79(1):77-87.
10. The 2020 revised comprehensive diagnostic (RCD) criteria for IgG4-RD. Umehara H, Okazaki K, Kawa S, Takahashi H, Goto H, Matsui S, Ishizaka N, Akamizu T, Sato Y, Kawano M; Research Program for Intractable Disease by the Ministry of Health, Labor and Welfare (MHLW) Japan. Mod Rheumatol. 2021 May;31(3):529-533. Avincsal MO et al: The histopathology of IgG4-related disease. Curr Top Microbiol Immunol. 401:45-60, 2017
11. Weindorf SC et al: IgG4-related disease: a reminder for practicing pathologists. Arch Pathol Lab Med. 141(11):1476-83, 2017
12. Ferry JA et al: IgG4-related disease in the head and neck. Semin Diagn Pathol. 29(4):235-44, 2012
13. Immunoglobulin G4-related diseases in the head and neck: a systematic review. Mulholland GB, Jeffery CC, Satija P, Côté DW. J Otolaryngol Head Neck Surg. 2015 Jun 20;44(1):24.
14. Mulholland GB et al: Immunoglobulin G4-related diseases in the head and neck: a systematic review. J Otolaryngol Head Neck Surg. 44:24, 2015
15. IgG4 related disease of the head and neck. Deshpande V. Head Neck Pathol. 2015 Mar;9(1):24-31.
16. Thompson A et al: Imaging of IgG4-related disease of the head and neck. Clin Radiol. 73(1):106-20, 2018
17. Eosinophilic angiocentric fibrosis is a form of IgG4-related systemic disease. Deshpande V, Khosroshahi A, Nielsen GP, Hamilos DL, Stone JH. Am J Surg Pathol. 2011 May;35(5):701-6.
18. Yamamoto M et al: A new conceptualization for Mikulicz's disease as an IgG4-related plasmacytic disease. Mod Rheumatol. 16(6):335-40, 2006

19. Moriyama M et al: Clinical characteristics of Mikulicz's disease as an IgG4-related disease. Clin Oral Investig. 17(9):1995-2002, 2013
20. Fragoulis GE et al: IgG4-related sialadenitis and Sjögren's syndrome. Oral Dis. 23(2):152-6, 2017
21. Oral and maxillofacial manifestations of IgG4-related disease: A clinicopathological study. Pereira GG, Pontes FSC, Soares CD, de Carvalho MGF, da Silva TA, Calderaro DC, Ferreira GA, Tanure LA, de Souza LL, Rodrigues-Fernandes CI, de Almeida OP, Fonseca FP, Pontes HAR. J Oral Pathol Med. 2022 May;51(5):493-500.
22. IgG4-associated sialadenitis. Geyer JT, Deshpande V.Curr Opin Rheumatol. 2011 Jan;23(1):95-101.
23. Clinicopathological analysis of salivary gland tissue from patients with IgG4-related disease. Takano K, Nomura K, Abe A, Kamekura R, Yamamoto M, Ichimiya S, Takahashi H, Himi T. Acta Otolaryngol. 2016 Jul;136(7):717-21.
24. Puxeddu I et al: Salivary gland pathology in IgG4-related disease: a comprehensive review. J Immunol Res. 2018:6936727, 2018
25. Salivary Gland Pathology in IgG4-Related Disease: A Comprehensive Review. Puxeddu I, Capecchi R, Carta F, Tavoni AG, Migliorini P, Puxeddu R. J Immunol Res. 2018 Apr 1;2018:6936727.
26. Chan JK: Kuttner tumor (chronic sclerosing sialadenitis) of the submandibular gland: an underrecognized entity. Adv Anat Pathol. 5(4):239-51, 1998
27. Ahuja AT et al: Kuttner tumour (chronic sclerosing sialadenitis) of the submandibular gland: sonographic appearances. Ultrasound Med Biol. 29(7):913-9, 2003
28. Kitagawa S et al: Abundant IgG4-positive plasma cell infiltration characterizes chronic sclerosing sialadenitis (Küttner's tumor). Am J Surg Pathol. 29(6):783-91, 2005
29. Chow TL et al: Kuttner's tumour (chronic sclerosing sialadenitis) of the submandibular gland: a clinical perspective. Hong Kong Med J. 14(1):46-9, 2008
30. Geyer JT et al: Chronic sclerosing sialadenitis (Küttner tumor) is an IgG4-associated disease. Am J Surg Pathol. 34(2):202-10, 2010
31. Wang Z et al: CT features and pathologic characteristics of IgG4-related systemic disease of submandibular gland. Int J Clin Exp Pathol. 8(12):16111-6, 2015
32. Takano K et al: Clinicopathological analysis of salivary gland tissue from patients with IgG4-related disease. Acta Otolaryngol. 136(7):717-21, 2016
33. Abraham M et al: Diagnostic and treatment workup for IgG4-related disease. Expert Rev Clin Immunol. 13(9):867-75, 2017
34. Tabata T et al: Serum IgG4 concentrations and IgG4-related sclerosing disease. Clin Chim Acta. 408(1-2):25-8, 2009
35. Dhobale S et al: IgG4 related sclerosing disease with multiple organ involvements and response to corticosteroid treatment. J Clin Rheumatol. 15(7):354-7, 2009
36. Rituximab for IgG4-related disease: a prospective, open-label trial. Carruthers MN, Topazian MD, Khosroshahi A, Witzig TE, Wallace ZS, Hart PA, Deshpande V, Smyrk TC, Chari S, Stone JH. Ann Rheum Dis. 2015 Jun;74(6):1171-7.
37. Gill J et al: Salivary duct carcinoma arising in IgG4-related autoimmune disease of the parotid gland. Hum Pathol. 40(6):881-6, 2009
38. Ochoa ER et al: Marginal zone B-cell lymphoma of the salivary gland arising in chronic sclerosing sialadenitis (Küttner tumor). Am J Surg Pathol. 25(12):1546-50, 2001
39. Numerous IgG4-positive plasma cells are ubiquitous in diverse localised non-specific chronic inflammatory conditions and need to be distinguished from IgG4-related systemic disorders Johanna D Strehl, Arndt Hartmann, Abbas Agaimy. J Clin Pathol 2011;64:237-243.
40. IgG4-positive plasma cells in nonspecific sialadenitis and sialolithiasis. Peuraharju E, Hagström J, Tarkkanen J, Haglund C, Atula T. Mod Pathol. 2022 Oct; 35(10):1423- 1430.
41. Ophthalmic manifestations of IgG4-related disease: single-center experience and literature review. Wallace ZS, Deshpande V, Stone JH. Semin Arthritis Rheum. 2014 Jun;43(6):806-17.

42. The histological diagnosis of IgG4-related disease on small biopsies: challenges and pitfalls. Arora K, Rivera M, Ting DT, Deshpande V. Histopathology. 2019 Apr;74(5):688-698.
43. Sakamoto M et al: The diagnostic utility of submandibular gland sonography and labial salivary gland biopsy in IgG4-related dacryoadenitis and sialadenitis: its potential application to the diagnostic criteria. Mod Rheumatol. 1-6, 2019
44. Cheuk W et al: Kuttner tumor of the submandibular gland: fine-needle aspiration cytologic findings of seven cases. Am J Clin Pathol. 117(1):103-8, 2002
45. Arora K et al: The histological diagnosis of IgG4-related disease on small biopsies: challenges and pitfalls. Histopathology. 74(5):688-98, 2019
46. Needle biopsy compared with surgical biopsy: pitfalls of small biopsy in histologial diagnosis of IgG4-related disease. Liu Y, Yang F, Chi X, Zhang Y, Fu J, Bian W, Shen D, Li Z. Arthritis Res Ther. 2021 Feb 10;23(1):54.

12TH INTERNATIONAL AMR PATHOLOGY SLIDE SEMINAR SYMPOSIUM IN ANATOMIC PATHOLOGY

Case – 30

Head and Neck Pathology

Contributed by: ***Vania Nosé***

Clinical History

20-year-old female discovered to have a 5.0cm left thyroid nodule in 2019. Prior biopsy: 11/12/2019: Follicular Lesion of Undetermined Significance - FLUS (Bethesda Category III

In 2022, then 23-year-old female with a left thyroid nodule has been needled as Thyroseq benign but is nearly 8 cm.

CT scan and ultrasound showed a large mixed cystic and solid nodule replacing the left lobe of the thyroid gland with shift of the trachea to the right but no substernal extension. No definite suspicious cervical lymph nodes. US thyroid performed in October 2022 showed a 7.7 cm mixed cystic and solid nodule replaces the majority of the left thyroid lobe. No right thyroid nodules identified. Heterogeneous thyroid parenchyma suggestive of changes of Hashimoto thyroiditis.

Mother with history of papillary thyroid carcinoma.

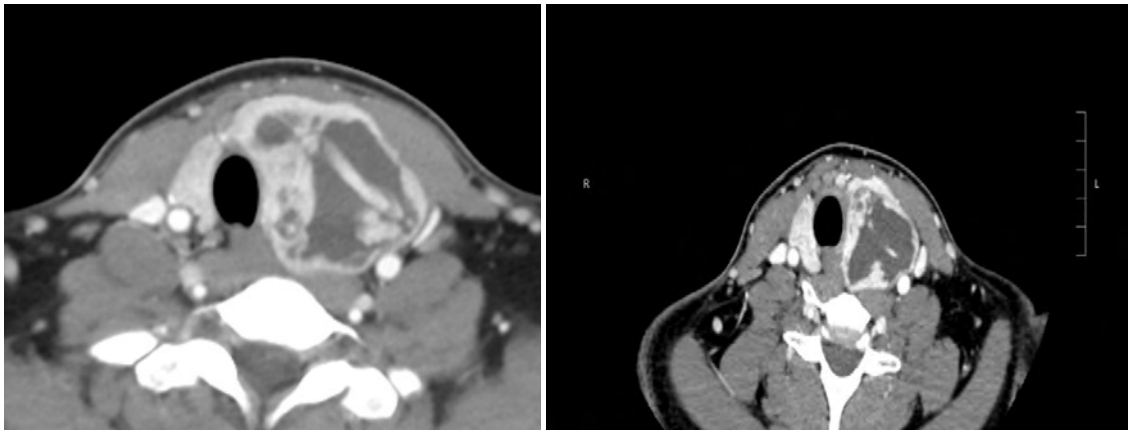

Pathological Findings

Received in formalin labeled "left goiter" is a 75 g (post fixation), 6.6 x5.5 x 3.8 cm distorted, enlarged left thyroid lobe with an attached 2.4 x 0.9 x0.9 cm portion of possible isthmus. The surface is pink-tan with scatteredloosely adherent red-brown fibromuscular tissue. The presumed isthmic margin is inked blue, and the remainder of the specimen is inked black. Involving the majority of the lobe, there is a 6.4 x 4.9 x 3.6 cm encapsulated heterogeneous nodular mass that is approximately 75% tan-white cystic and approximately 25% tan-pink to red-brown solid/gelatinous. The cystic component is filled with cloudy brown fluid. The mass is 0.4 cm from the isthmic margin. The scant amount of uninvolved parenchyma is pale pink-brown with no additional discrete lesions noted.

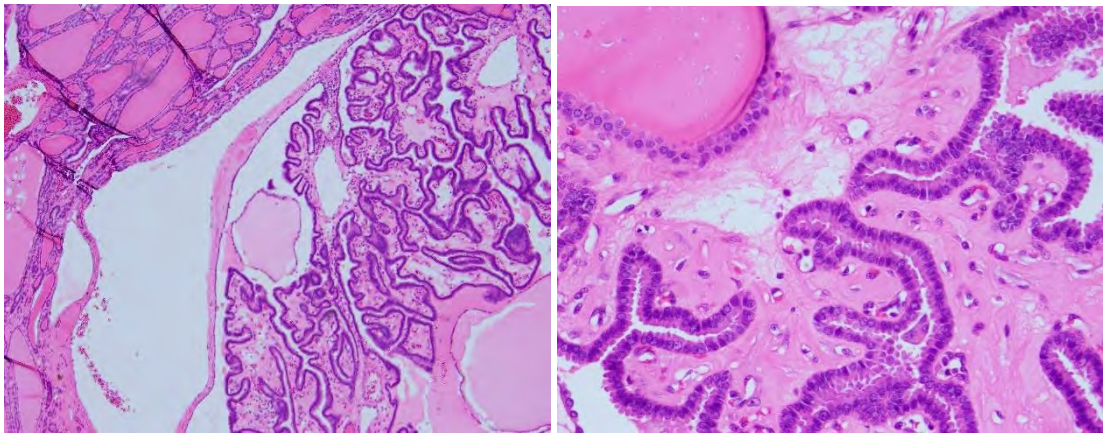

Molecular Studies

The NGS PGDx assay was performed and it is a next-generation sequencing tumor profiling test. The NGS PGDX assay utilizes a targeted, hybrid-capture based next-generation sequencing (NGS) assay for somatic single nucleotide variant (SNV), insertion/deletion (indel), copy number detection (amplification), and select gene fusion detection, microsatellite instability (MSI), and tumor mutational burden (TMB) in genomic DNA obtained from formalin-fixed, paraffin-embedded tumor tissue using the PGDx elio (TM) tissue complete platform. The NGS PGDx assay covers the full-coding sequence of 505 genes for the identification of key genomic alterations in accordance with professional guidelines in oncology for previously diagnosed patients with solid tumors.

KRAS p.G12V 12.5% (NM_033360)

DICER1 p.N65Kfs*15 34.2% (CCDS9931.1)

DICER1 p.D1709N 38.1% (CCDS9931.1)

COMMENT: Mutations in the *DICER1* gene, are associated with thyroid abnormalities, including multinodular goiter and differentiated thyroid carcinoma. While the mutation at codon 1709 is a known somatic hotspot mutation, the frameshift N65Kfs*15 may be of germline origin.

Diagnosis

Thyroid Follicular Nodular Disease

Thyroid follicular nodular disease with a dominant adenomatous nodule with prominent centripetal papillary growth, 6.4 cm. See note. Lymphocytic thyroiditis with germinal center formation. No lymph nodes or parathyroid glands are identified.

Note: This thyroid nodule has very unusual morphological findings. The nodule has a solid component, composed by follicles with a dark colloid and marked prominent centripetal papillary growth. The nodule has also a cystic component.

Comments

Abbreviations

- Thyroid follicular nodular disease (FND)
- ○ Multinodular hyperplasia (MNH)
- ○ Multinodular goiter (MNG)
- ○ Adenomatous nodules (AN)

Synonyms

- Adenomatous nodules
- Nodular hyperplasia
- Adenomatous hyperplasia
- Multinodular hyperplasia

Definitions

- Thyroid FND is a multifocal non-inflammatory benign proliferation of thyroid follicular cells that results in multiple clonal and non-clonal nodules with highly variable architecture (WHO 5th edition; 2022)
- Benign, nonneoplastic enlargement of thyroid gland
- Varying degrees of nodularity

Etiology/Pathogenesis: DICER1 Syndrome

- Childhood early onset &/or familial MNGs/FND suggest DICER1 syndrome
- Presence of hyperplastic nodules with centripetal hyperplasia and adenomatous nodules

Histologic Features

- Multiple variably sized nodules identifiable
    - Varying degrees of cellularity and colloid
- Enlarged follicles with flattened epithelium
- Smaller follicles with taller epithelium
    - Sanderson polsters
    - Papillary-type projections into lumina of follicles
- May mimic papillary thyroid carcinoma; however, nuclear features of Sanderson polsters are benign
- Cellular atypia may be present
- Oncocytic changes
- Nuclear clearing
- Signet ring changes
- Variable degree of fibrosis, cystic changes, evidence of hemorrhage, and calcification

Cytology

- Abundant colloid
- Low cellularity
- Degenerative features may be present
- Benign nuclear features
- However, nuclear atypia may be present in some cases

Immunohistochemistry

- Loss of staining for PTEN in thyroid glands with nodular hyperplasia
- Suggested as means of detecting patients with Cowden/PTEN hamartoma tumor syndrome
- Otherwise, normal immunoprofile of thyroid gland remains intact

Genetic Testing

- May demonstrate genetic abnormalities associated with syndromes that lead to clinical presentations of goiter
- Dyshormonogenetic goiter: Genetic disorder that may have mutations in any of number of proteins associated with thyroid hormonogenesis
- PTEN mutation in suspected cases of PTEN-hamartoma tumor syndrome
- Childhood &/or familial MNGs suggest DICER1 syndrome
- Particularly when other highly characteristic diseases like CN or lung cysts co-occur
- Genetic counseling is strongly recommended before *DICER1* mutation analysis
- In patients with *DICER1* mutations, tumor surveillance critical: Increased risk of multiple tumors, including ovarian tumors and pleuropulmonary blastoma
- Epigenetic analysis shows significant promoter hypermethylation of tumor-suppressor gene *RASSF1A*
- Silencing of tumor suppressor *RASSF1A* in subset of MNH

Pathologic Interpretation Pearls

- Essential criteria for diagnosis:
  - Follicular cell proliferations without invasive growth and lacking nuclear features of papillary thyroid carcinoma
  - Papillary hyperplastic protrusions into dilated follicles (Sanderson polsters)
- Desirable criteria:
  - Multiple variably sized nodules
  - Admixture of follicular and papillary growth patterns

References

1. Nosé V, Gill A, Teijeiro JMC, Perren A, Erickson L. Overview of the 2022 WHO Classification of Familial Endocrine Tumor Syndromes. Endocr Pathol. 2022;33(1):197-227. doi:10.1007/s12022-022-09705-5
2. Jonathan D Wasserman, Nelly Sabbaghian, Somayyeh Fahiminiya, Rose Chami, Ozgur Mete, Meryl Acker, Mona K Wu, Adam Shlien, Leanne de Kock, William D Foulkes, DICER1 Mutations Are Frequent in Adolescent-Onset Papillary Thyroid Carcinoma, The Journal of Clinical Endocrinology & Metabolism, Volume 103, Issue 5, May 2018, Pages 2009–2015
3. Nosé V. Thyroid Follicular Nodular Disease. In: Diagnostic Pathology: Endocrine, 3rd Ed, Elsevier 74-79, 2023.
4. Son EJ, Nosé V. Familial follicular cell-derived thyroid carcinoma. Front Endocrinol (Lausanne). 2012;3:61. Published 2012 May 3. doi:10.3389/fendo.2012.00061
5. Nosé V. DICER1 gene alterations in thyroid diseases. Cancer Cytopathol. 2020;128(10):688-689. doi:10.1002/cncy.22327

12TH INTERNATIONAL AMR PATHOLOGY SLIDE SEMINAR SYMPOSIUM IN ANATOMIC PATHOLOGY

Case – 31

Thoracic Pathology

Contributed by: ***David Suster***

Clinical History

A 75-year-old man with no significant past medical history was seen for symptoms of persistent cough. CT scans showed a mass involving the right upper lobe of lung. Following a core needle biopsy, the patient was scheduled for surgery. A thoracotomy with right upper lobectomy was performed. The gross specimen showed a large subpleural mass that measured 5.4 x 4.5 x 3.0 cm. The regional lymph nodes were all free of tumor.

Pathological Findings

Sections from the tumor showed a neoplastic proliferation composed of nests and irregular islands of tumor cells with large central areas of comedo-type necrosis. The tumor cells displayed large, irregular nuclei with prominent nucleoli and scattered mitotic figures, and were surrounded by an ample rim of clear to lightly eosinophilic cytoplasm. There was no evidence of gland formation or areas of maturing keratinization throughout the lesion. Immunohistochemical studies showed strong nuclear positivity of the tumor cells for p40 and cytoplasmic staining for CK5/6. Immunostains for Napsin-A and TTF1 were negative in the tumor cells. Next generation sequencing (NGS) analysis using the Oncomine Precision Assay (ThermoFisher) identified a *FGFR3::TACC3* fusion.

Diagnosis

Clear cell squamous cell carcinoma of the lung with *FGFR3::TACC3* translocation.

Comments

Lung cancers composed predominantly of clear cells are extremely rare and most often confused for metastases from clear cell tumors from other organs. Primary clear cell carcinomas of the lung have been rarely reported in the literature and have been effectively eliminated from the WHO classification of lung tumors since 2004. Clear cells in lung carcinomas tends to usually be focal and are considered within the spectrum of cytologic changes that any type of lung cancer can display. Only 2 large studies have been published on this topic in the literature. The first one was by Katzenstein et al[1] in 1980, who in a study of 348 consecutive lung carcinomas found 15 cases which contained >50% clear cells; 10 tumors showed epidermoid features and the rest showed gland formation. The authors concluded that clear cell carcinoma should not be considered a distinct clinicopathologic entity because there were not sufficient features which allowed for their separation. More recently, Yousem[2] presented the largest study on these tumors, including immunohistochemical and molecular characterization and found that adeno and squamous carcinomas with clear cell features showed an unusually high incidence of *KRAS* mutations compared to other types of lung carcinomas. Conventional non-small cell lung carcinoma (NSCLC), particularly adenocarcinoma, with clear cell features also need to be distinguished from the so-called fetal adenocarcinoma of the lung

that is characterized by a glandular neoplasm with “piano-key like” clearing of the cytoplasm, occasional squamous morules, and underlying *CTNNB1* mutations[4]

We recently reviewed cases from our files and identified 29 cases of lung carcinoma with predominant clear cell changes. The patients were 10 women and 19 men, aged 47-92 years (mean: 70 years). 25 patients had a history of tobacco smoking. By immunohistochemistry, 9 cases were TTF1/Napsin+ and typed as adenocarcinomas; 20 cases were positive for p40 and CK5/6 and negative for TTF1/Napsin and typed as squamous cell carcinomas. Some of the cases demonstrated aggressive histologic features such as pleomorphic giant cells or features of both adeno and squamous carcinomas (i.e. adenosquamous carcinoma). Next generation sequencing identified a variety of abnormalities in these tumors, including alterations in *BRAF, AKT1, KRAS, PIK3A, EGFR,* and *p53.* An interesting finding was the demonstration of a *FGFR3::TACC3* translocation in 7 cases.[3]

Only a subset of non-small cell lung carcinomas (NSCLC) has been described that are characterized by *FGFR* abnormalities; approximately 0.2-3% of cases of NSCLC harbor *FGFR3::TACC3* translocations and their histology has not been well characterized[5]. These fusions have been described so far mostly in the setting of secondary treatment resistance in NSCLC. Our cases were treatment-naïve patients and apparently represented de-novo translocations found in these tumors.

Figure 1: Clear cell squamous cell carcinoma.

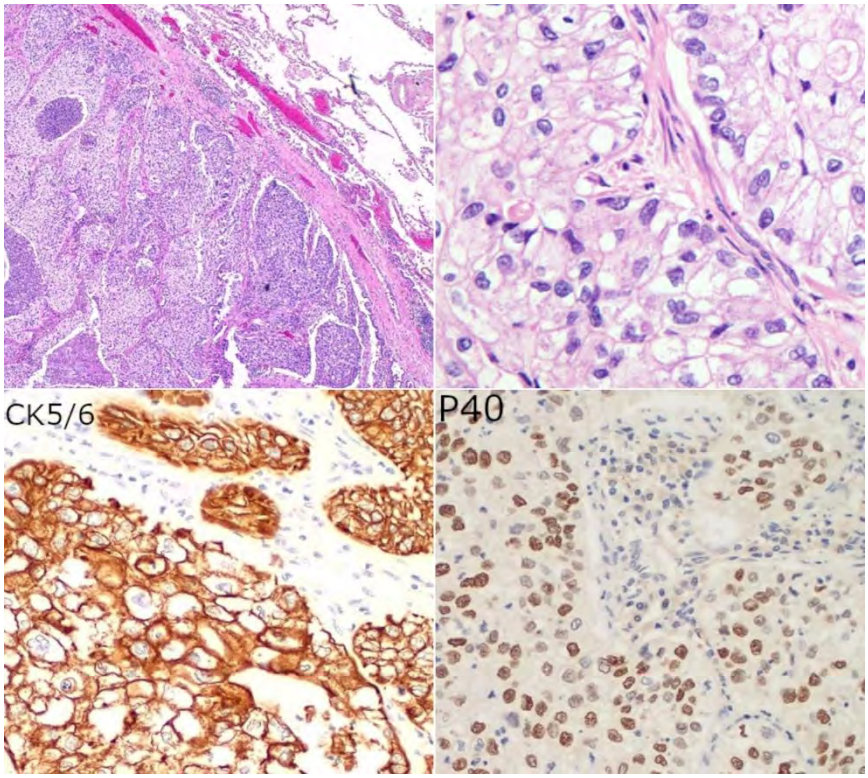

In our cohort, 4 patients were men and 3 were female, and 3 cases typed as adenocarcinoma while 4 typed as squamous cell carcinoma. The high incidence of this translocation in tumors displaying clear cell morphology may underlie a genetic link with this particular morphology and indicate a predisposition of these tumors to exhibit clear cell features at the light microscopic level. Our cases demonstrate that *FGFR3::TACC3* translocations may occur de-novo in treatment naïve patients and appear to be enriched in smokers or former smokers. Numerous trials are currently underway investigating targeted therapies against tumors with *FGFR* gene abnormalities. Identification of *FGFR* alterations may be of particular importance given the lack of targeted therapy options for patients with squamous cell carcinoma.

References

1. Katzenstein AL, Prioleau PG, Askin FB. The histologic spectrum and significance of clear-cell change in lung carcinoma. Cancer 1980; 45:943-947.
2. Yousem SA. Immunohistochemical and molecular characterization of clear cell carcinoma of lung. Hum Pathol 2013; 44:2467-2474.
3. Suster D, Mackinnon AC, Mejbel H, Ronen N, Suster S. Clear cell non-small cell lung carcinoma: Clinicopathologic and molecular genetic analysis of 7 treatment-naïve cases demonstrating *FGFR3::TACC3* gene rearrangements. Mod Pathol 2023; (A).
4. Ricaurte LM, Arrieta O, Zatarain-Barrón ZL, Cardona AF. Comprehensive review of fetal adenocarcinoma of the lung. Lung Cancer (Auckl). 2018 Aug 23;9:57-63.
5. Ou SI, Horn L, Cruz M, Vafai D, Lovly CM, Spradlin A, Williamson MJ, Dagogo-Jack I, Johnson A, Miller VA, Gadgeel S, Ali SM, Schrock AB. Emergence of FGFR3-TACC3 fusions as a potential by-pass resistance mechanism to EGFR tyrosine kinase inhibitors in EGFR mutated NSCLC patients. Lung Cancer. 2017 Sep;111:61-64.

12TH INTERNATIONAL AMR PATHOLOGY SLIDE SEMINAR SYMPOSIUM IN ANATOMIC PATHOLOGY

Case – 32

Thoracic Pathology

Contributed by: ***Alberto Cavazza***

Clinical History and Pathological Findings

A 33-year-old previously healthy woman presented with exertional dyspnoea and non-productive cough, which she reported following the exposure to the smokes of a fire. No other risk factors for lung disease nor systemic symptoms were present. Laboratory parameters were normal except for mild thrombocytopenia. Pulmonary function tests revealed a restrictive pattern, and HRCT of the chest showed bilateral ground-glass opacities with focal thickening of interlobular septa. A bronchoscopy with bronchoalveolar lavage (BAL) and transbronchial biopsy (TBB) was performed: both showed only foamy macrophages and were considered non diagnostic, so a video-assisted thoracoscopic biopsy was obtained (the material you received). Histologically, the lung architecture was preserved. The most stricking finding was the diffuse filling of the alveolar spaces by foamy macrophages. A different type of histiocytes focally expanded the pleura and interlobular septa: their cytoplasm contained a green, strongly PAS-positive material which contrasted with the finely vacuolated, fintly PAS-positive cytoplasm of the intra-alveolar macrophages. The bronchiolar epithelium had a clear cytoplasm similar to the cytoplasm of the intra-alveolar macrophages. At that time (20 years ago) a descriptive diagnosis was rendered and the patient was discharged with prednisone therapy. After 3 months she presented again for worsening dyspnea and abdominal pain. A CT-scan showed a progression of the lung opacities, hepatomegaly and 3 hypodense lesions of the spleen suggestive for infarcts. At this point the multidisciplinary team suggested a metabolic disorder. A skin biopsy was obtained to measure the acid sphingomyelinase (ASM) activity on cultured fibroblasts, which was decreased, and mutation of the sphingomyelin phosphodiesterase 1 gene (*SMPD1*) was detected.

Diagnosis

Niemann-Pick disease involving the lung.

Comments

Niemann-Pick dieases (NPD), also known as acid sphingomyelinase deficiency (ASMD), is a rare disorder caused by mutations in *SMPD1*, resulting in the abnormal storage of macrophages filled with lipids, mostly sphingomyelin and cholesterol. NPD is a clinically and biochemically heterogeneous disorder, with 6 variants recognized (types A to F). Type B NPD is characterized by hepatosplenomegaly, absence of neurologic involvement and a protracted clinical course, with many patient surviving to adulthood. Lung involvement in the form of interstitial lung disease is frequent and may precede NPD diagnosis or may develop during follow-up. It may occur at any age, with no sex predilection. The clinical presentation varies from asymptomatic to pulmonary failure, but in many patients respiratory symptoms are mild, consisting in exertional dyspnea and cough. Pulmonary function tests generally show a restrictive pattern with DLCO reduction. CT scan abnormalities consist in ground-glass opacities and interlobular septal thickening, sometimes combined (so called “crazy paving” pattern).

Histologically, the most significant finding is the intra-alveolar accumulation of finely vacuolated macrophages, so called endogenous lipoid pneumonia. In contrast, in *exogenous* lipoid pneumonia (i,e, aspiration of oily material) vaculoles are larger, irregular with nuclear indentation, and there is an associated fibrosis and granulomatous reaction typically absent in *endogenous* lipoid pneumonia. Other, more frequent causes of endogenous lipoid pneumonia are downstram of bronchial/bronchiolar obstrucions and drug reactions (i.e. amiodarone), but in surgical lung biopsy the combination of foamy macrophages with interstitial PAS-positive macrophages and cytoplasmic clarification of the bronchiolar epithelium, without other significant alterations, is characteristic of type B NPD.

After this case I have seen a few other examples of lung involvement in type B NPD: their clinical, radiologic and histologic findings where stereotyped. For this reason, I think a surgical lung biopsy is generally not necessary for the diagnosis: a BAL and/or a TBB showing only intra-alveolar foamy macrophages, albeit non-specyfic, in the correct clinical-radiologic scenario are enough to suggest the possibility of type B NPD, leading to the appropriate genetic tests and avoiding a surgical lung biopsy.

References

1. Falco F et al. Pulmonary involvement in an adult female affected by type B Niemann-Pick disease. Sarcoidosis Vasculitis DiffLung Dis 2005;22:229-233.
2. Nicholson AG et al. Pulmonary involvement by Niemann-Pick disease. Report of six cases. Histopathology 2006;48:596-603.
3. Borie R et al. Interstitial lung disease in lysosomal storage disorders. Eur Respir Rev 2021;30:200363.
4. Mendelson DS et al. Type B Niemann-Pick disease: findings at chest radiography, thin-section CT, and pulmonary function testing. Radiology 2006;238:339-345.

12TH INTERNATIONAL AMR PATHOLOGY SLIDE SEMINAR SYMPOSIUM IN ANATOMIC PATHOLOGY

Case – 33

Thoracic Pathology

Contributed by: ***Alberto M. Marchevsky***

Clinical History

The patient is a 29 year-old male with a history of cystic fibrosis, diabetes, and chronic respiratory failure requiring bilateral orthotopic lung transplantation at another institution, approximately 3 years prior to current admission. He had several post-operative episodes of acute cellular rejection, and an episode of right pneumothorax after a transbronchial lung biopsy; it required chest tube placement. Approximately 1 years after transplantation, he developed progressive dyspnea on exertion and severe gastroenteric reflux disease (GERD). The forced expiratory volume at 1 second (FEV1) decreased more than 10% predicted to 60% predicted and he was diagnosed with bronchiolitis obliterative syndrome (BOS). This diagnosis requires an FEV1 <75% predicted, an irreversible ≥10% decline in FEV1 <2 years, a FEV1-to-vital capacity (VC) ratio <0.7 or the lower limit of the 90% confidence interval of the ratio, absence of infection, and a preexisting diagnosis of chronic graft versus host disease or of air trapping on physical examination and imaging studies.

He was referred to Cedars-Sinai Medical Center with the diagnosis of chronic lung allograft disfunction (CLAD) syndrome for possible redo bilateral orthotopic lung transplantation. On admission he was in chronic hypoxemic respiratory failure requiring 10 liters of oxygen at rest. He was severely disabled with a Karnofsky score of 30%. Physical examination showed diffuse bilateral basilar crackles with poor bilateral apical air movement. Chest CT showed diffuse air trapping on expiratory phase, diffuse mild bronchial wall thickening and bronchiectasis. He was diagnosed with CLAD, bronchiolitis obliterans subtype and treated with redo-bilateral orthotopic lung transplantation.

The slide sent for review was collected from his right lung explant.

Pathological Findings

Both lungs were overinflated prior to placing in formalin and showed focal areas of pleural thickening. The lower lobes had a few cylindrical bronchiectasis, but the airways showed no mucus impaction or other gross abnormalities suggestive of cystic fibrosis. Alveolated lung parenchyma was grossly unremarkable, without areas of fibrosis, emphysema, or focal lesions.

Microscopically, the lungs were remarkable for the paucity of abnormal histopathologic changes. Alveoli were normal with only focal areas of minimal inflammation. Examination of multiple sections showed the presence of focal obliterative bronchiolitis (OB), with minimal chronic inflammation and variable fibrosis that narrowed or obliterated the lumina of distal bronchioles. Few small arteries showed intimal fibrosis. No perivascular lymphoid infiltrates were seen.

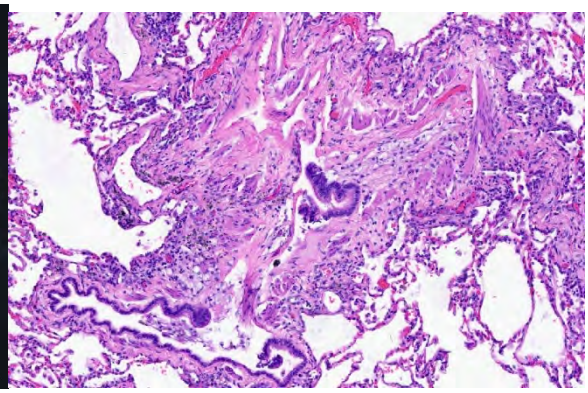

Diagnosis

Obliterative Bronchiolitis (Grade D rejection).

Comments

This case illustrates the presence of OB as the main manifestation of chronic rejection in a patient with chronic allograft disfunction (CLAD) syndrome.

Lung transplantation has become a widely used method to treat a variety of severe pulmonary diseases resulting in chronic respiratory failure. The results have steadily improved with the use of surgical techniques, better organ preservation solutions and modern immunosuppressive therapy, with survival rates of approximately 70% and 50% at 1 year and 5 years, respectively.

A variety of post-surgical complications and problems related to acute and chronic allograft rejection have been described. The immediate post-operative period can be complicated by the development of hyperacute rejection or allograft disfunction characterized by the development of diffuse alveolar damage and/or acute pulmonary hemorrhage, and/or by various surgical complications such as airway dehiscence, vascular obstruction, and others. Patients can also develop acute allograft disfunction resulting from antibody mediated rejection (AMR) caused by circulating antibodies that were present prior to transplantation. In this condition, the lungs develop acute lung injury changes such as diffuse alveolar damage and intrapulmonary hemorrhage and exhibit deposition of C4d in vascular walls. To my knowledge, there is still some controversy about how to distinguish AMR from harvest injury, reimplantation response and hyperacute rejection.

Days or weeks after transplantation, patients can develop large airway stenosis, infections such as bacterial pneumonias and others and acute cellular rejection. Acute cellular rejection can first develop approximately a week after transplantation and is diagnosed in the presence of perivascular lymphoid infiltrates in intrapulmonary arterioles and venules. The histopathologic changes are graded using a working formulation proposed by the International Society for Heart and Lung Transplantation (ISHLT) in 1996 and updated in 2007. It is shown in this table:

Table 1. Revised Working Formulation for Classification and Grading of Pulmonary Allograft Rejection

A: Acute rejection
Grade 0—none
Grade 1—minimal
Grade 2—mild
Grade 3—moderate
Grade 4—Severe
B: Airway Inflammation
Grade 0—none
Grade 1R—low grade
Grade 2R—high grade
Grade X—ungradeable
C: Chronic airway rejection—obliterative bronchiolitis
0—absent
1—present
D: Chronic vascular rejection—accelerated graft vascular sclerosis

"R" denotes revised grade to avoid confusion with 1996 scheme.

Grade I acute cellular rejection is characterized by the presence of perivascular lymphoid infiltrates in few vessels. Multiple deeper cuts need to be performed on the transbronchial biopsies and the changes can be usually detected after careful review of all sections at 100x microscopy. A minimum of 5 fragments of alveolated lung parenchyma are needed for a reliable diagnosis. It is recommended to list the number of lung fragments in the biopsy report. In cases with fewer than 5 lung fragments a note is included to alert the pulmonologists that the results are limited by scanty tissue availability. In grade II acute cellular rejection, the perivascular infiltrates can be readily identified at 40x magnification and are present in several arterioles and/or venules. Focal endothelialitis is often present. In grade III acute cellular rejection, numerous perivascular lymphoid infiltrates are present and extend into adjacent alveoli. The lungs show numerous perivascular infiltrates, interstitial infiltrates, and hemorrhagic necrosis in grade IV acute cellular rejection.

The working formulation includes a rB (Revised B) category to designate the presence of lymphocytic bronchiolitis. This nomenclature can create confusion, as this finding is not diagnostic of acute cellular rejection. It was included in the schema to document the presence of airway inflammation and collect data about a potential predictive factor for the development of grades C or D rejection. To my knowledge, no significant correlation between rB grade and chronic rejection has been reported.

Obliterative bronchiolitis (OB) is characterized by the presence of concentric or eccentric dense eosinophilic hyaline fibrosis in the sub-mucosa of membranous and respiratory bronchioles, resulting in partial or complete occlusion of their lumina. Some authors prefer to use the terminology of fibrosing bronchiolitis, not to confuse OB for bronchiolitis obliterans (BO), a feature of cryptogenic organizing pneumonia (COP). The latter is characterized by the presence of early fibrosis characterized by the presence in the lumina of respiratory bronchioles and alveolar ducts of fibroblasts admixed with a myxoid stroma. Adjacent alveoli often show mucostasis, and/or intraalveolar foamy histiocytes in a pattern reminiscent of endogenous lipoid pneumonia. Trichrome and EVG stains are very helpful to identify bronchioles with obliterative bronchiolitis and these stains should be performed routinely during the evaluation of biopsies from CLAD patients. Grade C rejection can often be missed on transbronchial biopsies due to sampling error. Pulmonologists usually diagnose the bronchiolitis obliterans syndrome (BOS) based on clinical findings and pulmonary function.

D rejection is characterized by the presence of intimal fibrosis and thickening in the wall of pulmonary arteries and veins. It cannot be diagnosed on transbronchial lung biopsies.

References

1. Berry GJ, Brunt EM, Chamberlain D, Hruban RH, Sibley RK, Stewart S, Tazelaar HD. A working formulation for the standardization of nomenclature in the diagnosis of heart and lung rejection: Lung Rejection Study Group. The International Society for Heart Transplantation. J Heart Transplant 1990; 9, 593-601.
2. Billingham ME, Cary NR, Hammond ME, Kemnitz J, Marboe C, McCallister HA, Snovar DC, Winters GL, Zerbe A. A working formulation for the standardization of nomenclature in the diagnosis of heart and lung rejection: Heart Rejection Study Group. The International Society for Heart Transplantation. J Heart Transplant 1990; 9, 587-593.
3. Winters GL. The international society for heart and lung transplantation working formulation for heart transplant rejection: Is it making the grade? Cardiovasc Pathol 1992; 1, 93-95.
4. Cooper JD, Billingham M, Egan T, Hertz MI, Higenbottam T, Lynch J, Mauer J, Paradis I, Patterson GA, Smith C, et al. A working formulation for the standardization of nomenclature and for clinical staging of chronic dysfunction in lung allografts. International Society for Heart and Lung Transplantation. J Heart Lung Transplant 1993; 12, 713-716.

5. Yousem S. A perspective on the Revised Working Formulation for the grading of lung allograft rejection. Transplant Proc 1996; 28, 477-479.
6. Yousem SA, Berry GJ, Cagle PT, Chamberlain D, Husain AN, Hruban RH, Marchevsky A, Ohori NP, Ritter J, Stewart S, Tazelaar HD. Revision of the 1990 working formulation for the classification of pulmonary allograft rejection: Lung Rejection Study Group. J Heart Lung Transplant 1996; 15, 1-15.
7. Stewart S, Fishbein MC, Snell GI, Berry GJ, Boehler A, Burke MM, Glanville A, Gould FK, Magro C, Marboe CC, McNeil KD, Reed EF, Reinsmoen NL, Scott JP, Studer SM, Tazelaar HD, Wallwork JL, Westall G, Zamora MR, Zeevi A, Yousem SA. Revision of the 1996 working formulation for the standardization of nomenclature in the diagnosis of lung rejection. J Heart Lung Transplant 2007; 26, 1229-1242.
8. Snell GI, Boehler A, Glanville AR, McNeil K, Scott JP, Studer SM, Wallwork J, Westall G, Zamora MR, Stewart S. Eleven years on: a clinical update of key areas of the 1996 lung allograft rejection working formulation. J Heart Lung Transplant 2007; 26, 423-430.

12TH INTERNATIONAL AMR PATHOLOGY SLIDE SEMINAR SYMPOSIUM IN ANATOMIC PATHOLOGY

Case – 34

Thoracic Pathology

Contributed by: ***Alberto M. Marchevsky***

Clinical History

The patient is a 67-year-old male who developed COVID-19 syndrome with fever, congestion, body aches and cough about 2 ½ years prior to this admission. He was overweight and had no previous preexistent illnesses such as diabetes, hypertension, or others. The respiratory symptoms worsened, and he developed progressive dyspnea that required hospitalization to a respiratory intensive care unit (RICU). On admission, he was diagnosed with respiratory failure and bilateral pneumonia. Imaging studies showed extensive bilateral pulmonary infiltrates. He was intubated and treated with antibiotics, steroids, and other medications. He was extubated after several weeks in the RICU and discharged with a diagnosis of chronic respiratory failure on 5-6 liters of oxygen. He remained extremely dyspneic and was unable to climb one flight of stairs. The respiratory insufficiency worsened, and lung transplantation was recommended.

On admission he was in hypoxic respiratory failure requiring 40 liters of oxygen delivered by high flow nasal cannula. Chest CT showed extensive bilateral interstitial fibrosis, greater in the right lung than in the left lung and including bibasilar predominant bronchiectases, reticulation, and honeycombing. The right lung was almost completely fibrotic with some sparing at the apex. The left lung also had extensive fibrotic changes in the lower lobe with slightly less severe involvement of the upper lobe. The main pulmonary artery was mildly dilated to 34 mm, consistent with pulmonary hypertension.

He underwent bilateral orthotopic lung transplantation approximately 30 weeks after the initial symptoms of acute COVID-19 syndrome. The slide sent for review and discussion was taken from the native right lung explant.

Pathological Findings

Both explanted lungs showed similar pathologic findings with severe fibrotic changes that were more extensive in the right lung than in the left lung. Multiple cystic bronchiectasis with dilated bronchi showing variable chronic inflammation, extensive goblet cell hyperplasia, focal squamous metaplasia and extensive peribronchial fibrosis were present in all lobes, with predominant distribution in the lower lobes. The alveoli were mostly fibrotic with extensive areas showing interstitial chronic inflammation and/or thin fibrosis, in a pattern akin that seen in patients with nonspecific interstitial pneumonia (NSIP). These fibrotic areas were interspersed with larger irregular areas of fibrosis and small foci of organizing pneumonia with reactive pneumocyte hyperplasia and poorly formed Masson bodies. Other histopathologic findings included foci of endogenous lipoid pneumonia, hemosiderosis and a small number of scattered multinucleated giant cells. No viral changes, well-formed epithelioid granulomas, vasculitis, or thrombi were seen.

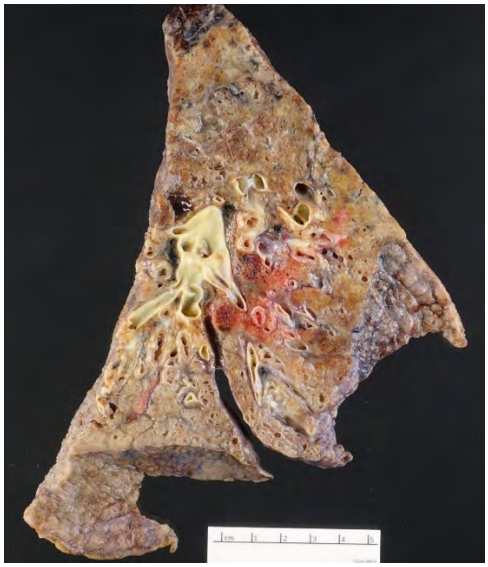

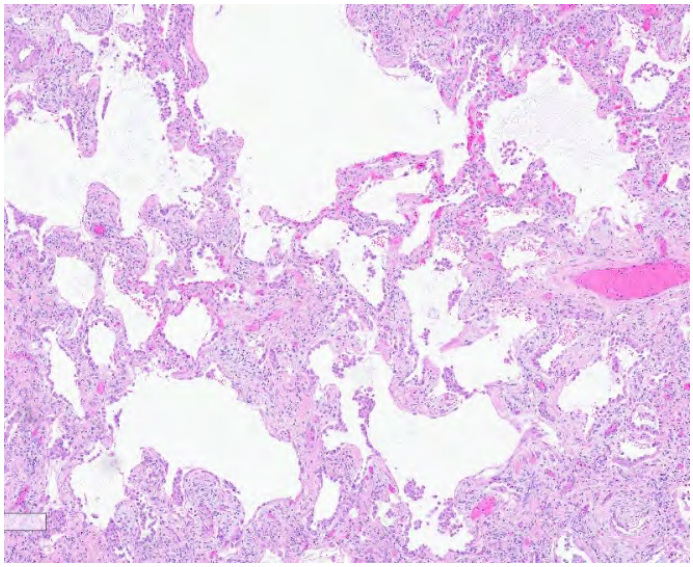

Diagnosis

Severe Interstitial Fibrosis with features resembling Nonspecific Interstitial Pneumonia (NSIP) in a patient with post-acute COVID-19 syndrome.

Comments

The coronavirus disease 2019 (COVID-19) pandemic, caused by the severe acute respiratory syndrome coronavirus 2 (SARS-CoV-2), has posed the greatest medical and public health challenge in decades, with more than 450 million total cases and 6 million deaths worldwide. The SARS-CoV-2 virus infects the respiratory tract and other organs, resulting in a multi organ disease with respiratory, cardiac, neurologic, and other manifestations. Approximately 33% of hospitalized COVID-19 patients develop acute respiratory distress syndrome and pneumonia that can progress to respiratory failure requiring Extracorporeal Membrane Oxygenation (ECMO)/mechanical ventilation**.** COVID-19 patients treated with ECMO have a 39% in-hospital mortality and a 1.34 higher risk mortality ratio than in those with influenza treated in a similar manner. Several autopsy studies have shown that the lungs of patients dying from acute/subacute COVID-19 syndrome often show diffuse alveolar damage (DAD) changes in either exudative or proliferative phase that are often associated with intraalveolar hemorrhage, superimposed bacterial or fungal pneumonias, multiple thromboemboli, and/or vasculitis in pulmonary vessels. Other pulmonary findings can include interstitial/alveolar edema, interstitial lymphocytic infiltrates, pneumocyte reactive hyperplasia, multinucleated giant cells, arteriolar microthrombi, organizing pneumonia and others. Extrapulmonary findings include myocarditis, acute tubular injury, gastric hemorrhage, shock liver, encephalitis, and others.

Post-acute or long COVID-19 syndrome is defined by the Center for Disease Control (CDC) as the presence of persistent symptoms and delayed or long-term complications beyond 4 weeks of the initial infection. Various clinical problems have been described, such as progressive interstitial fibrosis, superimposed bacterial and other infectious pneumonias, pulmonary thromboemboli, pulmonary hypertension and others. There is only limited information in case reports and small case series about the histopathologic findings in the lungs of patients with post-acute COVID-19 syndrome that suffer from chronic pulmonary disease. For example, Aesif et al reported the presence of diffuse interstitial fibrosis and lung infarction in a small retrospective series of 3 patients. Konopka et al reported a spectrum of pathologic changes including organizing diffuse alveolar damage, usual interstitial fibrosis, and other patterns of interstitial fibrosis in surgical lung biopsies from 18 patients. Rohr el al described the presence of pulmonary hypertensive changes in a single patient with post-acute COVID-

19 syndrome that underwent bilateral lung transplantation. Flaifel at al reported a spectrum of fibrotic changes in the explants of 3 patients that underwent lung transplantation. Konopka et al reported that interstitial pneumonia in a pattern consistent with usual interstitial pneumonia (UIP) was the most frequent finding in surgical lung biopsies from patients with persistent interstitial lung disease following infection with SARS-CoV-2.

We are in the process of reviewing our experience with the lungs explanted from 45 patients with severe interstitial fibrosis secondary to post-acute COVID-19 syndrome treated with bilateral orthotopic lung transplantation. All specimens showed extensive areas of interstitial fibrosis in a pattern similar to nonspecific interstitial fibrosis (NSIP), admixed with irregular areas of fibrosis exhibiting an unclassifiable pattern. In contrast with the experience by Konopka et al, none of our explants exhibited fibrotic changes consistent with the UIP pattern of fibrosis.

In addition to NSIP and nonspecific patterns of fibrosis, bronchiectasis, bronchioloectasia, and focal peribronchiolar metaplasia were present in all cases and focal multinucleated giant cells were seen in all but 3 cases. Other focal changes present in a few cases included obliterative bronchiolitis and microthrombi. About ¾ of the cases also had scattered areas of acute alveolitis consistent with superimposed bacterial infections.

Interestingly, none of our lung explants exhibited histopathologic features of diffuse alveolar damage, thrombosis in large pulmonary vessels, vasculitis and/or lung infarcts, as seen in the autopsies of patients dying with acute COVID-19 syndrome.

References

1. Thakur V, Ratho RK, Kumar P, et al. Multi-Organ Involvement in COVID-19: Beyond Pulmonary Manifestations. J Clin Med 2021; 10.
2. Lai CC, Hsu CK, Yen MY, et al. Long COVID: An inevitable sequela of SARS-CoV-2 infection. J Microbiol Immunol Infect 2022.
3. Bertini P, Guarracino F, Falcone M, et al. ECMO in COVID-19 Patients: A Systematic Review and Meta-analysis. J Cardiothorac Vasc Anesth 2022; 36, 2700-2706.
4. Wichmann D, Sperhake JP, Lutgehetmann M, et al. Autopsy Findings and Venous Thromboembolism in Patients With COVID-19: A Prospective Cohort Study. Ann Intern Med 2020; 173, 268-277.
5. Bosmuller H, Traxler S, Bitzer M, et al. The evolution of pulmonary pathology in fatal COVID-19 disease: an autopsy study with clinical correlation. Virchows Arch 2020; 477, 349-357.
6. Calabrese F, Pezzuto F, Fortarezza F, et al. Pulmonary pathology and COVID-19: lessons from autopsy. The experience of European Pulmonary Pathologists. Virchows Arch 2020; 477, 359-372.
7. Borczuk AC. Pulmonary pathology of COVID-19: a review of autopsy studies. Curr Opin Pulm Med 2021; 27, 184-192.
8. Flaifel A, Kwok B, Ko J, Chang S, Smith D, et al Pulmonary Pathology of End-Stage COVID-19 Disease in Explanted Lungs and Outcomes After Lung Transplantation. Am J Clin Pathol 2022; 157, 908-926.
9. Rohr JM, Strah H, Berkheim D, et al. Pulmonary Hypertensive Changes Secondary to COVID-19 Pneumonia in a Chronically SARS-CoV-2-Infected Bilateral
10. Konopka KE, Perry W, Huang T, Farver CF, Myers JL. Usual Interstitial Pneumonia is the Most Common Finding in Surgical Lung Biopsies from Patients with Persistent Interstitial Lung Disease Following Infection with SARS-CoV-2. EClinicalMedicine 2021; 42, 101209.
11. Aesif SW, Bribriesco AC, Yadav R, et al Pulmonary Pathology of COVID-19 Following 8 Weeks to 4 Months of Severe Disease: A Report of Three Cases, Including One With Bilateral Lung Transplantation. Am J Clin Pathol 2021; 155, 506-514.

12. Luo WR, Yu H, Gou JZ, Li XX, et al. Histopathologic Findings in the Explant Lungs of a Patient With COVID-19 Treated With Bilateral Orthotopic Lung Transplant. Transplantation 2020; 104, e329-e331.
13. Roden AC, Boland JM, Johnson TF, et al. Late Complications of COVID-19. Arch Pathol Lab Med 2022; 146, 791-804.

12TH INTERNATIONAL AMR PATHOLOGY SLIDE SEMINAR SYMPOSIUM IN ANATOMIC PATHOLOGY

Case – 35

Thoracic pathology

Contributed by: ***Brandon Larsen***

Clinical History

A 62-year-old man was found to have a large mass in the left lung and multiple bony metastases. A biopsy of the lung mass was obtained, and this showed a poorly differentiated malignancy with features diagnostic of NUT carcinoma. IHC for NUT was diffusely positive with a speckled nuclear pattern; diffuse expression of p40 was also present, along with patchy staining for AE1/AE3 and Cam5.2, without staining for TTF-1, SOX10, CD34, CD45, or S100 protein, and normal (retained) expression of INI1 and BRG1. Next-generation sequencing confirmed the presence of a *BRD3-NUTM1* fusion. The patient received multiple cycles of palliative chemotherapy with carboplatin and paclitaxel and radiation to his spine and hip. Because of severe hip pain from a large metastatic tumor deposit in his pelvis and an impending pathologic fracture, a resection and reconstruction of the right hemipelvis was performed.

Pathological Findings

The sections from the resected bone show metastatic non-small cell carcinoma with diffuse squamous differentiation and patchy keratinization, in a markedly fibrotic tumor bed with exuberant desmoplasia. The tumor itself shows marked treatment-induced cytologic changes with varying degrees of atrophy, vacuolization, and degenerative change. Immunohistochemistry shows focal, very weak nuclear NUT expression in the tumor but most of the tumor completely lacks NUT immunoreactivity.

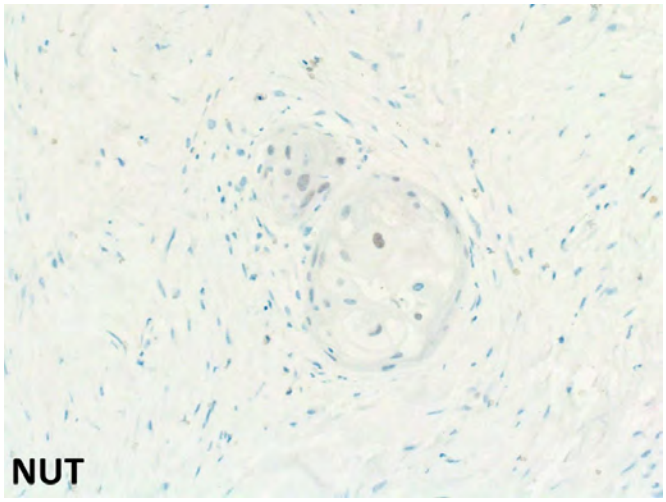

Diagnosis

Metastatic NUT carcinoma with *BRD3-NUTM1* fusion, with diffuse treatment-induced squamous differentiation.

Comments

NUT carcinoma is an uncommon and particularly aggressive non-small cell carcinoma defined by the presence of a rearrangement of the *NUTM1* gene, most commonly fused with the *BRD4* gene. Less commonly, *NUTM1* may be fused with other genes encoding BRD4-interacting proteins such as *BRD3*, *NSD3*, and others. This tumor most commonly arises in the thorax, but this tumor is now recognized to occur at other anatomic sites, particularly in the head and neck.

Diagnosis of NUT carcinoma hinges on demonstration of a *NUTM1* gene rearrangement, with NUT immunohistochemistry representing a highly sensitive and specific surrogate marker for this molecular alteration. However, NUT overexpression is typically seen only in the undifferentiated component of the tumor and is not typically seen in areas of abrupt squamous differentiation and keratinization. While not generally a diagnostic problem in treatment-naïve tumors composed primarily or entirely of undifferentiated cells, NUT carcinoma may undergo marked treatment-induced squamous differentiation with little to no residual undifferentiated component, resulting in a tumor with minimal NUT overexpression by immunohistochemistry, representing a potential diagnostic pitfall in the post-treatment setting.

References

1. French CA. NUT carcinoma: Clinicopathologic features, pathogenesis, and treatment. Pathol Int. 2018;68(11):583-95.
2. Bishop JA, Westra WH. NUT midline carcinoma of the sinonasal tract. Am J Surg Pathol. 2012;36(8):1216-21.
3. Torre M, Qian X. Cytopathologic and immunophenotypic changes in NUT midline carcinoma after targeted therapy. Cancer Cytopathol. 2017;125(1):70.
4. Stathis A, Zucca E, Bekradda M, et al. Clinical response of carcinoma harboring the BRD4-NUT oncoprotein to the targeted bromodomain inhibitor OTX015/MK-8628. Cancer Discov. 2016;6:492-500.
5. Filippakopoulos P, Qi J, Picaud S, et al. Selective inhibition of BET bromodomains. Nature. 2010;468:1067-73.

12TH INTERNATIONAL AMR PATHOLOGY SLIDE SEMINAR SYMPOSIUM IN ANATOMIC PATHOLOGY

Case – 36

Thoracic Pathology

Contributed by: ***Alberto Cavazza***

Clinical History and Pathological Findings

A 76-year-old previously healthy man presented with cough and mild fever persisting for more than 1 month. Blood exam showed an increase in inflammatory markers and neutrophilia, with negative autoimmune and oncologic markers. At CT-scan multiple nodules were present in both lungs, some of them cavitating and associated with minimal ground-glass opacities: the radiologic differential diagnosis was metastases, septic emboli/infection and granulomatosis with polyangiitis (Wegener's granulomatosis). A percutaneous fine-needle biopsy was performed, showing suppurative inflammation with negative culture results. A bronchoscopy with bronchoalveolar lavage (BAL) and transbronchial biopsy (TBB) was obtained: BAL was negative, whereas TBB (the biopsy you received) demonstrated a focal intra-alveolar accumulation of granular, eosinophilic and PAS-positive material, with dense eosinophilic globules and cholecterol clefts, diagnostic of alveolar proteinosis. At multidisciplinary discussion it was clear that TBB sampled only the ground-glass opacities and not the nodules: however, knowing that the ground-glass opacities corresponded to alveolar proteinosis increased the probability that the nodules were due to infection, particularly *nocardia* (see "comments" below). The patient's clinical conditions worsened and the clinician decided to obtain a surgical lung biopsy to reach a firm diagnosis. Histologically, surgical lung biopsy showed an inflammatory suppurative nodule containing GMS-positive filaments suggestive of *nocardia*. In the surrounding lung a single focus of alveolar proteinosis was present. Cultural exams performed on lung tissue confirmed *nocardia asteroides*. Serum granulocyte/macrophage colony stimulating factor (GM-CSF) autoantibodies were tested and were found at high concentration.

Diagnosis

Nocardia pneumonia in a patient with underlying autoimmune pulmonary alveolar proteinosis (the latter probably remained asymptomatic for a longtime, until infected).

Comments

Follow-up: the patient was treated with antibiotics for 6 months, with marked clinical improvement. Follow-up CT-scan showed the disappearance of the lung nodules, but the appearance of a diffuse "crazy paving".

I presented this case as an example of fruitful cross-talk between clinician, radiologist and pathologist in the diagnosis of interstitial lung diseases.

Nocardia pneumonia is generally associated with underlying conditions causing immunosuppression, including pulmonary alveolar proteinosis (PAP). PAP is a rare syndrome characterized by abnormal accumulation of alveolar surfactant, a fluid preventing alveolar collapse that is produced by type 2 pneumocytes, secreted into the alveolar spaces and cleared by alveolar macrophages. A recent classification of the disorders of surfactant homeostasis has been proposed, distinguishing conditions due to reduced clearance (PAP) from those due to abnormal production

(pulmonary surfactant metabolic dysfunction – PSMD). PAP is further subdivided into primary and secondary forms. Primary PAP can be an autoimmune disease caused by GM-CSF autoantibodies, or a genetic disease caused by mutations of different genes coding for the GM-CSF receptor, whereas secondary PAP arises in association with several diseases including hematologic disorders, malignant tumors, immune deficiencies, chronic inflammatory diseases, chronic infections and silica inhalation. On the other hand, PSMD is due to mutations of several genes of the surfactant synthesis pathway.

All these disorders are rare, with autoimmune PAP being the most frequent accounting for 90% of cases. It occurs mostly in adults, with a slight male predominance. Symptoms generally consist in dyspnea of insidious onset with or without cough and tend to be mild, frequently milder than expected from radiographic findings. At least 30% of patients with autoimmune PAP are asymptomatic. Depending on the severity of the disease, the results of the pulmonary function tests may be normal, or may show a restrictive defect with DLCO reduction. CT scan, albeit non-specific, is characteristic and typically consists in areas of ground-glass opacities with sharp margins and with superimposed reticular lines, giving an appearance that has been described as “crazy paving”. Bronchoscopy is frequently diagnostic, in particular BAL that macroscopically has a milky appearance and on cytologic examination reveals the typical granular, PAS positive material. In our patient BAL was negative, probably due to the focal distribution of the disease at onset. GM-CSF autoantibodies are important not only for the pathogenesis of the disease, but also for the diagnosis: high levels of serum GM-CSF autoantibodies are diagnostic of autoimmune PAP, with a sensitivity and specificity of 100%.

Biopsies are generally not necessary, but when obtained show the classical eosinophilic, granular material filling the alveolare spaces: dense eosinophilic globules and cholesterol clefts are frequently present and are helpful to exclude histologic simulators, like mucus, dense edema and *pneumocystis*. When partial resorption occurs, the diagnostic material can be very focal and may be overlooked: in these cases a florid granulomatous reaction to cholesterol clefts is frequently present and is a helpful clue of an underlying PAP. On the other hand, it is worth noting that a focal proteinaceous material can be seen occasionally as an incidental finding in other conditions, particularly secondary interstitial lung diseases.

The natural history is variable, including progressive deterioration, stable disease and spontaneous resolution. Patients with PAP have an increased risk to develop infections, particularly due to *nocardia* and *mycobacteria*, mostly in the lungs but also in extra-pulmonary locations. Whole-lung lavage and inhaled GM-CSF supplement are the main therapeutic options and are effective in the majority of the patients.

References

1. Carbonelli C et al. Cavitating pulmonary nodules growing in a favourable medium. Thorax 2013;68:1078-1083.
2. McCarthy C et al. Autoimmune pulmonary alveolar proteinosis. Am J Respir Crit Care Med 2022;205:1016-1035.
3. Trapnell BC et al. Pulmonary alveolar proteinosis syndrome. In Murray & Nadel. Textbook of respiratory medicine. Seventh edition, 2022.
4. Punatar AD et al. Opportunistic infections in patients with pulmonary alveolar proteinosis. J Infect 2012;65:173-179.

12TH INTERNATIONAL AMR PATHOLOGY SLIDE SEMINAR SYMPOSIUM IN ANATOMIC PATHOLOGY

Case – 37

Thoracic pathology

Contributed by: ***Brandon Larsen***

Clinical History

A 33-year-old woman with end-stage renal disease of unclear etiology at age 18 and prior renal transplantation at age 22 was found to have numerous bilateral pulmonary nodules. After a biopsy performed at an outside hospital was non-diagnostic, the patient underwent a wedge resection of one of the lung nodules.

Pathological Findings

Sections of the resected lung nodule show a nodular deposit of amorphous eosinophilic material associated with a foreign body-type giant cell inflammatory reaction and surrounded by chronic lymphoplasmacytic inflammatory infiltrates in the adjacent parenchyma. Though the morphologic appearance of the amorphous material was initially suggestive of amyloidosis, a Congo red stain was negative. This prompted Masson trichrome and sulfated alcian blue stains, which stained the amorphous nodular deposit with a bright red color and salmon pink color, respectively. Immunohistochemistry for CD3, CD5, CD10, CD20, CD21, CD43, BCL2, BCL6, and cyclin D1 was performed, along with in situ hybridization of kappa and lambda light chains, to characterize the lymphoplasmacytic infiltrates adjacent to the nodule. This workup revealed a kappa light chain-restricted population of plasma cells, along with scattered aggregates of small B-cells and scattered small T-cells without aberrant antigen expression. Molecular testing was negative for the MYD88 L265P gene mutation. Mass spectrometry confirmed abundant kappa immunoglobulin light chains in the nodule, without amyloid chaperone proteins or other evidence of amyloidosis.

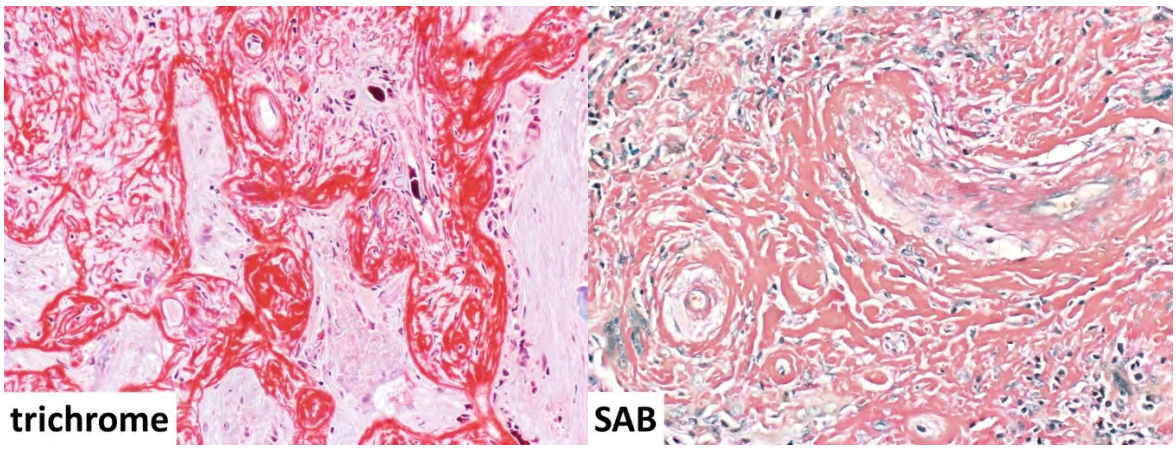

Diagnosis

Light chain deposition disease (kappa-type), associated with extranodal marginal zone lymphoma of mucosa-associated lymphoid tissue (MALT lymphoma).

Comments

Light chain deposition disease (LCDD) is a non-amyloidogenic monoclonal immunoglobulin deposition disorder that almost always involves the kidneys, but LCDD may also involve the heart, liver, and other anatomic sites. Pulmonary involvement by LCDD is rare with less than 100 cases reported in the literature. Patterns of deposition in the lung include diffuse deposition in alveolar walls (without disruption of pulmonary architecture) sometimes accompanied by cystic parenchymal change, and nodular deposits that may be solitary or multiple (as in the present case). LCDD is generally associated with plasma cell neoplasms or low-grade lymphomas and may occur in patients with Sjogren syndrome.

In the past, diagnostic difficulty in cases of LCDD primarily stemmed from its rareness and lack of familiarity with this disease, and lack of useful stains. A presumptive diagnosis was often made based on the presence of amorphous "amyloid-like" material that failed to stain with Congo red. More recent data supports the use of Masson trichrome and sulfated alcian blue stains as screening tools to distinguish LCDD from amyloidosis in an appropriate clinical and histologic context, as LCDD deposits show a distinctive bright red color with Masson trichrome staining and a distinctive salmon pink color when stained with sulfated alcian blue. In contrast, amyloid deposits show blue-gray staining with Masson trichrome and blue-green staining with sulfated alcian blue, and collagen shows bright blue staining with Masson trichrome and magenta staining with sulfated alcian blue. Other clinical and laboratory testing may be helpful to further support the diagnosis (e.g. serum or urine protein electrophoresis with immunofixation for light chains), but mass spectrometry with proteomic analysis is confirmatory and represents the gold standard for diagnosis of LCDD, and is generally recommended if available.

References

1. Kunnath-Velayudhan S, Larsen BT, Coley SM, et al. Masson trichrome and sulfated alcian blue stains distinguish light chain deposition disease from amyloidosis in the lung. Am J Surg Pathol. 2021;45:405-13.
2. Bhargava P, Rushin JM, Rusnock EJ, et al. Pulmonary light chain deposition disease: report of five cases and review of the literature. Am J Surg Pathol. 2007;31:267-76.

12TH INTERNATIONAL AMR PATHOLOGY SLIDE SEMINAR SYMPOSIUM IN ANATOMIC PATHOLOGY

Case – 38

Thoracic pathology

Contributed by: ***Cesar Moran***

Clinical History

A 46-year-old woman presents with shortness of breath and chest pain. Diagnostic imaging revealed the presence of an intrapulmonary mass in the right upper lobe. Lobectomy was performed.

Pathological Findings

Grossly, the tumor measured 2.5 cm in greatest diameter. The tumor appears to be well circumscribed, light brown with focal areas of hemorrhage.

Histologically, at low power magnification, the tumor consisted of a solid cellular proliferation with a subtle nested pattern alternating with dilated blood vessels. Intermediate magnification showed the cellular proliferation replacing lung parenchyma; however, in some areas endobronchial glands were preserved. On high power magnification, the cellular proliferation was seen to be composed of intermediate-sized cells with ovoid to plump nuclei and clear cytoplasm. Prominent nucleoli were not readily identifiable. Discrete areas of hyalinization were present. Mitotic activity and necrosis were not present.

Immunohistochemical studies were performed which showed positive staining only for vimentin with absence of staining in all other markers performed including cytokeratins, EMA, TTF1, p40, chromogranin, synaptophysin, CD56, CD34, CD31 (Figure. 5), STAT6, desmin, calponin, smooth muscle actin, GATA3, SOX10, Bcl-2, S-100, and HMB-45.

Diagnosis

Hemangioblastoma-like clear cell stromal tumor of the lung.

Comments

This represents an unusual primary tumor in the lung. Less than 25 cases have been reported in the literature. The initial description of similar tumors is credited to Falconieri et al (1) who described two tumors that also show similar morphology and IHC. However, in one of those cases, there was some focal positivity for CD34. In 2020, Lindholm, et al (2) described five cases in which extensive IHC was performed with only positive staining for vimentin. More recently, Agaimy et al (3) described 4 additional cases identifying the presence of YAP1-TFE3 fusion in three of those tumors.

Based on the available literature, it appears that these tumors are of low malignant potential. Complete surgical resection has been performed in all the cases described and so far, there are no reports of recurrences.

References

1. Falconieri G, Mirra M, Michal M, Suster S. Hemangioblastoma-like clear cell stromal tumor of the lung. Adv Anat Pathol 2013;20:130-5.
2. Lindholm KE, Moran CA. Hemangioblastoma-like clear cell stromal tumor of the lung. A clinicopathologic and immunohistochemical study of 5 cases. Am J Surg Pathol 2020; 44:771-775.
3. Agaimy A, Stroehr R, Michal M, et al. Recurrent YAP-TEF3 gene fusions in clear cell stromal tumor of the lung. Am J Surg Pathol 2021; 45:1541-1549.

12TH INTERNATIONAL AMR PATHOLOGY SLIDE SEMINAR SYMPOSIUM IN ANATOMIC PATHOLOGY

Case – 39

Thoracic Pathology

Contributed by: ***Michael Michal***

Clinical History

A 47-year-old man presented with pulmonary and brain metastases of a tumor that had presented initially 9 years prior in the pelvis and was then diagnosed at the time as a clear cell malignant tumor of unknown origin.

Pathological Findings

Microscopically, the tumor demonstrated an admixture of tubulopapillary, microcystic, and solid architectural patterns. While focal areas of mucoid materials were present in the microcystic areas, the tubulopapillary areas were reminiscent of clear cell renal cell carcinoma. The tumor cells harbored ample clear to lightly eosinophilic cytoplasm and round to ovoid nuclei. By immunohistochemistry, the tumor cells were diffusely strongly positive with the following markers: calretinin, WT1, D2-40, cytokeratins 5/6, cytokeratin 7, cytokeratins AE1/AE3, mesothelin, and carbonic anhydrase IX. Conversely, the tumor cells were negative for MOC31, Claudin-4, PAX8, TTF-1, Napsin A, PSA, HMB45, and Melan A, with intact BAP1 and MTAP expression. Ultrastructurally, the apical cell surface was covered by numerous thin elongated microvilli, characteristic of mesotheliomas.

Targeted DNA sequencing revealed the presence of a *VHL* frameshift mutation c.280_286del p.E94Sfs*63, while other mutations frequently occurring in mesotheliomas including *BAP1, NF2, SETD2*, and *PBRM1*, were lacking. Low-pass whole genome sequencing assay revealed a near-haploid genome with the retention of two copies of chromosomes 1q, 5, 7, and 20.

Diagnosis

Clear cell epithelioid mesothelioma with *VHL* mutation and near haploid genomic features.

Comments

First described by Ordonez et al. in 1996, clear cell mesothelioma is characterized by predominance of clear cells with resemblance to clear cell carcinomas (1). Clear cell mesothelioma is uncommon, with 27 cases previously published to date. Ultrastructurally, the clear cell change in clear cell mesotheliomas represents accumulation of intracytoplasmic glycogen, while lipid accumulation, presence of intracytoplasmic vesicles, and mitochondrial swelling may additionally contribute. (1-3) Similarly, the clear cytoplasm in clear cell renal cell carcinoma appears to be secondary to accumulation of intracytoplasmic lipids and glycogen; lipid accumulation has also been described in other von Hippel–Lindau syndrome-associated tumors such as pancreatic neuroendocrine tumors. (4, 5) These examples suggest an association between clear cell change and VHL in the metabolic regulation and development of diverse tumor types. Recently, the presence of VHL mutations in clear cell mesotheliomas was noted in three case reports. (6–8). In our recent paper, we described the clinicopathologic and molecular features of four clear cell mesotheliomas and identified, for the first

time, the presence of both inactivating VHL mutations (in the absence of other alterations typical of most mesotheliomas including BAP1, NF2, and SETD2) and genomic near-haploidization in clear cell mesotheliomas (3).

The pathologic diagnosis of clear cell mesothelioma can be challenging, as it overlaps microscopically with clear cell renal cell carcinoma and diverse other clear cell tumors. Immunohistochemical and/or ultrastructural studies can confirm the diagnosis of clear cell mesothelioma and exclude mimics. Clear cell mesothelioma expresses mesothelial markers such as calretinin, WT1, and D2-40 and is negative for epithelial markers such as claudin-4. Of note, while the strong staining of carbonic anhydrase IX as seen in our case is a common feature of mesotheliomas in general, in the case of clear cell mesothelioma this may lead to confusion with clear cell renal cell carcinoma and represent a diagnostic pitfall. While PAX8 expression, characteristic of clear cell carcinomas of renal and gynecologic primaries, has been described in a subset of epithelioid mesotheliomas without clear cell histology, it was negative in all four clear cell mesotheliomas tested in the literature and herein (3). Based on next-generation sequencing in 3 cases and low-pass whole-genome sequencing in one case, we identified evidence of genomic near-haploidization in clear cell mesotheliomas, with extensive loss of heterozygosity involving nearly all chromosomes but consistently sparing chromosomes 5, 7, and 20. Since genomic near-haploidization is present in ~3% of mesotheliomas (3), the four VHL-mutant clear cell mesotheliomas represent a minor fraction (estimated <10%) of all mesotheliomas with genomic near-haploidization. In fact, the five mesotheliomas with genomic near-haploidization first described in the TCGA study lacked mutations in VHL and instead harbored mutations in TP53 and/or SETDB1 (9). The identification of VHL alterations in clear cell mesothelioma raises a possibility of targeted therapy, such as belzutifan in tumors associated with von Hippel–Lindau disease (10).

References

1. Ordonez NG, Myhre M, Mackay B. Clear cell mesothelioma. Ultrastruct Pathol. 1996;20:331-336.
2. Ordonez NG. Mesothelioma with clear cell features: an ultrastructural and immunohistochemical study of 20 cases. Hum Pathol. 2005;36: 465-473.
3. Michal M, Kravtsov O, Ross JS, Skanderová D, Martínek P, Mosaieby E, Mata DA, Williams EA, Hung YP. Clear cell mesotheliomas with inactivating VHL mutations and near-haploid genomic features. Genes Chromosomes Cancer. 2022 Dec 14. doi: 10.1002/gcc.23119. Epub ahead of print. PMID: 36515470.
4. Kwon TJ, Ro JY, Mackay B. Clear-cell carcinoma: an ultrastructural study of 57 tumors from various sites. Ultrastruct Pathol. 1996;20:519-527.
5. Lubensky IA, Pack S, Ault D, et al. Multiple neuroendocrine tumors of the pancreas in von Hippel-Lindau disease patients: histopathological and molecular genetic analysis. Am J Pathol. 1998;153:223-231.
6. Smith-Hannah A, Naous R. Primary peritoneal epithelioid mesothelioma of clear cell type with a novel VHL gene mutation: a case report. Hum Pathol. 2019;83:199-203.
7. Saeed OAM, Armutlu A, Zhang X, Saxena R. Primary peritoneal mesothelioma with clear cell morphology presenting with multiple liver masses: report of a case with a unique VHL Y98fs*24 mutation and indolent clinical course. Am J Surg Pathol Rev Rep. 2020;25:295-297.
8. Du XM, Wei YP, Gao Y, et al. Clinicopathological characteristics of primary peritoneal epithelioid mesothelioma of clear cell type: a case report. Medicine. 2021;100:e25264.
9. Hmeljak J, Sanchez-Vega F, Hoadley KA, et al. Integrative molecular characterization of malignant pleural mesothelioma. Cancer Discov. 2018;8:1548-1565.
10. Jonasch E, Donskov F, Iliopoulos O, et al. Belzutifan for renal cell carcinoma in von Hippel-Lindau disease. N Engl J Med. 2021;385:2036-2046,

12TH INTERNATIONAL AMR PATHOLOGY SLIDE SEMINAR SYMPOSIUM IN ANATOMIC PATHOLOGY

Case – 40

Thoracic pathology

Contributed by: ***Cesar Moran***

Clinical History

A 59-year-old woman presents with chest pain, cough, and dyspnea. Diagnostic imaging revealed the presence of an anterior mediastinal mass. Surgical resection of the mass was performed.

Pathological Findings

Macroscopically, the tumor was described as well circumscribed, surrounded by adipose tissue, and measuring from 3 cm in greatest diameter. It was light brown, soft, without grossly identifiable areas of necrosis or hemorrhage.

Histologically, at low power view, the tumor was characterized by the presence of a rim of adipose tissue containing remnants of thymic tissue in the form of thymic epithelium and Hassall's corpuscles. The tumor appears to be well circumscribed but not encapsulated. In other areas, cystic changes were also identified. At higher magnification, the tumor was characterized by the presence of a neoplastic cellular proliferation composed of small round cells with scant amounts of cytoplasm, small round nuclei, and inconspicuous nucleoli. Areas of neurophil were present in different amounts. Scattered mitotic figures were identified.

Immunohistochemical stains were performed showing pan keratin decorating the remnants of thymic tissue, while synaptophysin strongly stained the neurophil. Neuron specific enolase was positive in tumor cells, while S-100 protein, chromogranin, synaptophysin, and CD-99 were negative in tumor cells.

Diagnosis

Primary thymic neuroblastoma in an adult patient.

Comments

Neuroblastomas and ganglioneuroblastomas are tumors predominantly of the pediatric age group. In the thoracic area, the posterior mediastinum is the more common location, and the vast majority of neuroblastoma and ganglioneuroblastomas occur in children under the age of 5 years. Neuroblastomas in adults have been described and essentially follow the same anatomical distribution than those in the pediatric age group (posterior mediastinum). Therefore, the presence of these tumors in the anterior mediastinum although it has been reported, it is highly unusual. From the diagnostic point of view, the diagnosis in a complete surgical resection does not pose a major challenge; however, in small biopsies from the anterior mediastinum in an adult patient, it can be a diagnostic problem as neuroblastic changes can be associated with other neoplasms such as teratomatous tumors. From the immunohistochemical point of view, the most consistent marker is NSE but we all know the non-specificity of this particular marker. Synaptophysin may be useful in

cases in which there is the presence of neurophil, as synaptophysin will show a strong positive reaction. Regarding the behavior of these tumors in the anterior mediastinum, it is possible that if complete surgical resection is accomplished and the tumor is limited to the mediastinal compartment, the outcome may be better. However, there are not enough cases described in the literature with a meaningful follow-up.

References

1. Moran CA, Truong M. Primary thymic neuroblastomas in adults: a clinicopathological and immunohistochemical study of three cases. Ann Diagn Pathol 2023; 62:152071; PMID 36495734
2. Talerman A, Gratama S. Primary ganglioneuroblastoma of the anterior mediastinum in a 61-year-old woman. Histopathology 1983; 7:967-975.
3. Hutchinson JE, Nash AD, McCord CW. Neuroblastoma of the anterior mediastinum in an adult. J Thorac Cardiovasc Surg 1968; 56(1):147-152.
4. Asada Y, Marutsuka K, Mitsukawa T, et al. Ganglioneuroblastoma of the thymus: an adult case with the syndrome of inappropriate secretion of antidiuretic hormone. Hum Pathol 1996; 27:506-509.

12TH INTERNATIONAL AMR PATHOLOGY SLIDE SEMINAR SYMPOSIUM IN ANATOMIC PATHOLOGY

Case – 41

Soft tissue and bone pathology

Contributed by: ***David Suster***

Clinical History

A 63-year-old man was seen in the clinic for back pain and abdominal discomfort. CT scan of the abdomen revealed a large retroperitoneal mass. The patient's past history was significant for a hernia operation and cataract surgery. An en-block resection was scheduled. At surgery, the mass was unencapsulated but well circumscribed and attached to the colon. It showed a smooth outer surface with a small amount of attached adipose tissue and measured 15 x 13 x 10.9 cm. The cut surface was tan-pink and homogeneous, with focal areas of softening. The segment of colon was unremarkable.

Pathological Findings

Histologic sections showed sheets of large epithelioid cells with haphazard distribution and varying degrees of stromal hyalinization. The tumor cells contained round to oval nuclei with finely dispersed chromatin and abundant clear to lightly eosinophilic cytoplasm. Scattered mitoses, averaging 4 per 10 high power fields could be seen. There were no areas of necrosis. The tumor was well-circumscribed and did not invade neighboring structures. A hemangiopericytic vascular pattern composed of branching vessels with open lumens could be seen focally. Immunohistochemical stains showed strong nuclear positivity of the tumor cells for STAT6 and CD34. Stains for cytokeratins, EMA, SMA, desmin, S100, SOX10, MUC4, bcl-2, CD31 and ERG were negative. Fusion gene analysis using the RNA-based Archer FusionPlex system showed a *NAB2::STAT6* translocation.

Diagnosis

Epithelioid and clear cell solitary fibrous tumor.

Comments

Solitary fibrous tumors are ubiquitous neoplasms that were first described in the pleura but later recognized in parenchymatous organs and in soft tissue locations.[1] The tumors are characterized by a spindle cell proliferation set against a fibrotic stroma and by showing striking variegation of growth patterns.[2,3] The most characteristic appearance is that of a bland spindle cell proliferation showing linear arrays of dense collagen that have been described as "rope-like". The majority of these tumors are benign and show very little mitotic activity, usually not exceeding 3 per 10 high power fields; however, about 10% can behave aggressively. Recently, a risk-assessment algorithm has been proposed which divides these tumors into low-risk, intermediate-risk, and high-risk categories.[3]

The existence of soft tissue neoplasms characterized by a predominance of large, epithelioid cells instead of spindle cells has been widely recognized in the literature and includes epithelioid sarcoma, sclerosing epithelioid fibrosarcoma, angiosarcoma, leiomyosarcoma, malignant peripheral nerve sheath tumors, myxoinflammatory fibroblastic sarcoma, and others. Such cases can pose difficulties for diagnosis due to their unusual cytologic appearances. Solitary fibrous tumors composed

of round, epithelioid cells are extremely rare and have rarely been reported in the literature, usually as single case reports. We recently presented our experience with 13 cases of these tumors, including immunohistochemical and molecular genetic studies of the lesions.[4] The tumors occurred in 8 women and 5 men, aged 36 to 80 years (mean= 63). They were located in the orbit, lower extremities, retroperitoneum, abdominal cavity, and in superficial soft tissues of the neck, pelvis, and pubis. The tumors measured from 3.5 to 24.5 cm in maximum dimension. Using the Demicco risk assessment system, 6 cases were stratified as low-risk tumors, 5 as intermediate risk, and 2 as high-risk. The tumors in the high-risk category behaved predictably aggressive with tumor metastases and death. The majority of the intermediate risk patients, however, showed no evidence of recurrence or metastases from 3 to 4 years follow-up. The low-risk tumors also showed no evidence of recurrence or metastases over a follow-up period between 6 to 18 years, except for one orbital tumor which recurred and eventually caused the death of the patient. Our patient corresponded to the intermediate risk category and was alive and well and free of disease after 3 years.

The role of immunohistochemistry for the diagnosis of solitary fibrous tumors has been well-established.[5] Nuclear positivity for STAT6 has been acknowledged as a reliable method for establishing the diagnosis of solitary fibrous tumor. All cases in our study showed the *NAB2::STAT6* translocation by molecular studies; however, only 10 cases showed nuclear positivity for STAT6 by immunohistochemistry. This may be an indication that unusual morphologic variants of these tumors may not always show the expected reactivity by immunohistochemistry; molecular testing is therefore recommended when there is a strong suspicion of solitary fibrous tumor and the immunohistochemical results are inconclusive.

The differential diagnosis of epithelioid solitary fibrous tumor with other types of epithelioid sarcomas can be facilitated by the combined use of immunohistochemistry and molecular pathology, and in some cases may be arrived at by elimination, but the consistent demonstration of the characteristic translocation in these tumors can be very helpful for correct diagnosis. Of note; SFT with these features needs to be distinguished from an emerging group of sarcomas characterized by *KTM2A* rearrangements[6]. Epithelioid and clear cell solitary fibrous tumor should be considered in the differential diagnosis of soft tissue neoplasms with epithelioid and clear cell morphology.

Figure 1: Two cases of epithelioid and clear cell solitary fibrous tumor.

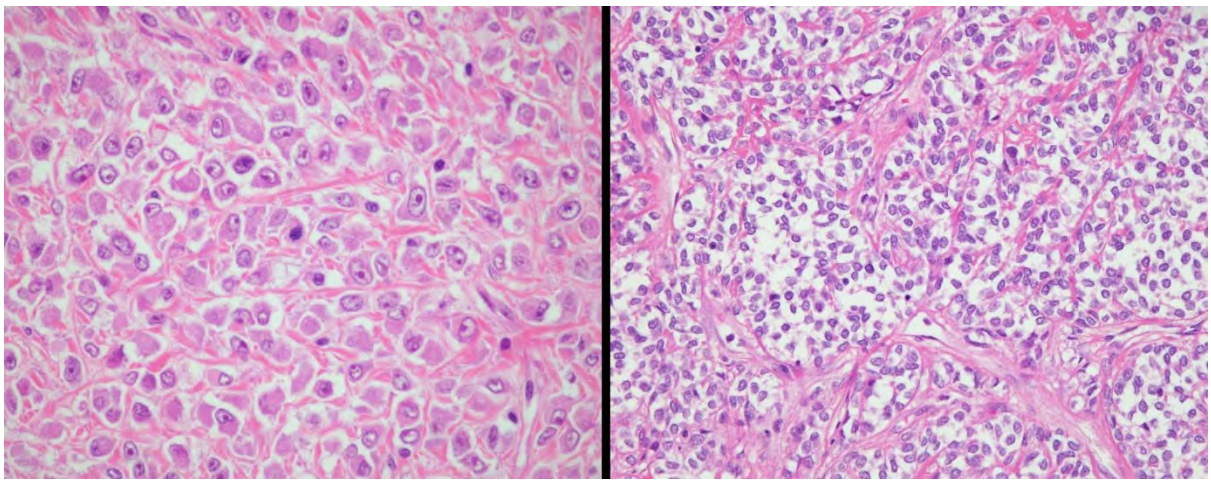

References

1. Suster S, Nascimento AG, Miettinen M, et al. Solitary fibrous tumor of soft tissue. A clinicopathologic study of 12 cases. Am J Surg Pathol 1995; 19:1257-1266.

2. Moran CA, Suster S, Koss MN. The spectrum of histologic growth patterns in benign and malignant fibrous tumors of the pleura. Semin Diagn Pathol 1992; 9:169-180.
3. Tariq MU, Din NU, Abdul-Ghafar J et al. The many faces of solitary fibrous tumor: diversity of histological features, differential diagnosis and role of molecular studies and surrogate markers in avoiding misdiagnosis and predicting the behavior. Diagn Pathol 2021; 16:32.
4. Suster D, Mackinnon AC, Mejbel HA et al. Epithelioid and clear cell solitary fibrous tumors. Clinicopathologic, immunohistochemical, and molecular genetic study of 13 cases. Am J Surg Pathol 2023; 47:259-269.
5. Doyle LA, Vivero M, Fletcher CDM, et al. Nuclear expression of STAT6 distinguishes solitary fibrous tumor from histologic mimics. Mod Pathol 2014; 27:390-395.
6. Kao YC, Lee JC, Zhang L, Sung YS, Swanson D, Hsieh TH, Liu YR, Agaram NP, Huang HY, Dickson BC, Antonescu CR. Recurrent YAP1 and KMT2A Gene Rearrangements in a Subset of MUC4-negative Sclerosing Epithelioid Fibrosarcoma. Am J Surg Pathol. 2020 Mar;44(3):368-377.

12TH INTERNATIONAL AMR PATHOLOGY SLIDE SEMINAR SYMPOSIUM IN ANATOMIC PATHOLOGY

Case – 42

Soft tissue and bone pathology

Contributed by: ***Michael Michal***

Clinical History

A 55-year-old man presented with a sharply circumscribed right inguinal tumor sized 4 x 3 x 2 cm (Fig. 1) which was excised. The patient was without signs of metastatic disease at presentation.

The excised tumor was sharply circumscribed, measuring 4 x 3 x 2 cm.

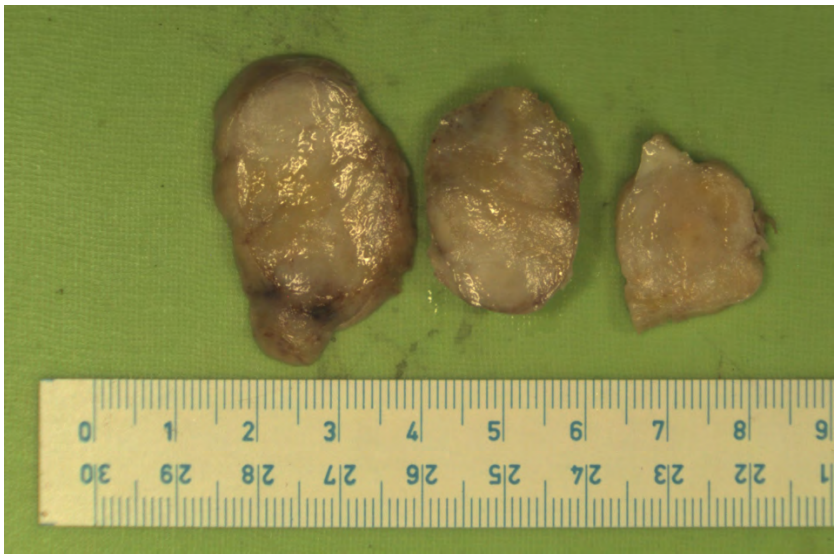

Pathological Findings

Microscopically, the tumor was composed of a variable mixture of mostly bland spindled, ovoid and round cells with low mitotic activity. The cellularity varied greatly in different areas but was predominantly low to moderate. However, small nodules with markedly increased cellularity composed almost purely of round cells were present. Nevertheless, the mitotic activity was still low. Besides these nodules, the stroma was hyalinized with admixture of adipocytes. The vasculature was inconspicuous. Scant, lightly eosinophilic or cytoplasm was seen in most cells.

Immunohistochemically, the tumor cells were diffusely positive for S100 protein and multifocally expressed GFAP, MyoD1 and PAX7, desmin focally decorated the tumor cells as well. SOX10, myogenin and CD34 were negative. RNA sequencing revealed *EWSR1::PATZ1* gene fusion. FISH for CDKN2A was negative.

Diagnosis

EWSR1::PATZ1 soft tissue sarcoma.

Comments

Although the first case of this unique neoplasm was described 20 years ago (1), it was not until the recent advent of high-throughput NGS techniques when more cases of *EWSR1::PATZ1*-rearranged sarcoma (EPS) began to appear in the literature. As of 2018, 18 more cases have been published (2). Combining data from our recent paper (2) with those reported previously allows some general observations to be made. Clinically, EPS have an equal gender distribution and occur over a very broad age range (1–81 years) with a mean age of 44 years. The most characteristic and diagnostically useful clinical feature of EPS is its marked predilection for soft tissues of the trunk, especially for thoracic soft tissues and/or lungs. In fact, 12 out of 25 reported cases with available data affected this anatomical area. Another eight cases occurred in the abdominal soft tissues (including both abdominal wall and intraabdominal sites) and 3 tumors involved the soft tissues of the head and neck. It is noteworthy that only 2/25 cases of EPS so far reported occurred on the limbs (thigh and shoulder) and none affected the skeleton [2-4].

While a subset of EPS exhibits almost exclusively round cell morphology, similar to most other members within the most recent 2020 WHO classification category of "undifferentiated small round cell sarcomas of bone and soft tissue" (i.e., CIC-rearranged sarcoma, sarcoma with BCOR alterations, EWSR1/FUS-NFATC2-rearranged sarcomas), EPS features variable mixture of spindled, ovoid, round, and epithelioid cells. The architectural and stromal features also vary and as a result, the morphologic spectrum is very broad. The nine cases in our recent cohort (and according to available figures probably all cases reported so far) could be roughly divided into three subgroups based on the predominant shape and nuclear grade of the neoplastic cells. While even then, the morphology within these subsets is not entirely homogeneous and the clinical impact of such subdivision is not known, we found this approach very useful for differential diagnostic purposes. Similar to the case presented herein, the first group included low-grade appearing tumors composed of spindled, ovoid, round, and epithelioid cells, which grew within predominantly hyaline stroma. These tumors were somewhat reminiscent of solitary fibrous tumors (when more spindled) or myoepitheliomas (when round/epithelioid cells predominated). The second group encompassed intermediate/high-grade tumors with a round or ovoid cell phenotype, few spindled cells and a less prominent stromal component. The differential diagnosis included other small round cell tumors. High-grade sarcomas with mixed spindled and round cell morphology were included in the last group. Rhabdomyosarcoma and sarcomas with BCOR and CIC gene rearrangements constitute the most likely differential diagnosis for these cases. It remains unclear whether the morphologically low-grade tumors can transform into the higher-grade variety or if the latter arise de novo. Despite the aforementioned differences, there were also several recurring traits shared by tumors across these categories, some of which were also noted previously (2). According to all available data, 9/14 cases had a mitotic count of less than 1 mitosis per 10 HPF, whereas the remaining cases showed 3–6 mitoses per 10 HPF (2-4). In line with a predominantly low mitotic rate, necrosis was rare, with two cases showing a single small necrotic focus and only one reported case containing more prominent areas of necrosis (2-4).

The immunohistochemical features of EPS are unique and in contrast to morphology, they are much more consistent between individual cases. Our study corroborates findings of several previous reports, which found most EPS to stain with S100-protein, GFAP and with the myogenic markers desmin and MyoD1 [2-4]. A novel finding of our study was frequent Pax-7 expression detected in 4/5 analyzed cases. In contrast to a previous report, myogenin was the least sensitive skeletal muscle marker as it stained only 2/9 cases (3).

EWSR1 and PATZ1 genes are both located on chromosome 22 only about 2Mb apart and such a close genomic proximity results in significant visualization and interpretation difficulties of the break-apart FISH signals (2). Therefore, other techniques such as NGS should be preferably used for molecular confirmation. The gene expression profiling analysis of small round cell sarcomas performed by Watson et al. showed EPS to form a distinct tight cluster, separate from all other tumors included in the study cohort (5). These molecular data lend further support to suggest that EPS represents a unique entity, different from EWSR1/FUSNFATC2 sarcomas or any other round cell tumor (2, 5).

Due to variable spindle and/or round cell morphology with different levels of atypia, the complete list of differential diagnostic entities is extraordinarily broad. The coexpression of S100-protein, GFAP, desmin, and MyoD1 found in most cases of EPS is very unusual and therefore suggestive of the diagnosis. Nonetheless, some cases of EPS may lack this characteristic immunoprofile and in such cases, molecular detection of the fusion is required for diagnosis. Based on similar clinical, morphological, and/or immunohistochemical features, solitary fibrous tumor, myoepithelioma, desmoplastic small round cell tumor (DSRCT), Ewing sarcoma, BCOR or CIC-rearranged sarcomas, rhabdomyosarcoma and malignant peripheral nerve sheath tumor (MPNST) with skeletal muscle differentiation are among the entities most likely to be confused with EPS (2).

Previous reports suggested very aggressive clinical behavior in most cases of EPS as 4/5 patients with followup either died or experienced distant metastasis within 2–30 months. The only patient with follow-up (19 months) that was alive without any adverse event was an 81-year-old female in a study by Bridge et al. (4). Based on available data, it seems that cases with copy number loss or deletion of CDKN2A/ CDKN2B genes may have a higher risk of aggressive behavior (2, 4)). Apart from secondary molecular abnormalities, our data indicated that certain morphological features might be associated with a more favorable prognosis. Two cases we presented in our study – as well as the case presented herein - were well-circumscribed, partially encapsulated tumors with negligible mitotic activity and similar low-grade morphology. Both tumors were completely excised, and the patients were free of disease 19 months after initial diagnosis. Notably, neither of them received any adjuvant therapy. However, despite intermediate-grade morphology, higher mitotic activity (3 mitoses/10 HPF) and widespread parietal and visceral pleural involvement at presentation, another patient in our study was free of disease 5 years after tumor resection. Adjuvant chemotherapy was administered as well but no response was noted by imaging or histology. Similarly, chemotherapy in four other published cases and in an aggressive case in our study showed little to no clinical benefit (2).

In summary, *EWSR1::PATZ1*-rearranged tumors have a very wide morphological spectrum with recurrent microscopic features. They also have a characteristic immunophenotype distinguished mainly by the co-expression of neural (S100-protein, GFAP) and skeletal muscle (desmin, MyoD1, Pax-7) markers in most cases. Both findings, as well as gene expression data from previous studies confirm that EPS is a distinct clinicopathologic entity. The uneventful outcome in some recently published cases indicate that a subset of EPS might follow a more indolent clinical course than previously appreciated.

References

1. Mastrangelo T, Modena P, Tornielli S, Bullrich F, Testi MA, Mezzelani A, et al. A novel zinc finger gene is fused to EWS in small round cell tumor. Oncogene. 2000;19:3799–804.
2. Michal M, Rubin BP, Agaimy A, et al. EWSR1-PATZ1-rearranged sarcoma: a report of nine cases of spindle and round cell neoplasms with predilection for thoracoabdominal soft tissues and frequent expression of neural and skeletal muscle markers. Mod Pathol. 2021 Apr;34(4):770-785. doi: 10.1038/s41379-020-00684-8.

3. Chougule A, Taylor MS, Nardi V, Chebib I, Cote GM, Choy E, et al. Spindle and round cell sarcoma with EWSR1-PATZ1 gene fusion: a sarcoma with polyphenotypic differentiation. Am J Surg Pathol. 2019;43:220–8.
4. Bridge JA, Sumegi J, Druta M, Bui MM, Henderson-Jackson E, Linos K, et al. Clinical, pathological, and genomic features of EWSR1-PATZ1 fusion sarcoma. Mod Pathol. 2019;32:1593–604.
5. Watson S, Perrin V, Guillemot D, Reynaud S, Coindre JM, Karanian M, et al. Transcriptomic definition of molecular subgroups of small round cell sarcomas. J Pathol. 2018;245:29–40.

12TH INTERNATIONAL AMR PATHOLOGY SLIDE SEMINAR SYMPOSIUM IN ANATOMIC PATHOLOGY

Case – 43

Soft tissue and bone pathology

Contributed by: ***Kyle Perry***

Clinical History

A 75 y/o female with a history of rheumatoid arthritis presented to an orthopedic clinic with a mass at the base of the left ring finger. An MRI identified a T2 hyperintense mass with an irregular margin measuring 1.2 cm in greatest dimension in the palmar and radial aspect of the left fourth finger. Ultrasound also noted a complex cystic lesion at the anterior base of the left fourth digit with thick vascular septations that would be atypical for a ganglion cyst. During the procedure, the surgeon excised the lesion, which was clinically felt to be compatible with a retinacular cyst emanating from the flexor sheath.

Pathological Findings

Histologically, the tumor was well circumscribed and exhibited a lymphoid cuff (Fig 2A). A prominent portion of the tumor exhibited background myxoid to hyalinized stroma with nodules/aggregates of epithelioid like mesenchymal cells (Fig 2B). On higher power, these cells exhibited a vaguely whorled or reticular like architecture (Fig 2C, Fig 2D).

Immunohistochemical stains were performed and the cells showed partial staining for desmin, smooth muscle actin and weak nonspecific staining for AE1/AE3. The cells showed retained nuclear staining for INI-1. ERG, CK5/6, high molecular weight cytokeratin, CD31, S100 and CD68 stains are negative in the areas of interest. Next generation sequencing was performed and demonstrated an *EWSR1-CREB1* fusion transcript.

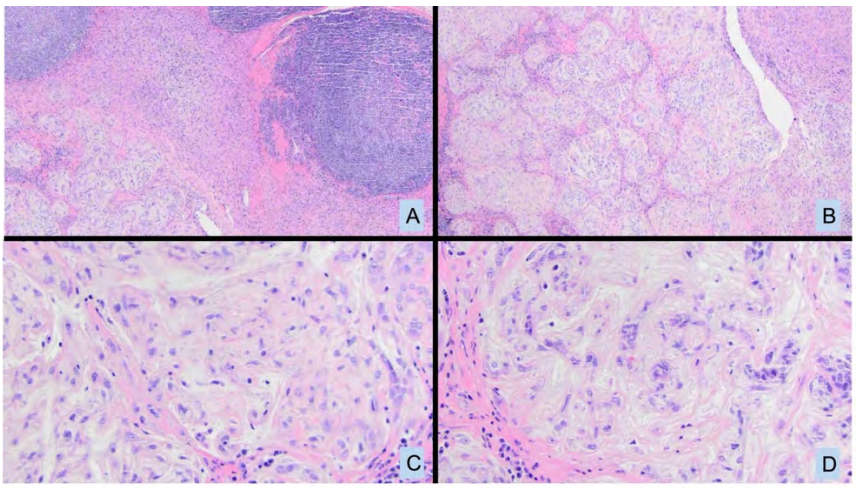

Fig 1A. Myxoid angiomatoid fibrous histiocytoma with lymphoid cuff. Fig 1B. Majority of tumor shows oval cells embedded in myxoid stroma. Fig 1C and 1D. On higher power, the cells exhibit a vaguely reticular like architecture.

Diagnosis

Myxoid angiomatoid fibrous histiocytoma.

Comments

Angiomatoid fibrous histiocytoma is a soft tissue tumor of intermediate biologic potential that historically has been identified as arising in the subcutaneous tissue or deep dermis of young adults and children. These tumors have also been found to occasionally arise in older adults and other anatomic locations. [1] They can sometimes cause local tenderness but can also be associated with constitutional symptoms such as weight loss and fever through production of cytokines such as IL-6. [2]

Histologically, these tumors are typically composed of cells that somewhat resemble histiocytes in the background of hemorrhage and chronic inflammation. Areas of increased vascularity and a peripheral lymphoid cuff are often seen. Occasionally (less than 5% of the time), angiomatoid fibrous histiocytomas can exhibit conspicuous areas of myxoid changes which can sometimes complicate the diagnostic process for the unsuspecting pathologist. This variant will often retain features of conventional angiomatoid fibrous histiocytoma such as a lymphoid cuff and fibrous pseudocapsule but will exhibit a prominent area of cells in myxoid stroma. The cells typically contain oval to stellate nuclei and show a whorled or reticular architecture.[3]

Myxoid angiomatoid fibrous histiocytoma behaves in a similar manner to its conventional counterpart which is considered "intermediate" in biologic behavior. The primary goal for a pathologist is to be aware of this morphologic variation such that it is not confused for a more aggressive myxoid tumor such as low-grade myxofibrosarcoma, extraskeletal myxoid chondrosarcoma, or myxoid liposarcoma. Fortunately, angiomatoid fibrous histiocytomas usually exhibit an *EWSR1-CREB1* or *EWSR1-ATF1* fusion transcript which (although not completely specific) can help distinguish this tumor from other common diagnostic considerations in the appropriate morphologic context.

Special thanks to Dr. Fatimah Alruwaii for allowing me to present this case.

References

1. Chen G, Folpe AL, Colby TV, et al. Angiomatoid fibrous histiocytoma: unusual sites and unusual morphology. *Modern pathology : an official journal of the United States and Canadian Academy of Pathology, Inc*. Dec 2011;24(12):1560-70. doi:10.1038/modpathol.2011.126
2. Goldblum JR, Enzinger FM, Folpe AL, Weiss SW. *Enzinger and Weiss's soft tissue tumors*. Saunders/Elsevier; 2014.
3. Schaefer IM, Fletcher CD. Myxoid variant of so-called angiomatoid "malignant fibrous histiocytoma": clinicopathologic characterization in a series of 21 cases. *The American journal of surgical pathology*. Jun 2014;38(6):816-23. doi:10.1097/pas.0000000000000172.

12TH INTERNATIONAL AMR PATHOLOGY SLIDE SEMINAR SYMPOSIUM IN ANATOMIC PATHOLOGY

Case – 44

Soft Tissue and bone pathology

Contributed by: ***John Gross***

Clinical History

A 71-year-old female presented with left thigh pain. Non-significant past medical history. Subsequent imaging revealed a deep left thigh mass eroding the femur and small (indeterminant pulmonary nodules) bilaterally.

Pathological Findings

A core needle biopsy was performed revealing a high-grade pleomorphic sarcoma with extensive necrosis. Immunohistochemical results were negative for SMA, Desmin, CAM5.2, CK AE1/AE3, S100, myoD1,HMB45, Melan-A, MDM2 FISH negative. A diagnosis of undifferentiated pleomorphic sarcoma was rendered on the core needle and a radical resection of the mass and portion of femur was performed demonstrating a 6.5 cm partially necrotic soft tissue sarcoma extending into bone. Histologic sections of the resection specimen showed high-grade pleomorphic, epithelioid, and rhabdoid nuclei growing in close association with background stromal vasculature. In addition, the cells of interest showed variable lightly eosinophilic to clear cytoplasm. Extensive lymphovascular invasion and necrosis was seen and mitotic activity was brisk. Repeat immunohistochemical stains showed strong and diffuse GPNMB and cathepsin but very limited/focal Melan-A, TFE3, desmin, and MITF. SMA, S100, SOX10, CK AE1/AE3, HMB45, BRAFV600E, and myogenin were negative. INI1 was retained. Subsequent molecular analysis detected a TSC1 p.R509 mutation, a RB1 p.R579 mutation, a TGFBR2 p.K153fs mutation, and a TP53 p.R248W mutation.

Diagnosis

Malignant PEComa, high-grade.

Comments

PEComa rare mesenchymal tumors often expressing both melanocytic and smooth muscle markers but can be focal and inconsistent which may pose significant diagnostic challenges especially on limited biopsies. Regarding the genetics of PEComa, two distinct molecular groups have been described:

(1) Classic PEComas with TSC mutations;

(2) TFE3 translocation associated PEComas with TFE3.

Mutations in TSC1 resulting in activation of the MTOR/PI3K signaling pathway have been detected. Treatment strategies with drugs targeting this pathway may be therapeutic options for this patient.

Recently, Salles et al showed GPNMB (glycoprotein nonmetastaticB), a transmembrane protein and MITF/TFE3 transcriptiona target, to be highly expressed in kidney neoplasms with TSC1/2/MTOR alteration-associated renal tumors and translocation-associated renal cell carcinoma (tRCC). Our preliminary data suggests strong and diffuse expression of GPNMB is a highly sensitive and fairly specific immunohistochemical surrogate for the diagnosis of PEComa which, in concert with compatible morphology, is amenable to targeted therapy.

References

1. Salles, DC et al. GPNMB expression identified TSC1/2/mTOR-associated and MIT family translocation-driven renal neoplasms. J Pathol June 2022. 257 158-171

12TH INTERNATIONAL AMR PATHOLOGY SLIDE SEMINAR SYMPOSIUM IN ANATOMIC PATHOLOGY

Case – 45

Soft tissue and bone pathology

Contributed by: ***Kum Cooper***

Clinical History

A 21-year-old woman with no significant past medical or surgical history was found to have a large pelvic mass during routine annual gynecologic examination. She noted urinary frequency, dysuria, constipation, abdominal fullness, and cold sweats. Pelvic ultrasound demonstrated a 14 x 10 x 11 cm solid, vascular, central pelvic mass. Contrast-enhanced abdominal and pelvic magnetic resonance imaging (MRI) demonstrated a 15.7 x 13.5 x 11.8 cm heterogeneously enhancing pelvic mass of indeterminate origin with focal cystic change. The mass abutted the rectum and ovaries with inferior compression of the uterus and bladder. The uterus and ovaries were otherwise without abnormality, with the mass appearing separate from the uterus and ovaries. There was compression of the left ureter with secondary hydronephrosis. There was no adenopathy nor osseous abnormality. There was no evidence of metastatic disease within the chest or abdomen. Differential diagnostic considerations based on these imaging findings included gastrointestinal stromal tumor, exophytic uterine leiomyosarcoma, and primary peritoneal sarcoma. CT-guided biopsy was performed for definitive characterization.

Pathological Findings

Microscopy demonstrated a heterogeneous neoplasm, even within just a single core biopsy (Fig. 1). Cellular areas of plump spindle cells with foci of stromal fibrosis transitioning to hypocellular myxoid areas with loose stellate cells were present. Some of the myxoid areas harbored greater numbers of chronic inflammatory cells. Other areas consisted of more eosinophilic and epithelioid cells. Yet others were myxohyaline. Abundant hyalinized blood vessels and focal hyalinzed stroma were present. Overt cytologic atypia, mitotic activity, and necrosis were not appreciated. A panel of immunohistochemical stains (Fig. 2) demonstrated expression of s100 and CD34, prompting consideration of an NTRK-rearranged tumor. However, pan-TRK immunoreactivity was only focal and weak, and fluorescent in situ hybridization (FISH) for NTRK1, NTRK2, and NTRK3 all demonstrated intact genes. TLE1, focal SMA, and strong and diffuse ALK expression were also identified by immunohistochemistry. The tumor cells were not immunoreactive for SOX10, desmin, pancytokeratin, AE1/AE3, CD117, DOG1, STAT6, MUC4, ER, SF1, inhibin, or calretinin. RB1 was intact. SYT and CHOP (DDIT3) FISH demonstrated intact genes, however ALK FISH demonstrated a gene rearrangement (Fig. 3).

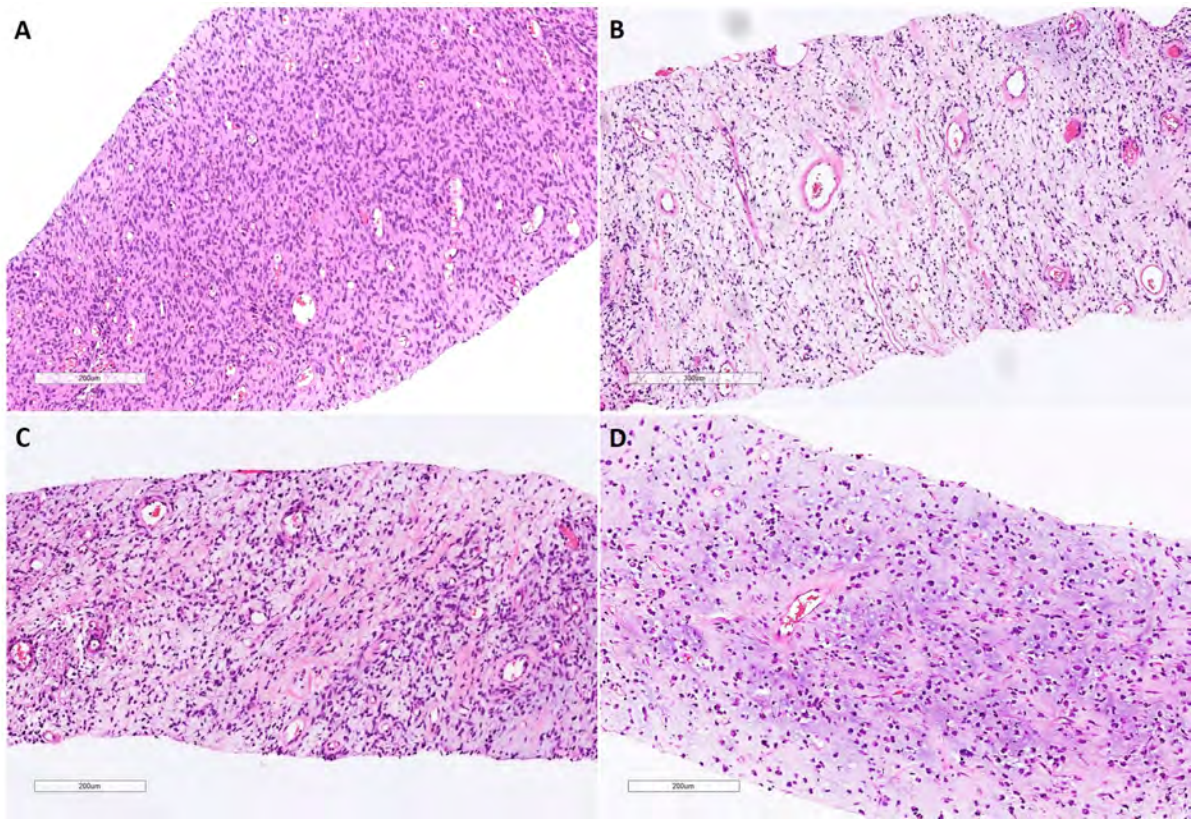

Figure 1. The tumor demonstrated various histomorphologies on H&E stain of the core biopsy, from spindled (A) to myxoid (B) and myxoinflammatory (C) to myxohyaline with small epithelioid cells (D).

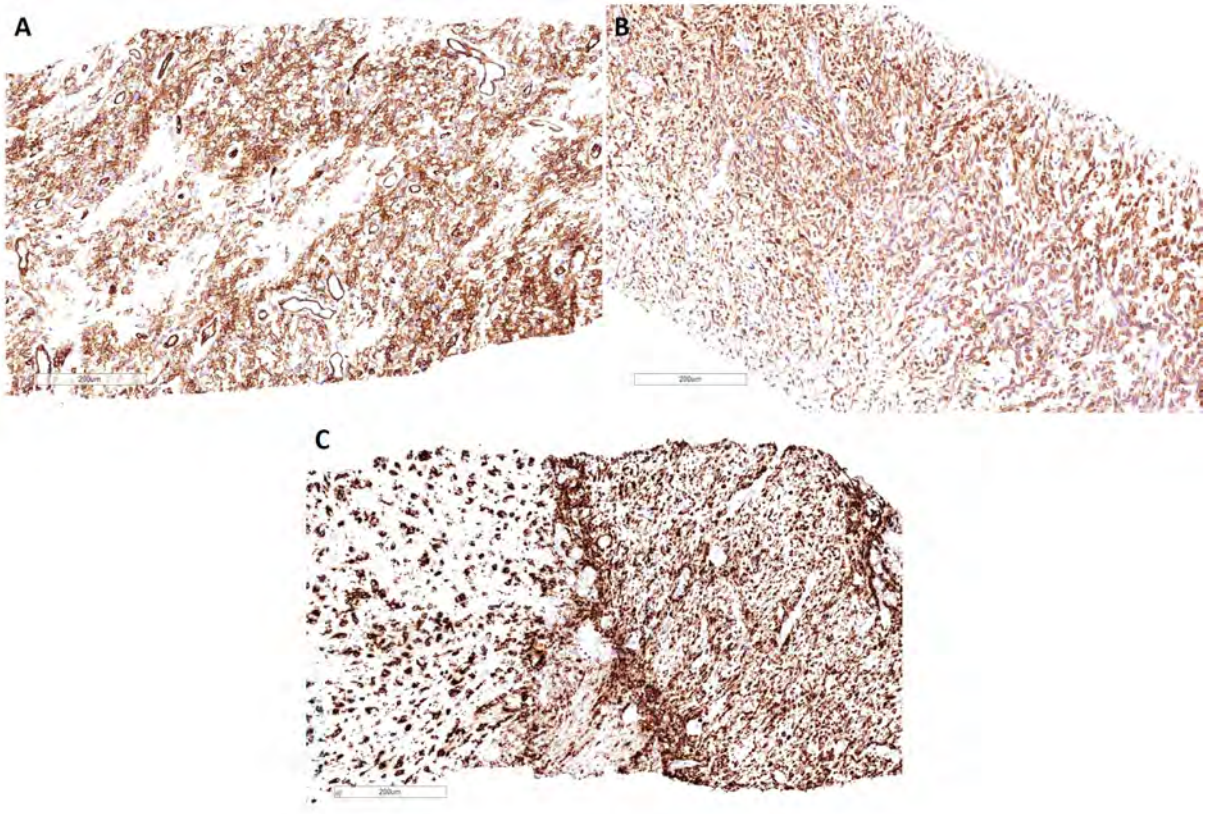

Figure 2. Immunohistochemical st ains for CD34 (A), S100 (B), and ALK (C) all demonstrated diffuse expression.

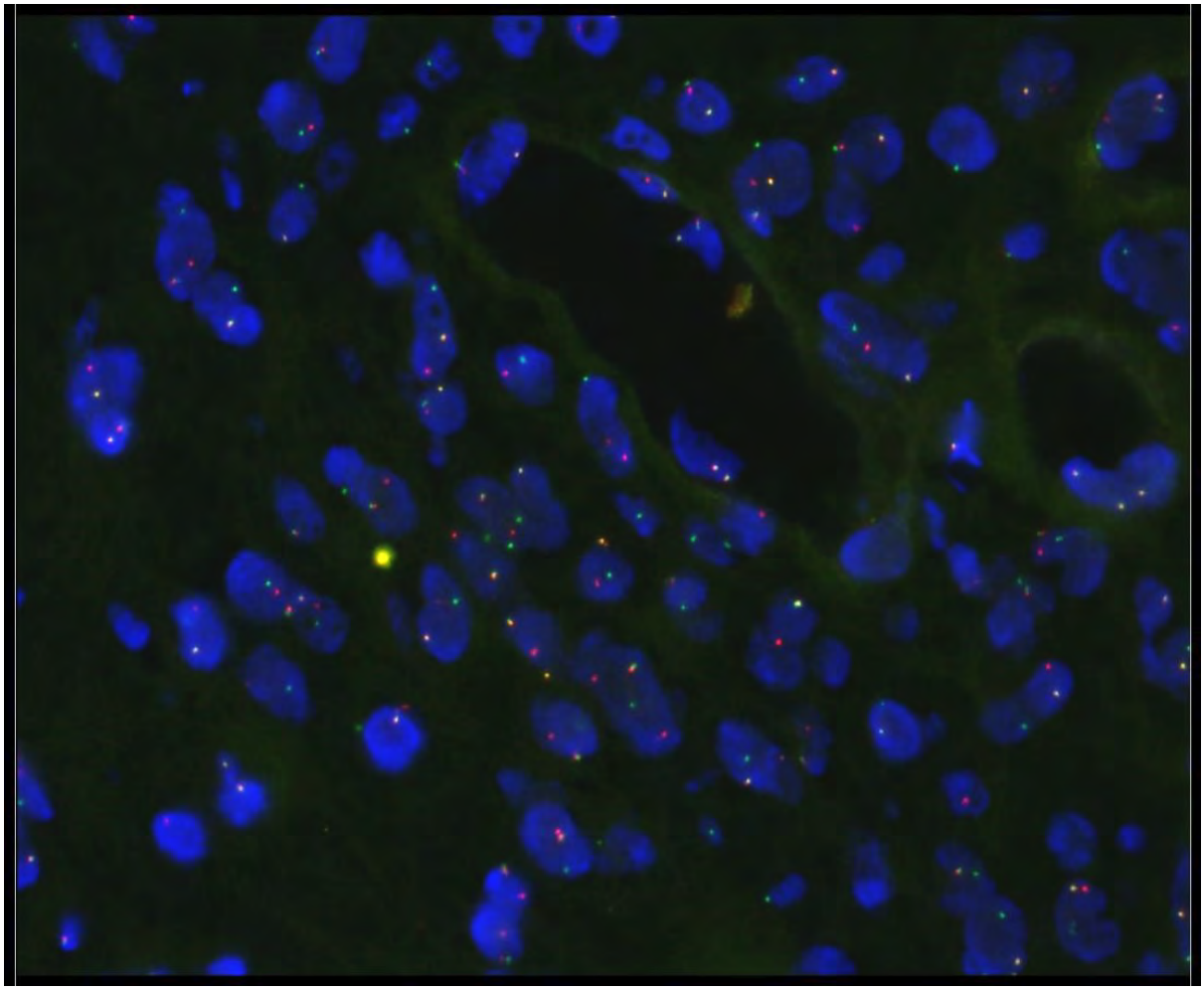

Figure 3. Fluorescence in situ hybridization (FISH) for ALK (break-apart probe) demonstrated numerous tumor cells with a break-apart signals (1 red, 1 green, 1 yellow), indicating an ALK gene rearrangement.

Diagnosis

S100 and CD34 expressing mesenchymal neoplasm with rare *PLEKHH2-ALK* fusion.

Comments

The clinical presentation of a pelvic mass in a young woman together with ALK rearrangement were most consistent with an inflammatory myofibroblastic tumor (IMT). However, as the histomorphology and immunophenotype were somewhat unusual for IMT, particularly the myxohyaline differentiation and s100 and CD34 expression, a comprehensive solid tumor next generation sequencing panel was performed. This study confirmed an ALK fusion, with a heretofore extremely rarely reported pleckstrin homology domain-containing protein, family H, member 2 (PLEKHH2) fusion partner [PLEKHH2 (NM_172069.4) exon 6 - ALK (NM_004304.4) exon 20]. Presurgical therapy was initiated with the ALK inhibitor, brigatinib, 90 mg oral daily. Imaging one month later demonstrated an interval decrease in size of the pelvic mass (12.4 x 11.0 x 9.3 cm) with improved heterogeneous enhancement compared to the prior exam. Oral brigatinib was continued at 90 mg oral daily for eight additional weeks, followed by interval imaging, which demonstrated continued volume reduction to 10.8 x 9.2 x 9.0 cm (Fig. 4). The patient underwent definitive surgical resection two weeks later, with brigatinib discontinued two days prior to the procedure. The grossly

11.0 cm residual tumor was resected, removed en bloc (Fig. 5). Microscopic examination of the tumor and peritoneal nodule demonstrated predominantly hyalininzing fibrosis, with foci of histiocytic inflammation, edema, myxoid and cystic degeneration, and calcification, consistent with robust treatment response (Fig. 6). There was no definitive necrosis. Only scattered foci of residual low-grade spindle cells remained, particularly perivascularly, with approximately 5% residual tumor cells. While functionally presenting and being treated as an IMT, the histomorphologic and immunophenotypic findings in the presented case, save for the ALK expression, are not typical of IMT. Furthermore, the specific ALK rearrangement identified is very unusual. Though the fusion partners in IMT are accepted as vast, the PLEKHH2-ALK fusion is not an established fusion and has not been published in an IMT in the primary literature. We propose that this tumor is of a better histomorphologic, immunophenotypic, and genetic fit in the emerging group of mesenchymal neoplasms with oncogenic kinase alterations akin to NTRK-rearranged mesenchymal neoplasms, particularly as the presented neoplasm demonstrated s100 and CD34 expression, often a clue to an NTRK-rearranged tumor and not characteristic of IMT.2,3 Various ALK fusions are being increasingly recognized in this emerging family of tumors, with PLEKHH2-ALK being a novel addition. The PLEKHH2-ALK fusion has only been extremely rarely reported to date, with a majority of reports in lung adenocarcinoma and only a single abstract reporting this finding in an IMT.

We herein report the second case of a mesenchymal neoplasm with PLEKHH2-ALK fusion, and substantiate the finding of sensitivity to ALK inhibition in tumors with this gene rearrangement. With histomorphology and an immunophenotype deviant to that of inflammatory myofibroblastic tumor, this tumor appears to represent one with a novel ALK fusion in the emerging family of s100 and CD34 expressing mesenchymal neoplasms with oncogenic kinase alterations.

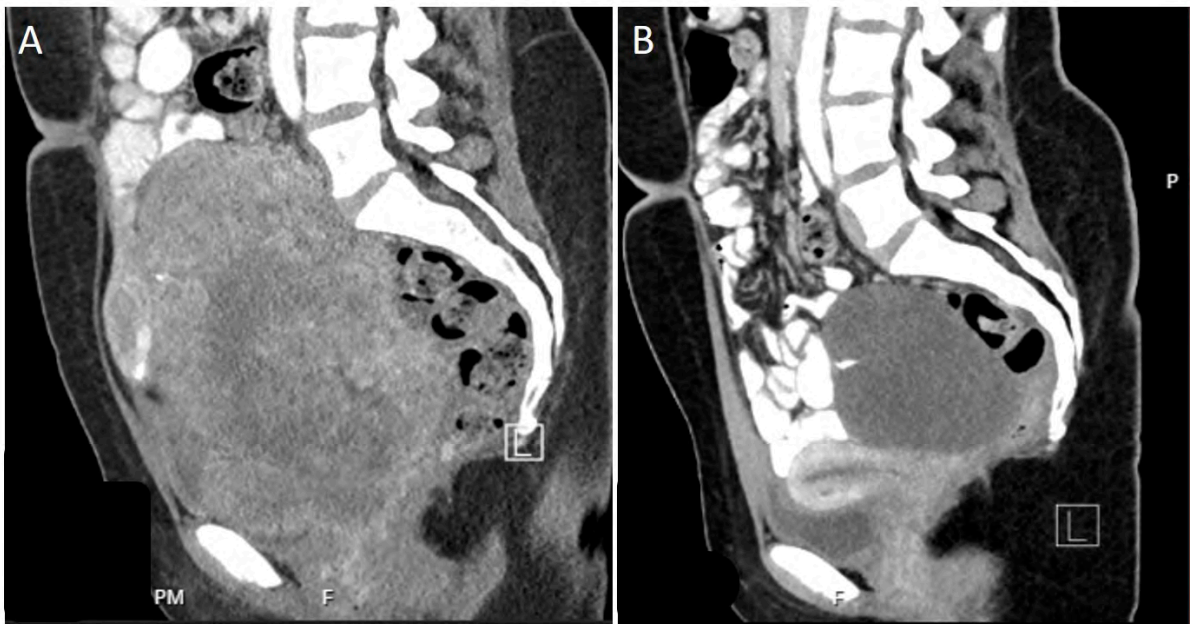

Figure 4. Pelvic CT scan before (A) and three months after (B) initiation of treatment with brigatinib, demonstrating significant volume reduction and improvement of mass effect on visceral organs.

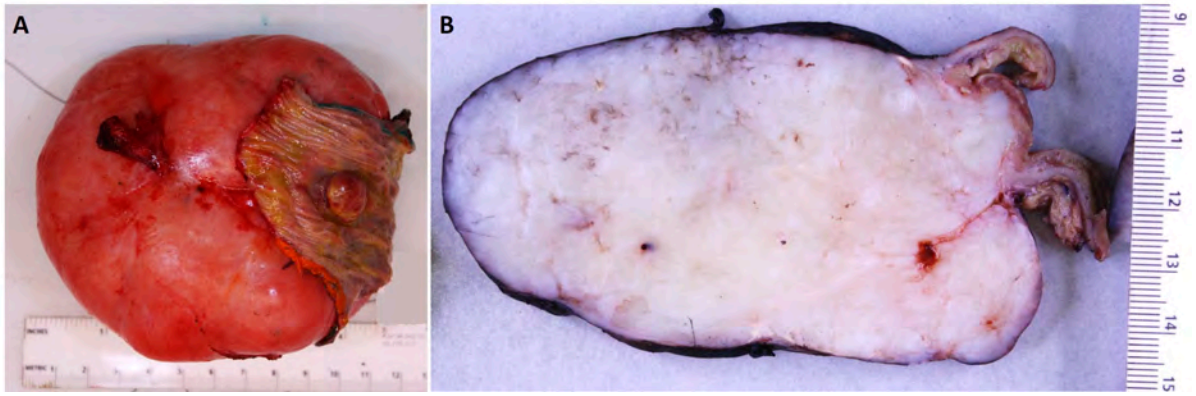

Figure 5. Gross resection specimen with opened attached segment of jejunum (A) and full-thickness section (B) demonstrating the polypoid protrusion of the tumor into the small bowel and the homogenous fibrotic cut surfaces of the tumor post-treatment.

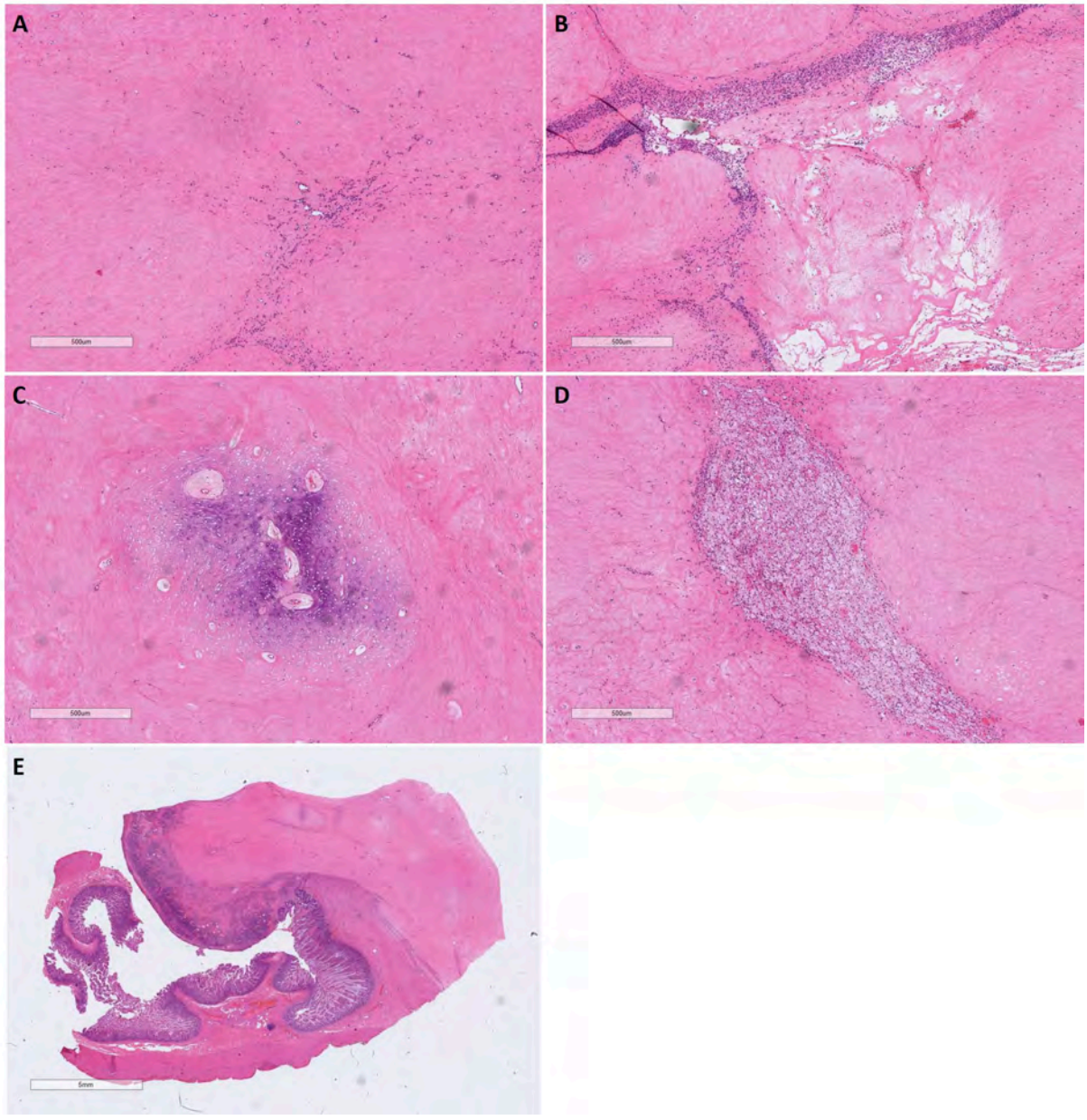

Figure 6. Microscopic examination of the treated resection specimen demonstrated robust treatment response, consisting predominantly of hyalinizing fibrosis (A). Only scattered foci of residual spindle

cells were present, and myxoid and cystic degeneration were noted (B). Rare residual myxohyaline foci (C) and foci of histiocytic inflammation (D) were also identified. The tumor appeared to possibly be arising from the submucosa of the jejunum, with polypoid expansion through the muscularis propria and protrusion into the small bowel lumen (E), overlying mucosal ulceration, and extension into the peritoneum.

References

1. Suurmeijer AJH, Dickson BC, Swanson D, et al. A novel group of spindle cell tumors defined by S100 and CD34 co-expression shows recurrent fusions involving RAF1, BRAF, and NTRK1/2 genes. Genes. Chromosomes Cancer 2018;57:611. doi:10.1002/GCC.22671.
2. Tan SY, Al-Ibraheemi A, Arhens WA, et al. ALK rearrangements in infantile fibrosarcoma-like spindle cell tumours of soft tissue and kidney. Histopathology 2021. doi:10.1111/HIS.14603.
3. Abs D, Landman S, Osio A, et al. Spindle cell tumor with CD34 and S100 co-expression and distinctive stromal and perivascular hyalinization showing EML4-ALK fusion. J. Cutan. Pathol. 2021;48:896–901. doi:10.1111/CUP.13926.
4. Lopez-Nunez O, Surrey LF, Alaggio R, et al. Novel PPP1CB-ALK fusion in spindle cell tumor defined by S100 and CD34 coexpression and distinctive stromal and perivascular hyalinization. Genes. Chromosomes Cancer 2020;59:495–499. doi:10.1002/GCC.22844.
5. Kao YC, Suurmeijer AJH, Argani P, et al. Soft tissue tumors characterized by a wide spectrum of kinase fusions share a lipofibromatosis-like neural tumor pattern. Genes. Chromosomes Cancer 2020;59:575–583. doi:10.1002/GCC.22877.
6. Li B, Hu Y, He Q, et al. Loss of 5'ALK leads to better response to crizotinib in sarcomas with ALK rearrangement. J. Clin. Oncol. 2021;39:e23554. doi:10.1200/JCO.2021.39.15_suppl.e23554.
7. Li T, Zhang F, Wu Z, et al. PLEKHM2-ALK: A novel fusion in small-cell lung cancer and durable response to ALK inhibitors. Lung Cancer 2020;139:146–150. doi:10.1016/J.LUNGCAN.2019.11.002.
8. Nagasaka M, Fisher A, Chowdhury T, et al. PLEKHH2-ALK: A Novel In-frame Fusion With Durable Response to Alectinib: Utilizing RNA Sequencing in Search for Hidden Gene Fusions Susceptible to Targeted Therapy. Clin. Lung Cancer 2021;22:e51–e53. doi:10.1016/J.CLLC.2020.07.017.
9. Butrynski JE, D'Adamo DR, Hornick JL, et al. Crizotinib in ALK-rearranged inflammatory myofibroblastic tumor. N. Engl. J. Med. 2010;363:1727–1733. doi:10.1056/NEJMOA1007056.

12TH INTERNATIONAL AMR PATHOLOGY SLIDE SEMINAR SYMPOSIUM IN ANATOMIC PATHOLOGY

Case – 46

Soft Tissue and bone pathology

Contributed by: ***John Gross***

Clinical History

A 60-year-old male presented with shoulder pain. His past medical history is non-significant. Subsequent imaging revealed a 9 cm mass within the infraspinatous muscle eroding into the scapula.

Pathological Findings

A core needle biopsy was performed revealing a high-grade spindled and epithelioid sarcoma with brisk mitotic activity and necrosis. Despite the high-grade features, the cytology was relatively uniform / monotonous. Immunohistochemical results were variably positive (patchy) for CD34 and S100 whereas it was negative for SOX10, CK AE1/AE3, desmin, SMA, HMB45, ALK, CAM5.2, CD45, CD31, MART1, TFE3, Myogenin, CD1a, Langherin, and ERG. Subsequent targeted RNA sequencing revealed a *FIP1L1::RAF1* fusion. Diagnosis of high-grade spindled and epithelioid sarcoma (FNCLCC Grade 3 of 3) with *FIP1L1::RAF1* fusion. The patient underwent interdigitated chemotherapy and radiation. The tumor was subsequently resected revealing a 9.2 cm mass with only a mild response to neoadjuvant therapy. Surgical margins were negative for tumor.

Diagnosis

Spindle and epithelioid sarcoma with *FIP1L1::RAF1* fusion, high-grade (FNCLCC grade 3 of 3).

Comments

NTRK-rearranged spindle cell neoplasms are an emerging group of soft tissue tumors, currently molecularly-defined, and included into a separate category / chapter in the 2020 WHO 5th Edition Bone and Soft Tissue Tumor Classification. This group of molecularly defined rare soft tissue tumors has a wide spectrum of morphologies and histologic grades. In general, these tumors tend to show co-expression of S100 and CD34 (can be variable or diffuse) but lack expression of SOX10. These tumors are typically composed of monomorphic spindle cells with variable stromal hyalinization and perivascular collagen deposition. The tumors are generally harbor gene fusions involving *NTRK1/2/3*, *RAF1*, or *BRAF1* but, just like the morphologic spectrum, the genetic spectrum is constantly expanding. Briefly, *RAF1* is an oncogene located on chromosome 3 which provides instructions for making an important protein in the *RAS/MAPK* signaling pathway. *RAF1* soft tissue sarcoma partners in literature include *PDZRN3::RAF1, SLMAP::RAF1, TMF1::RAF1, MTAP::RAF1, FMR1::RAF1*. *FIP1L1* is a gene found on chromosome 4 and plays a role in creation of a protein complex named CPSF which is important for creating the poly(A) tail for various proteins. *FIP1L1::PDGFRA* fusion is seen in chronic eosinophilic leukemia but, to our knowledge, *FIP1L1::RAF1* is a novel fusion in sarcoma. Interestingly, unlike various mimics, this family of tumor is potentially targetable with NTRK oncogenic receptor tyrosine kinase inhibitors.

References

1. Agaram, N. P., Zhang, L., Sung, Y.-S., Chen, C.-L., Chung, C. T., Antonescu, C. R., & Fletcher, C. D. (2016). Recurrent NTRK1 Gene Fusions Define a Novel Subset of Locally Aggressive Lipofibromatosis-like Neural Tumors. *The American Journal of Surgical Pathology*, *40*(10), 1407–1416.
2. Brčić, I., Godschachner, T. M., J., & Liegl-Atzwanger, B. (2021). Broadening the spectrum of NTRK rearranged mesenchymal tumors and usefulness of pan-TRK immunohistochemistry for identification of NTRK fusions. In *Modern Pathology* (Vol. 34, Issue 2, pp. 396–407). https://doi.org/10.1038/s41379-020-00657-x
3. Caprini, E., Verkhovskaia, S., Casini, B., Testi, A., Dagrada, G. P., Palese, E., & Rahimi, S. (2023). A spindle cell neoplasm with MYH9::EGFR fusion and co-expression of S100 and CD34, further expanding the family of kinase fusion positive spindle cell neoplasms. *Genes, Chromosomes & Cancer*. https://doi.org/10.1002/gcc.23134
4. Davis, J. L., Lockwood, C. M., Hawkins, D. S., & Rudzinski, E. R. (2019). Expanding the Spectrum of Pediatric NTRK-rearranged Mesenchymal Tumors. In *The American Journal of Surgical Pathology* (Vol. 43, Issue 4, pp. 435–445). https://doi.org/10.1097/pas.0000000000001203
5. Suurmeijer, A. J. H., Dickson, B. C., Swanson, D., Zhang, L., Sung, Y.-S., Cotzia, P., Fletcher, C. D. M., & Antonescu, C. R. (2018). A novel group of spindle cell tumors defined by S100 and CD34 co-expression shows recurrent fusions involving RAF1, BRAF, and NTRK1/2 genes. *Genes, Chromosomes & Cancer*, *57*(12), 611–621.
6. Zhang, T., Wang, Q., Yi, X., & Zhu, P. (2021). RAF1-rearranged spindle cell tumour: report of two additional cases with identification of a novel FMR1-RAF1 fusion. *Virchows Archiv: An International Journal of Pathology*. https://doi.org/10.1007/s00428-021-03178-3

12TH INTERNATIONAL AMR PATHOLOGY SLIDE SEMINAR SYMPOSIUM IN ANATOMIC PATHOLOGY

Case – 47

Soft tissue and bone pathology

Contributed by: ***Hugo Ricardo Dominguez-Malagon***

Clinical History and Pathological Findings

A 57-year-old male admitted to our hospital in October 2017 for postoperative control of a soft tissue abdominal wall. The tumor was resected three times recurred twice in the last 20 years, in another institution, the last resection in June 2017. No recurrence was detected on admision. We received the paraffin block and HyE slides of the last surgery (June 26, 2017). The histology had the typical appearance was of a DFSP (storiform and lace-like). By immunochemistry it was positive for CD 34 and BCL-2, negative for C-Kit, DOG-1, TLE-1, Anti-alpha smooth muscle actin and S-100. As one of the differential diagnosis was with synovial sarcoma, a search for the rearrangement of SS18 was carried out by FISH, which was positive, however, even with the confirmation of such rearrangement, it was considered a DFSP because the histology and clinical behavior was consistent with such entity. The patient was not considered candidate for radiotherapy, negative for adenopathy and tumor activity by magnetic resonance and PET-SCAN studies, the clinical decision was follow-up monitoring the patient every 3 months. The patient was free of disease for 4 years, but in Octuber 2021 a computed axial tomography showed one nodule in the area of the last surgery that measured 22.5mm with contrast uptake. A trucut was done, a DFSP with fibrosarcomatous component was rendered A wide local excision of left abdominal wall was done. In the pathology department we received a 4.3 cm tumor was found, it was round, well defined borders, firm, localized in the dermis with extension to subcutis. Histologically displayed the storiform and lace-like pattern typical of DFSP.plus a fibrosarcomatous component. By IHQ It was positive for CD 34, CD 56 (weak) and was negative for SS18, BCL2, STAT6 and TLE-1. Because of the previous FISH study that was positive for SS18 rearrangement in the material obtained more than 4 years ago, it was decided to repeat the study. It was again positive for the SS18 rearrangement. The last consultation of the patients was in November 28, 2022, with computed axial tomography without evidence of tumoral activity. The patient continues under close surveillance with medical check-up every 3 months.

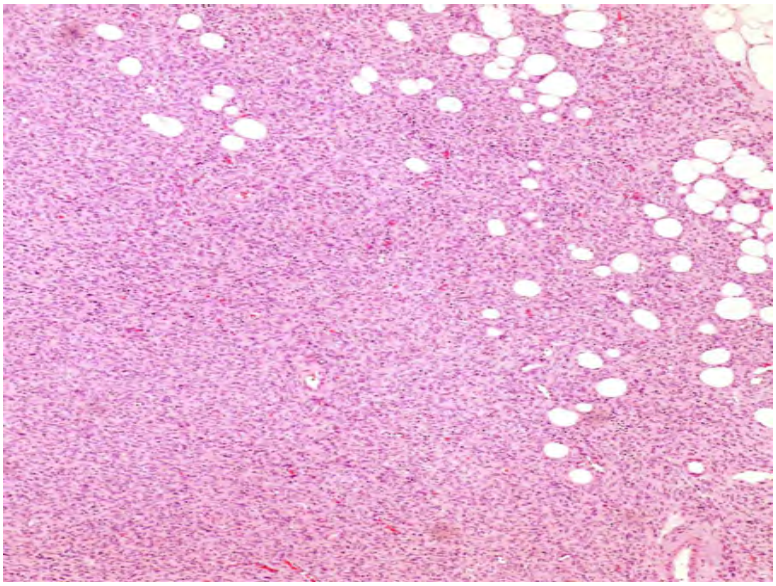

Diagnosis

Dermatofibrosarcoma protuberans with fibrosarcomatous transformation, and SS18 rearrangement by FISH.

Comments

DFSP is a locally aggressive superficial mesenchymal neoplasm, most cases contain COL1A1/PDGFB. mostly exophytic, nodular cutaneous mass or a flat plaque. Initially may show persistent slow growth, often for many years, then sudden progression with fibrosarcomatous transformation. Metastases typically occur following multiple local recurrences. Tumors are generally centered within the dermis or subcutis and characterized by spindle cells with a storiform to whorled pattern. Tumors infiltrate and expand fibrous septa; interdigitation amongst lobules of fat yields a so called "honeycomb" pattern By electron microscopy it is characterized by dendritic cells with long slender processes with scant cutoplasm and few organelles including some subplasmalemmal plates, surrounded by mature collagen. The nuclei are often convoluted with deep indentations. A case of DFSP, with typical clinical, histological, immunohistochemical, ultrastructural and follow-up features is presented, however by fish it showed the molecular features of synovial sarcoma.

12TH INTERNATIONAL AMR PATHOLOGY SLIDE SEMINAR SYMPOSIUM IN ANATOMIC PATHOLOGY

Case – 48

Soft tissue and bone pathology

Contributed by: ***Markku Miettinen***

Clinical History

A 53-year-old male presented with a 5x4.5x4cm psoas muscle mass. He also had a large jejunal mass about 20 cm in maximum diameter. There was a history of HIV/ AIDS.

Pathological findings

The presented example is a large, internal tumor mass. This is histologically different from typical Kaposi sarcoma with undifferentiated appearance and pleomorphism. This differs from typical Kaposi sarcoma that is composed of mildly atypical spindle cells and may contain vascular differentiation. As observed in typical Kaposi sarcoma, this example was positive for CD34 and HHV8. Mutation analysis revealed somatic mutations in genesTP53 (p53 gene) and ARID1A. Sarcoma DNA methylation classifier matches this tumor as an angiosarcoma.

Diagnosis

Kaposi sarcoma, tumorigenic/ aggressive form.

Comments

Kaposi sarcoma is generally known as a small skin tumor that can involve otherwise healthy elderly patients, malnourished individuals (especially in Africa), organ transplant recipients, and HIV/ AIDS patients of any age. The latter patients often have multiple skin lesions. Internal organ involvement may also occur.

Kaposi sarcoma may evolve into a tumorigenic and organ metastatic form, and this is often referred as “aggressive Kaposi sarcoma”. Histologically this form of Kaposi sarcoma is not well-described but has been reported (1). This form of Kaposi sarcoma seems to retain HHV8- positivity, but contains various pathogenic mutations, involving cell cycle regulating genes, such TP53 and chromatin-organizer protein ARID1A, and others (2). Sarcoma DNA methylation classifier is a new, currently experimental diagnostic tool, which is more developed for brain tumor classification (3-5).

References

1. Basra P, Paramo J, Alexis JJ Disseminated Kaposi sarcoma with epithelioid morphology in an HIV/AIDS patient: A previously unreported variant. Cutan Pathol. 2018 Jul;45(7):526-529.
2. Malouf GG, Lu X, Mouawad R, Spano JP, Grange P, Yan F, Aractingi S, Su X, Dupin NJ. Genetic landscape of indolent and aggressive Kaposi sarcomas. Eur Acad Dermatol Venereol. 2022;36:2343-2351.
3. Koelsche C, Schrimpf D, Stichel D, et al. Sarcoma classification by DNA methylation profiling. Nature Communications 2021;12:498:1-10.

4. Lyskjaer I, De Noon S, Tirabosco R, et al. DNA methylation-based profiling of bone and soft tissue tumours: a validation study of the DKFZ sarcoma classifier. J Pathol Clin Res 2021;7:350-360.
5. Papanicolau-Sengos A, Aldape K. DNA methylation profiling: An emerging paradigm for cancer diagnosis. Annu Rev Pathol Mech Dis 2022;17:295-321

12TH INTERNATIONAL AMR PATHOLOGY SLIDE SEMINAR SYMPOSIUM IN ANATOMIC PATHOLOGY

Case – 49

Soft tissue and bone pathology

Contributed by: ***Markku Miettinen***

Clinical History

A 35-year-old female presented with a 7.5 x 5 x 2.5 cm periscapular mass. Patient had a history of neurofibromatosis 1.

Pathological findings

The presented example is an intraneural/ plexiform neurofibroma evolving into MPNST. The slide contains elements of plexiform neurofibroma and atypical neurofibromatous neoplasm with varying cellularity containing areas resembling neurofibroma and those that have evolved into an MPNST (high cellularity, mitotic activity, in some areas >10/ 10 HPFs). The MPNST areas showed loss of SOX10 and p16, aberrant CD34 expression, and essentially retained H3K27me3. Mutation analysis showed loss of NF1 and MET amplification, but CDKN2A/B loss was not observed.

Diagnosis

Malignant peripheral nerve sheath tumor

Comments

Neurofibromatosis 1 patients with NF1 gene loss of function germline mutations develop cutaneous and intraneural neurofibromas, and the latter may evolve into MPNST.

About 2.7% of NF1 patients are reported to develop MPNST by age of 20 years [1] and around 10% in lifetime [2]. This case is example of an MPNST arising in a neurofibroma but only partly involving it. Loss of SOX10/ S100 protein is typical in high-grade MPNST. Tumor is unusual in having CDKN2A/B and H3K27me3 retained; both typically show losses in MPNST [3]. MET oncogene involvement is known in a subset of MPNST and may be a therapeutic oncogene target [4].

References

1. Peltonen S, Kallionpää RA, Rantanen M, et al . Pediatric malignancies in neurofibromatosis type 1: A population-based cohort study. Int J Cancer. 2019;145:2926- 2932.
2. Evans DG, Baser ME, McGaughran J. Malignant peripheral nerve sheath tumours in neurofibromatosis 1. Med Genet. 2002;39:311-4.
3. Mantripragada KK, Spurlock G, Kluwe L, et al . High-resolution DNA copy number profiling of malignant peripheral nerve sheath tumors using targeted microarray-based comparative genomic hybridization. Clin Cancer Res. 2008;14:1015-24.
4. Peacock JD, Pridgeon MG, Tovar EA, et al. Genomic Status of MET Potentiates Sensitivity to MET and MEK Inhibition in NF1-Related Malignant Peripheral Nerve Sheath Tumors.Cancer Res. 2018 Jul 1;78(13):3672-3687.

12TH INTERNATIONAL AMR PATHOLOGY SLIDE SEMINAR SYMPOSIUM IN ANATOMIC PATHOLOGY

Case – 50

Soft tissue and bone pathology

Contributed by: ***Hugo Ricardo Dominguez-Malagon***

Clinical History

A seven year-old female with a 2 year history of left shoulder pain and microfractures in the proximal humerus. Radiography and CAT demonstrated an expansile osteolytic lesion involving the proximal metaphisis of the right humerus, with popcorn appearance (chondroid matrix).

Pathological findings

The lesion has three main components, one is the presence of abundant hyaline cartilage with well differentiated chondrocytes arranged in columns, resembling the growth plate; other is encondral ossification resulting in bone trabeculae delineated by polygonal osteoblasts and some osteoclasts; he third component is connective tissue matrix with reparative changes.

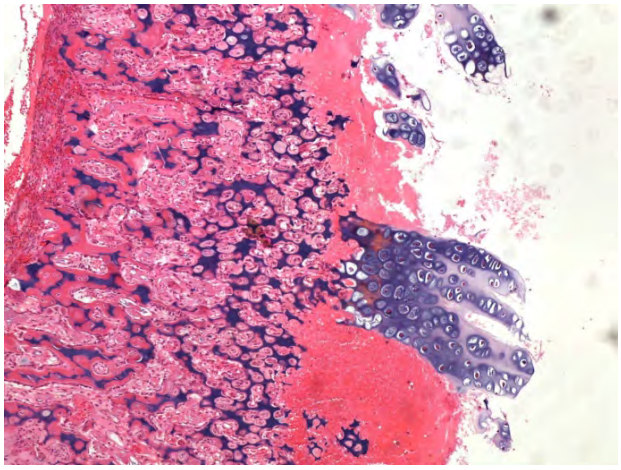

Diagnosis

Fibrocartilaginous mesenchimoma.

Comments

Fibroartilaginous Mesenchimoma (FCM) is a rare tumor that primarily arises in the long bones of children, it grows quickly despite its benign nature. It has proved a challenging diagnosis and can be mistaken with a sprectum of benign and malignant tumors. The histological presentation is unique with plate like cartilage (chondrocytes arranged in columns, destruction of surrounding cortical bone and fibrous stroma).

FCM was originally reports by Dahlin 1n 1984 (1), to date only 33 cases have been published, in addition to long bones other locations include metatarsals, pubis, ribs and vertebrae.

Radiologically FCM is described as radiolucent with scattered ring like calcification. Histologically is characterized by variable proportions of: fibroblastic proliferation without atypia; islands of cartilage displaying characteristic resemblance to epiphyseal growth plate-like cartilage, capillaries in the stroma, irregular borders and encondral ossification with osteoblast rimmed lamellar bone formation.

The origin of the growth-plate-like cartilage is unclear, Mirra proposed that chondroid areas represent residues of the growth plate. However the fact that FM can occur in bones where the epiphyseal plate does not exist like vertebrae and pubis, runs against this theory.

Differential diagnosis include Fibrocartilaginous dysplasia (FCD) and chest wall hamartoma of infancy among others. FCM and FCD have similar clinical, radiological and histoptahological characteristics and some authors even consider the two to be equivalent (2); however FCD shows fibrous stroma with woven bone trabeculae lacking osteoblastic rimming and nodules of cartilage de not contain growth plate-like configuration.

Chest wall hamartoma of infancy shares growth plate appearance with FCM, however it only affects infants and only occurs in the chest-wall.

Molecularly, no GNAS and IDH ½ mutation of MDM2 amplification were found (3), concluding that FCM is not related to fibrous dysplasia, dedifferentiates chondrosarcoma and well differentiated osteosarcoma. Only one case recurred 1 year following intralesional resection. None died of disease.

References

1. Dahlin DC, Bertoni F, Beabout JW, Campanacci M. Fibrocartilaginous mesenchimoma with lw-grade malignancy. Skeletal Radiol. 1984;12(4):263-269.
2. Bhaduri A, DEsphande RB. Fibrocartilaginous mesenchimoma versus fibrocartilaginous dysplasia: are these a single entity? Am J Surg Pathol. 1995;19 (12): 1447-1448.
3. Gambarotti M, Righi A, Vanel D, et al. Fibrocatilaginous mesenchimoma of bone: a single institution experience with molecular investigations and a review of the literature. Histopathology 2017;71:134-142

12TH INTERNATIONAL AMR PATHOLOGY SLIDE SEMINAR SYMPOSIUM IN ANATOMIC PATHOLOGY

Case – 51

Soft tissue and bone pathology

Contributed by: ***Kum Cooper***

Clinical History

A 30-year-old male presented with history of right middle back pain for 5 months. He also complained of right sided rib pain/discomfort and associated numbness.

MRI showed an expansile lesion centered in the right posterior elements of T7 with associated mass effect upon the thecal sac and narrowing of right T6-7 and T7-8 neural foramina. Differential diagnoses included aneurysmal bone cyst, chondroid lesions and giant cell tumor. Radiologically ABC was the favored diagnosis.

Patient underwent pre-operative spinal angiogram with embolization of both segmental arteries at T7-8. This was followed by needle core biopsy and surgical resection with T6-8 laminectomy and transpedicular resection of the T7 mass and partial removal of chest wall.

Pathological findings

Designated spinal column tumor the specimen measured 4.7 x 4.5 x 4.4 cm tan-white soft tissue and osseous elements. The cut surface revealed tan-white to pink, soft to firm dense intraosseous lesion measuring 3.8 x 3.2 x 2.0 cm. Numerous cysts ranging from 1.0 to 4.0 mm were also noted. In addition, the lesion invaded into soft tissue.

The tumor comprised solid sheets of fibroblastic/myofibroblastic proliferation without prominent and large blood-filled cysts with fibromembranous septae. Isolated focal tiny cysts were appreciated with smooth lining. Although cortical destruction was present, the peripheral margin of the tumor showed reactive woven bone rimmed by osteoblasts. The tumor was cellular with bland spindle cells with vesicular nuclei and minute nucleoli; arranged in fascicles with storiform or haphazard patterns in which foci of hemorrhages with extravascated blood was noted. Mitoses were rare, ranging from 1-4/10HPF. Chronic inflammatory infiltrate with cystic changes and variable collagen deposition reminiscent of nodular fasciitis was seen. Varying numbers of osteoclast giant cells ranging from scattered to focal aggregates were noted often clustered around foci of hemorrhages. Reactive bone with osteoblast-like cells rimming lace-like or trabeculae of woven bone were also seen.

USP-6 gene rearrangement was confirmed by fluorescent in situ hybridization.

Diagnosis

Aneurysmal bone cyst, solid variant (SVABC).

Comments

The diagnosis of solid variant of ABC is based on histological features demonstrating the solid component of ABC. On imaging SVABC usually presents with an expansile and osteolytic solid lesion

with or without small cystic spaces but without characteristic fluid-fluid levels on CT or MRI. In fact, there appears to be no differences in clinical and radiologic presentations between SVABC and primary ABC (PABC). This is further supported by the presence of t(16::17) which represents a juxtaposition of *CDH11* and *USP6* that is shared between SVABC and PABC, implying close association and inseparable entities. Evidence suggests that SVABC is putatively the early stage of PABC.

USP6 overexpression may induce matrix metalloproteinases, prompting inflammation, osteolysis and vascularization leading to a repair-like and hemorrhagic appearance in SVABC and PABC. Therefore, other types of florid fibroblastic proliferation of soft tissue such nodular fasciitis, myositis ossificans or fibro-osseous pseudotumor of the digit may histologically resemble SVAB/PABC due to distinct USP6 rearrangements.

SVABC is rare accounting for 3.5-7.5% of all ABCs; although the incidence may be inaccurate since SVABC and giant cell reparative granuloma (GCRG) was considered interchangeable as they shared similar histologic features. The latter has since been revised since USP6 rearrangement was demonstrated in the small bones of hands and feet but NOT in gnathic GCRGs. Hence the term GCRG is now reserved for the gnathic location, considered to be pathogenetically different from extra-gnathic locations.

CDH11-USP6 fusion transcripts are identified only in PABCs but not in secondary ABCs; hence being useful in distinguishing entities like chondroblastoma, giant cell tumor, fibrous dysplasia, osteoblastoma, etc. which may have secondary ABC-like changes both radiologically and histologically.

The differential diagnosis of SVABC includes tumors with spindle cells and osteoid predominantly rimmed by osteoblasts and osteoclast like giant cells. Giant cell tumors typically display evenly distributed polyhedral mononuclear cells with H3G34 being helpful (mutation *H3F3A*). Osteoblastoma is characterized by prominent osteoblast-rimmed trabeculae of woven bones with intervening loose fibrovascular tissue and demonstrate *FOSB* rearrangement; lacking spindle cells and *USP6* rearrangement. GCRGs, Brown tumor (BT), and phosphaturic mesenchymal tumor (PMT) show considerable morphologic overlap with admixture of fibroblasts, extravasated blood cells, and scattered giant cells, clustering around hemorrhagic areas. GCRGs always arise in gnathic sites (see above), clinical/laboratory results may support hyperparathyroidism for BT, and FGF expression supporting a diagnosis of PMT; all three of these entities are negative for *USP6* rearrangements.

References

1. Sanerkin et al. “Solid” Variant of ABC. Cancer. 1983;51:2278-86.
2. Zhou et al. Solid ABC with USP6 rearrangement. Pathology International. 2020;70:502-512.
3. Agaram et al. USP6 rearrangements in GCRG of hands and feet (not gnathic). Human Pathology. 2014;45:1147-1152.
4. Hiemcke-Jiwa et al. USP6 associated neoplasms. IJSP. 2020;28:816-825.

12TH INTERNATIONAL AMR PATHOLOGY SLIDE SEMINAR SYMPOSIUM IN ANATOMIC PATHOLOGY

Case – 52

Soft Tissue and bone pathology

Contributed by: ***John Gross***

Clinical History

A 46-year-old female with PMH of fibromyalagia, presenting with increasing back pain, osteomalacia with multiple fractures in different stages of healing, weakness and paresthesia. Clinical concern was for a systemic disease / myeloma. Imaging also revealed a paraspinal mass with features concerning for spinal cord compression. Bone marrow biopsy showed a 0.4% monoclonal plasma cell population, kappa-positive (IgA kappa). Subsequent random urine protein electrophoresis was normal as well a urine immunofixation electrophoresis (IFE) was normal. Given the concern for spinal cord compression, urgent mass excision and spinal cord decompression surgery was performed.

Pathological Findings

Surgical excision revealed a bland spindle cell neoplasm with admixed mature adipose tissue with prominent stromal hemangiopericytyomoa-like vasculature pattern. The cells of interest are uniform / monotonous and have fine condensed chromatin. Small pools of grungy mucoid fluid was also seen. No concerning nuclear atypia/anaplasia, mitotic activity, or tumor necrosis. Diffusely positive for SSTR2A, SATB2 and CD56 whereas ERG is negative.

Diagnosis

Phosphaturic mesenchymal tumor, mixed-connective tissue type, histologically benign, forming a 3.1 cm mass.

Comments

PMT is a rare mesenchymal tumor associated with tumor-induced osteomalacia (TIO). PMT mostly occurs in older adults in the soft tissues (acral, extremities, H&N) or bones and is rare in parenchymal organs and RP. Major variants / patterns of PMT include: Mixed-connective tissue type (most common; 70-80%), osteoblastoma-like and giant-cell rich (may have ABC-like areas). In general, PMT consists of bland spindle cells, myxoid stroma, mature fat, HPC-like vessels, grungy calcifications. The immunophenotype is variable but often shows positive IHC expression of ERG, SATB2, SSTR2A, CD56, SMA, CD34. FGFR23 chromogenic in situ hybridization is sensitive and specific but not readily available (difficult test to perform test / send out, not available in most practice settings). Most cases harbor *FN1::FGFR1* (majority) fusions whereas a subset will have *FN1::FGF1* gene fusions. The overwhelming majority of PMTs are benign but rare malignant (frankly sarcomatous) examples exist. Occasionally, histologically benign examples can metastasize. Surgical excision often cures phosphaturia. The basic pathophysiology of TIO is hypophosphatemia secondary to tumor secretion of FGF23 which leads to inhibition of renal phosphorus reabsorption *compounded* by a vitamin D synthetic defect that blocks the compensatory rise in calcitriol stimulated by the hypophosphatemia. Non-phosphaturic variants of PMT exist and are likely related to inactive secretion of FGF-23, insufficient FGF-23 secretion (often

in a tumor caught early), tumors which secrete MEPE but not FGF-23, tumors that secrete FGF-23 but the patient compensates to handle the increased FGF-23 secretion are challenging to accurately diagnose.

In our patient, serum phosphate levels were very low prior to surgery at 0.7 mg/dL and began to increase postoperatively. Phosphate levels are expected to continue to improve over time with phosphate supplementation. Vitamin D3 levels were also low at 12 pg/mL. Alkaline phosphatase elevated at 251 U/L. Progressive tumor-induced osteomalacia likely explains the patient's prior diagnoses of polyneuropathy and fibromyalgia. The course of the disease was likely indolent until she developed spinal canal stenosis. The possibility of altered mineral metabolism for the extensive insufficiency fractures was not initially considered based on the CT and XR. The presence of prominent adjacent soft tissue mass and prior history of MGUS were a diagnostic pitfall, which led to many of the healing fractures being characterized as associated with lytic bone lesions, and an incorrect initial suspicion of myeloma. PMT was not suspected until tissue sampling was performed and correlation of both the low phosphate levels in the serum and radiologic findings by the pathologist, highlighting the importance of clinical, radiological, and pathological correlation. Phosphaturic mesenchymal tumors should be considered by the radiologist/clinician/pathologist when there is a dominant soft tissue or bone mass accompanied by osteomalacia / insufficiency fractures. The pathologist is critical to secure this diagnosis, which is a very rare disease, and may not present with classic clinical or radiologic sequelae.

References

1. Folpe, A. L. (2019). Phosphaturic mesenchymal tumors: A review and update. *Seminars in Diagnostic Pathology*, *36*(4), 260–268.
2. Folpe, A. L., Fanburg-Smith, J. C., Billings, S. D., Weiss, S. W. (2004). Most Osteomalacia-associated Mesenchymal Tumors Are a Single Histopathologic Entity: An Analysis of 32 Cases and a Comprehensive Review of the Literature. *The American Journal of Surgical Pathology*, *28*(1), 1–30
3. Jan de Beur S. Tumor-Induced Osteomalacia. Journal of the American Medical Association 2005; Vol 294, No. 10.
4. Agaimy, A., Michal, M., Haller, F., & Michal, M. (2017). Phosphaturic Mesenchymal Tumors: Clinicopathologic, Immunohistochemical and Molecular Analysis of 22 Cases Expanding their Morphologic and Immunophenotypic Spectrum. *The American Journal of Surgical Pathology*, *41*(10), 1371–1380.

12TH INTERNATIONAL AMR PATHOLOGY SLIDE SEMINAR SYMPOSIUM IN ANATOMIC PATHOLOGY

Case – 53

Soft tissue and bone pathology

Contributed by: ***Kyle Perry***

Clinical History

A 22-year-old (otherwise healthy) male presented after experiencing a year of hip pain. He had no history of malignancy or radiation therapy. An MRI demonstrated a 13.4 cm mass in the left tensor fasciae latae muscle belly that was predominantly composed of fat. The mass had moderate heterogeneously enhancing central irregular soft tissue elements, radiologically interpreted as concerning for lipoma or atypical lipomatous tumor (Fig A and B). During the procedure, the surgeon found the consistency of the mass to be unusual and questioned whether it could be necrotic. He decided to perform an incisional-type biopsy.

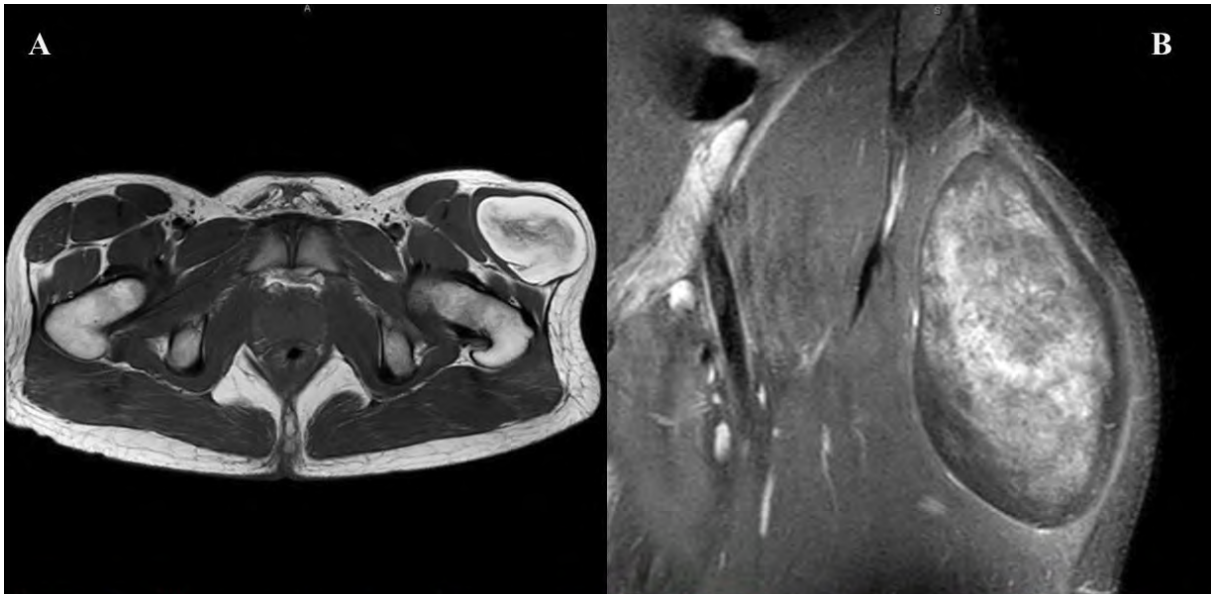

Figures A and B. MRI showing features compatible with adipocytic tumor with heterogenous enhancement.

Pathological Findings

Histologically, the tumor was overwhelmingly composed of irregular adipocytes (Fig C and D). In very focal areas of the tumor (less than 2%), there was increased capillary density, minimal myxoid stroma and occasional immature adipocytes/ lipoblasts (Fig E and F). The tumor was negative for MDM2 gene amplification by fluorescent in-situ hybridization. However, next generation sequencing (NGS) identified a FUS-DDIT3 fusion transcript.

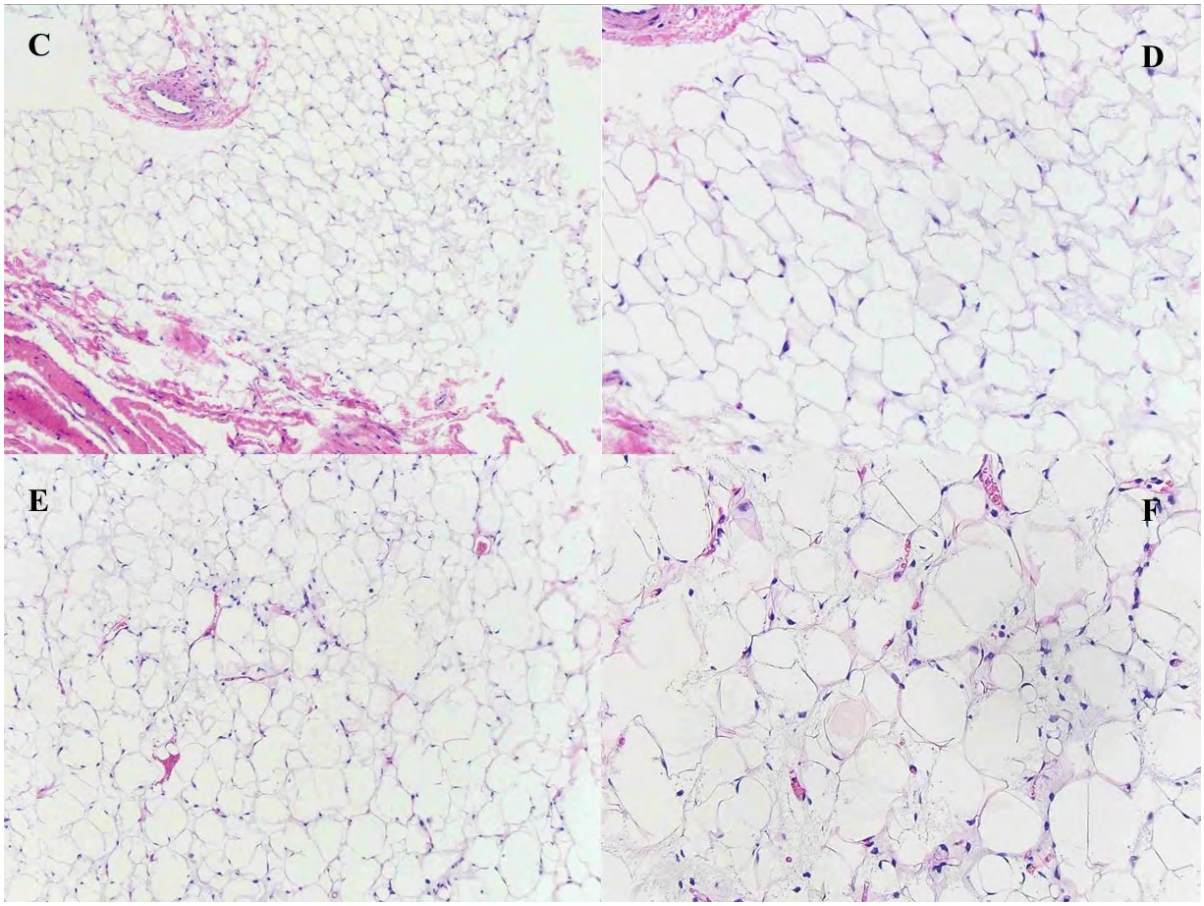

Figures C and D. The overwhelming majority of the tumor appeared to be composed of relatively mature adipocytes. Figures E and F. Focal areas of delicate capillaries and myxoid stroma were noted.

Diagnosis

Myxoid liposarcoma with a predominant mature adipocytic component.

Comments

While myxoid liposarcoma is not a particularly exotic diagnosis, this case highlights an interesting potential pitfall created by this variant morphology. Myxoid liposarcomas usually present as a proliferation of round to ovoid cells in the background of a delicate network of capillaries and myxoid matrix. Higher grade tumors (i.e., “round cell sarcoma”) show more cellular areas of a neoplastic cells with overlapping nuclei. While immature/more mature adipocytes can be present, these typically compose a minority of an untreated tumor. 1 In tumors which have been previously treated with radiation therapy, a significant portion of the myxoid liposarcoma can show a more mature “lipoma-like” morphology.2 This presentation was unusual in that the patient’s initial (untreated) tumor exhibited almost complete (>98%) mature adipocytic differentiation. This phenomenon has been nicely described in a recent paper by Iwasaki and colleagues in which they describe a series of “myxoid liposarcomas with extensive lipoma-like changes.”3 As soft tissue tumors are increasingly diagnosed on needle core biopsies (which can constitute less than 0.1% of the tumor mass), this morphologic variant of myxoid liposarcoma could present a potential pitfall to the unsuspecting pathologist. Next generation sequencing or fluorescent in-situ hybridization studies for DDIT gene rearrangements could be helpful in adipocytic tumors with unusual intraoperative or imaging characteristics.

References

1. Goldblum JR, Enzinger FM, Folpe AL, Weiss SW. Enzinger and Weiss's soft tissue tumors. Saunders/Elsevier; 2014.
2. Engstrom K, Bergh P, Cederlund CG, et al. Irradiation of myxoid/round cell liposarcoma induces volume reduction and lipoma-like morphology. Acta Oncol. 2007;46(6):838-45. doi:10.1080/02841860601080415
3. Iwasaki H, Ishiguro M, Nishio J, et al. Extensive lipoma-like changes of myxoid liposarcoma: morphologic, immunohistochemical, and molecular cytogenetic analyses. Virchows Arch. Apr 2015;466(4):453-64. doi:10.1007/s00428-015-1721-z

12TH INTERNATIONAL AMR PATHOLOGY SLIDE SEMINAR SYMPOSIUM IN ANATOMIC PATHOLOGY

Case – 54

Soft tissue and bone pathology

Contributed by: ***Paul Wakely***

Clinical History

A 48-year old man presented with a gradually increasing neck mass and 30 lb. weight loss. He had intermittent dysphagia to liquids, associated cough and episodes of choking. CT scan from an outside hospital demonstrated a 2.5 x 2.4 x 2.4 cm. ovoid expansile mass limited to the left thyroid cartilage. The mass had radiologic features exhibiting chondroid matrix deposition. Radiologic impression was chondrosarcoma versus chondroma. The right thyroid cartilage and cricoid cartilage were radiologically unremarkable. Vertical hemilaryngectomy and left thyroplasty with tracheotomy was performed.

Pathological Findings

A left partial laryngectomy specimen contained a 1.7 cm. tan-brown, friable mass without the translucent off-white appearance typical of conventional chondrosarcoma. Most tissue sections contained a proliferation of large polygonal tumor cells mixed with woven bone. Replacement of marrow was by tumor cells having sharply defined cell borders, and voluminous amounts of balloon-like cytoplasm that varied from optically clear to partly eosinophilic. Nuclear cytoplasmic pseudoinclusions were not infrequent. Tumor cells were PAS-positive, PAS-D negative, and expressed diffuse, strong S-100 staining.

Diagnosis

Clear cell chondrosarcoma of the larynx.

Comments

Chondrosarcoma (ChS) of the entire head and neck region is uncommon. For the larynx in particular, evaluation of the NCI's SEER registry over the past 38 years (ending 2010) uncovered only 143 examples of laryngeal ChS representing 0.2 % of all laryngeal tumors. SEER registry data found a predilection for laryngeal ChS to arise primarily in Caucasians, males (3:1, M:F), and to only rarely develop regional or distant metastases even with T4 neoplasms. Obenauer et al. described the initial case of clear cell ChS (CCC), and to my knowledge only 5 additional examples have been reported. CCC of bone was initially described by Unni et al. It is the rarest histologic form of ChS with its prime location being the epiphysis of the neck and head of the femur, and head of the humerus. Mokharti et al. found only 9 examples of CCC in the head and neck including one in the skull, and the aforementioned laryngeal examples.

Since most examples of CCC also contain foci of conventional matrix-producing ChS, it is possible with a small biopsy specimen that only the conventional ChS portion of a mass may be sampled, and thus be misdiagnosed. As in our case, tissue sections of CCC show a solid proliferation of large cells with pale to lightly eosinophilic cytoplasm, single enlarged nuclei, and discrete cell

borders intersecting among bony trabeculae. If one focused only on the clear cells without recognizing foci of chondroid matrix, one could potentially mistake CCC for a metastatic or locally invasive carcinoma having predominantly clear cell histology. Unlike CCC, chondroblastoma has much smaller cells, lacks the enormous clear cytoplasm, and characteristically contains delicate lace-like calcification in areas. Immunohistochemically, CCC cells are strongly S-100 positive, and may show reactivity with cytokeratin AE1/AE3, CK 18.

References

1. Dubal PM, Svider PF, Kanumuri VV et al. Laryngeal chondrosarcoma: a population-based analysis. Laryngoscope. 2014;124: 1877-8
2. Unni KK, Dahlin DC, Beabout JW, et al. Chondrosarcoma: clear cell variant. A report of sixteen cases. J Bone Joint Surg Am. 1976;58:676–83.
3. Mokhtari S, Mirafsharieh A. Clear cell chondrosarcoma of the head and neck. Head Neck Oncol. 2012;4:13.
4. Obenauer S, Kunze E, Fischer U, et al. Unusual chondrosarcoma of the larynx: CT findings. Eur Radiol. 1999;9: 1625–8.
5. Hendriks T, et al. Clear cell chondrosarcoma of the larynx. BMJ Case Rep. 4: 2018.
6. Velez Torres JM et al. Primary Sarcomas of the Larynx: A Clinicopathologic Study of 27 Cases. Head Neck Pathology 2021; 15:905–916.
7. Alexander J, Wakely PE Jr. Primary laryngeal clear cell chondrosarcoma: report of a case and literature review. Head Neck Pathol. 2014;8(3):307-10.

12TH INTERNATIONAL AMR PATHOLOGY SLIDE SEMINAR SYMPOSIUM IN ANATOMIC PATHOLOGY

Case – 55

Soft tissue and bone pathology

Contributed by: ***Fredrik Petersson***

Clinical History

A 40 year-old woman presented with a central neck lump of 2 years duration that was progressively increasing in size. The patient had a subtotal thyroidectomy performed overseas 3 years ago for a tumor that was told to be benign. Clinical examination revealed a 2 cm hard, central neck mass that did not move on swallowing. A CT-scan of the neck showed a 1.9 cm, hyperdense, poorly circumscribed focus with irregular radiating tongue-like extensions in the central neck region. The patient initially underwent an FNA-biopsy (which was signed out as "a low-grade spindle cell neoplasm, likely of mesenchymal origin"), and the tumor was subsequently excised.

Pathological Findings

The epicenter of the tumor was located in the deep subcutis and showed a multi-nodular to plexiform arrangement separated by dense collagenous stroma. The tumor was infltrative with radiating tongue-like fibroblastic bands extending to the margins multifocally. The radiating tongue-like extensions extended far from the center of the tumor mass and were associated with scattered smaller plexiform nodules of histiocytoic cells. These tongue-like bands were composed of variably cellular, fbroblastic/fbromatosis-like areas. The tumor also infltrated skeletal muscle focally. On higher magnification, the tumor was composed of two cell types; (A) histiocytoid cells with round vesicular nuclei and ample pale cytoplasm and (B) fibroblastic-type spindle cells with longer tapering cytoplasmic processes. Numerous interspersed osteoclasttype giant cells were also present. Nuclear atypia was minimal. Mitotic activity was up to 5 per 10 HPFs with no atypical mitotic figures seen. On IHC, SMA-expression was seen in the spindle and some histiocytoid cells while CD68 was strongly expressed only in the histiocytoid cells and multinucleated giant cells. There was patchy expression of CD163 in the spindle and histiocytoid cells. The tumor cells showed no expression of cytokeratins (AE1/3, CAM5.2), HMB-45, SOX10 and S-100 protein, desmin, CD31, ERG, CD21, CD23, CD35 and HHV8.

Diagnosis

Plexiform fibrohistiocytic tumor.

Comments

Plexiform fbrohistiocytic tumor is an uncommon low-grade malignant mesenchymal tumor that was first described by Enzinger and Zhang in 1988 [1]. In the initial series, PFHT seemed to have a predilection for young female patients. Subsequently, with increasing number of reported cases, there seems to be no sharp gender difference. Although the age range is wide (congenital to elderly), PFHT is predominantly a tumor that affects children and young adults. The tumor most frequently involves the extremities in both proximal and distal locations. The tumor is usually centered in subcutaneous

adipose tissue but dermal extension may occur. Less frequently, tumors may infltrate into skeletal muscle. PFHT occurring in the head and neck region is distinctly uncommon with seven out of sixty-five (10%) cases reported in Enzinger and Zhang's series, one out of fourteen (7%) cases reported in Hollowood's series and none in Remstein's series of 22 cases [1, 2, 3]. Complete surgical clearance can be potentially difficult as microscopic infiltration into subcutaneous tissue and skeletal muscle at the periphery of the tumor may not be apparent on pre-operative radiological imaging. Local recurrence is thus quite common (12-40%). Regional lymph node metastasis is uncommon and distant metastasis is (very) rare. Death of disease is exceptional (one reported case).

PFHT exhibis a plexiform growth pattern of small- to medium-sized sometimes whorling nodules. Three histologic variants/patterns are recognized; (1) histiocytoid, (2) fibroblastic and (3) mixed. A frequent finding is presence of (mainly osteoclast type) giant cells. The purely fibroblastic variant often lacks giant cells and often display peri-tumoral inflammation. Stromal hyalinization, focal myxoid change, metaplastic bone formation may uncommonly be encountered. Although cytologically quite bland, increased both cytologic atypia and mitotic activity have been described [4]. The immunophenotypic features of PFHT reveal a fibro-histiocytic phenotype, with the histiocytoid and multinucleated giant cells being variably positive for CD68, CD163 and CD11c and the fibroblastic cells positive for SMA. CD34 is generally negative. Thangaiah et al. [5] have presented evidence that the histiocytoid nodules contain a CD163/CD11c-negative population of "null-cells" which CSF-1 expression. PFHT is not known to have any recurrent molecular genetic abnormalities.

The differential diagnostic considerations depend on which component predominates. When the histiocytic and osteoclast-type giant cells predominate, especially when deep, despite a plexiform growth pattern, one could consider a giant cell tumor of soft parts or cellular neurothekeoma (vide infra). When the fibroblastic component predominates, one might consider fibromatosis, nodular fasciitis or lipofibromatosis. The rare fibroma-like variant of epithelioid sarcoma and possibly monophasic spindle cell synovial sarcoma also may need consideration. Benign mesenchymal neoplasms that can display a plexiform growth pattern include plexiform variants of neurofbroma, schwannoma and myofibroblastoma [6]. In cases with significant haemorrhage/extravasation of RBCs, Kaposi sarcoma becomes a consideration. Spindle cell melanoma (including desmoplastic melanoma), spindle cell carcinoma, follicular dendritic cell sarcoma and other spindle cell sarcomas generally display more pronounced cellular/nuclear atypia and higher mitotic activity than PFHT. The nodular arrangement of histiocytoid mononuclear cells with admixed giant cells may suggest the possibility of a granulomatous process. However, close inspection will reveal osteoclast-like rather than Langhans-type giant cells. Central necrosis is also not a feature of the histiocytic and giant cell-rich nodules of PFHT. In this case (close to the thyroid and with previous thyroid surgery), the extremely rare monophasic variant of spindle epithelial tumor with thymus-like differentiation of the thyroid is also conceivable but the majority of the reported cases are truly biphasic with a distinct epithelial component [7].

The relation between between PFHT and cellular neurothekeoma (CNT) is controversial. PFHT shows similar demographic and anatomic distributions as CNT. CNT and PFHT can show overlapping histologic features when both are predominantly composed of histiocytoid cells. As a result, some authors believe that these two entities might be closely related, or even identical [1,8]. MiTF may be a reliable marker for distinguishing CNT from PFHT as it is found to be strongly and diffusely expressed in CNT and not PFHT [9]. NKI-C3 and NSE are not reliable as these may also be expressed in PFHT.

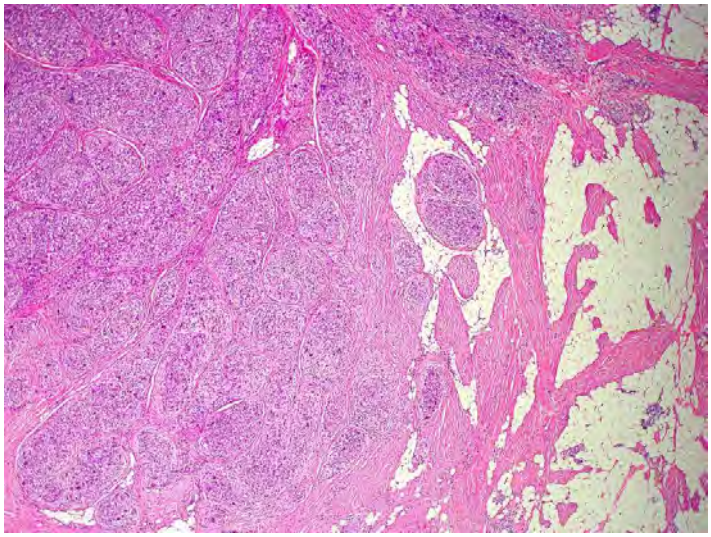

Plexiform, multinodular pattern.

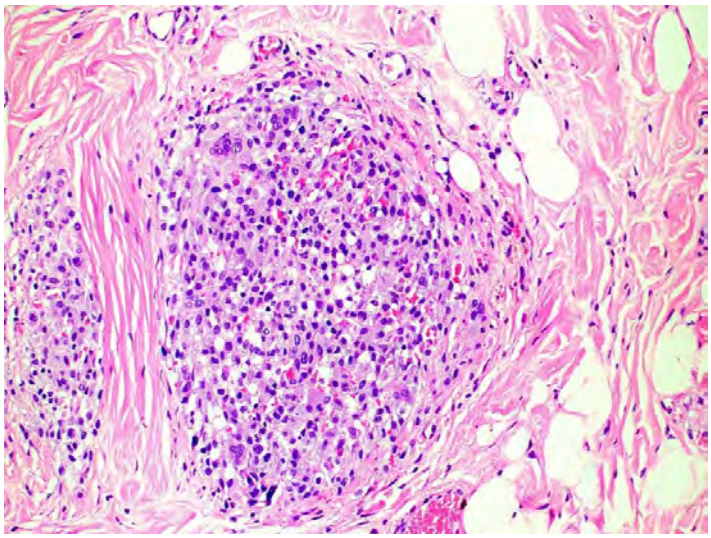

Nodule composed of mononuclear histiocytoid and osteoclast-type giant cells.

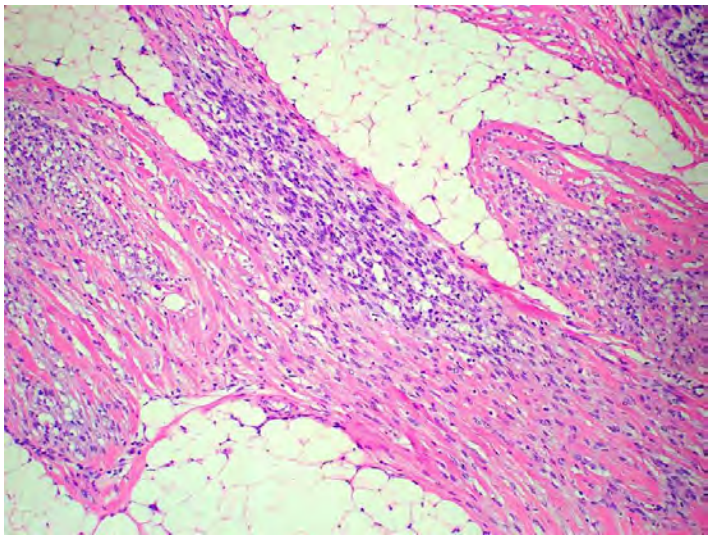

Fibromatosis-like spindle cell (fibroblastic) component.

References

1. Enzinger FM, Zhang RY. Plexiform fbrohistiocytic tumor presenting in children and young adults. An analysis of 65 cases. Am J Surg Pathol. 1988;12:818–26.
2. Hollowood K, Holley MP, Fletcher CD. Plexiform fbrohistiocytic tumour: clinicopathological, immunohistochemical and ultrastructural analysis in favour of a myofbroblastic lesion. Histopathology. 1991;19:503–13.
3. Remstein ED, Arndt CA, Nascimento AG. Plexiform fbrohistiocytic tumor: clinicopathologic analysis of 22 cases. Am J Surg Pathol. 1999;23:662–70.
4. Moosavi C, Jha P, Fanburg-Smith JC . An update on plexiform fibrohistiocytic tumor and addition of 66 new cases from the Armed Forces Institute of Pathology, in honor of Franz M. Enzinger, MD..Ann Diagn Pathol. 2007 Oct;11(5):313-19.
5. Thangaiah JJ, Dashti NK, Agaimy A, Fritchie K, Folpe AL. Plexiform fibrohistiocytic tumor: a clinicopathological and immunohistochemical study of 39 tumors, with evidence for a CSF1-producing "null cell" population. Virchows Arch. 2022 Nov;481(5):739-750.
6. Papke DJ Jr, Al-Ibraheemi A, Fletcher CDM. Plexiform Myofibroblastoma: Clinicopathologic Analysis of 36 Cases of a Distinctive Benign Tumor of Soft Tissue Affecting Mainly Children and Young Adults. Am J Surg Pathol. 2020 Nov;44(11):1469-78.
7. Tong GX, Hamele-Bena D, Wei XJ, O'Toole K. Fine-needle aspiration biopsy of monophasic variant of spindle epithelial tumor with thymus-like diferentiation of the thyroid: report of one case and review of the literature. Diagn Cytopathol. 2007;35(2):113–19.
8. Hornick JL, Fletcher CD. Cellular neurothekeoma: detailed characterization in a series of 133 cases. Am J Surg Pathol. 2007;31:329–40.
9. Fox MD, Billings SD, Gleason BC, Moore J, Thomas AB, Shea CR, et al. Expression of MiTF may be helpful in diferentiating cellular neurothekeoma from plexiform fbrohistiocytic tumor (histiocytoid predominant) in a partial biopsy specimen. Am J Dermatopathol. 2012;34(2):157–60.

12TH INTERNATIONAL AMR PATHOLOGY SLIDE SEMINAR SYMPOSIUM IN ANATOMIC PATHOLOGY

Case – 56

Urologic and miscellaneous pathology

Contributed by: ***Reza Alaghehbandan***

Clinical History

A 49-year-old woman with a 2.2 cm left renal mass.

Pathological Findings

Sectioning of the left partial nephrectomy reveals a 2.2 x 2.1 x 1.6 cm well-circumscribed, tanyellow friable soft mass with small cystic areas abutting the capsular surface. Histologically, the tumor is unencapsulated and shows predominantly solid and focal cystic architecture. The neoplastic cells are polygonal and have voluminous eosinophilic cytoplasm with basophilic cytoplasmic stippling. Immunohistochemically, the tumor is positive for CK20 (strong/diffuse), Cytokeratin CAM 5.2 (patchy), Cathepsin-K (patchy), while being negative for CA-IX. Fumarate hydratase was retained.

Diagnosis

Eosinophilic solid and cystic renal cell carcinoma (ESC RCC).

Comments

Follow-up: the patient is alive with no local recurrence or metastatic disease.

ESC RCC is a recently described renal entity that was included as a novel entity in the WHO 2022 classification, under the category “other renal tumours”. ESC RCC is found mostly as a sporadic and solitary tumour in patients of broad age range, with marked female predilection. Rare cases have also been identified in patients with tuberous sclerosis complex (TSC). Great majority of ESC RCCs had indolent behavior, but rare tumours with metastases have also been reported, typically of larger size, and showing necrosis and hemorrhage

ESC RCC exhibits grossly identifiable solid and cystic components in great majority of cases; only rare cases had almost exclusive solid growth with rare microcysts. The solid areas are composed of eosinophilic cells exhibiting diffuse, compact acinar or tight nested growth, and voluminous cytoplasm; other growth patterns may also be focally seen. The cells lining the cysts typically show hobnailing. A characteristic feature is the presence of coarse basophilic to purple, coarse cytoplasmic granules (stippling). Scattered foamy histiocytes and lymphocytes are also common.

Immunohistochemically, ESC RCC shows either diffuse or focal CK20 expression, but rare cases may be CK20 negative; CK7 is typically negative. At least focal cathepsin K expression has been reported in most cases Other positive stains include PAX8, AE1/AE3, and vimentin. ESC RCC is consistently negative for CD117 and CAIX. ESC RCCs have been found to demonstrate biallelic loss in TSC2 or TSC1, resulting in activation of the mTOR complex 1.

References

1. Trpkov K, et al. Novel, emerging and provisional renal entities: The Genitourinary Pathology Society (GUPS) update on renal neoplasia. Mod Pathol. 2021 Jun;34(6):1167-1184.
2. Siadat F, Trpkov K. ESC, ALK, HOT and LOT: Three Letter Acronyms of Emerging Renal Entities Knocking on the Door of the WHO Classification. Cancers (Basel). 2020 Jan 9;12(1):168.
3. Palsgrove DN, et al. Eosinophilic Solid and Cystic (ESC) Renal Cell Carcinomas Harbor TSC Mutations: Molecular Analysis Supports an Expanding Clinicopathologic Spectrum. Am J Surg Pathol. 2018 Sep;42(9):1166-1181.
4. Mehra R, et al. Somatic Bi-allelic Loss of TSC Genes in Eosinophilic Solid and Cystic Renal Cell Carcinoma. Eur Urol. 2018 Oct;74(4):483-486.
5. Trpkov K, et al. Eosinophilic Solid and Cystic Renal Cell Carcinoma (ESC RCC): Further Morphologic and Molecular Characterization of ESC RCC as a Distinct Entity. Am J Surg Pathol. 2017 Oct;41(10):1299-1308.
6. Trpkov K, et al. Eosinophilic, Solid, and Cystic Renal Cell Carcinoma: Clinicopathologic Study of 16 Unique, Sporadic Neoplasms Occurring in Women. Am J Surg Pathol. 2016 Jan;40(1):60- 71.

12TH INTERNATIONAL AMR PATHOLOGY SLIDE SEMINAR SYMPOSIUM IN ANATOMIC PATHOLOGY

Case – 57

Urologic and miscellaneous pathology

Contributed by: Delia Perez-Montiel

Clinical History

A 69-year-old Mexican male, smoker for 50 years, one pack a day, complaints of pelvic pain and dysuria for 6 months. TAC with bladder mass and unilateral hydronephrosis.

Pathological Findings

A TUR of a 4 cm bladder tumor located in right wall was performed, (patient did not accept radical cystectomy), we received many chips, brown, soft with white areas.

Microscopically the neoplasia shows an endophytic pattern with nests and trabecular pattern lined by polygonal cells with clear cytoplasm and large irregular nuclei with apparent nucleoli in transition with microcystic areas lined by one line of cuboidal to flat cells with small nuclei. The neoplastic cells infiltrated the muscularis propiae. Other areas showed more classic areas of urothelial carcinoma.

Neoplastic cells show same expression in trabecular and microcystic areas. GATA3, P63, CK7, CK20 and Uroplakin were positive. PAX8, NKX3.1, S100, chromogranin and synaptophysin were negative.

Diagnosis

Urothelial carcinoma with microcystic and nested pattern.

Comments

The plasticity of the urothelial carcinoma is a well-recognized phenomenon, many histological variants have been described, some of them with prognostic value and others are important to pathologists because of the difficulties in differential diagnosis.

The microcystic variant is a rare morphology in the bladder, was described by Young and Zukerberg in 1991, and since then a few series have been described. The largest an recent is the one of Lopez-Beltran et al series where they show 20 cases, all cases were at least pTNM T2; twelve were associated to conventional high grade component and lymph node metastases were present in at least 30% of the cases. No differences were seen with conventional carcinoma in the same TNM stage, but, microcystic variant is associated to higher stage at diagnosis.

Many cases were associated with other variants like plasmacytoid, lymphoepithelioma like or nested.

Because of bland cytology, the differential diagnosis include, mainly in small biopsies, benign lesions as cystitis cystica glandularis, nephrogenic adenoma, and Gleason 3+3 prostatic adenocarcinoma.

By immunostains microcystic carcinomas are positive to MUC5AC, CK7, MUC1, CK30, P63 and GATA3, however, same immunostains were positive in cystitis glandularis, the difference between

both entities is lower Ki67 labelling index, low P53 expression and up regulation of p27 in the later in comparison to microcystic carcinomas.

References

1. Lobo N, Shariat SF, Guo CC, Fernandez MI, Kassouf W, Choudhury A, Gao J, Williams SB, Galsky MD, Taylor JA 3rd, Roupret M, Kamat AM. What Is the Significance of Variant Histology in Urothelial Carcinoma? Eur Urol Focus. 2020 Jul 15;6(4):653-663. doi: 10.1016/j.euf.2019.09.003. Epub 2019 Sep 15.PMID: 31530497 Review.
2. Lopez-Beltran A, Henriques V, Montironi R, Cimadamore A, Raspollini MR, Cheng L. Variants and new entities of bladder cancer. Histopathology. 2019 Jan;74(1):77-96. doi: 10.1111/his.13752.PMID: 30565299 Review.
3. Lopez Beltran A, Montironi R, Cheng L. Microcystic urothelial carcinoma: morphology, immunohistochemistry and clinical behaviour. Histopathology. 2014 May;64(6):872-9. doi: 10.1111/his.12345. Epub 2014 Feb
4. Mai KT, Hakim SW, Ball CG, Flood TA, Belanger EC. Nested and microcystic variants of urothelial carcinoma displaying immunohistochemical features of basallike urothelial cells: an immunohistochemical and histopathogenetic study. Pathol Int. 2014 Aug;64(8):375-81. doi: 10.1111/pin.12187.PMID: 25143125

12TH INTERNATIONAL AMR PATHOLOGY SLIDE SEMINAR SYMPOSIUM IN ANATOMIC PATHOLOGY

Case – 58

Urologic and miscellaneous pathology

Contributed by: ***Reza Alaghehbandan***

Clinical History

A 59 year-old woman with a 1.8 cm right renal mass.

Pathological Findings

Sectioning of the right partial nephrectomy reveals a 1.8 x 1.6 x 1.3 cm well-circumscribed, tangrey solid mass with no areas of hemorrhage or necrosis. Histologically, the tumor is unencapsulated and shows a predominantly nested growth pattern. The neoplastic cells have eosinophilic cytoplasm and exhibit marked intracytoplasmic vacuoles. The nuclei are enlarged and pleomorphic with prominent nucleoli. There are also thick-walled vessels present in the tumor and also at the periphery. Immunohistochemically, the tumor is patchy positive for CD117, Cytokeratin CAM 5.2 and Cathepsin-K (patchy), while being negative for CK20, and vimentin. CK7 is reactive only in rare cells.

Diagnosis

Eosinophilic vacuolated tumour (EVT).

Comments

Follow-up: the patient is alive with no local recurrence or metastatic disease.

Eosinophilic vacuolated tumour (EVT) is a recently described entity that has been included as an emerging renal entity in the WHO 2022 classification. More than 50 EVTs have been documented to date and all reported cases were benign, without evidence of recurrence or metastases.

EVT is typically solitary and sporadic tumour, about 3-4 cm in size. It has been rarely found in patients with TSC. EVT is a solid tumour that lacks a distinct cystic component and a wellformed capsule. Thick-walled vessels are almost always present at the periphery. The cells have an eosinophilic cytoplasm and exhibit marked intracytoplasmic vacuoles. The nuclei are round to oval, with prominent nucleoli that focally can be quite large. EVT is typically positive for CD117, CD10, and Cathepsin-K (in some cases focally). CK7 is reactive only in rare, scattered cells.

Complete losses or gains of multiple chromosomes have not been found, although isolated losses of chromosomes 1 and 19p have been reported. TSC/MTOR mutations leading to mTORC1 activation have consistently been documented in EVT. A recent study also highlighted the existence of non-overlapping mutations in MTOR, TSC2, and TSC1 in all evaluated cases, associated with low mutational rates.

References

1. Trpkov, K., et al. Novel, emerging and provisional renal entities: The Genitourinary Pathology Society (GUPS) update on renal neoplasia. Mod Pathol. 2021; 34, 1167–1184.
2. Chen YB, et al. Somatic Mutations of TSC2 or MTOR Characterize a Morphologically Distinct Subset of Sporadic Renal Cell Carcinoma with Eosinophilic and Vacuolated Cytoplasm. Am J Surg Pathol. 2019 Jan;43(1):121-131.
3. He H, et al. "High-grade oncocytic renal tumor": morphologic, immunohistochemical, and molecular genetic study of 14 cases. Virchows Arch. 2018 Dec;473(6):725-738.
4. Gupta S, et al. Renal Neoplasia in Tuberous Sclerosis: A Study of 41 Patients. Mayo Clin Proc. 2021 Jun;96(6):1470-1489.

12TH INTERNATIONAL AMR PATHOLOGY SLIDE SEMINAR SYMPOSIUM IN ANATOMIC PATHOLOGY

Case – 59

Urologic and miscellaneous pathology

Contributed by: Delia Perez-Montiel

Clinical History

A 43-year-old female with urinary bleeding and loss of weight. CA19-9 and CA125 markers were negative.

Pathological Findings

A nephrectomy specimen shows a heterogenous tumor, with brown papillary areas in the renal pelvis with transition to white-yellow solid areas in the renal parenchyma. The tumor size was 12 cm.

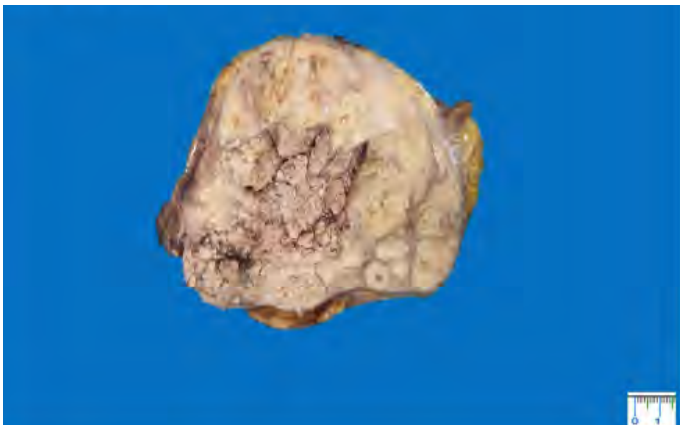

Microscopically the neoplasia shows a well differentiated urothelial high grade carcinoma with papillae in the renal pelvis in transition to solid areas with nest of polygonal cells, pseudo-alveolar areas with polygonal cells with rhabdoid features and areas with pleomorphic fusocellular cells.

Neoplastic cells showed different expression in well differentiated areas vs dedifferentiated areas. Urothelial area was positive for GATA3, P63, CK7, CD10 and Uroplakin, negative to PDL1. Rhabdoid, solid and fusiform areas were positive to PDL1, P63, CK7 and CD10, negative to GATA3 and Uroplaklin. Both components were negative to PAX8, CK20.

Diagnosis

Dedifferentiated urothelial carcinoma with rhabdoid and sarcomatoid features.

Comments

Rhabdoid and sarcomatoid morphological features have been described as a dedifferentiated changes not only in urothelial carcinomas but in other carcinomas as renal, endometrial, lung, pancreas etc. These changes represent part of the heterogeneous neoplastic spectrum of the well know highly variable histology of the urothelial carcinomas, and, together with

pleomorphic giant cell and undifferentiated are defined as poorly differentiated carcinomas, according to WHO classification.

Dedifferentiated phenomenon is more frequent in women, with an aggressive clinical behavior in which 2/3 of the patients have progression of disease and an average survival of 15 months.

The main differential diagnosis includes RCC with rhabdoid and sarcomatoid features in which, the sampling of the tumor is more important than immunostains.

Immunostains in dedifferentiated areas, as in our case, lose expression for GATA3 and Uroplakin, aberrant expression to CD10, sometimes with expression only to keratins. The same happens with RCC in which the expression for immunostains is lost or aberrant, because of that, thew sampling of the tumor looking for better differentiated areas is the most useful tool for the diagnosis. Other differential diagnoses include metastasis, direct infiltration or, in bladder, reactive stromal changes.

References

1. Agaimy A, Hartmann A, Trpkov K, Hes O. Undifferentiated and dedifferentiated urological carcinomas: lessons learned from the recent developments. Semin Diagn Pathol. 2021 Nov;38(6):152-162. doi: 10.1053/j.semdp.2021.09.004. Epub 2021 Sep 20.PMID: 34579992 Review.
2. Kuroda N, Naroda T, Tamura M, Perez-Montiel D, Michal M, Hes O High grade urothelial carcinoma, plasmacytoid variant, of the renal pelvis with osteoclast-like giant cells and focal rhabdoid features. Pol J Pathol. 2014 Oct;65(3):237- 40. doi: 10.5114/pjp.2014.45788.
3. WHO Classification of Tumors Editorial Board. Urinary and male genital tumours.Lyon (France): International Agency for Research on Cancer; 2022. (WHO Classification of tumours series, 5th ed.;vol.8) https://publications.iarc.fr/610.

12TH INTERNATIONAL AMR PATHOLOGY SLIDE SEMINAR SYMPOSIUM IN ANATOMIC PATHOLOGY

Case – 60

Urologic and miscellaneous pathology

Contributed by: Thomas Mentzel

Clinical History

A 71-year-old female patient developed an indurated lesion at the right hand. After a marginal excision a complete excision with tumour free margins had been performed and there is no sign of recurrence at 10 months.

Pathological Findings

The cellular lesion is composed of enlarged tumour cells with a clear cytoplasm and enlarged hyperchromatic or vesicular nuclei showing some variation in size and shape. Numerous multinucleated giant cells (so-called wreath-like giant cells) are present. Few tumour cells contain melanin pigment. The neoplastic cells are separated by hypocellular fibrous bands and septa of variable thickness. The proliferative activity of tumour cells is not increased and no tumour necrosis is seen. Immunohistochemically, neoplastic cells stained positively for S-100 protein and Sox10, and focally for Melan-A. A *CRTC1-TRIM11* fusion was detected by RT-PCR, whereas no *EWS* or *ATF1* fusion was present.

Diagnosis

Cutaneous melanocytoma with *CRTC1-TRIM11* fusion.

Comments

Cutaneous melanocytoma with *CRTC1-TRIM11* fusion represents a rare and recently described entity in the spectrum of dermal tumours with expression of melanocytic markers including cellular blue naevus, metastasis of melanoma, rare primary dermal melanoma, paraganglioma-like dermal melanocytic tumour, and rare cutaneous clear cell sarcoma. Cutaneous melanocytoma with *CRTC1-TRIM11* fusion may arise in children and adults and show a wide variety of anatomic location. Although follow-up informations are limited, it seems that these neoplasms represent low-grade neoplasms, and local recurrences and lymph node metastases have been reported but are rare. Cellular blue naevus is characterized by a biphasic growth pattern, and tumour cells are diffusely positive for HMB45 and Melan-A, whereas S-100 protein can be absent. The presence of intersecting nests and bundles of tumour cells and the uniformity of the cytology in cutaneous melanocytoma with *CRTC1-TRIM11* fusion are distinguishing features from metastatic and primary dermal melanoma. Paraganglioma-like dermal melanocytic tumours are nodular lesions characterized by a prominent nested growth pattern but there is probably some overlap. Clear cell sarcoma that occurs only rarely in the dermis represents the entity morphologically closest to cutaneous melanocytoma with *CRTC1-TRIM11* fusion, and it seems that molecular confirmation is needed in establishing the correct diagnosis, what is important given the prognostic difference.

References

1. Cellier L, Perron E, Pissaloux D et al. Cutaneous melanocytoma with *CRTC1-TRIM11* fusion. Report of 5 cases resembling clear cell sarcoma. Am J Surg Pathol 2018; 42: 382-391
2. Deyrup AT, Althof P, Zhou M et al. Paragangloma-like dermal melanocytic tumor: a unique entity distinct from cellular blue nevus, clear cell sarcoma, and cutaneous melanoma. Am J Surg Pathol 2004; 28: 1579-1586
3. Hanna J, Ko JS, Billings SD et al. Cutaneous melanocytic tumor with *CRTC1::TRIM11* translocation. An emerging entity analyzed in a series of 41 cases. Am J Surg Pathol 2022; 46: 1457-1466
4. Ko JS, Billings SD, Pissaloux D et al. *CRTC1-TRIM11* fusion defined melanoctic tumors: a series of four cases. J Cutan Pathol 2019; 46: 810-818
5. Vest BE, Harview CL, Liu V et al. Cutaneous melanocytic tumor with *CRTC1::TRIM11* fusion and prominent epidermal involvement: A case report. J Cutan Pathol 2022; 49: 1025-1030

12TH INTERNATIONAL AMR PATHOLOGY SLIDE SEMINAR SYMPOSIUM IN ANATOMIC PATHOLOGY

Case – 61

Urologic and miscellaneous pathology

Contributed by: Tiziana Salviato

Clinical History

A 44-year-old immunocompromised man performs a colonoscopy for suspected CMV colitis and a gastro-duodenoscopy because of severe pancytopenia. At gastro-duodenoscopy, the stomach appears distensible and the mucosa diffusely hyperemic, while starting from the duodenal bulb up to the third duodenal portion numerous, reddish-colored papules are seen, ranging in size from 2 to 10 mm. At colonoscopy all the tracts were in the normal range.

Pathological Findings

Duodenal lesion consists in spindle cell proliferations forming irregular vascular channels or slits in the submucosal layer, spreading also in the lamina propria. It is associated with red blood cell extravasation and hemosiderin-laden macrophage deposits which gives it a characteristic red to dark, bruise-like appearance. Additionally, significant lymphoplasmacytic infiltration occurs. Neoplastic cells are HHV8 positive, CD31 and CD34 positive, S100 negative HMB45 negative.

Diagnosis

Duodenal Kaposi's sarcoma.

Comments

Despite our decades of experience with KS, its true nature remains elusive. This angioproliferative low grade disease of the vascular endothelium has a propensity to involve visceral organs in the immunocompromised population.

Kaposi's sarcoma (KS) of the gastrointestinal tract is not an uncommon disease among individuals with acquired immunodeficiency syndrome (AIDS). The majority is asymptomatic, and for this reason, gastrointestinal KS (GI-KS) remains undiagnosed. KS is classified into four clinical variants which have coevolved in certain human populations: classic KS, endemic (or African) KS, Iatrogenic (or immuno suppression related) KS, and epidemic (or AIDS related) KS.

The presence of spindle shaped cells can exclude many benign and malignant lesions:

- GIST
- Spindle cell melanoma
- Angiosarcoma

To make a diagnosis of KS, the presence of HHV8 is necessary and immunohistochemical testing is recommended for all specimens with spindle cell morphology. Other biomarkers that are expressed include CD34 and CD117 (or c-KIT), which overlap with other stromal tumors making it a less reliable marker for KS diagnosis.

Similar to Gastrointestinal KS, gastrointestinal stromal tumors also express CD34 and CD117, but it is distinguished by the absence of HHV8, and positive DOG 1 expression. Furthermore, spindle cell melanomas also share similar endoscopic and histologic features with GI-KS, but these tumors typically lack the CD34 marker and express S100 immunopositivity. Although a rare entity, physicians should be aware of this condition that is far more common than originally thought, in order to facilitate a prompt diagnosis and necessary intervention.

References

1. Kaposi's sarcoma of the gastrointestinal tract: report of two cases and review of the literature. Kahl P, Buettner R, Friedrichs N, Merkelbach-Bruse S, Wenzel J, Carl Heukamp L.Pathol Res Pract. 2007;203(4):227-31. doi: 10.1016/j.prp.2007.01.007. Epub 2007 Mar 26.PMID: 17379429
2. Gastrointestinal Kaposi Sarcoma Involving Stomach and Colon: Diagnostic Pitfall for Pathologists with Expression of CD117. Bozdag Z, Toprak S, Karadag N, Akbulut S.J Gastrointest Cancer. 2022 Jan 21. doi: 10.1007/s12029-021-00785-w. Online ahead of print.PMID: 35060100
3. Gastric Kaposi sarcoma presenting as an upper gastrointestinal bleeding in a non-AIDS patient. Zanganeh E, Hosseini SA, Alimadadi M, Seyyedmajidi M.Caspian J Intern Med. 2021;12(Suppl 2):S413-S416. doi: 10.22088/cjim.12.0.413.PMID: 34760095
4. Gastrointestinal Kaposi's sarcoma: Case report and review of the literature. Lee AJ, Brenner L, Mourad B, Monteiro C, Vega KJ, Munoz JC.World J Gastrointest Pharmacol Ther. 2015 Aug 6;6(3):89-95. doi: 10.4292/wjgpt.v6.i3.89.PMID: 26261737

12TH INTERNATIONAL AMR PATHOLOGY SLIDE SEMINAR SYMPOSIUM IN ANATOMIC PATHOLOGY

Case – 62

Urologic and miscellaneous pathology

Contributed by: Barbara Gazic

Clinical History

A 52-year-old female presented with uterine tumor. The myomectomy specimen was submitted for histology with a clinical diagnosis of uterine myoma. Malignant nature of the tumor was ascertained from the biopsy therefore hysterectomy with bilateral adnexectomy and resection of two additional tumor deposits from Douglas' space were performed.

Pathological Findings

The tumor measured 3 x 2.5 cm. It was nodular, well circumscribed. On a cut surface the tumor had pink-tan-white whorled appearance without tumor necrosis. The whole uterine cervix was infiltrated while corpus, fundus and adnexa were not macroscopically changed. Histologically the tumor was composed of spindle cells. In some areas the cells were bland with rare mitotic figures while other areas were hypercellular with interlacing fascicles and brisk mitotic activity. The tumor cells were strongly and diffusely positive for CD34, focally and weakly positive for CD10, and negative for SMA, h-Caldesmon, Desmin, Myogenin, MyoD1, s-100, Melanoma Cocktail, CKAE1/AE3, CK8/18, STAT6, CD117, DOG1 and pan-TRK. According to morphology and immunohistochemistry the tumor was diagnosed as undifferentiated sarcoma. Since there was visible gross disease in the right parametrium, adjuvant radiotherapy was indicated.

Two years later, a follow up contrast-enhanced MRI revealed several pelvic peritoneal metastases which were removed surgically. Metastatic deposits morphologically and immunohistochemically corresponded to the neoplasm in the primary biopsy but after considering the possibility of fusion sarcoma, FISH for COL1A-PDGFB fusion was also performed which was positive, reclassifying the tumor as dermatofibrosarcoma-like COL1A1-PDGFB fusion fibrosarcoma of uterine cervix.

Diagnosis

Dermatofibrosarcoma-like COL1A-PDGFB fusion fibrosarcoma of uterine cervix.

Comments

Uterine sarcomas comprise about 3-7% of uterine malignancies. After immunohistochemical exclusion of more common subtypes which include leiomyosarcoma, adenosarcoma and endometrial stromal sarcoma, an unclassified spindle cell sarcoma of uterine corpus, cervix or vagina with morphology resembling fibrosarcoma could represent an NTRKrearranged sarcoma or COL1A-PDGFB fusion sarcoma. All NTRK-rearranged uterine sarcomas reported so far displayed diffuse or focal positivity for CD34 and S100, and diffuse positivity for panTRK while all four previously reported COL1A-PDGFB fusion uterine sarcomas were diffusely positive for CD34 and negative for S-100 and pan-TRK. It is important to recognize both entities since effective treatment with targeted therapies

has become available. TRK inhibitors may be used for the therapy of NTRK-rearranged sarcoma, and Imatinib for COL1A-PDGFB fusion sarcoma.

References

1. Grindstaff SL, Di Silvestro J and Quddus MR. COL1A-PDGFB fusion uterine fibrosarcoma: A case report with treatment implication. Gynecol Oncol Rep. 2019:31:100523.
2. Croce S, Hostein I, Longacre TA, et al. Uterine and vaginal sarcomas resembling fibrosarcoma: a clinicopathological and molecular analysis of 13 cases showing common NTRK-rearrangements and the description of a COL1A1-PDGFB fusion novel to uterine neoplasms. Modern Pathology. 2019:1008-1022.
3. Gatalica Z, Xiu J, Swensen J, Vranic S. Molecular characterization of cancers with NTRK gene fusions. Modern Pathology. Published online 2018.
4. Libertini M, Hallin M, Thway K, et al. Gynecological Sarcomas: Molecular characteristics, Behavior, and Histology-driven therapy. Int J Surg Pathol. 2021:4-20.

12TH INTERNATIONAL AMR PATHOLOGY SLIDE SEMINAR SYMPOSIUM IN ANATOMIC PATHOLOGY

Case – 63

Urologic and miscellaneous pathology

Contributed by: Thomas Mentzel

Clinical History

An 87-year-old male patient complained about a fast-growing superficial tumour arising at the right elbow. After a biopsy a marginal excision had been performed and a 3.5 x 3.0 x 2.5 cm measuring lesion was described.

Pathological Findings

Histologically, sun-damaged skin with a dermosubcutaenous nodular lesion is noted. The lesion is composed of bland spindled, fibroblastic cells, numerous vessels and numerous inflammatory cells set in a collagenous stroma with cleft-like spaces. Scattered plasma cells are present. PCR-technique revealed the presence of Borrelia-DNA.

Diagnosis

Borrelia associated fibroid nodule.

Comments

Acrodermatitis chronica atrophicans (ACA) represents a chronic or late manifestation of infection by Borrelia burgdorferi and Borrelia afzeli is the predominant organism. Juxta-articular fibrous or fibroid nodules may develop in 10-25% of cases of ACA and regress under antibiotic treatment. The elbows and more rarely the back of hands are preferred anatomic locations. The downregulation of major histocompatibility complex class II molecules on epidermal Langerhans cells indicates a poorly effective immune response and may explain faulty elimination of the organisms from the skin and the immunologically induced tumour-like fibrosis. Other non-neoplastic mimickers of benign and malignant mesenchymal neoplasms include bacillary angiomatosis, tumour-stage of erythema elevatum et diutinum, biker´s nodule, amyloid tumour, extranodal Rosai-Dorfman disease, Lichen myxedematosus, and iatrogenic rhabdoid pseudotumor.

References

1. Lübbe J, Schlüpen EM, Fierz W, Panizzon RG, Burg G. Identification of Borrelia afzelii in jucta-articular nodule from a huma immunodeficiency virus-positive patient with acrodermatitis chronica atrophicans. Arch Dermatol 1995; 131: 1341-1342
2. Marsch WC, Mayet A, Wolter M. Cutaneous fibroses induced by Borrelia burgdorferi. Br J Dermatol 1993; 128: 674-678
3. Marsch WC, Wolter M, Mayet A. Juxta-articular fibrotic nodules in Borrelia infection – ultrastructural details of therapy induced regression. Clin Exp Dermatol 1994; 19: 394-398

4. Picken RN, Strle F, Picken MM et al. Identification of three species of borrelia burgdorferi sensu lato (B. burgdorferi sensu stricto, B. garinii, and B. afzelii) among isolates from acrodermatitis chronica atrophicans lesions. J Invest Dermatol 1998; 110: 211-214
5. Ko JS, Billings SD, Pissaloux D et al. *CRTC1-TRIM11* fusion defined melanoctic tumors: a series of four cases. J Cutan Pathol 2019; 46: 810-818
6. Vest BE, Harview CL, Liu V et al. Cutaneous melanocytic tumor with *CRTC1::TRIM11* fusion and prominent epidermal involvement: A case report. J Cutan Pathol 2022; 49: 1025-1030

12TH INTERNATIONAL AMR PATHOLOGY SLIDE SEMINAR SYMPOSIUM IN ANATOMIC PATHOLOGY

Case – 64

Urologic and miscellaneous pathology

Contributed by: Barbara Gazic

Clinical History

A 49-year-old female presented with abdominal discomfort which had been going on for more than two months. An abdominal computed tomography was performed which demonstrated a 3x2cm hypo-dense solid mass in lobus caudatus of the liver. The lesion was hypo-vascular and had an ill-defined border according to radiologist most probably hepatocellular carcinoma. Fine needle aspiration biopsy of the lesion was performed and diagnosed as metastasis of malignant melanoma. Because PET CT didn't show any other lesions, hepatic lesion was excised and sent for histology to our pathology department.

Pathological Findings

The lesion measured 3 cm in the largest diameter and was quite sharply demarcated from liver parenchyma. Histologically the neoplastic proliferation was composed of spindle and polygonal cells with clear to eosinophilic cytoplasm arranged in haphazard pattern and some trabeculae forming around small vascular spaces. Some cells were more pleomorphic and had prominent eosinophilic nucleoli. The tumor cells were strongly and diffusely positive for Melan-A, HMB45, Melanoma and SMA while S-100, CK8/18, CD34, DOG1 and CD117 were negative.

Diagnosis

Liver PEC-oma.

Comments

Hepatic PEC-omas are very rare and are markedly more frequent in females than males with a peak in young to middle-aged adults. Histological diagnosis of liver PEC-oma might be challenging because of pleomorphism and heterogeneity of the histological features as well as because of the rarity of the lesion in the liver. Several histological characteristics in a liver PEC-oma might be mistaken for features of HCC: polygonal cells in trabecular arrangement, peliosis, nuclear pleomorphism, prominent eosinophilic nucleoli and eosinophilic globules or for metastatic melanoma according to immunohistochemical findings.

References

1. Hyun-Jin Son et al. Hepatic perivascular epithelioid cell tumor (PEComa): a case report with a review of literatures. Clin Mol Hepatol. 2017 Mar; 23(1): 80–86.
2. Khaja F et al. PEComa: A Perivascular Epithelioid Cell Tumor in the Liver—A Case Report and Review of the Literature. Case reports in medicine 2013.

3. Mann SA, Saxena R. Differential diagnosis of epithelioid and clear cell tumors in the liver. Semin Diagn Pathol. 2017:183–91. 4. Bonetti, F, Pea M, Martignoni G, Zamboni G. PEC and sugar. Am. J. Surg. Pathol. 1992: 307–308.

12TH INTERNATIONAL AMR PATHOLOGY SLIDE SEMINAR SYMPOSIUM IN ANATOMIC PATHOLOGY

Case – 65

Urologic and miscellaneous pathology

Contributed by: Anamarija Morovic Perry

Clinical History

A 50-year-old male, with no significant past medical history, presented with left tonsil lesion.

Pathological Findings

Sections show ulcerated tonsillar tissue expanded by a polymorphic inflammatory infiltrate comprised of numerous plasma cells, mature appearing small lymphocytes, plasmacytoid lymphocytes, occasional eosinophils, neutrophils and histiocytes. Neutrophil clusters and focal granulation tissue is seen. Also, focal areas showing vasculitis are also present.

Spirochete immunohistochemical stain shows numerous organisms. Other performed immunohistochemical stains to rule out other entities: CD20, CD3, CD5, CD10, BCL6, CD23, CD30, CD56, IgG, IgG4, CD163, ALK, MPO. Kappa and lambda ISH – polyclonal plasma cells EBER-ISH – negative for EBV.

Diagnosis

Tonsil involved by syphilis.

Comments

Syphilis is a venereal disease caused by the spirochete Treponema pallidum, first clinically recognized back in 15th century, with discovery of T. pallidum as a causative agent at the beginning of the 20th century. Today, the incidence of primary and secondary syphilis is on the rise, with 80% increase in reported cases in the United States from 2014 to 2018. Syphilis can be a challenging disease to diagnose for clinicians and is sometimes referred to as “The Great Mimicker”, since the symptoms and clinical findings in syphilis overlap with many conditions.

Clinically, syphilis has three stages, as well as latent stages which can occur between primary and secondary as well as after the resolution of the secondary stage. Syphilis is sexually transmissible in primary and secondary stages. The primary stage is characterized by indurative and ulcerative syphilitic chancre, occurring at the site of contact with partner’s infectious lesion – most commonly genital area, rectum or oral cavity. Secondary syphilis is characterized by nonpruritic rash (characteristically on palms and soles), mucosal lesions (condyloma latum), fever, lymphadenopathy, as well as occasionally alopecia, periostitis, hepatitis, and nephritis. Tertiary syphilis occurs in approximately 30% of infected patients, 2-50 years after initial infection and can manifest as central nervous system disease (e.g. meningovascular disease, tabes dorsalis, etc.), gummas (tumorous lesions), cardiovascular syphilis, and ocular or otic syphilis.

With the increasing number of cases in the community, pathologists are also starting to see more syphilitic lesions (from all clinical stages of disease) under the microscope, which sometimes

pose a great diagnostic challenge. Lesions of syphilis can be seen in virtually any organ and can histologically overlap with other conditions. Therefore, pathologists should stay alert and think about syphilis in differential diagnosis. Diagnosis of syphilis in lymphoid tissue can be particularly challenging, as illustrated in this case. Occasionally, pathologists will encounter syphilitic lymphadenitis, that can be seen in all stages of disease. The most commonly observed histologic changes in lymph nodes involved by syphilis include follicular and paracortical hyperplasia, interfollicular plasmacytosis, capsular thickening with plasma cell infiltration, as well as obliterative vasculitis. Some cases can show collections of epithelioid histiocytes or well-formed granulomas, and stromal and vascular hyperplasia. In tertiary stage of syphilis, lymph node can show gummatous lymphadenitis, characterized by prominent necrosis surrounded by epithelioid histiocytes and multinucleated giant cells. In the affected lymph nodes, spirochetes can be demonstrated using Warthin-Starry staining, immunofluorescence, as well as by immunohistochemical stain which is the preferred method.

Differential diagnosis of syphilitic lymphadenitis includes other causative agents of necrotizing and non-necrotizing granulomatous inflammation (e.g. sarcoidosis, mycobacterial infections, etc.). Differential diagnosis in the current case (which was very challenging in my opinion) included entities such as inflammatory pseudotumor, IgGrelated disease, as well as other infectious etiologies. Morphologic appearance, however, did not fit well with any particular entity and clinical history was strongly suggestive of neoplasm.

References

1. Ghanem KG, Ram S, Rice PA. The modern epidemic of syphilis. NEJM. 2020;382(9):845-854. 2.
2. O'Malley DP, George TI, Orazi A, Abbondanzo SL, editors. Benign and reactive conditions of lymph node and spleen - Atlas of nontumor pathology. Washington DC, The American Registry of Pathology, 2009.

12TH INTERNATIONAL AMR PATHOLOGY SLIDE SEMINAR SYMPOSIUM IN ANATOMIC PATHOLOGY

Case – 66

Urologic and miscellaneous pathology

Contributed by: Anamarija Morovic Perry

Clinical History

A 75-year-old male, with no significant past medical history, presented with an acute abdomen and was found to have a small bowel perforation.

Pathological Findings

Resected 20 x 3 cm looped segment of small bowel is tethered by adhesions where a 3.5 x 2 cm transmural defect is noted with associated hemorrhage and fibrinous exudate.

Sections show bowel mucosa (terminal ileum) with an atypical lymphoid infiltrate that diffuselly involves entire bowel thickness. Infiltrate is composed of small to intermediate sized cells with irregular nuclear contours, inconspicuous nucleoli and moderately abundant cytoplasm. Adjacent bowel mucosa shows villous blunting with numerous intraepithelial lymphocytes.

Immunohistochemical stains:

- Positive: CD3, CD2, CD7, CD8, CD56, TIA-1, TCR delta.
- Negative: CD4, CD5, TCR alpha beta, CD30, ALK

EBER-ISH negative.

Diagnosis

Monomorphic epitheliotropic intestinal T-cell lymphoma.

Comments

Monomorphic epitheliotropic intestinal T-cell lymphoma (MEITL) is a primary intestinal lymphoma derived from intraepithelial T cells. This lymphoma used to be called type II eneteropathy-associated T-cell lymphoma (EATL), a name that was changed to MEITL in 2017 World Health Organization Classification. In contrast to EATL, MEITL shows no association with celiac disease and transcriptome sequencing showed distinct expression signatures between EATL and MEITL, warranting definitive separation of these two entities. MEITL is diagnosed worldwide but is the most common primary intestinal lymphoma in Asia. It is most commonly diagnosed in older individuals with median in 7th decade with a male-to-female ratio of 2:1.

Patients with MEITL commonly present with acute abdomen due to perforation and/or hemorrhage. Intestinal obstruction by tumor mass is seen in some patients. Small intestine, particularly jejunum is most frequently involved, and multifocal involvement is frequently seen. Most frequently, lymphoma presents as an ulcerated mass in the intestine. MEITL is an aggressive lymphoma with a 5-year survival of around 30%.

Morphologically, MEITL shows sheets of relatively monotonous (monomorphic), medium-sized lymphoma cells, with round to slightly irregular nuclei, fine chromatin, inconspicuous to small nucleoli, and moderately abundant pale cytoplasm. Interstinal villi show distorted architecture with widening and blunting, and lymphoma cells show prominent epitheliotropism. Lymphoma cells are positive for CD3, CD8, CD56, and cytotoxic granule-associated proteins (TIA-1 and granzyme B). The cells are negative for CD4, CD5, and CD30. Moreover, TCR gamma is often positive (up to 60% of cases), while occasional cases express TCR beta.

Over 90% all cases show clonal TRB and/or TRG gene rearrangement. Sequencing studies of MEITL showed a mutational profile that overlaps with EATL, with some significant differences. Inactivation of SETD2 is seen in 76-83% of cases. Mutations is JAK-STAT pathway are also common, including JAK1, JAK3, STAT3, STAT5B, and SH2B3. Other recurrent mutations include TP53, BCOR, GNAI2, and ATM.

Differential diagnosis of EATL includes other primary intestinal T cell lymphoma, primarily EATL and intestinal T-cell lymphoma (ITL), NOS. Main clinical, morphologic an immunophenotypic features/differences between these entities are summarized in Table 1.

Table 1

	EATL	**MEITL**	**ITL, NOS**
Age, gender	6th-7th decade, M>F	7th decade, M:F=2:1	Older adults, M>F
Most common site(s) of involvement	Jejunum, ileum	Jejunum	Colon
Prognosis	Poor, median survival <1 year	Poor, 5-year survival 32%	Poor, median survival 35 months
Gross appearance	Plaque, ulcerated mass, stricture	Ulcerated mass	Mass
Microscopic appearance	• Infiltrates entire bowel wall • Pleomorphic, medium-sized to large cells, irregular nuclei, prominent nucleoli • Angioinvasion, necrosis • Celiac disease in adjacent mucosa	• Infiltrates entire bowel wall • Monomorphic appearance, medium-sized cells, round nuclei, fine chromatin, inconspicuous nucleoli • Blunted and widened villi, prominent epitheliotropism	• Infiltrates entire bowel wall • Heterogeneous morphology, pleomorphic • Medium-sized to large cells • Angioinvasion, necrosis
Immunophenotype	• Positive: CD2, cCD3, CD7, TIA-1, granzyme B, perforin; subset cTCR • CD8 posiitve in up to 30% of cases • Negative: sCD3, CD4, CD5, CD56, sTCR	• Positive: CD3, CD8, CD56, TIA-1, granzyme B, TCR gamma • Negative: CD4, CD5	• Positive: CD4, TCR beta, cytotoxic granules • Some cases CD4/CD8 double negative

References

1. Swerdlow SH CE, Harris NL, Jaffe ES, Pileri SA, Stein H, Thiele J, Arber DA, Hasserjian RP, Le Beau MM, Orazi A, Siebert R WHO Classification of Tumours of Haematopoietic and Lymphoid Tissues. Lyon: IARC; 2017.

2. van Vliet C, Spagnolo DV. T- and NK-cell lymphoproliferative disorders of the gastrointestinal tract: review and update. Pathology. 2020;52(1):128-141.
3. Susan SH, Ng SB, Wang S, Tan SY. Diagnostic approach to T- and NK-cell lymphoproliferative disorders in the gastrointestinal tract. Semin Diagn Pathol. 2021;38(4):21-30.

12TH INTERNATIONAL AMR PATHOLOGY SLIDE SEMINAR SYMPOSIUM IN ANATOMIC PATHOLOGY

Case – 67

Urologic and miscellaneous pathology

Contributed by: Tiziana Salviato

Clinical History

A 45-year-old HIV-infected patient had an initial gastroscopy for stomachache that revealed an ulcer at the level of the posterior wall of the gastric body. On the first biopsies the morphology, although immunohistochemical investigation with HHV8 was negative, suggested the diagnosis of Kaposi's Sarcoma.
Abdominal CT scan after intravenous administration of contrast and after oral administration of water revealed focal thickening of the gastric wall at the level of the body-bottom passage of 37x25x10 cm. A partial gastrectomy was therefore performed.

Pathological Findings

On the macroscopic evaluation of the formalin-fixed specimen, a grayish, plaque-like, centrally depressed neoformation of 3.2 cm in the major axis was found at the gastric wall.

Microscopically, this was a mesenchyme neoplasm, arising from the submucosa, with an infiltrative growth pattern along the entire thickness of the gastric wall to the serosa, consisting of predominantly spindle-shaped cells, with occasional pleomorphic elements. Necrosis was absent.

Neoplastic cells presented the following immunophenotypic profile: negative for CD1a, Bcl2, D2-40, CK7, CD21, CD213, CD31, HMB45, CD99, CK and CD117 with variable expression of CD34 and S100.

The case was sent for a second opinion and further immunohistochemical stains were performed.

It resulted also negative for EMA, CD21, ERG, MUC4, NUT, STAT6, TLE1, DOG1 or ALK but showed diffuse cytoplasmic reactivity for Pan-TRK.

The targeted RNA-sequencing using the TruSight panel (Illumina) confirmed the presence of an NTRK fusion, specifically TPM3::NTRK1.

Diagnosis

NTRK-associated low-grade spindle cell mesenchymal neoplasm of the GI-tract.

Comments

Follow-up: currently the patient is well, without any recurrence. He underwent orchiectomy of the right testis for seminoma in 2022.

NTRK (neurotrophic tyrosine receptor kinase)- rearranged spindle cell neoplasms represent novel rare STS recently included in the 5th edition of the World Health Organization (WHO) Classification of Soft Tissue and Bone Sarcomas. Tropomyosin-related kinase (TRK) is a receptor tyrosine kinase family of neurotrophin receptors (NTs) expressed in human neuronal tissue.

Outside of the classic infantile fibrosarcoma, NTRK-rearranged mesenchymal gastrointestinal (GI) tumors are often associated with *NTRK1* fusions, spanning a morphological spectrum from low-grade to high-grade.

Neurotrophin tyrosine receptor kinase (NTRK)- rearrangements should be considered in any KIT(−)/DOG1(−) gastrointestinal stromal tumor-like lesion particularly in young individuals.

On immunohistochemistry, tumor cells are negative for CD117 and DOG1 and positive for CD34. The CD34+/S100+/SOX10− immunophenotype is a distinctive feature. Molecular confirmation is often needed to verify TRK immunohistochemistry results. Since these are low grade tumors complete excision and follow-up is the mainstay of treatment. In case of progressive or aggressive disease NTRK inhibitors may be administered.

The differential diagnosis may include solitary fibrous tumor, especially in the presence of the HPC-like vascular pattern, perivascular hyalinization, haphazard arrangement and CD34 positivity; yet STAT6 negativity excludes this possibility.

In addition to CD34, tumor cells also express S100, hence a nerve sheath tumor might be considered: however SOX10 reaction is lacking.

Further differential diagnosis includes an inflammatory myofibroblastic tumor (especially in young people) but it is more cellular, presents less inflammatory lymphocytic infiltrate and is ALK1 protein negative.

Furthermore, the combined morphological and immunohistochemical features reasonably rule out a number of proliferations such as epithelial differentiation and synovial sarcoma (pan-cytokeratin/EMA negative); smooth muscle differentiation (desmin/SMA-);; desmoid fibromatosis (beta-catenin-) and neuroendocrine tumors (synaptophysin/chromogranin-).

References

1. Mesenchymal tumors of the gastrointestinal tract with NTRK rearrangements: a clinicopathological, immunophenotypic, and molecular study of eight cases, emphasizing their distinction from gastrointestinal stromal tumor (GIST). Atiq MA, Davis JL, Hornick JL, Dickson BC, Fletcher CDM, Fletcher JA, Folpe AL, Mariño-Enríquez A**.**Mod Pathol. 2021 Jan;34(1):95-103. doi: 10.1038/s41379-020-0623-z. Epub 2020 Jul 15.PMID: 32669612
2. Intestinal *LMNA::NTRK1*-fused spindle cell neoplasm with S100 and CD34 coexpression: a new case. Rahim S, Alkhaldi SS, Alasousi K, Ali RH.BMJ Case Rep. 2022 Nov 10;15(11):e251270. doi: 10.1136/bcr-2022-251270.
3. GISTs with *NTRK* Gene Fusions: A Clinicopathological, Immunophenotypic, and Molecular Study. Cao Z, Li J, Sun L, Xu Z, Ke Y, Shao B, Guo Y, Sun Y.Cancers (Basel). 2022 Dec 23;15(1):105. doi: 10.3390/cancers15010105.